AD_____

Award Number: DAMD17-01-2-0036

TITLE: Gene and Protein Therapy for Poisoning by
Organophosphorus Agents

PRINCIPAL INVESTIGATOR: Oksana Lockridge, Ph.D.

CONTRACTING ORGANIZATION: University of Nebraska Medical Center
Omaha, Nebraska 68198-6810

REPORT DATE: September 2003

TYPE OF REPORT: Annual

PREPARED FOR: U.S. Army Medical Research and Materiel Command
Fort Detrick, Maryland 21702-5012

DISTRIBUTION STATEMENT: Approved for Public Release;
Distribution Unlimited

The views, opinions and/or findings contained in this report are
those of the author(s) and should not be construed as an official
Department of the Army position, policy or decision unless so
designated by other documentation.

REPORT DOCUMENTATION PAGE	Form Approved OMB No. 074-0188

Public reporting burden for this collection of information is estimated to average 1 hour per response, including the time for reviewing instructions, searching existing data sources, gathering and maintaining the data needed, and completing and reviewing this collection of information. Send comments regarding this burden estimate or any other aspect of this collection of information, including suggestions for reducing this burden to Washington Headquarters Services, Directorate for Information Operations and Reports, 1215 Jefferson Davis Highway, Suite 1204, Arlington, VA 22202-4302, and to the Office of Management and Budget, Paperwork Reduction Project (0704-0188), Washington, DC 20503

1. AGENCY USE ONLY (Leave blank)	2. REPORT DATE September 2003	3. REPORT TYPE AND DATES COVERED Annual (1 Sep 2002 – 31 Aug 2003)	
4. TITLE AND SUBTITLE Gene and Protein Therapy for Poisoning by Organophosphorus Agents		**5. FUNDING NUMBERS** DAMD17-01-2-0036	
6. AUTHOR(S) Andrea M. Allan, Ph.D.			
7. PERFORMING ORGANIZATION NAME(S) AND ADDRESS(ES) University of Nebraska Medical Center Omaha, Nebraska 68198-6810 E-Mail: olockrid@unmc.edu		**8. PERFORMING ORGANIZATION REPORT NUMBER**	
9. SPONSORING / MONITORING AGENCY NAME(S) AND ADDRESS(ES) U.S. Army Medical Research and Materiel Command Fort Detrick, Maryland 21702-5012		**10. SPONSORING / MONITORING AGENCY REPORT NUMBER**	

11. SUPPLEMENTARY NOTES

12a. DISTRIBUTION / AVAILABILITY STATEMENT Approved for Public Release; Distribution Unlimited	12b. DISTRIBUTION CODE

13. ABSTRACT (Maximum 200 Words)

The goal of this work is to find new protection strategies against the toxicity of nerve agents. A gene therapy protocol capable of delivering human acetylcholinesterase into dividing as well as nondividing cells has been developed, using adeno-associated virus to transfer the gene. Mice treated with this virus expressed human acetylcholinesterase.

A transgenic mouse line was established that expresses human C117H butyrylcholinesterase in all tissue. The G117H butyrylcholinesterase gene was selected for expression in mice because of its special properties. It hydrolyzes nerve agents, pesticides, and other organophosphorus esters, and also hydrolyzes the neurotransmitter acetylchoine. When G117H butyrylcholinesterase transgenic mice had only mild signs of toxicity and no lethality. This is the first transgenic mouse successfully engineered for resistance to organophosphate toxicity. It demonstrates that small quantities of human G117H buturulcholinesterase provide protection in a living animal.

14. SUBJECT TERMS Gene therapy, butyrylcholinesterase, nerve agent, organophosphorus toxicant, acetylcholinesterase	15. NUMBER OF PAGES 144
	16. PRICE CODE

17. SECURITY CLASSIFICATION OF REPORT Unclassified	18. SECURITY CLASSIFICATION OF THIS PAGE Unclassified	19. SECURITY CLASSIFICATION OF ABSTRACT Unclassified	20. LIMITATION OF ABSTRACT Unlimited

NSN 7540-01-280-5500

Standard Form 298 (Rev. 2-89)
Prescribed by ANSI Std. Z39-18
298-102

Table of Contents

Abbreviations

AAV	adenoassociated virus
AChE	acetylcholinesterase enzyme
ACHE	acetylcholinesterase gene
BChE	butyrylcholinesterase enzyme
BCHE	butyrylcholinesterase gene
BW284C51	1,5 bis(4-allyldimethylammoniumphenyl)-pentan-3-one; specific inhibitor of AChE
DFP	diisopropylfluorophosphate
DMEM	Dulbecco's Modified Eagle Medium
DTNB	dithiobisnitrobenzoic acid
Elisa	enzyme linked immunosorbent assay
ES	embryonic stem cells
FBS	fetal bovine serum
FLAG	8 amino acid peptide DYKDDDDK
G117H	human butyrylcholinesterase containing Histidine 117 in place of Glycine 117
HA	Hemagglutinin epitope
HEK293	Human embryonic kidney cells
IMDM	Iscove's Modified Dulbecco's Medium
Iso-OMPA	tetraisopropylpyrophosphoramide; specific inhibitor of BChE
MEPQ	7-(methylethoxyphosphinyloxy)-1-methylquinolinium iodide
OP	organophosphorus toxicant
PCR	polymerase chain reaction
PON1	paraoxonase
s.c.	subcutaneous
SDS	sodium dodecyl sulfate
TAT	Protein transduction domain from HIV, containing 11 amino acids
VX	O-ethyl S-[2-(diisopropylamino)ethyl] methylphosphonothioate; nerve agent

Introduction

The goal of this work is to protect the soldier from the toxicity of nerve agents. The research plan involves finding new ways to deliver protective cholinesterase enzymes into tissues. Gene therapy and protein therapy protocols are being developed.

Test animals are being made to test the idea that an organophosphate hydrolase enzyme in the right location will provide protection against organophosphorus toxins. The G117H knockin mouse and the G117H transgenic mouse will give information on the level of protection that can be achieved by introducing the gene for an organophosphorus hydrolase.

Task 1. Various types of AChE enzyme will be injected into mice for the purpose of determining whether AChE enters the brain and other tissues.
1.1 Tetramers of fetal bovine AChE will be injected intraperitoneally into AChE-/- mice. Completed in year 1.
1.2 Monomers of human AChE will be produced in Chinese Hamster Ovary cells, purified, and injected into AChE -/- mice.
1.3 A TAT fusion protein with human AChE will be produced in bacteria. The purified AChE fusion protein will be tested in cultured cells for ability to enter cells and fold into active enzyme. Progress in year 2
1.4 The AChE fusion protein will be injected into AChE-/- mice to determine whether it improves their phenotype, and into wild-type mice to test the protective effect against OP.

Task 2. A gene targeted mouse substituting the G177H mutant of human BChE for the ACHE gene will be made.
2.1 A gene targeting construct will be made. Completed in year 1.
2.2 Homologous recombination in embryonic stem (ES) cells will substitute the human G117H BCHE gene for the mouse ACHE gene. Completed in year 2.
2.3 Microinjection of targeted ES cells into blastocysts and transfer into pseudopregnant mice will lead to the birth of chimeric mice.
2.4 Mating of chimeric mice with C57Bl/6 mice will determine which of the chimeras transmit the targeted allele in their germline.
2.5 Chimeric mice that are known to transmit the targeted allele in their germline will be mated with 129sv mice to produce mice with a 129sv genetic background.
2.6 Homozygous G117H mice will be produced by mating. Their phenotype and their resistance to OP will be determined.

Task 3. A transgenic mouse that expresses human G117H BChE will be made.
3.1 A plasmid will be made that contains the mouse ACHE promoter, mouse ACHE exon 1, and mouse intron 1 attached to the cDNA of human G117H BCHE. Completed in year 1.
3.2 The linearized, digested, and purified DNA will be microinjected into mouse fertilized eggs of strain FVB/N. The injected embryos will be transferred into

pseudopregnant mice. The live pups will be tested for the presence of the transgene. Completed in year 2.

3.3 Mice that carry the transgene will be tested for expression of human G117H BCHE. Completed in year 2.

3.4 Founder mice expressing the highest levels of G117H BCHE will be mated to produce colonies of transgenic mice. Completed in year 2.

3.5 Transgenic mice will be characterized with respect to tissue location of the expressed transgene and the levels of expression. Started in year 2.

3.6 Transgenic mice will be tested for resistance to OP. Started in year 2.

Task 4. Gene therapy with AChE.

4.1 Human AChE cDNA will be cloned into a shuttle vector. The linearized shuttle vector and pAdEasy-1 will be cotransfected into bacteria to allow homologous recombination. Colonies resistant to kanamycin will be screened by restriction endonuclease digestion. Completed in year 1.

4.2 The adenoviral vector containing human AChE, pAd-ACHE, will be linearized and transfected into 293 cells. Virus production will be visualized by fluorescence of green fluorescence protein and by measuring AChE activity.

4.3 Viral stocks will be amplified in 293 cells to obtain 10^{11} to 10^{12} plaque forming units. The virus will be purified in preparation for injection into mice.

4.4 Mice will be injected intravenously with various doses of adenoviral vector. The site of localization of the adenovirus will be determined. Expression levels of AChE will be determined. The duration of expression of AChE will be measured.

Relation to statement of work. In this second year of the project, we have made progress on tasks 1, 2, 3, and 4.

Task 1. *Various types of AChE enzyme will be injected into mice for the purpose of determining whether AChE enters the brain and other tissues.*
1.3 A TAT fusion protein with human AChE will be produced in bacteria. The purified AChE fusion protein will be tested in cultured cells for ability to enter cells and fold into active enzyme.

Task 1.3

Abstract

Background. Pretreatment with purified acetylcholinesterase (AChE) or butyrylcholinesterase (BChE) enzyme protects monkeys against a maximum of 5 LD_{50} doses of soman.   The limited protection is explained by the fact that the scavenger enzymes stay in the peripheral system whereas nerve agents readily enter the brain.

Goal. Our goal is to enable scavenger enzymes to cross the blood-brain barrier.

Method An 11 residue peptide from the TAT protein of HIV has been reported to have the unusual ability to carry cargo across cell membranes in a receptor-independent manner. TAT-β-galactosidase injected i.p. was reported to cross the blood-brain barrier in mice. The 11 residue TAT peptide and other peptides rich in basic amino acids are called protein transduction domains. In Task 1.3, the protein transduction domain from the TAT protein of HIV was attached to human AChE, human BChE, and human PON1. TAT was added to the 5' end, the 3' end, or embedded in the signal peptide. The constructs gave low levels of expression in bacteria. To improve expression levels in *E. coli*, the 1.7 kb human BCHE gene was completely resynthesized from oligonucleotides, using codons preferred by bacteria.

Results. The new human BCHE gene constructed with bacterial codons gave greatly improved expression levels in *E. coli*. Most of the protein was in inclusion bodies. Some of the BChE was in the soluble periplasm.

A monoclonal antibody to denatured human BChE was made. This antibody has high specificity for human BChE and recognizes both folded and denatured human BChE.

Conclusion. Expression of human BChE in bacteria has been achieved. The protein transduction domain has not yet been evaluated.

Introduction

Injection of purified AChE or BChE enzymes into the periphery protects animals from the toxicity of nerve agents. Animals have no side-effects and behave as if they had never been exposed to nerve agent. However, there is a ceiling to the level of protection. Table 1.1 shows that protection was achieved against a maximum of 1 to 8 LD_{50} doses of sarin, soman, VX or MEPQ, but not against higher doses. Pretreatment with higher amounts of cholinesterase did not allow animals to survive a higher dose of nerve agent. A possible explanation is that high doses of nerve agent escape into brain and other compartments where AChE and BChE

cannot follow.   To protect the brain from organophosphorus agent (OP) toxicity, we have been trying to develop an OP-scavenger or OP-catalytic enzyme that crosses the blood-brain barrier.

Table 1.1. Protection against nerve agent toxicity by pretreatment with AChE or BChE.

Animal	Dose of ChE, mg	Dose of OP	Toxic signs	Reference
Monkey	39	$2 LD_{50}$ soman	none	Broomfield (1991)
Monkey	39	$1 LD_{50}$ sarin	none	Broomfield (1991)
Monkey	56	$4 LD_{50}$ soman	none	Wolfe (1992)
Monkey	42.6	$2 LD_{50}$ soman	behavioral decrement	Castro (1994)
Monkey	17 to 45	$2 LD_{50}$ VX	none	Raveh (1997)
Monkey	17 to 45	$3.3 LD_{50}$ soman	none	Raveh (1997)
Monkey	33 to 66	none	none	Matzke (1999)
Mouse	1.5	soman	survived	Ashani (1991)
Mouse	1.5	MEPQ	survived	Ashani (1991)
Mouse	4	$1.5 LD_{50}$ VX	none	Raveh (1993)
Rat	4	$1.5 LD_{50}$ soman	none	Raveh (1993)
Rat	4	$1.5 LD_{50}$ soman	no cognitive deficits	Brandeis (1993)
Rat	10	MEPQ	response rate slowed	Genovese (1995)
Guinea pig	12	$2 LD_{50}$ soman	none	Allon (1998)
Monkey	7.5 and 15 mg	$2.7 LD_{50}$ soman	none	Maxwell (1992)
Monkey	29 to 36 mg	$5 LD_{50}$ soman	none	Wolfe (1992)
Mouse	0.9 mg	$3 LD_{50}$ VX	survived	Wolfe (1987)
Mouse	0.5 mg	$4 LD_{50}$ MEPQ	slight tremors	Raveh (1989)
Mouse	0.5 mg	$2.6 LD_{50}$ soman	survived	Ashani (1991)
Mouse	0.5 mg	$4.1 LD_{50}$ MEPQ	survived	Doctor (1991)
Mouse	2.4 mg	$8 LD_{50}$ soman	slight cholinergic	Maxwell (1993)

The method for crossing the blood-brain barrier that we have been testing relies on the protein transduction domain. Proteins covalently linked to a protein transduction domain (Table 1.2) are reported to have the ability to cross biological membranes. An impressive example of the success of this method is the paper by Schwarze et al. (1999).   A bacterial protein, β-galactosidase, fused to the TAT protein transduction domain was injected into the peritoneum of a mouse. Within 4 hours this protein was found in an active form in the mouse brain. A requirement of the method was that the TAT-protein be produced in bacteria and that the TAT-protein be denatured at the time of injection. The TAT-protein was assumed to fold into an active enzyme as it crossed the cell membrane. A list of the successful use of protein transduction domains is in Table 1.3.

Table 1.2. Amino acid sequences of protein transduction domains

Protein transduction domain	Amino acid sequence
TAT from HIV-1	YGRKKRRQRRR
VP22 from herpes virus	DAATATRGRSAASRPTERPRAPARSASRPRRPVE
ANTP from Drosophila	RQIKIWFQNRRMKWKK
21 amino acid carrier peptide	KETWWETWWTEWSQPKKKRKV
12 residues from Kaposi fibroblast growth factor	AAVLLPVLLAAP
9Arg	RRRRRRRRR
9Lys	KKKKKKKKK

Table 1.3. Use of a protein transduction domain to transduce proteins across membranes.

Protein	kDa	Trans-duction domain	Domain location	Tissues or cells transduced	Reference	Comments
β-galactosidase	120	TAT	5'	All tissues in living mouse	Schwarze 1999	active β-gal in brain after i.p. injection
caspase-3		TAT	5'	Jurkat T cells	Vocero-Akbani 1999	
β-glucuronidase	80	TAT	3'	live mice, brain	Xia 2001	adenovirus
β-glucuronidase	80	TAT	3'	live mice, brain	Elliger 2002	AAV in spine and i.v.
IκBα		TAT	5'	bone marrow macrophages	Abu-Amer 2001	
anti-apoptotic proteins	25	TAT	5'	pancreatic islets	Embury 2001	
superoxide dismutase	22	TAT	5'	HeLa cells	Kwon 2000	
green fluorescent protein	30	11 Arg	5'	brain slices	Matsushita 2001	
green fluorescent protein	30	21 a.a. peptide		293 cells	Morris 2001	Peptide carrier
green fluorescent protein	30	9 Lys or 9 Arg	5'	HeLa cells	Park 2002	
APOBEC-1	85	TAT	5'	primary hepatocytes	Yang 2002	
Cre recombinase	43	12 aa	3'	live mice, brain	Jo 2001	injected i.p.
Cre recombinase	43	TAT	5'	ES cells	Joshi 2002	did not work in mice
glutamate dehydrogenase	28	TAT	5'	PC12 cells	Yoon 2002	
glutathione transferase		12 aa	3'	NIH 3T3 cells	Rojas 1998	
Bcl-xL	25	TAT	5'	live mice, brain	Cao 2002	injected i.p.
Bcl-XL	25	TAT	5'	live mice, brain	Kilic 2002	Injected i.v.
Bcl-XL	25	TAT	5'	Eye	Dietz 2002	

Most of the studies in Table 1.3 used cultured cells. However, 6 studies reported success in living mice. Xia et al. 2001 attached TAT to the 3' end of β-glucuronidase expressed in an adenovirus vector. Elliger et al. (2002) also attached TAT to the 3' end of β-glucuronidase but their vector was adenoassociated virus (AAV). In neither study was TAT attached to the 5' end nor was the expressed protein added in a denatured form. The β-glucuronidase-TAT was correctly folded, active and already inside a cell when it was synthesized. The presence of TAT added to the success of their gene therapy protocols. Untreated mutant mice were unable to breed, but neonates injected with AAV were fertile (Elliger et al., 2002).

TAT-proteins injected directly into living mice were reported to show cre-recombinase activity and Bcl-XL activity in mouse brain (Jo et al., 2001; Cao et al., 2002; Kilic et al., 2002). The TAT-proteins used by Jo et al. and Cao et al. were expressed in bacteria but were not denatured before injection. One study (Joshi et al., 2002) reported failure of TAT-protein to transduce membranes in living mice. Joshi et al. (2002) injected adult ROSA26 reporter mice intraperitoneally with 1 mg of TAT-cre-recombinase on four consecutive days and then examined various tissues for deletion of the reporter allele by Southern blot analysis. They found no cre-recombinase activity in mouse tissues. Joshi's TAT-cre-recombinase had been denatured in 8 M urea.

These results suggest that the TAT-proteins do not fold after entering a cell. Contrary to the hypothesis proposed by the Dowdy laboratory, TAT-proteins must be in an active conformation before injection into an animal, if they are to have a physiological effect.

Our efforts have been directed toward getting expression in bacterial cells. We have succeeded in expressing significant amounts of human BChE in E.coli.

Methods

Materials. The pTAT-HA bacterial expression vector and the positive control pTAT-β-galactosidase vector were a generous gift from Steven Dowdy at Washington University School of Medicine, St. Louis, Missouri (presently at Univ California San Diego, La Jolla, CA). The vector pTAT-HA has an N-terminal 6-histidine leader followed by the 11-amino acid TAT protein transduction domain flanked by glycine residues, a hemagglutinin (HA) tag, and a polylinker (Nagahara et al., 1998).

Anti-HA mouse monoclonal antibody (clone 12CA5) to a peptide epitope derived from the hemagglutinin protein of human influenza virus was from Boehringer-Mannheim (cat. No. 1 583 816). Anti-human PON1 mouse monoclonal was a gift from Dr. Richard James (Blatter Garin et al., 1994). Anti-mouse Ig, horseradish peroxidase linked whole antibody (from sheep) GPR was from Amersham Life Sciences (NXA 931). LumiGLO chemiluminescent substrate kit (2-C) was from Kierkegaard & Perry, (product code 54-61-00)

Monoclonal antibody to human BChE. The antibodies in the literature recognize folded BChE but not denatured BChE protein. Therefore we made our own monoclonal. The antigen for monoclonal antibody production was the same 99.9% pure recombinant human BChE that was used to solve the crystal structure of human BChE (Nachon et al., 2002; Nicolet et al., 2003). This BChE had 529 amino acids and 6 N-linked glycans. By contrast, wild-type BChE has 574 amino acids and 9 N-linked glycans. The missing 45 amino acids were in the tetramerization domain at the C-terminus. The BChE at a concentration of 10 mg/ml was boiled in 1% SDS, 5% mercaptoethanol to denature it before it was injected into mice. A total of 3 mg of pure BChE was used.

Three young adult female BALB/c mice were immunized i.p with 100 μg of BChE, emulsified in complete Freund's adjuvant. Mice were reinjected with another 100 μg of denatured BChE after 4, 8, 15, and 17 weeks. Mice were bled 2 months after the first injection to identify the mouse with the highest serum antibody titer. The final 100 μg of BChE was injected without adjuvant 5 days before in vitro splenocyte-myeloma hybridization. The Monoclonal Core Facility at the University of Nebraska made the hybridoma cells.

Mouse serum was screened for antibody against BChE by dot blot (Schleicher & Schuell Minifold apparatus). The BChE antigen was loaded onto PVDF membrane in amounts of 100, 10, 1, and 0 ng per well. The membrane was prehybridized in Tris buffered saline containing 0.2% Tween-20, 5% dry milk for 1 h at 37°C. Then the membrane was cut into strips and each strip was hybridized with antibody solution. Mouse sera were tested at 1:200 and 1:1000 dilution. Hybridization was in a seal-a-meal bag overnight at 4°C. The strips were washed with 8 different solutions containing milk and Tween-20 at various concentrations. Then they were hybridized with anti-mouse IgG conjugated to horse radish peroxidase for 2 h. They were washed and treated with chemiluminescent reagent.

Culture medium from hybridoma cells in eleven 96-well plates was also screened by dot blot. The BChE antigen was loaded onto PVDF membrane at a concentration of 20 ng in 100 μl per well. Hybridoma fluid, 50 to 120 μl, was applied under suction. PVDF membranes were hybridized with anti-mouse IgG conjugated to horse radish peroxidase and developed with chemiluminescent reagent. The initial screening identified 40 strong positives out of 1008. Five positives were purified by limiting dilution and rescreened. The final screening was on Western blots. The best cell line was called C191 2.1-1.

Plasmid construction. Human AChE, human BChE, and human PON1 cDNA were inserted into the polylinker of the pTAT-HA bacterial expression vector. When none of these gave good yields of protein in bacteria, we redesigned the signal peptide sequence. Later we also changed the codons to codons preferred by bacteria. The plasmids we made and tested are listed in Table 1.4.

Table 1.4. Plasmid constructs for bacterial expression of TAT-proteins

Number	Plasmid	Comment
1	6His-TAT-HA-ACHE	Dowdy expression vector; 69 aa in signal peptide MRGSHHHHHHGMASMTGGQQMGRDLYDDDD KDRWGSKLGYGRKKRRQRRRGGSTMSGYPYD VPDYAGSM
2	6His-TAT-HA-BCHE	"
3	6His-TAT-HA-PON1	"
4	6His-TAT-ACHE	Dowdy vector; 55 aa in signal peptide MRGSHHHHHHGMASMTGGQQMGRDLYDDDD KDRWGSKLGYGRKKRRQRRRGGSTM
5	6His-TAT-BCHE	"
6	TAT-PON-6His	HA deleted; 6His moved to 3' end
7	TAT-PON-6His	MGYGRKKRRQRRR LLLLLLLLSGALA Redesigned signal sequence, 26 aa
8	TAT-PON-6His	MGGRKKKRRQRRRFLFWFLLLCMLIGGSHAAKL Redesigned signal sequence, 33 aa
9	TAT-PON-6His	bacterial codons for the 33 aa signal peptide and the N-terminal 59 amino acids.
10	BCHE-9Lys	Protein transduction domain at C-terminus
11	BCHE	New gene with bacterial codons Fig. 1.1.
12	BCHE-9Lys-6His	New gene with bacterial codons and 9 Lys

Expression of TAT-proteins in mammalian cells. Constructs #7, 8, 9, and 11 were tested for expression in 293T cells to be sure the signal peptide was cleaved and active protein was secreted into the culture medium. The plasmid for mammalian expression was pcDNA3 (Invitrogen). When 293T cells were 70-80% confluent, cells were transfected by calcium phosphate coprecipitation. The DNA was left on the cells for 3-5 days, after which time the culture medium and cells were tested for enzyme activity.

Expression of TAT-proteins in E.coli. Plasmids in bacterial expression vector pET16b (Novagen) were transfected into BL21(DE3)pLysS (Novagen) cells or into Rosetta(DE3)pLysS (Novagen) cells. The Rosetta strain has tRNA genes for codons rarely used by bacteria but frequently used by mammalian systems. 1 Liter cultures were grown at 37°C to optical density of 0.6 . Expression was induced by addition of IPTG to 0.5 mM.

Expression of the new BCHE gene in bacteria. The new BCHE cDNA was cloned into the bacterial expression vector pEX. pEX is derivative of pET-17b with the signal peptide of the bacterial endoxylanase protein cloned into the NdeI/EcoRV sites of pET17b (Novagen). This signal peptide is expected to direct expression into the periplasm. Tuner(DE3) cells (Novagen) were transformed with pEX-newBChE. For expression, cells were grown at 37°C in NZCYM medium (Sigma). The NZCYM medium had a concentration of 22 g/L and contained no glucose. After the cells had

grown to an optical density at 590 nm of 0.6, the medium was cooled to 25°C. Expression was induced with 1 mM IPTG for 2h at 25°C.

Purification of TAT-protein. The protocol described by Vocero-Akbani et al. (2000) was followed. Bacterial cultures of 1000 ml were centrifuged at 4,000 x g for 10 min and the cells resuspended in 10 ml of 8 M urea, 20 mM HEPES, 0.1 M NaCl, 5 mM imidazole, pH 8.0. The cell suspension was sonicated on ice and centrifuged at 12,000xg at 4°C for 30 min. The cell extract solution was bound to 5 ml Ni-NTA (Qiagen) that had been preequilibrated with 8 M urea, 20 mM HEPES, 0.1 M NaCl, 5 mM imidazole, pH 8.0 at room temperature. Binding was in a beaker. The beads were packed into a column and washed with the same buffer. The bound TAT-protein was eluted with 10 ml of elution buffer (8 M urea, 20 mM HEPES, 0.1 M NaCl, pH 8.0) containing 10, 20, 50, 100, 250, 500, and 1 M imidazole. The TAT-protein was desalted on a Mono-Q ion exchange column attached to a Waters HPLC.

Results

Negative results
Bacterial expression using the Dowdy vector. Expression of human AChE, BChE, or PON in bacteria using the Dowdy vector gave no clear evidence of the desired protein band either by staining a gel with Coomassie blue or by hybridization of Western blots with antibodies. No improvement was obtained by using a bacterial strain that contains tRNA for rare codons.

Bacterial expression in pET16b. The signal peptide was redesigned to allow cleavage of the signal peptide in mammalian cells. We wanted the signal peptide to remain attached during expression in bacteria but to be cleaved during translocation into mammalian cells. The protein transduction domain was part of the signal peptide. None of the constructs in this set gave significant protein yields when expressed in bacteria.

Positive results
The new BCHE gene. The low expression level of human BCHE in bacteria led us to compare codon usage in human BChE and in *E. coli*. It was found that the human BChE cDNA coding region contained 57 rare codons for Ile, Arg, Gly Pro, and Leu. These rare codons were distributed throughout the sequence, making it impossible to alter the sequence in a simple way. Therefore, we decided to resynthesize the entire BCHE gene from oligonucleotides. Restriction sites were built into the sequence to make it convenient to subclone fragments. The new BCHE gene sequence is shown in Figure 1.1.

Bacterial signal peptide (Endoxylanase)

```
-28                                                                                                    +1
Met Phe Lys Phe Lys Lys Lys Phe Leu Val Gly Leu Thr Ala Ala Phe Met Ser Ile Ser Met Phe Ser Ala Thr Ala Ser Ala Glu
CAT ATG TTT AAG TTT AAA AAG AAA TTC TTA GTG GGT TTA ACG GCA GCT TTC ATG AGT ATC AGC ATG TTT TCT GCA ACC GCC TCT GCA GAA
NdeI                                                                                                          BbsI

                         10                              CHO        20                                   30
Asp Asp Ile Ile Ile Ala Thr Lys Asn Gly Lys Val Arg Gly Met Asn Leu Thr Val Phe Gly Gly Thr Val Thr Ala Phe Leu Gly Ile
GAC GAT ATC ATC ATC GCC ACC AAA AAC GGT AAA GTG CGT GGT ATG AAC CTG ACC GTG TTC GGT GGT ACC GTG ACC GCG TTC CTG GGT ATC
EcoRV

                         40                                        50                   CHO        60
Pro Tyr Ala Gln Pro Pro Leu Gly Arg Leu Arg Phe Lys Lys Pro Gln Ser Leu Thr Lys Trp Ser Asp Ile Trp Asn Ala Thr Lys Tyr
CCG TAC GCG CAG CCG CCG CTG GGT CGT CTG CGT TTC AAA AAA CCG CAG AGC CTG ACC AAA TGG AGC GAT ATT TGG AAC GCG ACC AAA TAC

                         70                                        80                              90
Ala Asn Ser Cys Cys Gln Asn Ile Asp Gln Ser Phe Pro Gly Phe His Gly Ser Glu Met Trp Asn Pro Asn Thr Asp Leu Ser Glu Asp
GCG AAT AGC TGC TGC CAG AAC ATT GAT CAG AGC TTT CCG GGT TTC CAC GGT AGC GAA ATG TGG AAC CCG AAC ACC GAT CTG AGC GAA GAT

                         100                            CHO        110                             120
Cys Leu Tyr Leu Asn Val Trp Ile Pro Ala Pro Lys Pro Lys Asn Ala Thr Val Leu Ile Trp Ile Tyr Gly Gly Gly Phe Gln Thr Gly
TGC CTG TAC CTG AAC GTG TGG ATC CCG GCC CCG AAA CCG AAA AAC GCG ACC GTG CTG ATC TGG ATC TAC GGT GGT GGT TTC CAG ACC GGT
                             BamHI

                         130                                       140                             150
Thr Ser Ser Leu His Val Tyr Asp Gly Lys Phe Leu Ala Arg Val Glu Arg Val Ile Val Val Ser Met Asn Tyr Arg Val Gly Ala Leu
ACC AGC AGC CTG CAC GTG TAC GAT GGT AAA TTC CTG GCG CGT GTG GAA CGT GTG ATC GTG GTG AGC ATG AAC TAC CGT GTG GGT GCG CTG

                         160                                       170                             180
Gly Phe Leu Ala Leu Pro Gly Asn Pro Glu Ala Pro Gly Asn Met Gly Leu Phe Asp Gln Gln Leu Ala Leu Gln Trp Val Gln Lys Asn
GGT TTC CTG GCC CTG CCG GGT AAT CCG GAA GCG CCG GGT AAC ATG GGT CTG TTC GAT CAG CAG CTG GCG CTG CAA TGG GTG CAG AAA AAC
                                                                       PvuII

                         190                                       200                             210
Ile Ala Ala Phe Gly Gly Asn Pro Lys Ser Val Thr Leu Phe Gly Glu Ser Ala Gly Ala Ala Ser Val Ser Leu His Leu Leu Ser Pro
ATC GCG GCG TTC GGT GGT AAT CCG AAA AGC GTG ACC CTG TTC GGT GAA AGC GCG GGT GCG GCT AGC GTG AGC CTG CAC CTG CTG AGC CCT
                                                                           NheI

                         220                                       230                             240 CHO
Gly Ser His Ser Leu Phe Thr Arg Ala Ile Leu Gln Ser Gly Ser Phe Asn Ala Pro Trp Ala Val Thr Ser Leu Tyr Glu Ala Arg Asn
GGT AGC CAC AGC CTG TTC ACC CGT GCG ATC CTG CAG AGC GGT AGC TTC AAC GCC CCG TGG GCA GTG ACC AGC CTG TAC GAA GCG CGT AAC
                                          PstI                   BglI

                         250                                       260                             270
Arg Thr Leu Asn Leu Ala Lys Leu Thr Gly Cys Ser Arg Glu Asn Glu Thr Glu Ile Ile Lys Cys Leu Arg Asn Lys Asp Pro Gln Glu
CGT ACC CTG AAC CTG GCG AAA CTG ACC GGT TGC AGC CGT GAA AAC GAA ACC GAA ATC ATC AAA TGC CTG CGT AAC AAA GAT CCG CAA GAA

                         280                                       290                             300
Ile Leu Leu Asn Glu Ala Phe Val Val Pro Tyr Gly Thr Pro Leu Ser Val Asn Phe Gly Pro Thr Val Asp Gly Asp Phe Leu Thr Asp
ATC CTG CTG AAC GAA GCG TTC GTG GTG CCG TAC GGT ACC CCG CTG AGC GTT AAC TTC GGT CCG ACC GTG GAT GGT GAT TTC CTG ACC GAT
                                                                   HincII&HpaI

                         310                                       320                             330
Met Pro Asp Ile Leu Leu Glu Leu Gly Gln Phe Lys Lys Thr Gln Ile Leu Val Gly Val Asn Lys Asp Glu Gly Thr Ala Phe Leu Val
ATG CCG GAT ATT CTG CTG GAA CTG GGT CAG TTC AAA AAA ACC CAG ATC CTG GTG GGT GTG AAC AAA GAT GAA GGT ACC GCG TTC CTG GTG

                         340 CHO                                   350                             360
Tyr Gly Ala Pro Gly Phe Ser Lys Asp Asn Asn Ser Ile Ile Thr Arg Lys Glu Phe Gln Glu Gly Leu Lys Ile Phe Phe Pro Gly Val
TAC GGT GCG CCG GGT TTC AGC AAA GAT AAC AAC AGC ATC ATC ACC CGT AAA GAA TTT CAG GAA GGC CTG AAA ATC TTC TTC CCG GGT GTG
                                                                       StuI                    AvaI&SmaI

                         370                                       380                             390
Ser Glu Phe Gly Lys Glu Ser Ile Leu Phe His Tyr Thr Asp Trp Val Asp Asp Gln Arg Pro Glu Asn Tyr Arg Glu Ala Leu Gly Asp
AGC GAA TTT GGT AAA GAA AGC ATC CTG TTC CAC TAC ACC GAT TGG GTG GAT GAT CAG CGT CCG GAA AAC TAC CGT GAA GCG CTG GGT GAT
                                                                                                AfeI

                         400                                       410                             420
Val Val Gly Asp Tyr Asn Phe Ile Cys Pro Ala Leu Glu Phe Thr Lys Lys Phe Ser Glu Trp Gly Asn Asn Ala Phe Phe Tyr Tyr Phe
GTG GTG GGT GAT TAC AAC TTC ATC TGC CCG GCG CTG GAA TTC ACC AAA AAA TTC AGC GAA TGG GGT AAC AAT GCG TTC TTC TAC TAC TTC
                                                       EcoRI

                         430                                       440                             450
Glu His Arg Ser Ser Lys Leu Pro Trp Pro Glu Trp Met Gly Val Met His Gly Tyr Glu Ile Glu Phe Val Phe Gly Leu Pro Leu Glu
GAA CAC CGT AGC AGC AAA CTG CCG TGG CCG GAA TGG ATG GGT GTG ATG CAC GGT TAC GAA ATC GAA TTT GTG TTC GGT CTG CCG CTG GAA

                  CHO       460                                    470                             480 CHO
Arg Arg Asp Asn Tyr Thr Lys Ala Glu Glu Ile Leu Ser Arg Ser Ile Val Lys Arg Trp Ala Asn Phe Ala Lys Tyr Gly Asn Pro Asn
CGT CGT GAT AAC TAC ACC AAA GCG GAA GAA ATC CTG AGC CGT AGC ATC GTG AAA CGT TGG GCG AAC TTT GCG AAA TAC GGT AAC CCG AAC
                                                                                                    BstEII

            CHO CHO        490                                    500                             510
Glu Thr Gln Asn Asn Ser Thr Ser Trp Pro Val Phe Lys Ser Thr Glu Gln Lys Tyr Leu Thr Leu Asn Thr Glu Ser Thr Arg Ile Met
GAA ACC CAG AAC AAC AGC ACG AGC TGG CCG GTT TTC AAA AGC ACC GAA CAG AAA TAC CTG ACC CTG AAC ACC GAA AGC ACC CGT ATC ATG

                         520                                       530
Thr Lys Leu Arg Ala Gln Gln Cys Arg Phe Trp Thr Ser Phe Phe Pro Lys Val *** ***
ACC AAA CTG CGT GCG CAG CAG TGC CGT TTC TGG ACC AGC TTC TTC CCG AAA GTG TGA TAA GGG CCC AAA
                                                                              ApaI&BanII
```

Figure 1.1. The new human BCHE gene with codons preferred by bacteria.
The 28 amino acid signal peptide is from the endoxylanase gene of bacteria.

Monoclonal antibody to human BChE. The monoclonal antibody to human BChE was found to be highly specific for human BChE. It did not recognize albumin in human serum (data not shown). In Western blots of bacterial cell lysates the monoclonal gave bands only in bacteria that expressed human BChE. Uninduced bacterial cultures were blank. See Figure 1.2. This gave us a reliable tool for detecting BChE expression in bacteria.
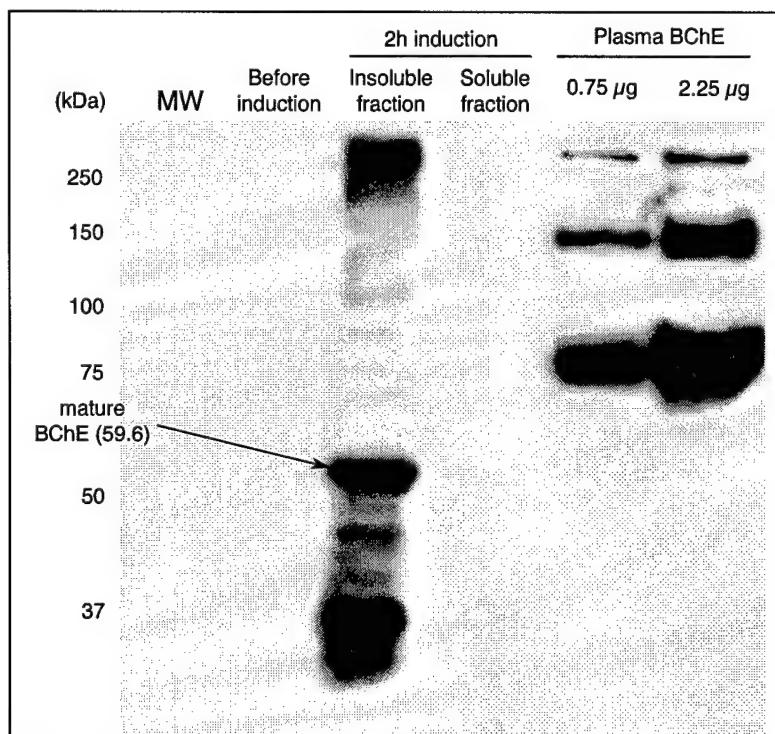
Figure 1.2. Western blot hybridized with monoclonal antibody to human BChE. The new BChE gene was expressed in bacteria. Cells were lysed by sonication and treatment with lysozyme. Insoluble and soluble fractions were loaded on an SDS gel. The positive controls are human BChE purified from human plasma. The monoclonal antibody is highly specific for human BChE as shown by the fact that the lane with uninduced bacteria is blank.

Expression of the new BCHE gene in bacteria. Several details of expression had to be refined before BChE protein expression was seen, even with the new BCHE gene. 1) All of the BChE protein was degraded when standard IPTG induction was used. Bacterial cells without a transporter for IPTG were the only strain that showed a BChE band. The strain used for expression of BChE was Rosetta(DE3)pLysS grown in the absence of chloramphenicol. This strain is called Tuner(DE3) when it is grown without chloramphenicol. The plasmid expressing the IPTG transporter was lost in the absence of chloramphenicol. The slow induction in this strain allowed some BChE protein to move into the periplasm.   2) The induction period with 1 mM IPTG had to be limited to 2 hours at room temperature to minimize proteolysis of

human BChE. 3) A third detail was the effect of freezing. When bacterial cell lysates were frozen and examined later for BChE protein bands, no bands were found. However, when newly prepared lysates were loaded on gels, BChE bands were found in inclusion bodies (Figure 1.3). It seems that proteolytic degradation of human BChE occurs rapidly in bacteria and that degradation is the major cause of low yields.
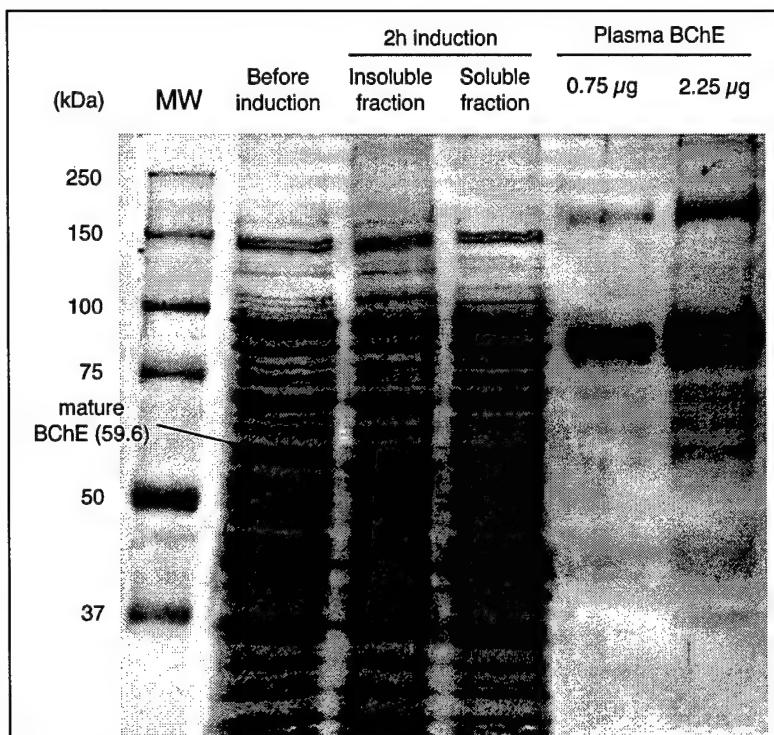
Figure 1.3. Coomassie stained SDS gel showing bacterial expression of human BChE. The band at 60 kDa is human BChE. It is smaller than the BChE purified from human plasma because it has no carbohydrates.

Discussion

Recent work on the mechanism of protein transduction disagrees with the claims of the Dowdy laboratory that translocation of TAT-proteins is independent of receptors. The six laboratories listed in Table 1.5 have found that TAT-proteins bind to the surface of cell membranes because of their positive charge. They bind to negatively charged heparan-sulfate. The TAT-proteins enter the cell by endocytosis. They are encapsulated in an endosome and only rarely enter the cytoplasm when an endosome bursts. There is no direct uptake into the cytoplasm or the nucleus. Reports of translocation into the cytoplasm and nucleus have been shown to be

artifacts of cell fixation. This suggests the β-galactosidase activity did not in fact cross the blood-brain barrier as claimed by Schwarze et al. (1999) but only entered the brain after cells had been fixed with methanol.

Table 1.5. Protein transduction domain does not translocate across membranes.

Protein	kDa	Trans-duction domain	Domain location	Tissues or cells transduced	Reference	Comments
Diphtheria toxin	21	TAT	5'	Vera cells	Falnes 2001	no translocation
Green fluorescent protein	30	TAT	5'	Eye; adenovirus	Cashman 2003	no translocation
Green fluorescent protein	30	TAT 8Arg 8 Lys	5'	CHO cells	Lundberg 2003	no translocation
Review; CD8+T cell epitope		TAT		cells	Leifert 2003	no translocation
fluorescein	1	TAT 9Arg	5'	Jurkat cells	Richard 2003	no translocation
Biotin-TAT FITC-avidin	68	TAT		HeLa, CHO	Console 2003	no translocation

We believe that the TAT-HA-β-galactosidase injected by Schwarze into mice was enzymatically active. We prepared TAT-HA-β-galactosidase by his method, denaturing the protein in 8 M urea, purifying it on Ni-NTA, and desalting. We tested the desalted enzyme for β-gal activity using o-nitrophenyl-D-galactopyranoside as substrate (Sambrook et al., 1989). To our surprise the desalted β-galactosidase was active. This control assay was not done by Schwarze nor by any other laboratory in the list in Table 1.3.   The finding that β-galactosidase was enzymatically active before injection negates the mechanism proposed by Schwarze wherein a denatured TAT-protein translocates across cell membranes and in the process of translocation folds into active enzyme with the aid of chaperones.

This reinterpretation of the data of Schwarze et al. (1999) affects our work. It no longer makes sense to express TAT-AChE, TAT-BChE, or TAT-PON in bacteria if the bacterially expressed protein is inactive. So far none of these enzymes has had measurable activity when expressed in bacteria. We are planning alternative approaches to getting an enzyme across the blood brain barrier, for example use of adenoassociated virus as in the paper by Elliger et al. (2002).

Task 2. *A gene targeted mouse substituting the G117H mutant of human BChE for the ACHE gene will be made.*
2.1 A gene targeting construct will be made.
2.2 Homologous recombination in embryonic stem (ES) cells will substitute the human G117H BCHE gene for the mouse ACHE gene.

Tasks 2.1 and 2.2

Abstract

        The G117H mutant of human BChE has the unique capability of being able to hydrolyze the neurotransmitter acetylcholine and to hydrolyze organophosphorus (OP) toxicants. We want to know whether substitution of G117H BChE for AChE will make the mouse resistant to OP toxicity. Toward this end, we have constructed a gene-targeting plasmid to be used for making the G117H knockin mouse. The linearized gene-targeting plasmid was transfected into mouse embryonic stem cells by electroporation. 480 colonies resistant to G418 and gancyclovir were selected. Genomic DNA from 480 colonies was screened by Southern blotting; one clone was found to have undergone homologous recombination.

Introduction

        Better protection from nerve agents would be achieved if an OP hydrolase were present in the nerve muscle junction and in neurons of the brain. Millard et al. (1995 and 1998) and Lockridge et al. (1997) have shown that the G117H mutant of human BChE hydrolyzed the OP agents sarin, VX, echothiophate, and paraoxon, as well as butyrylthiocholine and acetylthiocholine. Potentially, G117H BChE would perform the job that AChE normally performs, that of terminating nerve impulse transmission, with the advantage that G117H BChE is resistant to inactivation by OP. To test the idea that a mouse could be OP resistant, we are making a mouse that has the human G117H BCHE gene in the mouse ACHE gene locus.

Methods and Results

Design of gene targeting vector. We have designed and constructed the gene targeting vector to make the G117H knockin mouse. We designed the gene targeting vector so that expression of human G117H BChE would occur during development at the same time and in the same tissues as AChE in wild-type mice.
        The design of the gene targeting vector aims to retain as much of the control regions of the ACHE gene as possible so as not to alter the expression pattern. Therefore, mouse ACHE intron 1, the mouse ACHE signal peptide, mouse ACHE intron 3, exon 4, intron 4, exon 5, intron 5, exon 6, and the 3' untranslated region are retained. The human BCHE in this vector is represented by amino acids Glu 1 to Gly 478 encoded by human BCHE exon 2. This plan is missing one potential control region, namely intron 2 of the ACHE gene. It was not possible to include intron 2 because it would have given unwanted recombination. Luo et al., (1998) have shown that retention of either intron 2 or 3 of mouse ACHE is sufficient to control

exon 4 to exon 6 splicing. Since our construct contains intron 3, it is expected that normal control of splicing will be possible.

Structure of the gene targeting vector. See Figures 2.1 and 2.2. The gene targeting vector contains two selectable markers: the TK gene (2 kb) for negative selection, and the PGK-NEO gene (1.6 kb) for positive selection. The 34 nucleotide loxP sequence was placed on both sides of the NEO gene to allow deletion of the NEO gene by Cre recombinase.
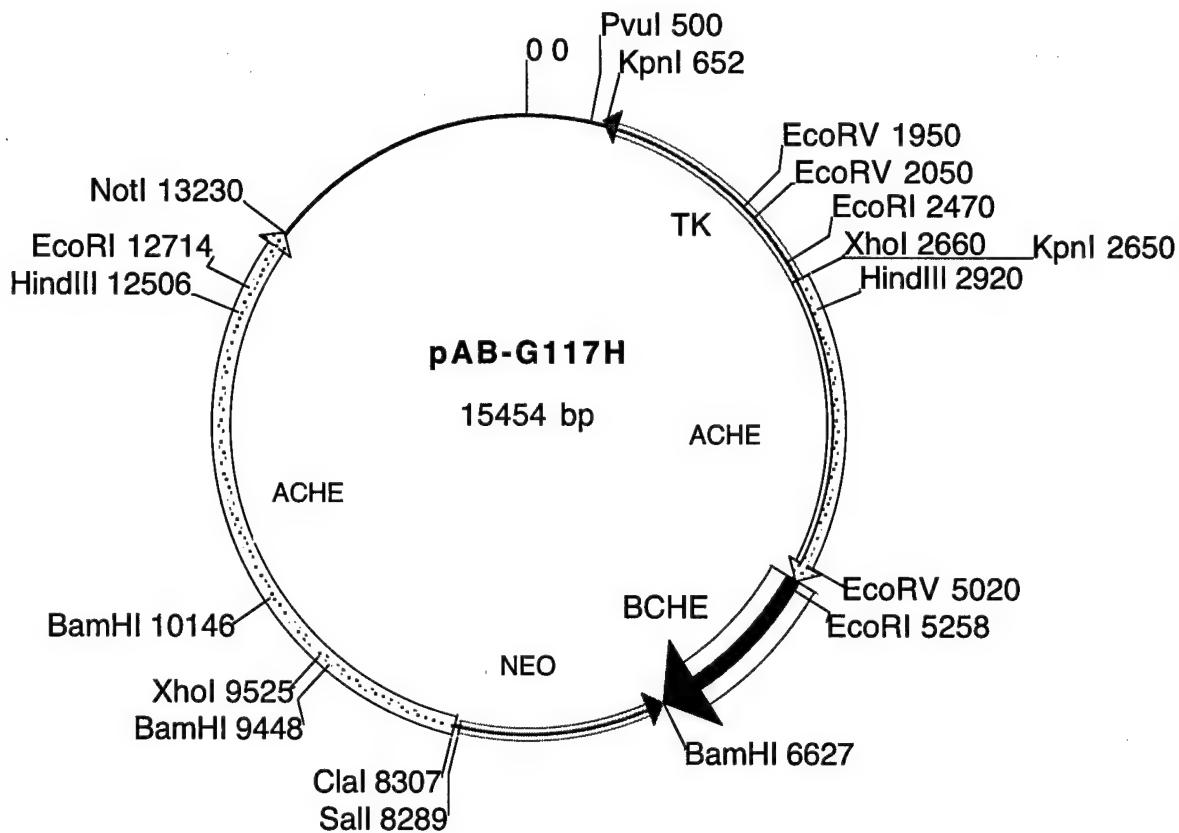
Figure 2.1. Map of the gene-targeting vector. The selectable markers are the TK gene (2 kb) and loxP NEO (1.66 kb). The 2502 bp of mouse ACHE are followed by 1433 bp of human BCHE, 1662 bp of loxP NEO, and 4923 bp of mouse ACHE. Human BCHE contains the G117H mutation.

The short arm of the gene targeting vector contains 2502 bp of mouse ACHE starting with 139 bp of intron 1b, followed by 292 bp of exon 1a, 226 bp of intron 1a, 84 bp of exon 1, 1644 bp of intron 1, and 115 bp of exon 2. The exon 2 portion of

mouse ACHE includes the splice site and the codons for the 31 amino acid signal peptide of mouse ACHE. The mouse AChE signal peptide was used rather than the human BChE signal peptide. The human BCHE gene starting with Glu+1 of the mature protein and ending at Gly 478 was placed immediately after the signal peptide. Gly 478 is at the end of exon 2 of human BCHE. A total of 1433 bp of the human BCHE gene are in this construct. At the end of exon 2 of human BCHE are 20 bp of intron 3 of mouse ACHE including the splice site. This is followed by the loxP PGK-NEO gene, and then by 4.9 kb of mouse ACHE. The 4.9 kb long arm contains 1340 bp of intron 3 of mouse ACHE, 170 bp of exon 4, 116 bp of intron 4, 128 bp of exon 5, 536 bp of intron 5, 122 bp of exon 6, and 3 kb of 3' untranslated region of mouse ACHE. The TK and NEO genes are oriented opposite to the direction of the ACHE-BCHE gene fusion. The sequence of the human BCHE gene was modified at residue Gly 117 to make the G117H mutant, because this mutant hydrolyzes organophosphorus toxicants including nerve agents.

The gene targeting vector was checked by DNA sequencing (Figure 2.2) and restriction enzyme digestion to be sure the construct was faithful to the design. The DNA sequence of the mouse ACHE portions was nearly identical to that in Genbank accession number NT_026533, even though our gene targeting vector was made from DNA of mouse strain 129SVj (Stratagene lambda FIX genomic library, catalog #946309) while the Genbank sequence is for mouse strain C57BL/6J. There were 5 differences: one nucleotide in intron 1a and 4 nucleotides in intron 1.

Figure 2.2. Sequence of the gene targeting vector.

```
1     ACCTAAGTTGTAAACGTTAATATTTTGTTAAAAATTCGCGTTAAATTTTTGTTAAATCAGCTCATTTTTTAACCAATAGGCCGAAATCGGCAAAATCCCTT
      Bluescript SK+    651nt
101   ATAAATCAAAAGAATAGACCGAGATAGGGTTGAGTGTTGTTCCAGTTTGGAACAAGAGTCCACTATTAAAGAACGTGGACTCCAACGTCAAAGGGCGAAA
201   AACCGTCTATCAGGGCGATGGCCCACTACGTGAACCATCACCCTAATCAAGTTTTTTGGGGTCGAGGTGCCGTAAAGCACTAAATCGGAACCCTAAAGGG
301   AGCCCCCGATTTAGAGCTTGACGGGGAAAGCCGGCGAACGTGGCGAGAAAGGAAGGGAAGAAAGCGAAAGGAGCGGGCGCTAGGGCGCTGGCAAGTGTAG
401   CGGTCACGCTGCGCGTAACCACCACACCCGCCGCGCTTAATGCGCCGCTACAGGGCGCGTCCCATTCGCCATTCAGGCTGCGCAACTGTTGGGAAGGGCG
501   ATCGGTGCGGGCCTCTTCGCTATTACGCCAGCTGGCGAAAGGGGGATGTGCTGCAAGGCGATTAAGTTGGGTAACGCCAGGGTTTTCCCAGTCACGACGT
      PvuI                         PvuII
601   TGTAAAACGACGGCCAGTGAATTGTAATACGACTCACTATAGGGCGAATTG/GGTACCGCGCCAGAAATCCGCGCGGTGGTTTTTGGGGGTCGGGGGTGTT
      M13 primer              T7 primer              KpnI end TK gene 1999nt
701   TGGCAGCCACAGACGCCCGGTGTTCGTGCGCGCCAGTACATGCGGTCCATGCCCAGGCCATCCAAAAACCATGGGTCTGTCTGCTCAGTCCAGTCGTGG
801   ACCTGACCCCACGCAACGCCCAAAATAATAACCCCCACGAACCATAAACCATTCCCCATGGGGGACCCCGTCCCTAACCCACGGGGCCCGTGGCTATGGC
901   AGGGCTTGCCGCCCCGACGTTGGCTGCGAGCCCTGGGCCTTCACCCGAACTTGGGGGTTGGGGTGGGGAAAAGGAAGAAACGCGGGCGTATTGGTCCCAA
1001  TGGGGTCTCGGTGGGGTATCGACAGAGTGCCAGCCCTGGGACCGAACCCCGCGTTTATGAACAAACGACCCAACACCCGTGCGTTTTATTCTGTCTTTTT
1101  ATTGCCGTCATAGCGCGGGTTCCTTCCGGTATTGTCTCCTTCCGTGTTTCAGTTAGCCTCCCCCATCTCCCGGGCAAACGTGCGCGCCAGGTCGCAGATC
                                                                                        BssHII
1201  GTCGGTATGGAGCCTGGGGTGGTGACGTGGGTCTGGACCATCCCGGAGGTAAGTTGCAGCAGGGCGTCCCGGCAGCCGGCGGGCGATTGGTCGTAATCCA
1301  GGATAAAGACGTGCATGGGACGGAGGCGTTTGGCCAAGACGTCCAAGGCCCAGGCAAACACGTTATACAGGTCGCCGTTGGGGGCCAGCAACTCGGGGGC
1401  CCGAAACAGGGTAAATAACGTGTCCCCGATATGGGGTCGTGGGCCCGCGTTGCTCTGGGGCTCGGCACCCTGGGGCGGCACGGCCGTCCCCGAAAGCTGT
1501  CCCCAATCCTCCCACCACGACCCGCCGCCCTGCAGATACCGCACCGTATTGGCAAGCAGCCCGTAAACGCGGCGAATCGCGGCCAGCATAGCCAGGTCAA
                                PstI
1601  GCCGCTCGCCGGGGCGCTGGCGTTTGGCCAGGCGGTCGATGTGTCTGTCCTCCGGAAGGGCCCCCAACACGATGTTTGTGCCGGGCAAGGTCGGCGGGAT
1701  GAGGGCCACGAACGCCAGCACGGCCTGGGGGGTCATGCTGCCCATAAGGTATCGCGCGGCCGGGTAGCACAGGAGGGCGGCGATGGGATGGCGGTCGAAG
1801  ATGAGGGTGAGGGCCGGGGGCGGGGCATGTGAACTCCCAGCCTCCCCCCCGACATGAGGAGCCAGAACGGCGTCGGTCACGGCATAAGGCATGCCCATTG
1901  TTATCTGGGCGCTTGTCATTACCACCGCCGCGTCCCCGGCCGATATCTCACCCTGGTCGAGGCGGTGTTGTGTGGTGTAGATGTTCGCGATTGTCTCGGA
                                                  EcoRV
2001  AGCCCCCAGCACCTGCCAGTAAGTCATCGGCTCGGGTACGTAGACGATATCGTCGCGCGAACCCAGGGCCACCAGCAGTTGCGTGGTGGTGGTTTTCCCC
                                                  EcoRV
2101  ATCCCGTGAGGACCGTCTATATAAACCCGCAGTAGCGTGGGCATTTTCTGCTCCAGGCGGACTTCCGTGGCTTCTTGCTGCCGGCGAGGGCGCAACGCCG
2201  TACGTCGGTTGCTATGGCCGCGAGAACGCGCAGCCTGGTCGAACGCAGACGCGTGTTGATGGCAGGGGTACGAAGCCATACGCGCTTCTACAAGGCGCTT
2301  GCCAAAGAGGTGCGGGAGTTTCACGCCACCAAGATCTGCGGCACGCTGTTGACGCTGTTAAGCGGGTCGCTGCAGGGTCGCTCGGTGTTCGAGGCCACAC
2401  GCGTCACCTTAATATGCGAAGTGGACCTGGGACCGCGCCGCCCCGACTGCATCGCGTGTTCGAATTCGCCAATGACAAGACGCTGGGCGGGGTTTGCTC
                                                       EcoRI
2501  GACATTGGGTGGAAACATTCCAGGCCTGGGTGGAGAGGCTTTTTGCTTCCTCTTGCAAAACCACACTGCTCGACATTGGGTGGAAACATTCCAGGCCTGG
2601  GTGGAGAGGCTTTTTGCTTCCTCTTGAAAACCACACTGCTCGACGGTACC|GGGCCCCCCTCGAG|CAAAGTGCATTGTAGCATCTCCCCACAGCCTTCTG
                             1999nt start of TK gene KpnI    ApaI      XhoI   mouse ACHE 2502 nt,      exon1a
2701  CTTGCCACTATGTGGTCTGGCTTCTCAGCTGTCCCCGTGTCACCTCTTCTTGCCCACAGGGGTCTTTTCCTATAAGGGAGAGCCTGTGTTTCTGTTATTT
2801  GTTCCTACAGGTGTTCTTTCGTCTCCACAGAGATGTCCCACGTCATCTTTTCTACCAGTGTCAGCTGAAGGGGGTCCTCAGTCAGGCTTTCTCGTGTCTC
2901  TTCTCTTATTACCCTGCCCCAAGCTTTGTCCTGGTTACAGATGCCAAATATTAGGCCTCTGATCTTTCTGGATTAGAGCTGTCAGTGTGTCCTTCCGTCC
                              HindIII
3001  GTGAAAGGCGACCGGTCTGTCTGTGACTTGTCACCGCAGGAGACTGTCGCCTGCGTGAACGGTGTCTGGTGTCTCCGCAGGCTGCGGTCCGTCTGTCACG
3101  TGGGTGTCTGCCCCGCCGCTGCGGGTCTGCGGGTCTGTCGGTCTGTCTGAATCTACCACTGGAGTGTGTCTGGGCTCCCGCTCCCCGGGGTCTCGGGGCT
3201  TGAAGGGAGGGGAGGAGGGGAGGTGGCAGCCCGGGGGAGCGGGGAGGGGCGGGGGCGGAGACAGTGGGCGGGCGGGGGCGCCGTGCGGCCCGGAGGGGTGT
3301  GTGCGGGGGGCCGGAGGCGGCTGTCACTGTCGGCTCAGCCTGCGCCGGGGAACATTGGCCGCCTCCAGCTCCCGGCGCGGCCCGACCCGGCCCGGCTTGG
3401  CCGCCTCAG|GTGAGTCTCCCAACCCACCCAGGACCCTCCACCGAGTCGGGACCAATCCGCATCCCGGGGGAAACGTGCGATCCTGGAACGATCGAAGCCC
      ACHE intron 1, 1644nt
3501  CCCAACAGAGCTCCTACTGCACCTCCTGCCCCGTGGGGCCTGCCTAGAGGGGCCCCTCCACTGCCTCGCACTCCTCTGAAACTCCCGCTAGCCGCTGCAT
           SacI                                                                              NheI
3601  ACTTACTGATGATGCTCGCTGGGCCGGCCGCTGCCTCTGCGCTCCCTTCCTGCAGGGACCCCCTGAAGGCCCCTTCCCCACTCTCTTCAAAGTCTGGGGA
3701  CACTGGAAGACGCCCCCTGTTTGGGGCGGAGCCCAAACTGCGCAGGTTACTGACATCCCGAATGCACCACCCCCCATCCCGAGGGCGCGACCCCAACGT
3801  CCCTACCCAGCTGAGCCCCTTGCCAGCTCCAGGACCCCTCCTGCGCTCTCTCTCTCTCTCTCTCTCTCTCTCTCTCTCTCTCTCTCTGACTCTGTCTCTC
3901  TCTATGTGTCTCTGTCTCTCTCTTTCCCTCCCTCCCTCCCTCCCTCCCTCCCTCCCTCTCACCCTCCCACCCTCCCTCTAAAAGGAGGCTCAGCGGAAGC
                                                                          Shelley Camp's enhancer
4001  CCCGAGTTATAATTAGCCCCACTCGGGTTTCCTGGTTAATCTCCAACAACGCCACTATCCCCAGATCCAGGCGACCAGAACTGGCTGGGTGGGTGATGGGTGAA
4101  CACCCGGAGGGGGTAGTTCCGACCCGGGGAATTTTGATCTCTTGGCTGGAGACGCCGGAACTACAGCAGCTGTTGCCCCCAAAATAGCGCCCCTGCCTTT
                                               N box reversed    E box
4201  GCTACGGGGATCTCCGGAGCTCCCGGAACACAGACGTCCTGGCTCGCCCTTCAACCCCCTCTGCGATGCTCACGATTCTCCAGATACCCCCACACCAAGG
           SacI    N box reversed
4301  CTCGGGCGGGGAGCTCTGGCCTCTTCTTGGTCTCTACTGCTCCCGGTTGGCAGCGGAGGGCATTGCAATATGGGGATGCAATAGGGGCTTGAGTTCTGGT
           SacI
4401  GAGCCCCACAAGGGGCGAGTGAGACAGTTGGCTGGAGTCAGGCGAGAGGGGTGCGGTTGATGTAAAGCAAACGGGTACCAACCGGCCGTACCAGTAAGAA
                                                                                KpnI
4501  GAGAGGCGGAGCAGGGTGGGGCAAGGTATCGACTGGACAAGATTCCAAGATGCCTTCAGAACCTGGGACTCCCGATACCTTGAATGCCCAACCCACTCCC
4601  CAGAAGGCTTTGGCTAACCCAGGAGAGGCTTGGGCTGTGCTTTCTTATAACTTGCAAGCTCCCGAAGGGGCCACACCCGTCCGTCCATGAGGGTCCCCTG
4701  CACCTGTCCTGGGGCTATACAAAGCCTTTCCAACCCTGTGCTGTATACTAGGGGTCTTAGCTCAAGCTGCAGGGGAAAGAGGTATGGAGGCCCTTGGAA
4801  CTTGCTGCGGCAAGGGAGACTATGTATTAGCCAGGCTTATCTCAGTTGGCTGCATTTGTTGCGGTATGGGTGTGTGTATGTCTGATCTTGTGTTTGTCTGC
4901  CTGTGTCGCGTCTCCTAGCTTGACTCCATTTCTCCCCTCCCCTTACCAATCTGCACACCTCCTCTGCAACTCCTTGATAAGCCCTGGGCAAGACTGTTT
5001  CTTAATCTCCCACTGAGCTGATATCTTCACACTTTGCCTTTCTTTCTCCCAGCAG|ACACCCAGCCTGTCCTGGCAGTCATGAGGCCTCCCTGGTATCCCCT
                      EcoRV                            end intron 1  start exon 2 mouse ACHE 115 nt signal peptide
```

Figure 2.2 continued

```
5101 GCATACACCTTCCCTGGCTTTTCCACTCCTCTTCCTCCTCCTCTCCCTCCTGGGAGGAGGGGCAAGGGCT|GAAGATGACATCATAATTGCAACAAAGAAT
                                                                          end ACHE    +1aa human BCHE 1433 nt
5201 GGAAAAGTCAGAGGGATGAACTTGACAGTTTTTGGTGGCACGGTAACAGCCTTTCTTGGAATTCCCTATGCACAGCCACCTCTTGGTAGACTTCGATTCA
                                                              EcoRI
5301 AAAAGCACAGTCTCTGACCAAGTGGTCTGATATTTGGAATGCCACAAAATATGCAAATTCTTGCTGTCAGAACATAGATCAAAGTTTTCCAGGCTTCCAT
5401 GGATCAGAGATGTGGAACCCAAACACTGACCTCAGTGAAGACTGTTTATATCTAAATGTATGGATTCCAGCACCTAAACCAAAAAAATGCCACTGTATTGA
5501 TATGGATTTATGGTGGTCATTTTCAAACTGGAACATCATCTTTACATGTTTATGATGGCAAGTTTCTGGCTCGGGTTGAAAGAGTTATTGTAGTGTCAAT
          G117H
5601 GAACTATAGGGTGGGTGCCCTAGGATTCTTAGCTTTGCCAGGAAATCCTGAGGCTCCAGGGAACATGGGTTTATTTGATCAACAGTTGGCTCTTCAGTGG
5701 GTTCAAAAAATATAGCAGCCTTTGGTGGAAATCCTAAAAGTGTAACTCTCTTTGGAGAAAGTGCAGGAGCAGCTTCAGTTAGCCTGCATTTGCTTTCTC
5801 CTGGAAGCCATTCATTGTTCACCAGAGCCATTCTGCAAAGTGGTTCCTTTAATGCTCCTTGGCGGTAACATCTCTTTATGAAGCTAGGAACAGAACGTT
5901 GAACTTAGCTAAATTGACTGGTTGCTCTAGAGAGAATGAGACTGAAATAATCAAGTGTCTTAGAAATAAAGATCCCCAAGAAATTCTTCTGAATGAAGCA
6001 TTTGTTGTCCCCTATGGGACTCCTTTGTCAGTAAACTTTGGTCCGACCGTGGATGGTGATTTTCTCACTGACATGCCAGACATATTACTTGAACTTGGAC
6101 AATTTAAAAAAACCCAGATTTTGGTGGGTGTTAATAAAGATGAAGGGACAGCTTTTTTTAGTCTATGGTGCTCCTGGCTTCAGCAAAGATAACAATAGTAT
6201 CATAACTAGAAAAGAATTTCAGGAAGGTTTAAAAATATTTTTTCCAGGAGTGAGTGAGTTTGGAAAGGAATCCATCCTTTTTCATTACACAGACTGGGTA
6301 GATGATCAGAGACCTGAAAACTACCGTGAGGCCTTGGGTGATGTTGTTGGGGATTATAATTTCATATGCCCTGCCTTGGAGTTCACCAAGAAGTTCTCAG
6401 AATGGGGAAATAATGCCTTTTTCTACTATTTTGAACACCGATCCTCCAAACTTCCGTGGCCAGAATGGATGGGAGTGATGCATGGCTATGAAATTGAATT
6501 TGTCTTTGGTTTACCTCTGAAAGAAGAGATAATTACACAAAAGCCGAGGAAATTTTGAGTAGATCCATAGTGAAACGGTGGGCAAATTTTGCAAAATAT
6601 GG|GTCAGTGGTATTGGAGTGGGGATCC ATAACTTCGTATAATGTATGCTATACGAAGTTAT GCCATAGAGCCCACCGCATCCCCAGCATGCCTGCTATTG
     end exon2 BCHE intron3 20nt BamHI   loxP 34nt                        end of NEO gene 1594nt
6701 TCTTCCCAATCCTCCCCCTTGCTGTCCTGCCCCACCCCACCCCCCAGAATAGAATGACACCTACTCAGACAATGCGATGCAATTTCCTCATTTTATTAGG
6801 AAAGGACAGTGGGAGTGGCACCTTCCAGGGTCAAGGAAGGCACGGGGGAGGGGCAAACAACAGATGGCTGGCAACTAGAAGGCACAGTCGAGGCTGATCA
6901 GCGAGCTATAGAGAATTGATCCCCTCAGAAGAACTCGTCAAGAAGGCGATAGAAGGCGATGCGCTGCGAATCGGGAGCGGCGATACCGTAAAGCACGAGG
7001 AAGCGGTCAGCCCATTCGCCGCCAAGCTCTTCAGCAATATCACGGGTAGCCAACGCTATGTCCTGATAGCGGTCCGCCACACCCAGCCGGCCACAGTCGA
7101 TGAATCCAGAAAAGCGGCCATTTTCCACCATGATATTCGGCAAGCAGGCATCGCCATGGGTCACGACGAGATCATCGCCGTCGGGCATGCGCGCCTTGAG
7201 CCTGGCGAACAGTTCGGCTGGCGCGAGCCCCTGATGCTCTTCGTCCAGATCATCCTGATCGACAAGACCGGCTTCCATCCGAGTACGTGCTCGCTCGATG
7301 CGATGTTTCGCTTGGTGGTCGAATGGGCAGGTAGCCGGATCAAGCGTATGCAGCCGCCGCATTGCATCAGCCATGATGGATACTTTCTCGGCAGGAGCAA
7401 GGTGAGATGACAGGAGATCCTGCCCCGGCACTTCGCCCAATAGCAGCCAGTCCCTTCCCGCTTCAGTGACAACGTCGAGCACAGCTGCGCAAGGAACGCC
7501 CGTCGTGGCCAGCCACGATAGCCGCGCTGCCTCGTCCTGCAGTTCATTCAGGGCACCGGACAGGTCGGTCTTGACAAAAAGAACCGGGCGCCCCTGCGCT
7601 GACAGCCGGAACACGGCGGCATCAGAGCAGCCGATTGTCTGTTGTGCCCAGTCATAGCCGAATAGCCTCTCCACCCAAGCGGCCGGAGAACCTGCGTGCA
7701 ATCCATCTTGTTCAATGCCGATCCCATATTGGCTGCAGGTCGAAGGGCCCGGAGATGAGGAAGAGGAGAACGCGCGGCAGACGTGCGCTTTTGAAGCG
7801 TGCAGAATGCCGGGCCTCCGGAGGACCTTCGGGCGCCCGCCCCGCCCCTGAGCCCGCCCCTGAGCCCGCCCCCGGACCCACCCCTTCCCAGCCTCTGAGC
7901 CCAGAAAGCGAAGGAGCAAAGCTGCTATTGGCCGCTGCCCCAAAGGCCTACCCGCTTCCATTGCTCAGCGGTGCTGTCCATCTGCACGAGACTAGTGAGA
8001 CGTGCTACTTCCATTTGTCACGTCCTGCACGACGCGAGCTGCGGGGCGGGGGGGAACTTCCTGACTAGGGGAGGAGTAGAAGGTGGCGCGAAGGGGCCAC
8101 CAAAGAACGGAGCCGGTTGGCGCCTACCGGTGGATGTGGAATGTGTGCGAGGCCAGAGGCCACTTGTGTAGCGCCAAGTGCCCAGCGGGGCTGCTAAAGC
8201 GCATGCTCCAGACTGCCTTGGGAAAAGCGCCTCCCCTACCCGGTAGAATTAATTC ATAACTTCGTATAATGTATGCTATACGAAGTTAT GTCGACGCGTC
                                           NEO gene promoter start          loxP 34nt                 SalI
8301 CATCGAT|GGCGTCTGGGGGTCCAGGGGGAGAGGGGTACCCATGGATGGCAGTGAAAAAGAAGAAGAAACCTTCACAAAGTTAAGGGGTGAAGAGAAAGTCT
     ClaI    ACHE 4923nt                   KpnI   1340nt of ACHE intron 3
8401 CAGGTGATGCCGGAGAACAAGGCAGGCAGAACAGGGAGTCCTTAAAAGACAAAACCAGCTGGGAACCTTGAATCCCAGCACAGGAGGGAGAAGACAGTCT
8501 AATGTACACAGTTCCAGACTAGCTGGGACACGACAGAGTGAGAGCCCCCATAAGGGCTGGGAACAGCTCCATGGTAGACGGCTGAAAAGCAAATGTATAT
8601 GAGGCCACCCCAGCACTCTAAAAGACAGCGAGGTAACTGGTATTCAACAGATAAAAGAGATTGCCCTGCAAGCCTATCTCAGTTGAATCCCTGAAACACA
8701 GAGAGTGGCTCTCCACAAAGCTACCCCTGACCTTCAAATCTCTCTCACTCACACACAAACCCACACAGATGATGATGATGACGACAGAGAAAGGCA
8801 GTAGAGGTTTGGGGGTGTAGCTCAGTTAGTACTTACCTACCTAGGCATGCACAAACCCTTGGGTGCATCTGATTTTCGTTTCCCAAAGTAAAAGTAATAAT
8901 TGTAGAGACAGGACTGCACCTACCTACACAGCTAAAAGCACAATCCTAGAATTTTTTATTTTAAAATAGGGTCTCGCTATGTAGCACTGGCTGGTCTGGAA
9001 ATCTCCATGTTGATCAGGCTGGCTTCAAACTCAGAAAAATTAGCCTGCCTCTGCCTCCCGGGTGCTGGGATTAAAGCCTGTAGTACCGCACCCAGCTAGA
9101 AAGACTTTGAAAACAAAGGGAAATGGAGAAAGAGACAGAGATGTCCAGTGGAAAGAAAACTTCCCTAGGTGGTGGAATGGTAGAGGTACTTAAAATGAG
9201 AAGGGAACCTATCCATGTCTGTAAATCCGTACTCTGGGAAACTGAGGCAGAAGCATTGGCAGCACTCATTTCTCTCTCTCTCTCTCTCTCTCTCTCTC
9301 TCTCTCTCTCTCTCTCTCCCTCTCTCACACACACACACACTCACACACACACTCACACGGGGCGAGGGCGGGGGTGGGGGGCTGGCTGGAGTAGGG
9401 AGAAGAGAGTTGGGTGTTAAGAGTTGAAGAGGGTCCAGAGTCAGGAAAAGGATCCACGTCTTCATTCCTTATTCCTCTGGGCAGGCTGAGATTTCCCTTT
                                                     BamHI
9501 CCTTCCTCAG|GGACCCCAATGACCCTCGAGACTCCAAATCTCCACAGTGGCCACCGTACACCACTGCCGCGCAGCAATATGTGAGCCTGAACCTGAAGCC
             exon4 170nt    XhoI
9601 CTTAGAGGTGCGGCGGGGACTGCGCGCCCAGACCTGCGCCTTCTGGAATCGCTTTCTCCCCAAATTGCTCAGCGCCACCG|GTAGGCGCATGGAGTGGGGG
                                                                                    intron 4 116nt
9701 GAGCAGGGAATGCACAAGGCGGCAAGGGTTGGAAGGAGGGGAGAGAGATGGGGTGCAAAACACAGGGTGTAATCCCTCTCTTCTCCACCTCCCCAG|CCAC
9801 GGAGGCTCCTTGCACCTGCCCAAGCCCCGCCCATGGGGAGGCGGCCCCGAGGCCCGGGCCGGACTTAGCCCTGTCCCTCCTCTTCTTCCTTTTCCTCCTC
     exon 5 128nt
9901 CACTCCGGGCTTCCGTGGCTC|TAACTGCAATCCTTTCCCCTTCTGGTCTCAAAGCACACTTACTCTAGTGTGTAGCTGAGAAGGGGCCCCTCTCAGGGAT
                        intron 5 536nt
10001 ACAGAACCCCACTCCATTCTCAAGCCGAGACAAAATGGACAGACTCAGGGATCTTTGTTAAACAAAAATTCAAAAAACAGGATTTATTTTTTTTTTAATG
10101 TAAAAAATTATCCTTTGGAGCTTGAGCCTGGTGTTGAGGGGAGAAGGATCCGGGCTAGTTGGCGTCAGCCAAAGGGCCTTATAATCGGGAACTATTTCT
                                                    BamHI
10201 GTATCTTCTCTCTTTTCCCCACTAACCCATGAACCCTTCTCCCACTCTGATCCTGTCCCTCCCCTCCGTCTTCCGGTGATTTTTATCTCTTCCTCTCCTT
10301 CCTGTTCCACCTCTCCCTTCATTCTCCGGATCATCCACTGTTCTCTTTCCACCACCCCGCTCGGCCTCCGACAATGCGTGTGTGCCGGCGCACTCACGAC
10401 CGGTCTCCACTACCCGACCTGTTCCGTTTCTCCCACTCTTGCGGGGTGCCCTGGCCGCAG|ATACTCTGGACGAGGCGGAGCGCCAGTGGAAGGCCGAGTT
                                                                exon 6 mouse ACHE
10501 CCACCGCTGGAGCTCCTACATGGTGCACTGGAAGAACCAGTTCGACCACTATAGCAAGCAGGAGCGCTGCTCAGACCTGTGA|CCCCTTGGGGGACCCCAG
          SacI                                                                      end exon 6
```

Figure 2.2 continued

```
10601 GTCCTGCCGCCCTGCCCGAGCCCCTAGCTGTATATACACTATTTATTTAAGGGCTGGGATATAATACGACCGAGCCCCCAGGCCCTGTCCACTCCTCCCC
10701 GACTTCCTCCCACTAGGGGCTCCCCATCTTCTGCATGTCTTGGGCTAAGCTCCCCTCCCCGCGGtGCCTTCGCCCCTCTGGGCCGCCAATAAACTGTTAC
10801 AGCCACCAGAGTCTGTGCAACACGCGGGAAGTTGGGGCGGGGATGAGGTCAGAGACGCTGGGAACAGAAGCCTCGGGATTGGTGAGCACTGAGGCACCCT
10901 GCCCGCAGCATCCGGCGGAAGCAAGCGCTGGGCCCGCCCCTAGGGGCGGAGCCTGCGACTGCGCAGCAAGGCTGGTTTGCCGGCGCCTTTTAGAAGGCTC
11001 CTTAATTCGTCTGCCTGTGGAATCATCTCTCCTGCCGCTAGCCTGCTTGCTGAGAGTTCTCCGGTTCTACGTGCCCACACTGCCCGTAGCTAGTCCCAGA
                                              NheI
11101 AAACACCAGGAACCCGGAATTGGCCCTGCCTCGATGACAGCTGCTCTACCGAGCACCCTGGAGCTGCTGAAGGACGTGCACCTGGGCCTGCCTGTGCCCT
11201 GCCATGATCCCGCCCGACTGGCCCTCCTCTCAGGCCACTACCTTTACTATCACTATGGTTGCGATGGACTGGATGACCGTGGCTGGGGATGCGGCTACCG
11301 CACCCTGCAGACGCTGTGCTCCTGGCCAGGGGGCCAGTCCTCAGGCGTGCCTGGACTGCCAGCCTTGCAGGGAGCCCTAGAGGCCATGGGCGACAAGCCC
11401 CCCGGATTCCGGGGCTCCCGTAACTGGATCGGCTGTGTAGAGGCCAGTCTCTGCCTAGAACACTTCGGAGGACCTCAAGGGCGCCTATGCCACTTACCCC
11501 GCGGAGTAGGGCTTAGGGGAGAAGAGGGAGCGGCTTTATTCACACTTTACAACGGGTGGGGGCCCAGTAATGGTAGGAGGGAGATGCAGATGCCCAGTCCAA
11601 GGCCCTGCTGGGGATCTGTGAGGGGCCAGGTTCAGAAGTCTATGTCTTGATACTGGACCCACACTACTGGGGCACTCCAAAAAAACCGTTGTGAACTACAA
11701 GCTGCTGGATGGGTGGGCTGGCAAAAGGTAAAAAGCGTCTTTGATTCCAATTCCTTCTACAACTTGTGCTTCACCAGAAATCTCTGAATCACCACGCCCT
11801 ACCTGCACCGTTGGGTAGATCCCAGAACTGAGACTAAACACAGCCACCTATTTACTTCGCACAGGCCCCCACCGCGATCAAGTTTGGGCCTGGCACAATG
11901 ATACGGCAGGTGAATCTGAGTTCAAAGCCAACTTGGTCTACACAGCAAGGCCAAGCTGGAATTAGAGATACTGTTCTGAAAAATAATAAATTGGCGTAA
12001 TTCAGCTTACTATGGC|CCAGCCTGTGTTTGGGAAGGGACATACAGCACACAGTTAACACACACTACCAAAGTGTTTTTACTAGCGGGTAAAATAACGTAC
                         from Genbank NT_026533 mouse ACHE gene 1215 nt
12101 AAAAAAACTTTTCAGCTGATGGGATAAAGTGGTCACGGGTACTGATGTAGCAATGCAGGAGGGGACATGGATGGCTCAAAAGAAGTCAACATCATCCGGGG
12201 CATCCAGGTCCCGATACTCCACTATGGCCCTTGGGTCTCCTCGAACCATCCTGTGAGATAAAGGAAATGTGAACAGATGTCCCTATAGTCAGAGACGGGG
12301 AAAGGCAGCCTGGGCATCGTTCGTGCTCACCTGTTCCGAGGTTTCCCAGGATAACCGCCTTGGCCTCGAAAAGCATCATAGTTCCCACGGCCGGCACCAT
12401 ATGGAGCATGGGGGTATGGAGGCCCTCCTGTTGGGACTGCAGGGCGGACAGCACCAGCTATGACAAAGACCCAGGGTGAACTAAAAACTGACCTCAACCT
12501 CAGCCTAAGCTTTGTAGCCGCCTACAGACACCAAACCCCTGCACTGCCTTTCCACACTCACCTCCATAGCCCAAGATGGGAGGCCGGGGCTGACCATACG
           HindIII
12601 GCATCAAGCCCTGTGGCGTCTGATGTGGGTAGGGAAGTCCTGGGGTCAGGCCTGGGGGGAGTACAACACGGACAGGAACATGAATTACTGCGGGGGAGGA
12701 AAGGGACTGACAAGAATTCTAGGAATAGGGCCTGAAGGTTAGTGGAGCACACTTCTCAAAGTAGAAGAAAGAAGTCAAAGGTATGGCAGCTACCACAGAT
            EcoRI
12801 CGTATCTTACTCTGGGCAGGGCCAGGTGGCTGAGCTGGCTTGATCTCAGGCAAAGCTGGGCGCTTGGCGTCTGTGAGAAAGTTATTGAAGAACGCCACCT
12901 CCTTCTTCACCTCCTCGATCTTCTCGGCATGCTTATTGAAGATATGCTTGCGCACAAACTCCGGGCCCTGGGAGGAGCGGATGAGGACGGACAGCATGCT
13001 GCAGTCTCTTCCCCACCGAACCCCGCTGGAAGGTAACAGCTTCCTCCAGGCTTTTAGGGGTTTTGCTACCCAAGCCCTCCTCCCAATCTACCCTCACAAT
13101 TCTTTTCACATCTCAGACCTTGAATTTCTTGCCACTGAGAGGACATAGCCACTTATCCTTGCCCAGTTCCTGCGTGTTGGAGGTGACAAACTTCTCCACT
13201 TCCTGCTCTGGGTCTTTTCGACCCATCTTC|GCGGCCGCCACCGCGGTGGAGCTCCAGCTTTTGTTCCCTTTAGTGAGGGTTAATTTCGAGCTTGGCGTAA
           end ACHE gene  NotI BstXI SacII  SacI            T3 primer Bluescript SK+  2223nt
13301 TCATGGTCATAGCTGTTTCCTGTGTGAAATTGTTATCCGCTCACAATTCCACACAACATACGAGCCGGAAGCATAAAGTGTAAAGCCTGGGGTGCCTAAT
13401 GAGTGAGCTAACTCACATTAATTGCGTTGCGCTCACTGCCCGCTTTCCAGTCGGGAAACCTGTCGTGCCAGCTGCATTAATGAATCGGCCAACGCGCGGG
13501 GAGAGGCGGTTTGCGTATTGGGCGCTCTTCCGCTTCCTCGCTCACTGACTCGCTGCGCTCGGTCGTTCGGCTGCGGCGAGCGGTATCAGCTCACTCAAAG
13601 GCGGTAATACGGTTATCCACAGAATCAGGGGATAACGCAGGAAAGAACATGTGAGCAAAAGGCCAGCAAAAGGCCAGGAACCGTAAAAAGGCCGCGTTGC
13701 TGGCGTTTTTCCATAGGCTCCGCCCCCCTGACGAGCATCACAAAAATCGACGCTCAAGTCAGAGGTGGCGAAACCCGACAGGACTATAAAGATACCAGGC
13801 GTTTCCCCCTGGAAGCTCCCTCGTGCGCTCTCCTGTTCCGACCCTGCCGCTTACCGGATACCTGTCCGCCTTTCTCCCTTCGGGAAGCGTGGCGCTTTCT
13901 CATAGCTCACGCTGTAGGTATCTCAGTTCGGTGTAGGTCGTTCGCTCCAAGCTGGGCTGTGTGCACGAACCCCCCGTTCAGCCCGACCGCTGCGCCTTAT
14001 CCGGTAACTATCGTCTTGAGTCCAACCCGGTAAGACACGACTTATCGCCACTGGCAGCAGCCACTGGTAACAGGATTAGCAGAGCGAGGTATGTAGGCGG
14101 TGCTACAGAGTTCTTGAAGTGGTGGCCTAACTACGGCTACACTAGAAGGACAGTATTTGGTATCTGCGCTCTGCTGAAGCCAGTTACCTTCGGAAAAAGA
14201 GTTGGTAGCTCTTGATCCGGCAAACAAACCACCGCTGGTAGCGGTGGTTTTTTTGTTTGCAAGCAGCAGATTACGCGCAGAAAAAAAGGATCTCAAGAAG
14301 ATCCTTTGATCTTTTCTACGGGGTCTGACGCTCAGTGGAACGAAAACTCACGTTAAGGGATTTTGGTCATGAGATTATCAAAAAGGATCTTCACCTAGAT
14401 CCTTTTAAATTAAAAATGAAGTTTTAAATCAATCTAAAGTATATATGAGTAAACTTGGTCTGACA|GTTACCAATGCTTAATCAGTGAGGCACCTATCTCA
                                                                       beta-lactamase gene 862nt
14501 GCGATCTGTCTATTTCGTTCATCCATAGTTGCCTGACTCCCCGTCGTGTAGATAACTACGATACGGGAGGGCTTACCATCTGGCCCCAGTGCTGCAATGA
14601 TACCGCGAGACCCACGCTCACCGGCTCCAGATTTATCAGCAATAAACCAGCCAGCCGGAAGGGCCGAGCGCAGAAGTGGTCCTGCAACTTTATCCGCCTC
14701 CATCCAGTCTATTAATTGTTGCCGGGAAGCTAGAGTAAGTAGTTCGCCAGTTAATAGTTTGCGCAACGTTGTTGCCATTGCTACAGGCATCGTGGTGTCA
14801 CGCTCGTCGTTTGGTATGGCTTCATTCAGCTCCGGTTCCCAACGATCAAGGCGAGTTACATGATCCCCCATGTTGTGCAAAAAAGCGGTTAGCTCCTTCG
14901 GTCCTCCGATCGTTGTCAGAAGTAAGTTGGCCGCAGTGTTATCACTCATGGTTATGGCAGCACTGCATAATTCTCTTACTGTCATGCCATCCGTAAGATG
15001 CTTTTCTGTGACTGGTGAGTACTCAACCAAGTCATTCTGAGAATAGTGTATGCGGCGACCGAGTTGCTCTTGCCCGGCGTCAATACGGGATAATACCGCG
15101 CCACATAGCAGAACTTTAAAAGTGCTCATCATTGGAAAACGTTCTTCGGGGCGAAAACTCTCAAGGATCTTACCGCTGTTGAGATCCAGTTCGATGTAAC
15201 CCACTCGTGCACCCAACTGATCTTCAGCATCTTTTACTTTCACCAGCGTTTCTGGGTGAGCAAAAACAGGAAGGCAAAATGCCGCAAAAAAGGGAATAAG
15301 GGCGACACGGAAATGTTGAATACTCAT|ACTCTTCCTTTTTCAATATTATTGAAGCATTTATCAGGGTTATTGTCTCATGAGCGGATACATATTTGAATGT
                 end beta-lactamase
15401 ATTTAGAAAAATAAACAAATAGGGGTTCCGCGCACATTTCCCCGAAAAGTGCC
```

Figure 2.2. DNA sequence of the gene targeting vector to make the G117H knockin mouse.

The parent vector is pBluescript SK+ (Stratagene). The total number of nucleotides in the gene targeting vector is 15,454 bp. The 2874 nucleotides of pBluescript, including the beta-lactamase gene for resistance to ampicillin, are between Not I (13230) and Kpn I (652). The 1999 nucleotides of the TK gene cassette are between KpnI 652 and KpnI 2650. The mouse ACHE gene begins after XhoI 2660

and ends at 5170; these 2502 nucleotides of mouse ACHE include exon 1a, exon 1, intron 1 with Shelley Camp's enhancer sequence, and the start of exon 2. Only 115 nucleotides of mouse exon 2 are present and these encode the mouse ACHE signal peptide. The signal peptide is followed by 1433 nucleotides of the human BCHE gene. These 1433 bp encode the first amino acid of the mature BChE protein, Glu+1, to Gly 478 at the end of BCHE exon 2. Exon 2 of human BCHE includes G117H, and the catalytic triad residues Ser198, Glu325, and His438.   20 bp of intron 3 precede the NEO gene cassette. These intron 3 nucleotides are expected to allow splicing. The NEO gene cassette of 1594 bp is surrounded by loxP sites and inserted into BamHI 6627 and SalI 8289. Mouse ACHE gene sequences of 4923 bp are inserted between ClaI 8307 and NotI 13230. These 4923 bp include mouse ACHE intron 3, exon 4, intron 5, exon 5, intron 5, and exon 6.

     Genbank accession number NW_000239 was used to verify the mouse ACHE gene sequences. Genbank J02224 has the HSV-TK sequence.

     The N and E boxes in intron 1 are enhancers required for expression of AChE in muscle (Chan et al 1999; Luo et al., 1998; Angus et al., 2001).

Screening ES cells for homologous recombination. The gene-targeting vector, linearized with Not I, was transfected into R1 mouse embryonic stem cells by the University of Michigan Transgenic Animal Model Core Facility directed by Dr. Thom Saunders. 480 colonies resistant to G418 and gancyclovir were picked into triplicate 96-well plates. DNA was purified from two sets of plates and sent to us for screening. The DNA was digested with EcoRI and electrophoresed on 0.8 % agarose gels. The DNA was transferred to Zeta-probe membrane (Bio-Rad catalog 162-0159) and hybridized with a P32-labeled probe. The 255 bp probe was located outside the targeted region, on the 5' side of the ACHE gene. See Figure 2.3. The expected size of the EcoRI fragment was 10.3 kb for the gene that had undergone homologous recombination, and 16.5 kb for the wild-type gene.

     One positive clone was found (see Figure 2.4). The positive clone had the expected two bands of 16.5 and 10.3 kb after hybridization of EcoRI digested genomic DNA with the 5' probe. The positive clone was expanded to yield more DNA for additional testing. The right panel in Figure 2.4 used a 3' probe and different restriction enzymes. The results confirmed that this positive clone was indeed the result of homologous recombination and that the clone did not contain random insertions.

     Chromosome analysis revealed that this positive clone had the correct chromosome count (85.7% of spreads had 40 chromosomes) and was therefore suitable for blastocyst injection.
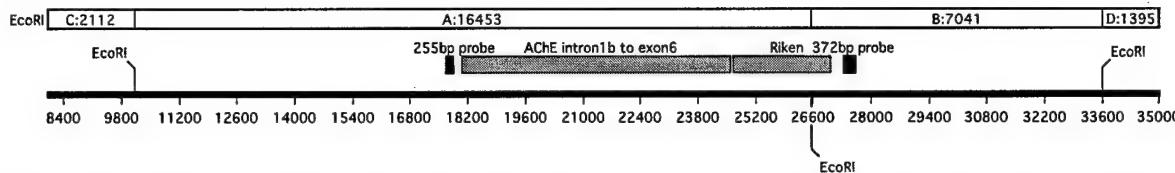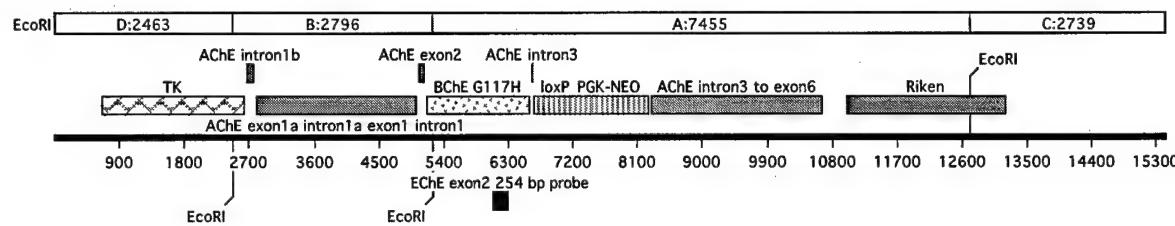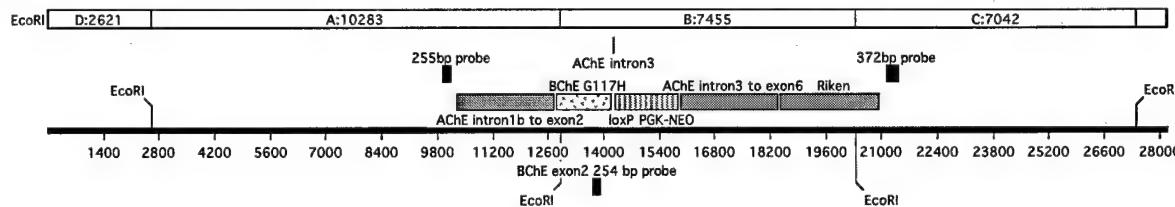
Figure 2.3. Restriction map of the mouse ACHE gene and location of probes.
The top panel represents the ACHE gene in the wild-type mouse; the EcoRI
restriction fragment probed with the 5' probe contains 16453 bp. The center panel
represents the gene-targeting vector; the 5' probe does not recognize any sequence
in the gene-targeting vector. The bottom panel represents the ACHE gene after it
has undergone homologous recombination to substitute the human BCHE G117H
gene for ACHE; the EcoRI fragment probed with the 5' probe contains 10283 bp.
The probes for screening and confirming homologous recombination in ES cells
were outside of the targeted region: the 5' probe contained 255 bp and the 3' probe
contained 372 bp. A 254 bp probe located inside the human BCHE gene is intended
for genotyping mice. Macvector software was used to make this figure.

Eco R1 digested ES clones 5' probe			BglII&ClaI BglII&SpeI 3' probe	
wt	1C3	wt	1C3	1C3

16.5 kb
10.3

12.3 kb

6.6
6.3
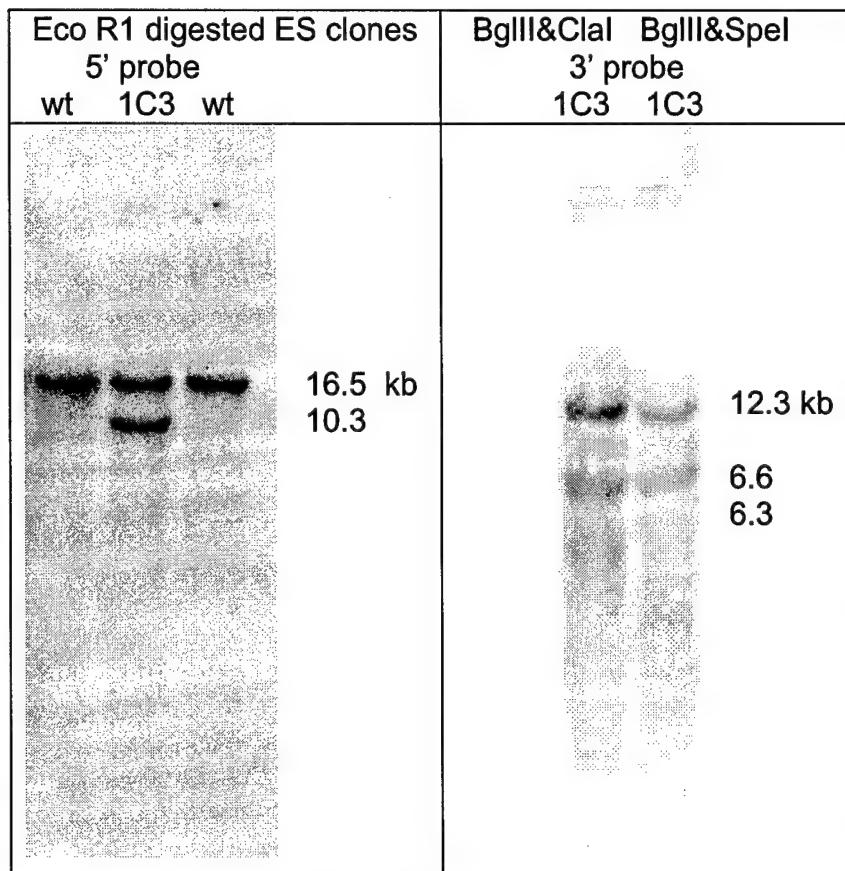
Figure 2.4. Southern blot showing the positive ES clone. The bands in the left panel were obtained by digesting genomic DNA with EcoRI and hybridizing with a 5' probe. One clone, called 1C3, shows two bands; the 10.3 kb band contains the desired recombination. Two clones show a single band of 16.5 kb; these contain only wild-type DNA. To confirm that homologous recombination had taken place, the positive clone 1C3 was digested with additional restriction enzymes and hybridized with a 3' probe. The right panel shows 12.3 and 6.3 kb bands for a Bgl II and Cla I digest, and 12.3 and 6.6 kb bands for a Bgl II and Spe I digest of clone 1C3. These results confirm that clone 1C3 has one allele that has undergone homologous recombination.

Discussion

We have completed the first two steps in the making of the G117H knockin mouse by constructing the gene targeting vector and by identifying one positive ES clone. The next step is to microinject these ES cells into mouse blastocysts.

Task 3. *A transgenic mouse that expresses human G117H BChE will be made.*
3.1 A plasmid will be made that contains the mouse ACHE promoter, mouse ACHE exon 1, and mouse intron 1 attached to the cDNA of human G117H BCHE.
3.2 The linearized, digested, and purified DNA will be microinjected into mouse fertilized eggs of strain FVB/N. The injected embryos will be transferred into pseudopregnant mice. The live pups will be tested for the presence of the transgene.
3.3 Mice that carry the transgene will be tested for expression of human G117H BCHE.
3.4 Founder mice expressing the highest levels of G117H BCHE will be mated to produce colonies of transgenic mice.
3.5 Transgenic mice will be characterized with respect to tissue location of the expressed transgene and the levels of expression.
3.6 Transgenic mice will be tested for resistance to OP.

Tasks 3.1, 3.2, 3.3, 3.4, 3.5, 3.6

Abstract

The G117H mutant of human butyrylcholinesterase (BChE) hydrolyzes organophosphorus toxicants. It also hydrolyzes the neurotransmitter acetylcholine and it is resistant to inhibition by OP. Transgenic mice were made that expressed human G117H BChE in all tissues. Expression was controlled by the ROSA26 promoter. The ROSA26 promoter directs expression in most tissue types throughout embryonic development and in adult tissues. A stable transgenic line expressed 0.5 µg/ml of human G117H BChE in plasma as well as 2 µg/ml of wild-type mouse BChE. Intestine, kidneys, stomach, lungs, heart, spleen, liver, brain and muscle expressed 0.6 to 0.15 µg/g of G117H BChE. An assay for G117H was developed which measured residual BChE activity after inhibition of wild-type BChE with 0.1 mM echothiophate. Transgenic mice were normal in fertility and behavior. The LD_{50} dose of echothiophate for wild-type mice was 0.1 mg/kg i.p. This dose caused severe cholinergic signs of toxicity and lethality in wild-type mice, but caused no deaths and only mild toxicity in transgenic animals. AChE and BChE activity were inhibited to the same extent in echothiophate treated wild-type and transgenic mice. This observation led to the hypothesis that protection against echothiophate toxicity was due to hydrolysis of acetylcholine rather than to hydrolysis of echothiophate.

Introduction

Methods to protect people against the toxicity of organophosphorus nerve agents and pesticides (OP) are being sought. Pretreatment with native human BChE is

effective in animals, but has the limitation that native BChE is a stoichiometric scavenger so that a molar equivalent of BChE is required for each mole of OP. An OP hydrolase, like G117H BChE (Millard et al., 1995 and 1998; Lockridge et al., 1997), is expected to be more efficient since it would destroy many molecules of OP per molecule of BChE. A transgenic mouse expressing human G117H BChE was made to test the protective effect of this OP hydrolase in mice.

Methods

Construction of the transgene. The ROSA26 promoter was selected because this promoter directs expression of the transgene in most tissue types throughout embryonic development and in adult tissues (Zambrowicz et al., 1997). A plasmid pBROAD (3.2 kb) containing the ROSA26 promoter was purchased from InvivoGen (San Diego, CA). A chimeric intron from pCI-neo (Promega) composed of the 5'-donor site from the first intron of the human beta-globin gene and the branch and 3'-acceptor site from the intron of an immunoglobulin gene heavy chain variable region (161 bp) was inserted into pBROAD between NcoI and Bgl II. The intron was added to pBROAD because the presence of an intron increases the number of animals that take up the transgene (Palmiter et al., 1991) and increases the level of expression of the transgene (Choi et al., 1991). The human BCHE cDNA encoded the 28 amino acid signal peptide and 574 amino acids of the full-length BChE protein. A single amino acid mutation at codon 117 substituted His for Gly to make the G117H mutation. Human BCHE was inserted into the Bgl II and Nhe I sites of pBROAD. A FLAG tag was placed at the 3' end of BCHE. The 3'untranslated region and polyadenylation sequence of the human elongation factor 1-alpha gene were in the pBROAD plasmid. The transgene was excised from the plasmid by digestion with Pac I to make a transgene of 3063 bp. See Figure 3.1.
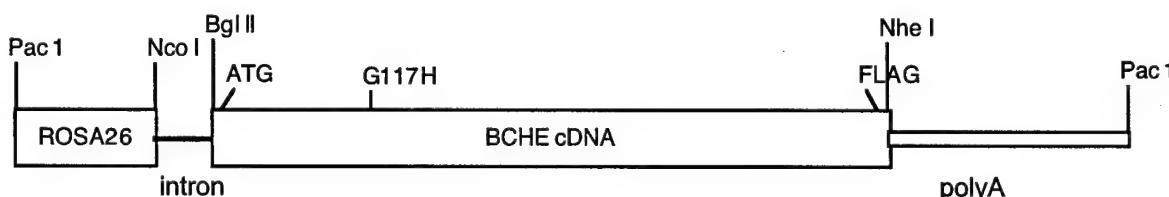
Figure 3.1. Schematic representation of the BCHE transgene. The ROSA26 promoter (382 bp) is followed by a chimeric intron (161 bp), the human BCHE cDNA (1859 bp) including a FLAG tag, and a poly A addition site (661 bp). The Pac I restriction site was used to produce a 3063 bp transgene for injection into fertilized mouse eggs.

The DNA sequence of the plasmid to make the transgenic G117H mouse is shown in Figure 3.2.

Figure 3.2. DNA sequence of G117H BCHE-FLAG in pBROAD

```
   1    TAATGTGTTGGCGGACTGGCGGGACTAGGGCTGCGTGAGTCTCTGAGCGCAGGCGGGCGG
        Pac I    ROSA26 promoter U83173   366 bp
  61    CGGCCGCCCCTCCCCCGGCGGCGGCAGCGGCGGCAGCGGCGGCAGCTCACTCAGCCCGCT
 121    GCCCGAGCGGAAACGCCACTGACCGCACGGGGATTCCCAGTGCCGGCGCCAGGGGCACGC
 181    GGGACACGCCCCCTCCCGCCGCGCCATTGGCCTCTCCGCCCACCGCCCCACACTTATTGG
 241    CCGGTGCGCCGCCAATCAGCGGAGGCTGCCGGGGCCGCCTAAAGAAGAGGCTGTGCTTTG
 301    GGGCTCCGGCTCCTCAGAGAGCCTCGGCTAGGTAGGGGATCGGGACTCTGGCGGGAGGGC
 361    GGCTTGGTGACCGGTCACCATGGGCAG|GTAAGTATCAAGGTTACAAGACAGGTTTAAGGA
                              Nco I       start chimeric intron
 421    GACCAATAGAAACTGGGCTTGTCGAGACAGAGAAGACTCTTGCGTTTCTGATAGGCACCT
         sense primer
 481    ATTGGTCTTACTGACATCCACTTTGCCTTTCTCTCCACAG|GTGTCCACTCCCAGATCTTC
                            end chimeric intron            Bgl II
 541    GGAAGCCACCATGGATAGCAAAGTCACAATCATATGCATCAGATTTCTCTTTTGGTTTCT
              Met -28
 601    TTTGCTCTGCATGCTTATTGGGAAGTCACATACTGAAGATGACATCATAATTGCAACAAA
                                           Glu1
 661    GAATGGAAAAGTCAGAGGGATGAACTTGACAGTTTTTGGTGGCACGGTAACAGCCTTTCT
 721    TGGAATTCCCTATGCACAGCCACCTCTTGGTAGACTTCGATTCAAAAAGCCACAGTCTCT
 781    GACCAAGTGGTCTGATATTTGGAATGCCACAAAATATGCAAATTCTTGCTGTCAGAACAT
        W56W antisense primer
 841    AGATCAAAGTTTTCCAGGCTTCCATGGATCAGAGATGTGGAACCCAAACACTGACCTCAG
 901    TGAAGACTGTTTATATCTAAATGTATGGATTCCAGCACCTAAACCAAAAAATGCCACTGT
 961    ATTGATATGGATTTATGGTGGTCATTTTCAAACTGGAACATCATCTTTACATGTTTATGA
              G117H
1021    TGGCAAGTTTCTGGCTCGGGTTGAAAGAGTTATTGTAGTGTCAATGAACTATAGGGTGGG
1081    TGCCCTAGGATTCTTAGCTTTGCCAGGAAATCCTGAGGCTCCAGGGAACATGGGTTTATT
1141    TGATCAACAGTTGGCTCTTCAGTGGGTTCAAAAAAAATATAGCAGCCTTTGGTGGAAATCC
1201    TAAAAGTGTAACTCTCTTTGGAGAAAGTGCAGGAGCAGCTTCAGTTAGCCTGCATTTGCT
1261    TTCTCCTGGAAGCCATTCATTGTTCACCAGAGCCATTCTGCAAAGTGGTTCCTTTAATGC
1321    TCCTTGGGCGGTAACATCTCTTTATGAAGCTAGGAACAGAACGTTGAACTTAGCTAAATT
1381    GACTGGTTGCTCTAGAGAGAATGAGACTGAAATAATCAAGTGTCTTAGAAATAAAGATCC
1441    CCAAGAAATTCTTCTGAATGAAGCATTTGTTGTCCCCTATGGGACTCCTTTGTCAGTAAA
1501    CTTTGGTCCGACCGTGGATGGTGATTTTCTCACTGACATGCCAGACATATTACTTGAACT
1561    TGGACAATTTAAAAAAACCCAGATTTTGGTGGGTGTTAATAAAGATGAAGGGACAGCTTT
1621    TTTAGTCTATGGTGCTCCTGGCTTCAGCAAAGATAACAATAGTATCATAACTAGAAAAGA
1681    ATTTCAGGAAGGTTTAAAAATATTTTTTTCCAGGAGTGAGTGAGTTTGGAAAGGAATCCAT
1741    CCTTTTTCATTACACAGACTGGGTAGATGATCAGAGACCTGAAAACTACCGTGAGGCCTT
1801    GGGTGATGTTGTTGGGGATTATAATTTCATATGCCCTGCCTTGGAGTTCACCAAGAAGTT
1861    CTCAGAATGGGGAAATAATGCCTTTTTCTACTATTTTGAACACCGATCCTCCAAACTTCC
1921    GTGGCCAGAATGGATGGGAGTGATGCATGGCTATGAAATTGAATTTGTCTTTGGTTTACC
1981    TCTGGAAAGAAGAGATAATTACACAAAAGCCGAGGAAATTTTGAGTAGATCCATAGTGAA
2041    ACGGTGGGCAAATTTTGCAAAATATGGGAATCCAAATGAGACTCAGAACAATAGCACAAG
2101    CTGGCCTGTCTTCAAAAGCACTGAACAAAAATATCTAACCTTGAATACAGAGTCAACAAG
2161    AATAATGACGAAACTACGTGCTCAACAATGTCGATTCTGGACATCATTTTTTCCAAAAGT
2221    CTTGGAAATGACAGGAAATATTGATGAAGCAGAATGGGAGTGGAAAGCAGGATTCCATCG
2281    CTGGAACAATTACATGATGGACTGGAAAAATCAATTTAACGATTACACTAGCAAGAAAGA
2341    AAGTTGTGTGGGTCTCGACTACAAGGACGACGATGACAAGTAAGGGCCCGTTTAAACGCT
                        FLAG peptide DYKDDDDK
2401    AGCATTATCCCTAATACCTGCCACCCCACTCTTAATCAGTGGTGGAAGAACGGTCTCAGA
        Nhe I
2461    ACTGTTTGTTTCAATTGGCCATTTAAGTTTAGTAGTAAAAGACTGGTTAATGATAACAAT
2521    GCATCGTAAAACCTTCAGAAGGAAAGGAGAATGTTTTGTGGACCACTTTGGTTTTCTTTT
2581    TTGCGTGTGGCAGTTTTAAGTTATTAGTTTTTAAAATCAGTACTTTTTAATGGAAACAAC
2641    TTGACCAAAAATTTGTCACAGAATTTTGAGACCCATTAAAAAAAGTTAAATGAGAAACCTG
```

29

```
2701   TGTGTTCCTTTGGTCAACACCGAGACATTTAGGTGAAAGACATCTAATTCTGGTTTTACG
2761   AATCTGGAAACTTCTTGAAAATGTAATTCTTGAGTTAACACTTCTGGGTGGAGAATAGGG
2821   TTGTTTTCCCCCCACATAATTGGAAGGGGAAGGAATATCATTTAAAGCTATGGGAGGGTT
2881   TCTTTGATTACAACACTGGAGAGAAATGCAGCATGTTGCTGATTGCCTGTCACTAAAACA
2941   GGCCAAAAACTGAGTCCTTGGGTTGCATAGAAAGCTTCATGTTGCTAAACCAATGTTAAG
3001   TGAATCTTTGGAAACAAAATGTTTCCAAATTACTGGGATGTGCATGTTGAAACGTGGGTT
3061   AAT
       Pac I
```

Figure 3.2. DNA sequence of G117H BCHE-FLAG in pBROAD between 2 Pac I sites (3063 nucleotides).   The primers highlighted above were used for PCR screening of mouse genomic DNA for the presence of the transgene.

Injection into fertilized mouse eggs and generation of transgenic mice. The DNA was microinjected into 164 fertilized (C57BL/6 X SJL)F2 eggs by the University of Michigan Transgenic Animal Model Core facility (Ann Arbor, MI) [Margaret Van Keuren mvkeuren@umich.edu and Dr. Thomas Saunders tsaunder@umich.edu; http://www.med.umich.edu/tamc]. The eggs were transferred into pseudopregnant recipient females. Out of 51 pups born, 13 carried the transgene. One founder mouse died before it could be bred, from bite injuries inflicted by other male mice.

Identification of mice that carry the transgene. For routine genotyping, DNA was extracted from hair roots by incubating hair in 50 mM NaOH at 95°C for 15 min (Schmitteckert et al., 1999). Animals were about three weeks old when hair was pulled for genotyping. Genomic DNA was tested for the presence of the BCHE transgene by PCR. The sense primer matched the chimeric intron, the antisense primer matched human BCHE. The PCR product had 392 bp.   The 34mer sense primer was 5'GGTTTAAGGAGACCAATAGAAACTGGGCTTGTCG, the 28mer antisense primer was   5'CCAAATATCAGACCACTTGGTCAGAGAC.

Southern blot. Genomic DNA was purified from tail snips with QIAamp DNA Mini Kit from Qiagen (Chatsworth, CA) and digested with EcoRI. Blots were probed with a single stranded P32-labeled probe containing 254 bases of the transgene. The 254 base probe encoded human BChE from Asp304 to Ala388. Blots were hybridized at 60°C in ExpressHyb solution from Clontech.

BChE activity assay. Blood was collected from the leg vein (Saphenous vein) of transgenic mice into heparinized tubes. Plasma was tested for BChE activity by the Ellman method (Ellman et al., 1961) using 1 mM butyrylthiocholine, 0.5 mM DTNB, 0.1 M potassium phosphate pH 7.0, at 25°C. Increase in absorbance at 412 nm was recorded in a Gilford spectrophotometer. Slopes were converted to μmoles substrate hydrolyzed per min per ml by using the extinction coefficient 13,600 M^{-1} cm^{-1}.

Tissue extracts were preincubated with DTNB in 0.1 M potassium phosphate buffer to react free sulfhydryl groups before addition of butyrylthiocholine.

Assay for G117H BChE activity. To assay G117H BChE activity, advantage was taken of a special property of the G117H BChE enzyme, that is, its resistance to inhibition by OP. By contrast, wild-type BChE is completely and irreversibly inhibited by OP. G117H activity in plasma was measured in the Ellman assay by adding echothiophate to a final concentration of 0.1 mM. G117H activity in tissues was measured after inhibiting wild-type BChE with 0.001 mM DFP. The residual rate of butyrylthiocholine hydrolysis after addition of OP was due to G117H BChE activity. Echothiophate was from Wyeth-Ayerst, Rouses Point, NY.

AChE activity assay. AChE activity was measured in the Ellman assay using 1 mM acetylthiocholine after preincubating the sample for 30 min in 0.1 mM iso-OMPA to inhibit wild-type BChE. Since G117H BChE was resistant to inhibition by iso-OMPA and since G117H BChE hydrolyzes acetylthiocholine, the contribution of G117H BChE was evaluated by inhibiting AChE activity with 0.1 mM BW284C51. The reported AChE activity has been corrected for acetylthiocholine hydrolysis by G117H BChE.

Units of activity for AChE, BChE, and G117H are defined as micromoles of substrate hydrolyzed per minute.

ELISA to measure FLAG epitope. The human G117H BChE has the 8 amino acid FLAG epitope at the carboxy-terminus. The presence of the FLAG epitope was measured in transgenic mouse blood with ELISA. In a first trial a 96 well plate coated with anti-FLAG antibody was purchased from Sigma (catalog # P2983). 3 to 30 μl of mouse serum from the test mice and from wild-type mice were placed into each well and allowed to bind to the anti-FLAG antibody. The positive control was culture medium containing a known amount of wild-type human BChE-FLAG or G117H BChE-FLAG. Wells were washed to remove unbound material, and then received butyrylthiocholine and DTNB to reveal BChE activity. No signal was found when Sigma precoated plates were used.

The assay was repeated but this time we coated our own 96-well plate (Nunc-Immuno Module) with M2 anti-flag antibody (Sigma), 6 μg/well. The antibody in each well was diluted to 200 μl with Tris buffered saline and incubated overnight at 4°C. Unbound antibody was washed out by rinsing 3 times with 0.05% Tween-20 in Tris buffered saline. The wells were blocked with 250 μl of 0.05% Tween-20 in Tris buffered saline, 1% non-fat dried milk at room temperature for one hour, and then rinsed 3 times with 0.05% Tween-20 in Tris buffered saline. 13 μl of mouse plasma from founder mouse M816T was diluted to 200 μl and allowed to bind at room temperature for one hour. Plasma volumes from other mice (M837T, M838T, M844T, F860wild-type control) ranged from 40 to 60 μl. The plate was rinsed three times with 0.05% Tween-20 in Tris buffered saline and then assayed for bound BChE activity by adding butyrylthiocholine and DTNB in buffer. The yellow color was allowed to develop for 1 hour and then it was read in a microtiter plate reader at 405 nm.

Tissue extraction. Mice were perfused with phosphate buffered saline through the heart to wash the blood out of tissues. Perfused tissues were removed and frozen.

Tissues were homogenized in 10 volumes of ice-cold 50 mM potassium phosphate pH 7.4 containing 0.5% Tween-20 in a Polytron (Brinkmann Instruments) for 10 seconds. The suspension was centrifuged 10 minutes in a microfuge in the cold room and the supernatant assayed for enzyme activity. 100 μl of tissue extract was assayed in a total reaction volume of 2 ml.

Nondenaturing gel electrophoresis. To visualize tetramers, dimers, and monomers of BChE, plasma samples were loaded onto a nondenaturing 4-30% polyacrylamide gradient gel (apparatus purchased from Hoefer Scientific, presently owned by Pharmacia) and electrophoresed for 24 hours at 120 volts at 4°C. 3 μl of mouse blood were loaded per lane. The gel was stained for BChE activity by the method of Karnovsky and Roots (1964) in the presence of butyrylthiocholine. To reveal G117H BChE activity, the gel was preincubated in 0.1 mM echothiophate for 30 min. Wild-type BChE was completely inhibited by echothiophate, but G117H BChE was resistant to inhibition.

Toxicity studies. 8 mice in the F4 generation of M844T were 45-110 days old at the time of the study; there were 5 female and 3 male mice. Control wild-type mice 8-10 weeks old were purchased from Taconic. The wild-type mice were the F1 cross of C57BL/6 X SJL and are called strain B6SJL/F1Tac. There were 6 female and 2 male wild-type mice. Mice weighed 18-26 g.

Mice were injected subcutaneously with about 20 μl of 0.1 mg/ml echothiophate dissolved in saline solution for a dose of 0.1 mg/kg s.c. Mice were observed for signs of toxicity. Body temperature was measured with a surface thermometer (Thermalert model TH-5 and a surface Microprobe MT-D, type T thermocouple, Physitemp Instruments Inc., Clifton, N.J.). Mice were euthanized 2 h after receiving echothiophate. Tissues were collected after intracardial perfusion with phosphate buffered saline. Tissue extracts were prepared as described above, and assayed for AChE, BChE, and G117H BChE activity.

Results

Transgenic founder mice. Out of 51 live births, 13 mice carried the human G117H BCHE gene. The mice were placed in quarantine at the University of Nebraska Medical Center for 6 weeks before being transferred to our care. During the quarantine period one mouse, M846T, was mauled to death by other male mice in its cage. Breeding of 12 transgenic founder mice to wild-type mice (strain B6SJL/F1Tac), and subsequent brother-sister matings were started in April 2002 and are continuing as of August 2003. During these 16 months two male founder mice, M837T and M844T, have produced stable transgenic lines (Table 3.1).

Table 3.1 shows that 2 of the founders did not transmit the G117H gene in their germline. Five founders had the human G117H gene but did not express the G117H enzyme at significant levels. Expression in the offspring of founder M838T was unstable even in the fifth generation. The founder with the highest expression level, M816T, impregnated one female when he was very young, but has been infertile since then. The male and female offspring from this one litter have been allowed to mate with each other and with wild-type mice for a year but have produced no litters.

Table 3.1. G117H activity in plasma of transgenic founder mice. Lack of correlation between gene copy number and transgene activity.

Founder transgenic mouse	BChE activity, u/ml	G117H activity, u/ml	G117H, µg/ml	Transgene copy number	Germline transmitter	Generation (8-18-03)
F813T	2.04	0.000	0	10-20*	Yes	F2
F825T	1.68	Not tested		Not tested	No	Not germline
F829T	2.18	0.000	0	Not tested	Yes	F2
F835T	1.93	0.002	0.013	2	Yes	F1
F855T	2.23	Not tested		Not tested	No	Not germline
F857T	Not tested	0.000	0	Not tested	Yes	
F859T	2.45	0.008	0.053	1	Yes	F3
M816T	1.49	0.640	4.27	1	Yes	F1
M837T	1.18	0.020	0.133	5-15	Yes	F4 stable
M838T	1.25	0.005	0.033	Not tested	Yes	F5 unstable
M844T	1.10	0.030	0.200	3-5	Yes	F6 stable
M846T	1.16	Not tested		Not tested	Dead	Dead
M853T	1.33	0.023	0.153	5-15*	Yes	F2

* two sites of insertion of the transgene into genomic DNA

For comparison, the plasma BChE activity was 0.65 and 1.31 u/ml in two male wild-type mice, and 1.87 in one female wild-type mouse of strain B6SJL/F1Tac. Units/ml of G117H activity were converted to µg/ml using a specific activity of 0.15 units/µg for pure G117H BChE (Lockridge et al., 1997). The G117H u/ml and µg/ml values have been corrected for the 30% inhibition of G117H BChE by 0.1 mM echothiophate.

Table 3.1 shows no correlation between BChE activity measured with butyrylthiocholine and G117H activity. G117H activity was detected by measuring

activity after inhibiting native BChE with echothiophate. It is known that G117H has reduced binding affinity for butyrylthiocholine compared to wild-type BChE; this partly explains why, under standard conditions G117H does not contribute significantly to BChE activity. Another way to estimate G117H content is to estimate G117H protein concentration. The specific activity of pure G117H of 0.15 units/µg was used to convert u/ml to µg/ml. Wild-type mouse BChE has a specific activity of about 0.7 u/µg. In terms of micrograms protein per ml, founder mouse M816T had 4.27 µg/ml G117H and 0.8 µg/ml wild-type BChE, that is 5 times more human BChE than mouse BChE. This founder mouse was fertile only when he was very young. His offspring were sterile. The sterility could be a consequence of where the transgene inserted into the chromosome. The two stable transgenic lines express 25% as much human BChE protein as mouse BChE protein in plasma.

After 16 months of breeding only one transgenic line, M844T, is in the 6th generation. Under ideal conditions a mouse can produce one litter every two months. The low productivity of most of our mouse lines is explained by a) cannibalism; the F1 female in the F813T line ate all pups in 4 litters, b) obesity; adults in this strain get grossly obese and unable to breed, c) neglect; the wild-type and F1 females in the M853T line allowed all pups to die in several litters, d) chance; some litters had all wild-type pups and no carriers of the G117H gene.

Transgene copy number. The number of copies of the transgene integrated into mouse chromosomal DNA was estimated by Southern blotting. Table 3.1 and Figure 3.3 show that founder M816T had the highest level of expression of G117H BChE but only one copy of the transgene. Three founders (F813T, M837T, and M853T) had multiple copies of the transgene. The F813T founder had the highest number of copies, but no detectable G117H activity. There was no correlation between gene copy number and level of expression. However, the mouse lines that stably expressed the transgene had multiple copies of the transgene.
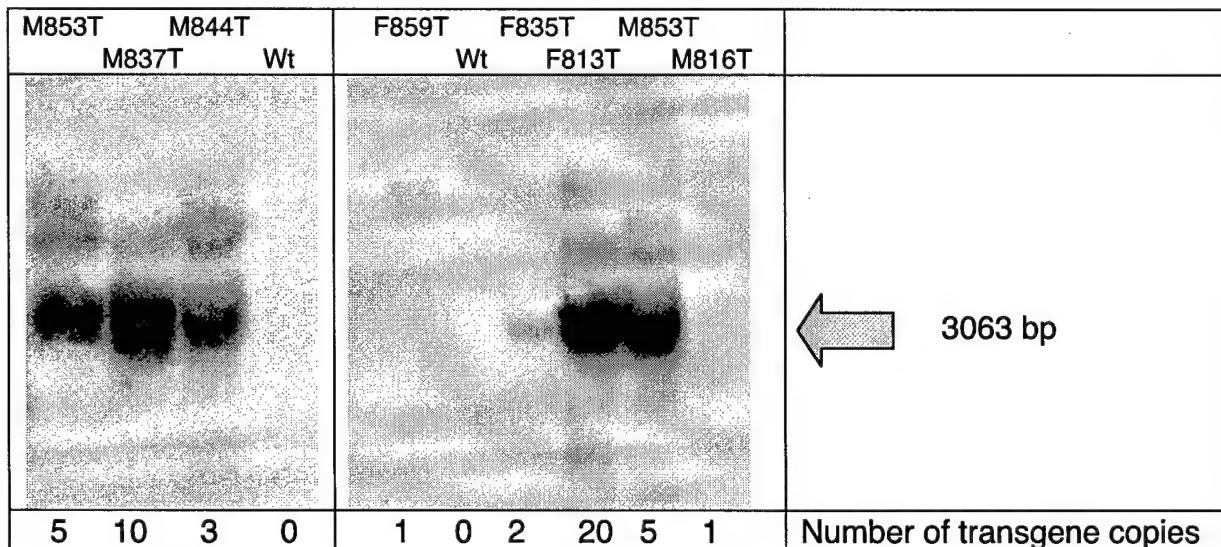
Figure 3.3. Southern blot of genomic DNA from transgenic mice. The DNA was digested with EcoRI. The P32 labeled probe is specific for the transgene. The

intense band has a size of 3063 bp. The number of copies of the transgene is 0 in wild-type mice, and up to 20 in the F813T mouse.

The number of integration sites within a chromosome was determined from the Southern blot results in Figure 3.3. The presence of two bands reflected one integration site, while three bands reflected two integration sites. Two integration sites were present in F813T and M853T. All other transgenic families in Table 3.2 had a single integration site.

Table 3.2. Number of integration sites and copy number of the transgene.

Transgenic family	Number of integration sites	Transgene copy number
F813T	2	10-20
F835T	1	2
F859T	1	1
M816T	1	1
M837T	1	5-15
M844T	1	3-5
M853T	2	5-15

Measurement of G117H activity. An assay was developed to reliably measure G117H activity levels in mouse tissues. This assay took advantage of the fact that G117H BChE was resistant to inhibition by OP, but wild-type BChE was completely and irreversibly inhibited by 100 µM echothiophate. Figure 3.4 shows activity traces for plasma containing only wild-type BChE and for plasma containing both G117H BChE and wild-type BChE. The butyrylthiocholine activity remaining after treatment of plasma with 100 µM echothiophate was due to the activity of G117H BChE.

Wild-type BChE in tissues other than plasma was not completely inhibited by 100 µM echothiophate. A high background rate was observed in kidney and liver. However, 1 µM DFP gave complete inhibition of wild-type BChE in tissue extracts. Therefore G117H activity in tissue extracts was measured in the presence of 1 µM DFP.

Highly purified human G117H BChE was tested for resistance to inhibition by OP. Echothiophate at 100 µM inhibited G117H BChE 30%, while 1 µM DFP inhibited G117H BChE 22%.   The human G117H BChE used for these assays was a recombinant BChE produced by CHO cells and purified from culture medium (Lockridge et al., 1997).

Other assays to determine G117H activity in mouse plasma did not work. Measurement of activity with butyrylthiocholine by the Ellman method (1961) in the absence of OP did not identify samples containing G117H BChE. Attempts to quantify G117H protein by measuring the FLAG epitope by ELISA were insensitive, and by Western blotting were nonspecific. The FLAG epitope is on the carboxy terminus of human G117H BChE. Only the high expressing founder mouse M816T had enough G117H BChE in plasma to allow detection of the FLAG epitope by ELISA.
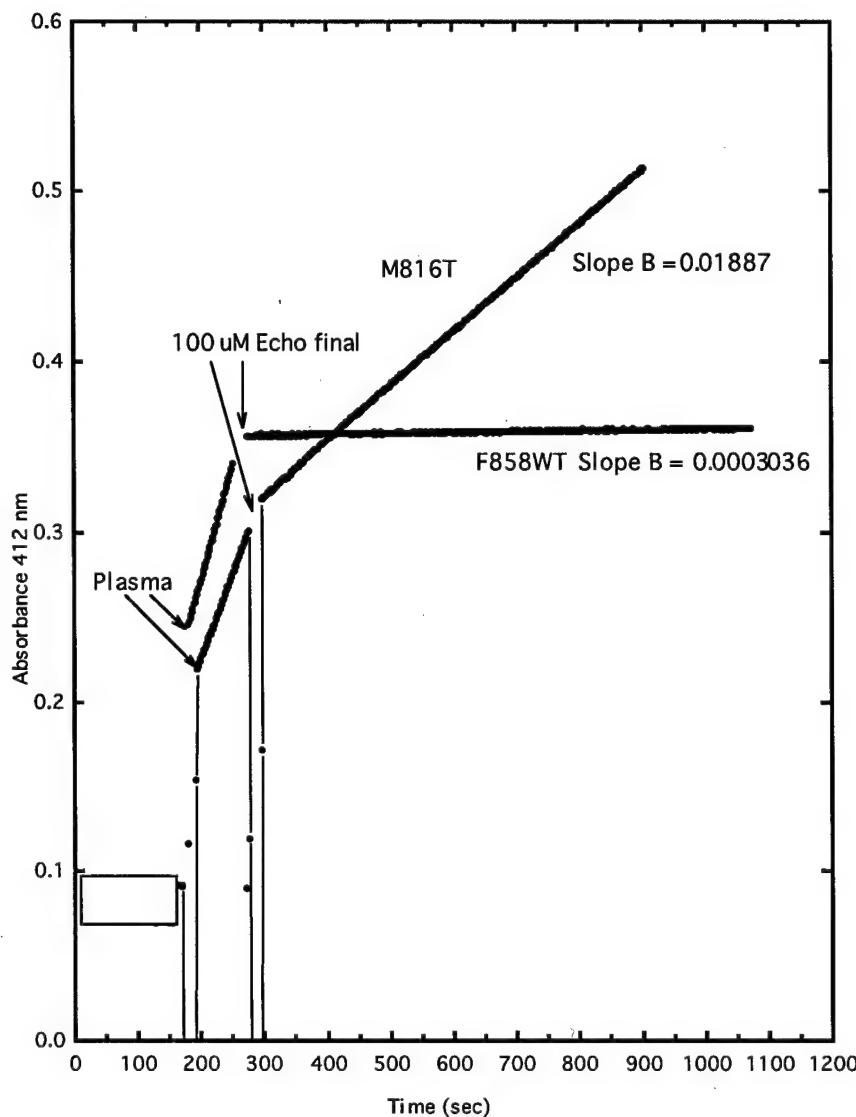
Figure 3.4. Measurement of G117H BChE activity. Hydrolysis of 1 mM butyrylthiocholine was measured initially in the absence of inhibitor. Then 10 µl of 20 mM echothiophate was added to the 2 ml reaction to give a final concentration of 100 µM. The echothiophate completely inhibited BChE activity in wild-type serum, but not in transgenic mouse serum. The echothiophate resistant activity in transgenic mouse serum was attributed to G117H BChE.

Establishing stable transgenic lines. All pups were genotyped by PCR at 3 weeks and tested for G117H BChE activity in plasma when they were 4-6 weeks old. Figure 3.5 shows that the F2 generation had a range of activities. This was expected since some mice in the F2 generation had positive chromosomes from both parents, some inherited a single positive chromosome, and some inherited no transgene. A male and female with the highest G117H activity were mated to produce the F3 generation.   4 sets of males and females from the F3 generation

were mated to produce the F4 generation. Animals with the highest activity were mated to produce the F5 generation. Similar levels of G117H activity were found in all animals in the fifth generation, suggesting that both chromosomes carried the transgene. All mice in the F5 generation had higher G117H activity than the founder mouse, supporting the conclusion that the F5 generation had two positive chromosomes.
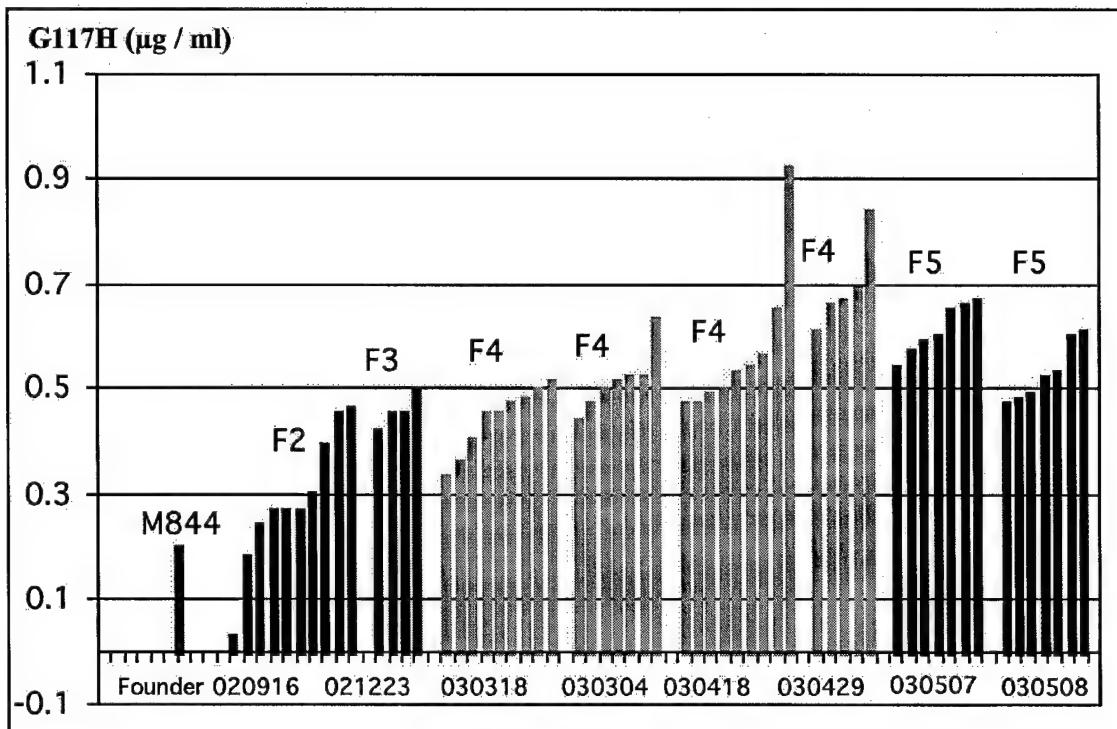
Figure 3.5. Establishment of a stable transgenic line from founder M844T. Stable G117H BChE activity in plasma was achieved by the fifth generation. The date of birth for each litter is on the x-axis. G117H activity has been corrected for 30% inhibition by 0.1 mM echothiophate.

Tissues that express G117H BChE. Tissues from adult mice in transgenic line M844T were tested for G117H activity. All tissues expressed G117H activity (Figure 3.6). The highest G117H activity was in intestine and plasma, the lowest in brain and muscle. There was a 4-fold difference in expression between the highest and lowest. By contrast, expression of wild-type BChE in the same transgenic line had a different pattern of expression (Figure 3.7). The highest wild-type BChE activity was in the intestine and liver, and the lowest in brain and muscle. There was a 60 fold difference in expression between the highest and lowest. These results support the finding of others (Soriano, 1999; Zambrowicz et al., 1997) that the ROSA26 promoter directs expression in most tissue types. The level of expression seems to be regulated not only by the ROSA26 promoter but also by the site of insertion of the transgene, since one transgenic founder, M816T, had higher G117H BChE activity than wild-type BChE activity.
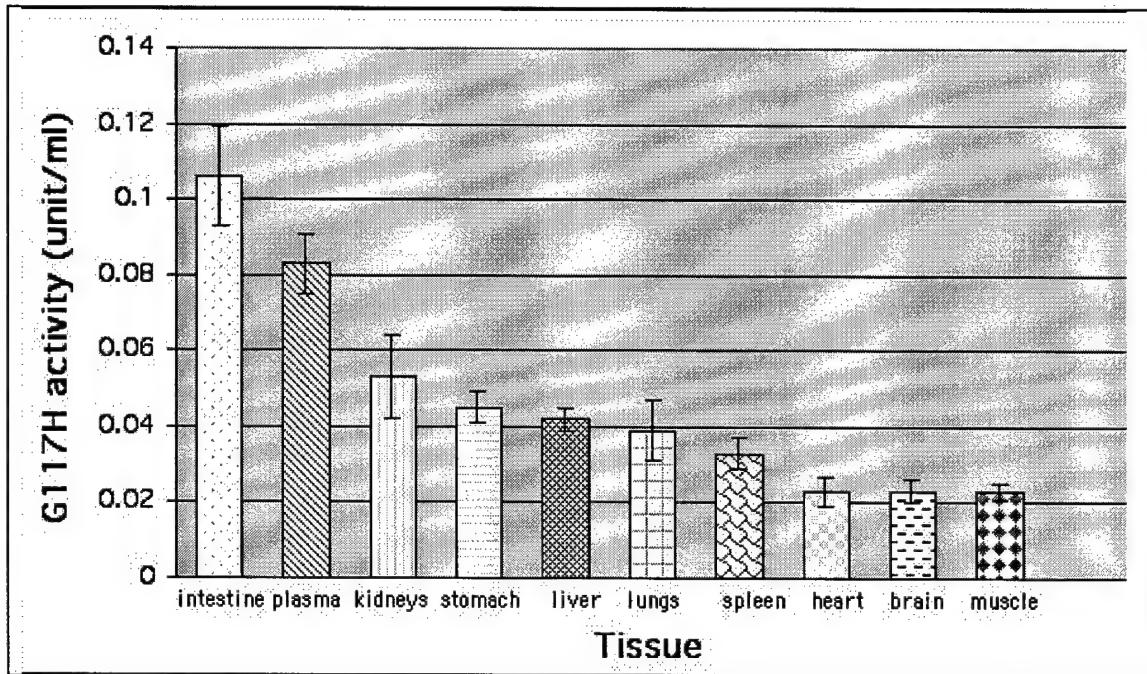
Figure 3.6. Tissue expression of G117H BChE in transgenic line M844T. Mice were perfused with saline to wash blood out of tissues, before tissues were removed. Mice were 3 months old. The mean ± s.d. is shown for 4 mice. The G117H activity values have been corrected for 22% inhibition by 1 µM DFP.
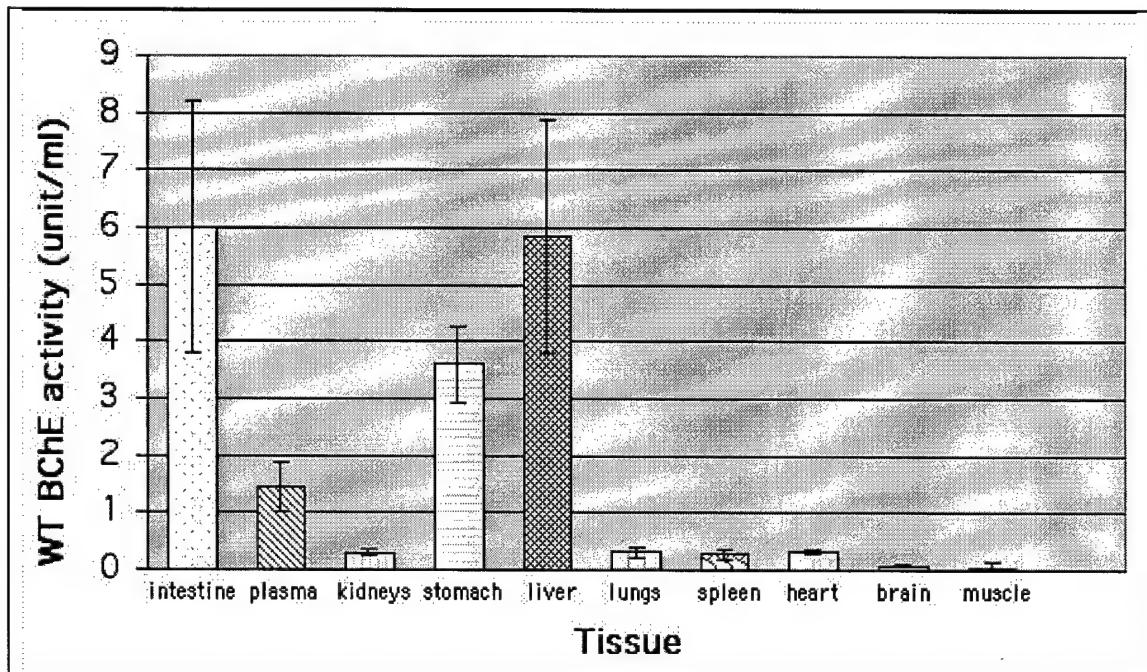
Figure 3.7. Tissue expression of wild-type BChE in transgenic line M844T. The same 4 mice were tested in Figures 3.6 and 3.7.

To determine whether expression of wild-type mouse BChE was affected by human BChE, the BChE activity levels were measured in the high-expressing M816T founder and his F1 progeny. The founder had 1.49 u/ml total BChE and 0.64 u/ml G117H BChE in plasma. The F1 had 3.03 u/ml total BChE and 1.38 u/ml G117H BChE. These activity values suggest that expression of wild-type mouse BChE was unaffected by expression of human G117H BChE. The BChE promoter and the ROSA26 promoter acted independently.

The different pattern of expression of G117H BChE and wild-type BChE in transgenic line M844T (Figures 3.6 and 3.7) supports the conclusion that the BChE and ROSA26 promoters acted independently.

Tetramers of G117H BChE. The subunit organization of human G117H BChE expressed in transgenic mouse plasma was determined as shown in Figure 3.8. Mouse plasma was electrophoresed on a nondenaturing polyacrylamide gel, and the gel stained for BChE activity. G117H BChE was revealed by inhibiting wild-type BChE with 0.1 mM echothiophate. Figure 3.8 shows that human G117H BChE was a tetramer.
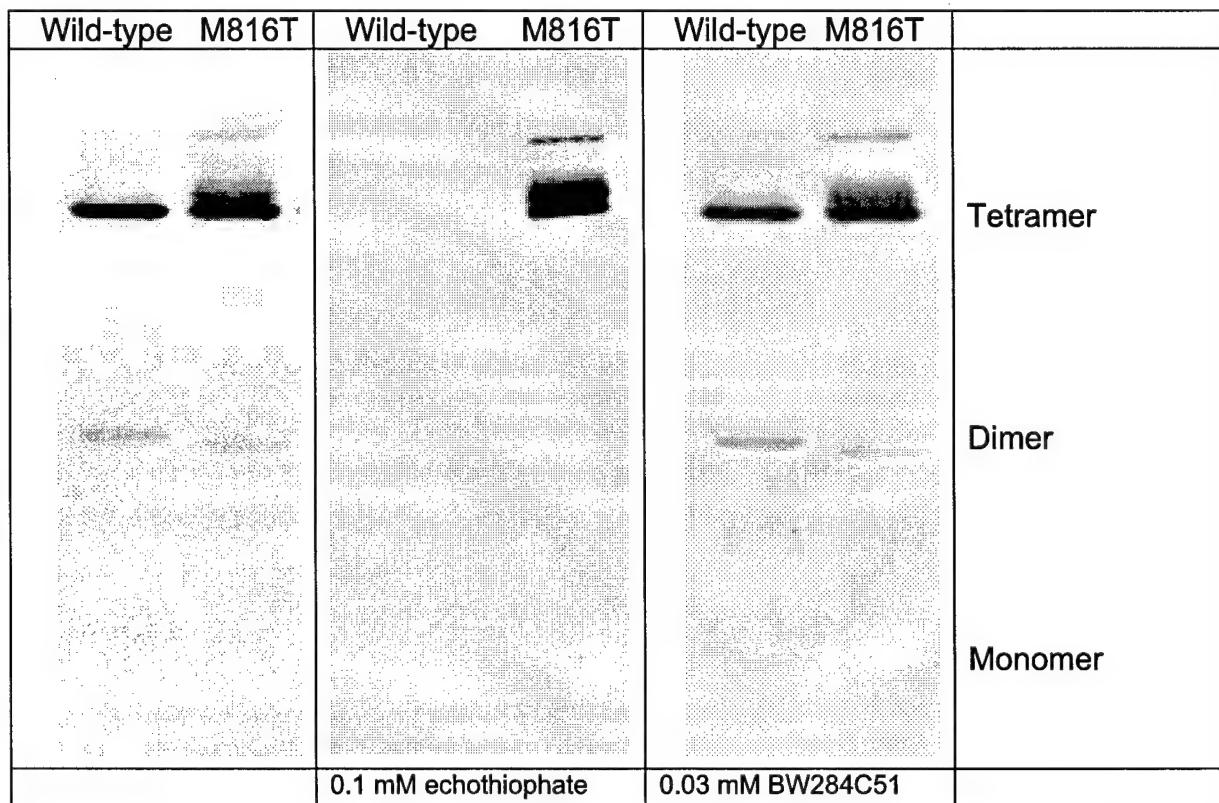
Figure 3.8. Subunit organization of G117H BChE in mouse plasma. A nondenaturing 4-30% polyacrylamide gradient gel was stained for BChE activity with butyrylthiocholine by the method of Karnovsky and Roots (1964) and for G117H BChE activity by inhibiting wild-type BChE with 0.1 mM echothiophate. The G117H BChE is a tetramer. The gel treated with AChE inhibitor BW284C51 has all the same bands as the gel treated with no inhibitor. This shows that this staining method specifically reveals BChE bands.

A tetramer doublet is present in lanes containing transgenic mouse blood but not in lanes containing wild-type mouse blood (Figure 3.8). The doublet might represent heterologous tetramers composed of a mixture of mouse and human BChE subunits. This possibility was not tested and is speculation at this point. Mouse BChE has 574 amino acids and 7 N-linked carbohydrate chains (Rachinsky et al., 1990). Human BChE has 574 amino acids, plus 8 amino acids from the FLAG epitope, 9 N-linked carbohydrate chains, and a subunit molecular weight of 85,000 (Lockridge et al., 1987).

Transgenic mice resist OP toxicity. Three out of 8 wild-type mice died after receiving 0.1 mg/kg echothiophate s.c., suggesting that this dose was approximately the LD_{50} dose for wild-type mice. None of the 8 transgenic mice died.

The wild-type mice had severe signs of toxicity including profuse salivation, lacrimation, whole body tremor, abnormal gait, impaired mobility, flattened posture, no response to being handled, and decrease in body temperature. By contrast transgenic mice had only slight salivation, slight tremor, and no significant decrease in body temperature (Figure 3.9). Transgenic mice showed no impairment in gait, mobility, posture, and no change in reactivity to being handled.
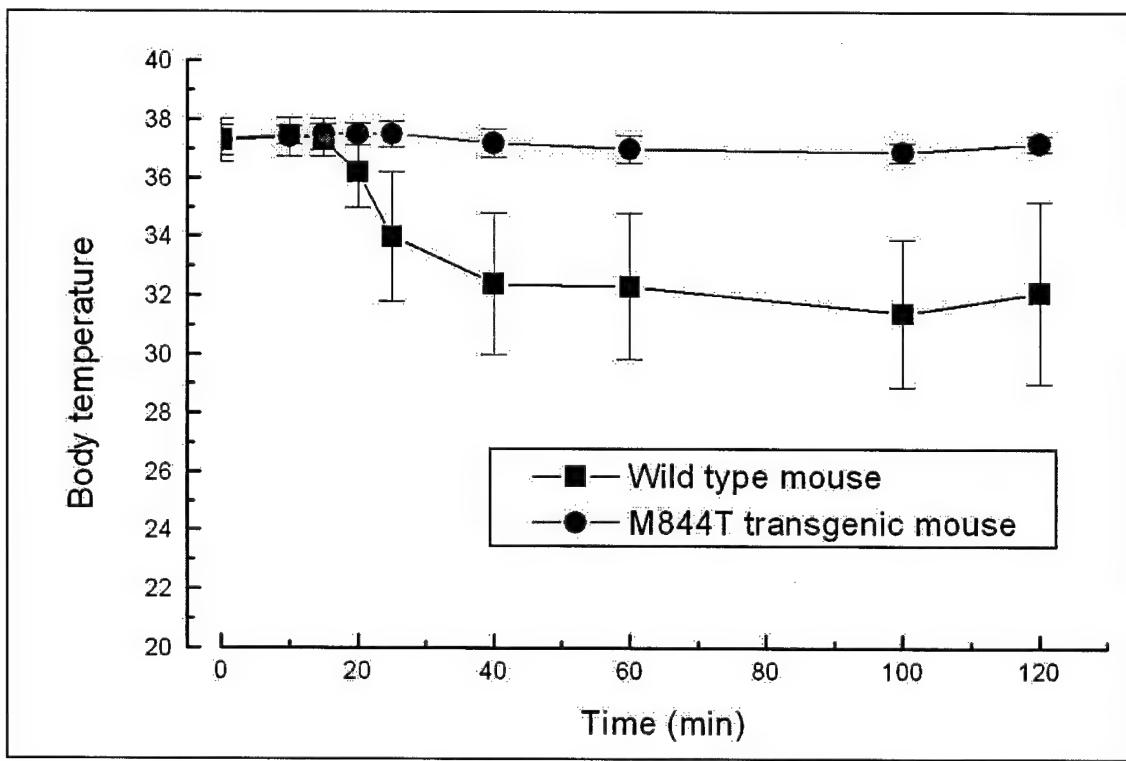
Figure 3.9. Transgenic G117H mice maintain body temperature after OP exposure. Echothiophate 0.1 mg/kg s.c caused a 6°C drop in body temperature in wild-type mice but not in transgenic mice. Data are for 5 wild-type and 8 transgenic mice. Three additional wild-type mice received echothiophate but they are not included in this graph because they died.

The LD$_{50}$ for transgenic mice has not been measured. Preliminary experiments with 2 mice suggested that a small increase in dose was lethal. One transgenic mouse was tested with 0.12 mg/kg and one with 0.15 mg/kg echothiophate. Both transgenic mice died. It is normal for dose response curves for OP to be very steep.

AChE, BChE, and G117H activity in OP treated mice. The question in these experiments is whether G117H BChE protected AChE and BChE from inhibition by OP. Results in Table 3.6 show that AChE and BChE activities decreased to the same extent in transgenic and wild-type mice after treatment with 0.1 mg/kg echothiophate s.c.

Table 3.6. AChE, BChE and G117H BChE activity in tissues of echothiophate-treated mice. Wild-type and transgenic mice received 0.1 mg/kg echothiophate s.c. Animals were euthanized 2 h later. Units of enzyme activity are micromoles substrate hydrolyzed per minute per gram wet weight of tissue.

Mouse	Tissue	AChE (mean±SD)	BChE (mean±SD)	G117H (mean±SD)
untreated wild-type	Brain	1.01±0.16	0.09±0.01	
wild-type	Brain	1.05±0.17	0.14±0.05	
untreated transgenic	Brain		0.09±0.01	0.023±0.003
transgenic	Brain	1.04±0.09	0.09±0.01	0.022±0.005
untreated wild-type	Muscle	0.32±0.14	0.16±0.01	
wild-type	Muscle	0.16±0.03	0.10±0.05	
untreated transgenic	Muscle		0.22±0.14	0.023±0.002
transgenic	Muscle	0.17±0.09	0.13±0.07	0.021±0.002
untreated wild-type	Liver	0.06±0.02	4.09±1.11	
wild-type	Liver	0.05±0.02	2.80±1.03	
untreated transgenic	Liver		5.84±2.03	0.042±0.003
transgenic	Liver	0.06±0.01	2.70±1.40	0.032±0.017
untreated wild-type	Heart	0.10±0.01	0.38±0.02	
wild-type	Heart	0.04±0.01	0.12±0.05	
untreated transgenic	Heart		0.32±0.04	0.023±0.004
transgenic	Heart	0.05±0.02	0.11±0.04	0.036±0.007
untreated wild-type	Lungs	0.15±0.09	0.27±0.07	
wild-type	Lungs	0.10±0.06	0.16±0.02	
untreated transgenic	Lungs		0.32±0.09	0.039±0.008
transgenic	Lungs	0.09±0.04	0.14±0.06	0.040±0.009
untreated wild-type	Plasma	0.45±0.15	1.71±0.56	
wild-type	Plasma	0.19±0.09	0.28±0.24	
untreated transgenic	plasma		1.44±0.44	0.083±0.008
transgenic	Plasma	0.13±0.03	0.33±0.19	0.080±0.025
untreated wild-type	Intestine	0.18±0.03	9.56±0.44	
wild-type	Intestine	0.10±0.01	4.25±1.96	
untreated transgenic	intestine		5.99±2.20	0.106±0.013
transgenic	Intestine	0.09±0.02	3.12±1.45	0.090±0.016

The data are for 8 treated transgenic mice (derived from founder M844T), 5 treated wild-type mice (another 3 died at 20 to 40 minutes after injection with echothiophate), 3 untreated wild-type mice, and 4 untreated transgenic mice.

The highest inhibition was in plasma; plasma BChE was inhibited 80-84% and plasma AChE was inhibited 70-75% both in transgenic and wild-type mice. In most other tissues BChE and AChE enzymes were inhibited about 50%. The level of inhibition of AChE and BChE in transgenic mice was not less than in wild-type mice. Echothiophate injected into the periphery did not inhibit AChE and BChE in the brain, thus demonstrating that the positively charged echothiophate did not cross the blood-brain barrier.

G117H BChE activity was not significantly inhibited by treatment of mice with 0.1 mg/kg echothiophate.

Comparison of AChE and BChE activities in untreated wild-type mice shows that most tissues have more BChE than AChE activity. Only brain and muscle have more AChE than BChE activity. This finding for strain B6SJL supports results for strain 129Sv reported by Li et al. (2000) and Duysen et al. (2001).

Catalytic activity of G117H BChE with acetylthiocholine. The above results led us to consider that G117H BChE might be protecting mice from OP toxicity not by catalysis of OP to inactive products, but by hydrolysis of acetylcholine. The potential of G117H BChE to hydrolyze acetylcholine was estimated by measuring the kcat and Km values for acetylthiocholine. For comparison, kcat and Km values were also measured with butyrylthiocholine. Table 3.7 shows that highly purified human G117H BChE binds acetylthiocholine with a Km value of 1.75 mM and that it hydrolyzes acetylthiocholine at a rate of 12,000 µmoles per min per µmole active site. Butyrylthiocholine is a better substrate for G117H BChE in terms of binding affinity and catalytic rate than acetylthiocholine.

Table 3.7. Binding affinity and catalytic rate for purified human G117H BChE

substrate	Km, mM	k_{cat}, min^{-1}
Acetylthiocholine	1.75 ± 0.09	12,000
Butyrylthiocholine	0.42 ± 0.02	18,300

Literature values: Millard et al., (1995) Km for butyrylthiocholine 0.23 mM; Millard et al. (1998) Km for butyrylthiocholine 0.1 mM, kcat 9000 min^{-1}.

Discussion

Mechanism of protection. The transgenic G117H BChE mouse is resistant to OP toxicity. Two possible ways in which G117H BChE could be protecting the mouse is by hydrolyzing OP or by hydrolyzing acetylcholine after AChE has been inhibited. We reasoned that if OP hydrolysis were the mechanism, then AChE and BChE should be less inhibited in the transgenic mouse. This was not found. The experimental result was that AChE and BChE were inhibited to similar extents in echothiophate-treated transgenic and wild-type mice. Therefore, OP hydrolysis is not the mechanism of protection in the transgenic mouse. This conclusion is supported by studies of the purified G117H enzyme, which hydrolyzes echothiophate at the slow rate of 0.75 min^{-1} (Lockridge et al., 1997).

We are left with the alternative hypothesis, that protection is explained by the resistance of G117H BChE to inhibition and the ability of G117H BChE to hydrolyze acetylcholine. It is known that inhibition of AChE causes accumulation of excess acetylcholine, and excess acetylcholine leads to death. The G117H BChE with its widespread distribution might be present in or near nerve synapses, where it could aid in metabolism of excess acetylcholine. Additional work needs to be done to support this hypothesis. There is no doubt that G117H BChE is resistant to inhibition by OP and that G117H is capable of hydrolyzing acetylcholine. What is not known is whether G117H BChE is found in locations where it could dispose of synaptic acetylcholine. Another problem with this hypothesis is that an LD_{50} dose of echothiophate inhibits muscle AChE 50%, but after 50% inhibition the muscle still has more AChE activity than G117H activity. Why should 0.02 units/g G117H BChE contribute significantly to acetylcholine hydrolysis in muscle that still has 0.16 units/g AChE activity?

A protective mechanism that relies on resistance to inhibition by OP rather than on ability to hydrolyze OP has examples in nature. OP-resistant AChE has been identified in the azinphos-methyl-resistant strain of the Colorado potato beetle (Zhu and Clark, 1997), paraoxon-resistant strains of house flies (Oppenoorth, 1982), malaoxon-resistant grain borer (Guedes et al, 1997), and dimethoate-resistant olive fruit fly (Vontas et al., 2001). There is one example of OP resistance combined with OP hydrolase activity. The diazinon-resistant sheep blowfly has a single amino acid mutation in carboxylesterase E3, that changes Gly 137 to Asp (Newcomb et al, 1997). Carboxylesterase is not found in nerve synapses and does not hydrolyze acetylcholine.

Two new assays to detect G117H activity. Two new assays to detect G117H activity were developed in this report, a spectrophotometric assay and a gel assay. Both assays relied on the resistance of G117H to inhibition by OP so that the only butyrylthiocholine hydrolysis activity remaining after treatment with OP was due to G117H activity. The spectrophotometric assay was useful for phenotyping transgenic mice to establish stable transgenic mouse lines. The assay distinguished animals with single and double doses of the heritable transgene locus. By contrast, genotyping by PCR did not distinguish between doses of the transgene.

The nondenaturing gel activity stain was useful for demonstrating subunit organization in G117H BChE.

Tetramers of human G117H BChE in mouse plasma. An unanswered question in the cholinesterase field is whether tetramers of plasma butyrylcholinesterase are composed simply of 4 identical subunits or whether they include a tetramer organizing peptide. A proline rich organizing peptide is required for assembly of recombinant butyrylcholinesterase and acetylcholinesterase into tetramers (Altamirano and Lockridge, 1999; Bon and Massoulié, 1997; Simon et al., 1998; Kronman et al., 2000). The tetramer organizing peptide, PRAD, derives from the N-terminus of the collagen tail (Bon et al., 1997; Krejci et al., 1997). A different proline rich membrane anchor, PRiMA, organizes AChE and BChE into tetramers and anchors them to brain and muscle membranes (Perrier et al., 2002). To date no evidence has been obtained to support the presence of a tetramer organizing peptide within the BChE tetramer. However, the possibility has not been ruled out.

The transgenic G117H mouse contains the gene for human BChE but does not contain the gene for human PRAD or human PRiMA. The G117H BChE in mouse plasma was a tetramer. This shows that mouse liver has the necessary machinery for assembling human BChE subunits into tetramers and exporting the tetramers into mouse blood. If a proline rich peptide is present in the tetramer, it has to be the mouse version.

The FLAG epitope at the carboxy terminus of the 574 amino acid human BChE subunit was detected in transgenic mouse plasma, suggesting that the FLAG epitope of 8 amino acids did not interfere with tetramer formation.

Characteristics of the G117H BChE transgenic mouse. This is the first BChE transgenic mouse. Beeri et al. (1994) attempted to make a BChE transgenic mouse but they found no expression of human BChE enzyme activity and undetectable human BCHE DNA after two generations. By contrast, transgenic mouse line M844T has stably transmitted the human BCHE gene for 6 generations. Two stable G117H BChE transgenic lines expressed 0.5 µg/ml (6th generation of M844T) and 0.7 µg/ml (4th generation of M837T) G117H BChE enzyme per ml plasma. This is 25-30% of the wild-type BChE in the same animals. All tissues tested expressed G117H BChE enzyme activity.

The transgenic mice are healthy and fertile. Litter sizes are normal at 7 to 9 pups per litter. Normal health was expected because expression of excess BChE in humans has no deleterious effect in humans. People with the Cynthiana variant of BChE have 2 to 4 times the normal amount of BChE and are resistant to the muscle relaxant succinylcholine (Neitlich, 1966; Yoshida and Motulsky, 1969; Delbrück and Henkel, 1979; Hada et al., 1985; Yao and Savarese,1997). Cynthiana variants have no other phenotype.

The only unusual feature of the G117H transgenic mouse is resistance to OP toxicity. This is the first transgenic mouse in the literature with inherited OP resistance. No other gene inserted into mice has protected mice from OP toxicity.

Task 4. *Gene therapy with AChE.*
4.1 Human AChE cDNA will be cloned into a shuttle vector. The linearized shuttle vector and pAdEasy-1 will be cotransfected into bacteria to allow homologous recombination. Colonies resistant to kanamycin will be screened by restriction endonuclease digestion.
4.2 The adenoviral vector containing human AChE, pAd-ACHE, will be linearized and transfected into 293 cells. Virus production will be visualized by fluorescence of green fluorescence protein and by measuring AChE activity.
4.3 Viral stocks will be amplified in 293 cells to obtain 10^{11} to 10^{12} plaque forming units. The virus will be purified in preparation for injection into mice.
4.4 Mice will be injected intravenously with various doses of adenoviral vector. The site of localization of the adenovirus will be determined. Expression levels of AChE will be determined. The duration of expression of AChE will be measured.

Tasks 4.1, 4.2, 4.3, 4.4

Abstract

Adenoassociated virus (AAV) is attractive as a gene transfer vector because it has no known pathogenicity, it is minimally immunogenic, and it can transduce nondividing cells. Use of AAV is approved by the Food and Drug Administration for treatment of a variety of diseases. For these reasons we selected AAV for gene therapy trials. The AChE knockout mouse was treated with a virus that delivers AChE. To date our progress includes construction of the viral expression plasmid (task 4.1), production of the virus (task 4.2), purification of the virus (task 4.3), and delivery of the virus to mice (task 4.4).

Several routes of administration of the virus have been tested. Intramuscular injection into adult AChE -/- mice resulted in expression of AChE in plasma at levels approaching 50% of the AChE activity in wild-type mouse plasma. Highest AChE activity was found on day 3 post-injection. AChE activity declined thereafter because the AChE was cleared from plasma by anti-human AChE antibodies.

Subcutaneous injection into newborn mice resulted in no expression of human AChE in AChE -/- plasma. Antibodies to human AChE were formed in AChE -/- mice.

Intrastriatal injection into the brains of 20-28 day old AChE -/- mice resulted in the only change in phenotype observed to date. The treated mice acquired the ability to hang on to an inverted screen. Untreated AChE -/- mice fell off within 4 seconds but treated mice stayed on for longer than 20 seconds. This finding is interpreted to mean that muscle coordination improved as a result of expression of AChE in the striatum.

Introduction

The AChE -/- mouse can be used as a model for testing the effectiveness of gene therapy to deliver the ACHE gene. The delivery of AChE via gene therapy is expected to have military applications for treatment and protection against OP.

Methods

Vector construction. Plasmid pAAV/AChE for expression of human AChE was constructed. Briefly, 1.9 kb of human AChE cDNA, encoding 31 amino acids in the signal peptide, 583 amino acids of the full-length AChE subunit (accession number NM 015831) , and 8 amino acids of the FLAG epitope was cloned into the pSCMF4 plasmid (BCCM^{TM}/LMBP plasmid collection Universiteit Gent, Belgium) for the purpose of acquiring an EcoRI site at the 5' end. The 1.9 kb piece was excised with EcoRI and SalI and cloned into the pAAV-MCS plasmid (catalog #240071 AAV Helper-Free System, Stratagene, La Jolla, CA). The vector contains the CMV promoter and beta-globin intron for high-level expression in mammalian cells. XL10-Gold$^{®}$ ultracompetent cells (catalog #200314, Stratagene) were used to amplify plasmid pAAV/AChE. It was essential to use XL10-Gold cells to avoid unwanted recombination through the inverted terminal repeat sequences. The pAAV/AChE plasmid was sequenced to verify the integrity of the inverted terminal repeats and to confirm the AChE sequence. The sequence of pAAV/AChE is in Figure 4.1.

Figure 4.1. Plasmid pAAV/AChE-FLAG encoding human AChE

```
CCTGCAGGCAGCTGCGCGCTCGCTCGCTCACTGAGGCCGCCCGGGCAAAGCCCGGGCGTC
---------------------------ITR-------------------------------
GGGCGACCTTTGGTCGCCCGGCCTCAGTGAGCGAGCGAGCGCGCAGAGAGGGAGTGGCCA
---------------------------ITR-------------------------------
ACTCCATCACTAGGGGTTCCTGCGGCCGCACGCGTGGAGCTAGTTATTAATAGTAATCAA 180
--------ITR-----------
TTACGGGGTCATTAGTTCATAGCCCATATATGGAGTTCCGCGTTACATAACTTACGGTAA
ATGGCCCGCCTGGCTGACCGCCCAACGACCCCCGCCCATTGACGTCAATAATGACGTATG
TTCCCATAGTAACGTCAATAGGGACTTTCCATTGACGTCAATGGGTGGAGTATTTACGGT 360
AAACTGCCCACTTGGCAGTACATCAAGTGTATCATATGCCAAGTACGCCCCCTATTGACG
TCAATGACGGTAAATGGCCCGCCTGGCATTATGCCCAGTACATGACCTTATGGGACTTTC
CTACTTGGCAGTACATCTACGTATTAGTCATCGCTATTACCATGGTGATGCGGTTTTGGC 540
AGTACATCAATGGGCGTGGATAGCGGTTTGACTCACGGGGATTTCCAAGTCTCCACCCCA
TTGACGTCAATGGGAGTTTGTTTTGCACCAAAATCAACGGGACTTTCCAAAATGTCGTAA
CAACTCCGCCCCATTGACGCAAATGGGCGGTAGGCGTGTACGGTGGGAGGTCTATATAAG 720
CAGAGCTCGTTTAGTGAACCGTCAGATCGCCTGGAGACGCCATCCACGCTGTTTTGACCT
CCATAGAAGACACCGGGACCGATCCAGCCTCCGCGGATTCGAATCCCGGCCGGGAACGGT
GCATTGGAACGCGGATTCCCCGTGCCAAGAGTGACGTAAGTACCGCCTATAGAGTCTATA 900
GGCCCACAAAAAATGCTTTCTTCTTTTAATATACTTTTTTGTTTATCTTATTTCTAATAC
TTTCCCTAATCTCTTTCTTTCAGGGCAATAATGATACAATGTATCATGCCTCTTTGCACC
ATTCTAAAGAATAACAGTGATAATTTCTGGGTTAAGGCAATAGCAATATTTCTGCATATA 1080
AATATTTCTGCATATAAATTGTAACTGATGTAAGAGGTTTCATATTGCTAATAGCAGCTA
CAATCCAGCTACCATTCTGCTTTTATTTTATGGTTGGGATAAGGCTGGATTATTCTGAGT
CCAAGCTAGGCCCTTTTGCTAATCATGTTCATACCTCTTATCTTCCTCCCACAGCTCCTG 1260
GGCAACGTGCTGGTCTGTGTGCTGGCCCATCACTTTGGCAAAGAATTGGGATTCGAACAT
```

```
CGATTGAATTCCCCGGGGATCCTCTAGAGTCGACCTGCAGAAGCTTGATATCTGCAGCC
    EcoR I                                      Hind III
-31
ATGAGGCCCCCGCAGTGTCTGCTGCACACGCCTTCCCTGGCTTCCCCACTCCTTCTCCTC 1439
MetArgProProGlnCysLeuLeuHisThrProSerLeuAlaSerProLeuLeuLeuLeu
                                    +1
CTCCTCTGGCTCCTGGGTGGAGGAGTGGGGGCTGAGGGCCGGGAGGATGCAGAGCTGCTG
LeuLeuTrpLeuLeuGlyGlyGlyValGlyAlaGluGlyArgGluAspAlaGluLeuLeu

GTGACGGTGCGTGGGGGCCGGCTGCGGGGCATTCGCCTGAAGACCCCCGGGGGGCCCTGTC
ValThrValArgGlyGlyArgLeuArgGlyIleArgLeuLysThrProGlyGlyProVal
                                                        Apa1
TCTGCTTTCCTGGGCATCCCCTTTGCGGAGCCACCCATGGGACCCCGTCGCTTTCTGCCA 1619
SerAlaPheLeuGlyIleProPheAlaGluProProMetGlyProArgArgPheLeuPro

CCGGAGCCCAAGCAGCCTTGGTCAGGGGTGGTAGACGCTACAACCTTCCAGAGTGTCTGC
ProGluProLysGlnProTrpSerGlyValValAspAlaThrThrPheGlnSerValCys

TACCAATATGTGGACACCCTATACCCAGGTTTTGAGGGCACCGAGATGTGGAACCCCAAC
TyrGlnTyrValAspThrLeuTyrProGlyPheGluGlyThrGluMetTrpAsnProAsn

CGTGAGCTGAGCGAGGACTGCCTGTACCTCAACGTGTGGACACCATACCCCCGGCCTACA 1799
ArgGluLeuSerGluAspCysLeuTyrLeuAsnValTrpThrProTyrProArgProThr

TCCCCCACCCCTGTCCTCGTCTGGATCTATGGGGGTGGCTTCTACAGTGGGGCCTCCTCC
SerProThrProValLeuValTrpIleTyrGlyGlyGlyPheTyrSerGlyAlaSerSer

TTGGACGTGTACGATGGCCGCTTCTTGGTACAGGCCGAGAGGACTGTGCTGGTGTCCATG
LeuAspValTyrAspGlyArgPheLeuValGlnAlaGluArgThrValLeuValSerMet

AACTACCGGGTGGGAGCCTTTGGCTTCCTGGCCCTGCCGGGGAGCCGAGAGGCCCCGGGC 1979
AsnTyrArgValGlyAlaPheGlyPheLeuAlaLeuProGlySerArgGluAlaProGly

AATGTGGGTCTCCTGGATCAGAGGCTGGCCCTGCAGTGGGTGCAGGAGAACGTGGCAGCC
AsnValGlyLeuLeuAspGlnArgLeuAlaLeuGlnTrpValGlnGluAsnValAlaAla

TTCGGGGGTGACCCGACATCAGTGACGCTGTTTGGGGAGAGCGCGGGAGCCGCCTCGGTG
PheGlyGlyAspProThrSerValThrLeuPheGlyGluSerAlaGlyAlaAlaSerVal

GGCATGCACCTGCTGTCCCCGCCCAGCCGGGGCCTGTTCCACAGGGCCGTGCTGCAGAGC 2159
GlyMetHisLeuLeuSerProProSerArgGlyLeuPheHisArgAlaValLeuGlnSer

GGTGCCCCCAATGGACCCTGGGCCACGGTGGGCATGGGAGAGGCCCGTCGCAGGGCCACG
GlyAlaProAsnGlyProTrpAlaThrValGlyMetGlyGluAlaArgArgArgAlaThr

CAGCTGGCCCACCTTGTGGGCTGTCCTCCAGGCGGCACTGGTGGGAATGACACAGAGCTG
GlnLeuAlaHisLeuValGlyCysProProGlyGlyThrGlyGlyAsnAspThrGluLeu

GTAGCCTGCCTTCGGACACGACCAGCGCAGGTCCTGGTGAACCACGAATGGCACGTGCTG 2339
ValAlaCysLeuArgThrArgProAlaGlnValLeuValAsnHisGluTrpHisValLeu

CCTCAAGAAAGCGTCTTCCGGTTCTCCTTCGTGCCTGTGGTAGATGGAGACTTCCTCAGT
ProGlnGluSerValPheArgPheSerPheValProValValAspGlyAspPheLeuSer

GACACCCCAGAGGCCCTCATCAACGCGGGAGACTTCCACGGCCTGCAGGTGCTGGTGGGT
AspThrProGluAlaLeuIleAsnAlaGlyAspPheHisGlyLeuGlnValLeuValGly

GTGGTGAAGGATGAGGGCTCGTATTTTCTGGTTTACGGGGCCCCCAGGCTTCAGCAAAGAC 2519
```

```
        ValValLysAspGluGlySerTyrPheLeuValTyrGlyAlaProGlyPheSerLysAsp
                                   ApaI
AACGAGTCTCTCATCAGCCGGGCCGAGTTCCTGGCCGGGGTGCGGGTCGGGGTTCCCCAG
AsnGluSerLeuIleSerArgAlaGluPheLeuAlaGlyValArgValGlyValProGln

GTAAGTGACCTGGCAGCCGAGGCTGTGGTCCTGCATTACACAGACTGGCTGCATCCCGAG
ValSerAspLeuAlaAlaGluAlaValValLeuHisTyrThrAspTrpLeuHisProGlu

GACCCGGCACGCCTGAGGGAGGCCCTGAGCGATGTGGTGGGCGACCACAATGTCGTGTGC 2699
AspProAlaArgLeuArgGluAlaLeuSerAspValValGlyAspHisAsnValValCys

CCCGTGGCCCAGCTGGCTGGGCGACTGGCTGCCCAGGGTGCCCGGGTCTACGCCTACGTC
ProValAlaGlnLeuAlaGlyArgLeuAlaAlaGlnGlyAlaArgValTyrAlaTyrVal

TTTGAACACCGTGCTTCCACGCTCTCCTGGCCCCTGTGGATGGGGGTGCCCCACGGCTAC
PheGluHisArgAlaSerThrLeuSerTrpProLeuTrpMetGlyValProHisGlyTyr

GAGATCGAGTTCATCTTTGGGATCCCCCTGGACCCCTCTCGAAACTACACGGCAGAGGAG 2879
GluIleGluPheIlePheGlyIleProLeuAspProSerArgAsnTyrThrAlaGluGlu

AAAATCTTCGCCCAGCGACTGATGCGATACTGGGCCAACTTTGCCCGCACAGGGGATCCC
LysIlePheAlaGlnArgLeuMetArgTyrTrpAlaAsnPheAlaArgThrGlyAspPro

AATGAGCCCCGAGACCCCAAGGCCCCACAATGGCCCCCGTACACGGCGGGGGCTCAGCAG
AsnGluProArgAspProLysAlaProGlnTrpProProTyrThrAlaGlyAlaGlnGln

TACGTTAGTCTGGACCTGCGGCCGCTGGAGGTGCGGCGGGGGCTGCGCGCCCAGGCCTGC 3059
TyrValSerLeuAspLeuArgProLeuGluValArgArgGlyLeuArgAlaGlnAlaCys

GCCTTCTGGAACCGCTTCCTCCCCAAATTGCTCAGCGCCACCGACACGCTCGACGAGGCG
AlaPheTrpAsnArgPheLeuProLysLeuLeuSerAlaThrAspThrLeuAspGluAla

GAGCGCCAGTGGAAGGCCGAGTTCCACCGCTGGAGCTCCTACATGGTGCACTGGAAGAAC
GluArgGlnTrpLysAlaGluPheHisArgTrpSerSerTyrMetValHisTrpLysAsn
                                           583
CAGTTCGACCACTACAGCAAGCAGGATCGCTGCTCAGACCTGGACTACAAGGACGACGAT 3239
GlnPheAspHisTyrSerLysGlnAspArgCysSerAspLeuAspTyrLysAspAspAsp
                                           -------FLAG-------
GACAAGTGAAGATCTCAACGGGTGGCATCCCTGTGACCCCTCCCCAGTGCCTCTCCTGGCC
AspLys
------    Bgl II
CTGGAAGTTGCCACTCCAGTGCCCACCAGCCTTGTCCTAATAAAATTAAGTTGCATCATT
TTGTCTGACTAGGTGTCCTTCTATAATATTATGGGGTGGAGGGGGGTGGTATGGAGCAAG 3420
GGGCAAGTTGGGAAGACAACCTGTAGGGCCTGCGGGGTCTATTGGGAACCAAGCTGGAGT
GCAGTGGCACAATCTTGGCTCACTGCAATCTCCGCCTCCTGGGTTCAAGCGATTCTCCTG
CCTCAGCCTCCCGAGTTGTTGGGATTCCAGGCATGCATGACCAGGCTCAGCTAATTTTTG 3600
TTTTTTTGGTAGAGACGGGGTTTCACCATATTGGCCAGGCTGGTCTCCAACTCCTAATCT
CAGGTGATCTACCCACCTTGGCCTCCCAAATTGCTGGGATTACAGGCGTGAACCACTGCT
CCCTTCCCTGTCCTTCTGATTTTGTAGGTAACCACGTGCGGACCGAGCGGCCGCAGGAAC 3780
                                                       --ITR-
CCCTAGTGATGGAGTTGGCCACTCCCTCTCTGCGCGCTCGCTCGCTCACTGAGGCCGGGC
--------------------------ITR-------------------------------
GACCAAAGGTCGCCCGACGCCCGGGCTTTGCCCGGGCGGCCTCAGTGAGCGAGCGAGCGC
--------------------------ITR-------------------------------
GCAGCTGCCTGCAGGGGCGCCTGATGCGGTATTTTCTCCTTACGCATCTGTGCGGTATTT 3960
-----------ITR-----------
CACACCGCATACGTCAAAGCAACCATAGTACGCGCCCTGTAGCGGCGCATTAAGCGCGGC
GGGTGTGGTGGTTACGCGCAGCGTGACCGCTACACTTGCCAGCGCCCTAGCGCCCGCTCC
```

```
TTTCGCTTTCTTCCCTTCCTTTCTCGCCACGTTCGCCGGCTTTCCCCGTCAAGCTCTAAA 4140
TCGGGGGCTCCCTTTAGGGTTCCGATTTAGTGCTTTACGGCACCTCGACCCCAAAAAACT
TGATTTGGGTGATGGTTCACGTAGTGGGCCATCGCCCTGATAGACGGTTTTTCGCCCTTT
GACGTTGGAGTCCACGTTCTTTAATAGTGGACTCTTGTTCCAAACTGGAACAACACTCAA 4320
CCCTATCTCGGGCTATTCTTTTGATTTATAAGGGATTTTGCCGATTTCGGCCTATTGGTT
AAAAAATGAGCTGATTTAACAAAAATTTAACGCGAATTTTAACAAAATATTAACGTTTAC
AATTTTATGGTGCACTCTCAGTACAATCTGCTCTGATGCCGCATAGTTAAGCCAGCCCCG 4500
ACACCCGCCAACACCCGCTGACGCGCCCTGACGGGCTTGTCTGCTCCCGGCATCCGCTTA
CAGACAAGCTGTGACCGTCTCCGGGAGCTGCATGTGTCAGAGGTTTTCACCGTCATCACC
GAAACGCGCGAGACGAAAGGGCCTCGTGATACGCCTATTTTTATAGGTTAATGTCATGAT 4680
AATAATGGTTTCTTAGACGTCAGGTGGCACTTTTCGGGGAAATGTGCGCGGAACCCCTAT
TTGTTTATTTTTCTAAATACATTCAAATATGTATCCGCTCATGAGACAATAACCCTGATA
AATGCTTCAATAATATTGAAAAAGGAAGAGTATGAGTATTCAACATTTCCGTGTCGCCCT 4860
TATTCCCTTTTTTGCGGCATTTTGCCTTCCTGTTTTTGCTCACCCAGAAACGCTGGTGAA
AGTAAAAGATGCTGAAGATCAGTTGGGTGCACGAGTGGGTTACATCGAACTGGATCTCAA
CAGCGGTAAGATCCTTGAGAGTTTTCGCCCCGAAGAACGTTTTCCAATGATGAGCACTTT 5040
TAAAGTTCTGCTATGTGGCGCGGTATTATCCCGTATTGACGCCGGGCAAGAGCAACTCGG
TCGCCGCATACACTATTCTCAGAATGACTTGGTTGAGTACTCACCAGTCACAGAAAAGCA
TCTTACGGATGGCATGACAGTAAGAGAATTATGCAGTGCTGCCATAACCATGAGTGATAA 5220
CACTGCGGCCAACTTACTTCTGACAACGATCGGAGGACCGAAGGAGCTAACCGCTTTTTT
GCACAACATGGGGGATCATGTAACTCGCCTTGATCGTTGGGAACCGGAGCTGAATGAAGC
CATACCAAACGACGAGCGTGACACCACGATGCCTGTAGCAATGGCAACAACGTTGCGCAA 5400
ACTATTAACTGGCGAACTACTTACTCTAGCTTCCCGGCAACAATTAATAGACTGGATGGA
GGCGGATAAAGTTGCAGGACCACTTCTGCGCTCGGCCCTTCCGGCTGGCTGGTTTATTGC
TGATAAATCTGGAGCCGGTGAGCGTGGGTCTCGCGGTATCATTGCAGCACTGGGGCCAGA 5580
TGGTAAGCCCTCCCGTATCGTAGTTATCTACACGACGGGGAGTCAGGCAACTATGGATGA
ACGAAATAGACAGATCGCTGAGATAGGTGCCTCACTGATTAAGCATTGGTAACTGTCAGA
CCAAGTTTACTCATATATACTTTAGATTGATTTAAAACTTCATTTTTAATTTAAAAGGAT 5760
CTAGGTGAAGATCCTTTTTGATAATCTCATGACCAAAATCCCTTAACGTGAGTTTTCGTT
CCACTGAGCGTCAGACCCCGTAGAAAAGATCAAAGGATCTTCTTGAGATCCTTTTTTTCT
GCGCGTAATCTGCTGCTTGCAAACAAAAAAACCACCGCTACCAGCGGTGGTTTGTTTGCC 5940
GGATCAAGAGCTACCAACTCTTTTTCCGAAGGTAACTGGCTTCAGCAGAGCGCAGATACC
AAATACTGTCCTTCTAGTGTAGCCGTAGTTAGGCCACCACTTCAAGAACTCTGTAGCACC
GCCTACATACCTCGCTCTGCTAATCCTGTTACCAGTGGCTGCTGCCAGTGGCGATAAGTC 6120
GTGTCTTACCGGGTTGGACTCAAGACGATAGTTACCGGATAAGGCGCAGCGGTCGGGCTG
AACGGGGGGTTCGTGCACACAGCCCAGCTTGGAGCGAACGACCTACACCGAACTGAGATA
CCTACAGCGTGAGCTATGAGAAAGCGCCACGCTTCCCGAAGGGAGAAAGGCGGACAGGTA 6300
TCCGGTAAGCGGCAGGGTCGGAACAGGAGAGCGCACGAGGGAGCTTCCAGGGGGAAACGC
CTGGTATCTTTATAGTCCTGTCGGGTTTCGCCACCTCTGACTTGAGCGTCGATTTTTGTG
ATGCTCGTCAGGGGGGCGGAGCCTATGGAAAAACGCCAGCAACGCGGCCTTTTTACGGTT 6480
CCTGGCCTTTTGCTGGCCTTTTGCTCACATGTC          6512
```

Figure 4.1. DNA sequence of plasmid pAAV/AChE. A signal peptide of 31 amino acids is followed by 583 amino acids of human AChE and 8 amino acids of the FLAG epitope. Two inverted terminal repeats (ITR) are underlined. The ITR are on each side of the human ACHE gene. The plasmid has a total of 6512 base pairs.

Virus preparation. rAAV virus was produced and purified using procedures established in Samulski's laboratory (Xiao et al., 1998; Haberman et al., 1999; Amiss and Samulski, 2001). Viral particles were prepared by adenovirus-free cotransfection of HEK293 cells with three plasmids: plasmid pAAV/AChE, plasmid pHelper (carrying adenovirus derived genes) and plasmid pAAV-RC (carrying AAV-2

replication and capsid genes). These three plasmids together supply all the trans-acting factors required for AAV replication and packaging in HEK293 cells. A kit from Stratagene includes the plasmids AAV-MCS, pHelper, and pAAV-RC (Stratagene, catalog #200314).

Cells were grown in twenty 15-cm dishes in 25 ml of DMEM/10% FBS per dish. Three hours before cotransfection, when cells were 70-80% confluent, the medium was replaced with Iscove's Modified Dulbecco's Medium (IMDM) containing 10% FBS to maintain a constant pH during transfection. Cells were cotransfected with 30 µg of DNA per plate (10 µg of each plasmid) by the calcium phosphate coprecipitation method. The IMDM/10% FBS was replaced with DMEM/2% FBS seven to eight hours after transfection. Incubation was continued for another 64 hours before medium and cells were harvested for purification of virus.

Purification of adenoassociated virus. Culture medium and cells were harvested 72 hours post-transfection (Amiss and Samulski, 2001). Virus was released from the cells by three cycles of freezing and thawing, and by sonication of cell debris. 500 ml of viral suspension was partially purified and concentrated by ammonium sulfate precipitation. 25 ml of viral suspension was overlayed on a cesium chloride gradient (Haberman et al., 1999) and centrifuged for 48 h at 288,000 x g (41,000 rpm in a Beckman SW-41 Ti rotor). The tube was punctured with a needle and 0.5 ml fractions collected. Fractions were frozen at –80˚C. After determination of viral titer by dot blot, the virus was desalted and concentrated in Amicon Ultra centrifugal filter device 100,000 molecular weight cut-off (catalog #UFC910002, Millipore Corp., Bedford, MA). The 1 ml of purified virus in phosphate buffered saline was aliquoted into 4 tubes and frozen at –80˚C. The desalted virus was titered for infectivity and expression of AChE enzyme activity.

A second batch of virus was produced and purified at the University of North Carolina Gene Therapy Center using the same pAAV/AChE plasmid. Virus was made by adenovirus-free triple cotransfection of HEK293 cells and purified by iodixanol gradient centrifugation followed by heparin column chromatography.

Viral titer. Two methods were used to determine viral titer. The dot blot method quantified viral DNA by hybridizing the dot blot with a P32 labeled probe for human ACHE and comparing the intensity of labeling against known quantities of plasmid pAAV/AChE.

A second method measured viral infectivity and AChE expression. HEK293 cells were plated in a 6-well plate in DMEM with 10% heat-inactivated FBS (Gibco #16140-071), at 3 ml culture medium per well. Heat-inactivated FBS was used because heat destroys the activity of bovine AChE in FBS. When cells were 70-80% confluent, they were infected with 1 to 10 µl of purified viral particles. Culture medium was harvested 23 hours later. Enzymatic AChE activity in the culture medium was measured by the Ellman (1961) method adapted to a 96-well plate. 10 µl of culture medium was assayed in 200 µl reaction mixture containing 0.1 M potassium phosphate pH 7.0, 0.5 mM DTNB, and 1 mM acetylthiocholine. The reaction was started by adding acetylthiocholine. Absorbance increase at 412 nm was read in a microtiter plate reader (Molecular Devices SpectraMax 190) for 20

minutes. The change in absorbance per min was converted to µmoles acetylthiocholine hydrolyzed per min by using the molar extinction coefficient 6,800 M^{-1} for the 0.5 cm pathlength. Units per ml of AChE activity were converted to µg AChE protein per ml using the specific activity of 5,200 units/mg for pure AChE (Rosenberry and Scoggin, 1984). Control assays measured AChE activity in culture medium from uninfected cells.

AChE knockout mice. Animal work was carried out in accordance with the Guide for the Care and Use of Laboratory Animals as adopted by the National Institutes of Health. Mice with no AChE activity in any tissue were the subjects for gene therapy trials. AChE-/- mice were made by gene-targeting (Xie et al., 2000) and raised to adulthood on a liquid diet of Ensure (Duysen et al., 2002). AChE-/- mice do not breed. Therefore, the colony is maintained by breeding heterozygotes. The AChE-/- mice have a strain 129Sv genetic background. Mice of both sexes were treated with rAAV/AChE. 12 adult (2 to 3 months old) AChE -/- were injected intramuscularly. 16 newborns (6 AChE -/-, 4 AChE +/-, and 6 AChE +/+) were injected subcutaneously. 6 young (17-29 days old) AChE -/-mice were injected in the brain.

AAV delivery. 50 µl of rAAV/AChE virus (titer 540 µg AChE/ml in the infectivity-expression assay) was injected into each hind leg tibialis anterior muscle of adult AChE-/- mice, for a total of 100 µl virus per mouse. 10 µl of rAAV/AChE (UNC) virus (titer 20 µg AChE/ml) was injected subcutaneously into newborn mice. Animals were genotyped by PCR using DNA from tail snips as template (Duysen et al., 2002). 2.5 µl of rAAV/AChE virus (titer 540 µg AChE/ml) was injected into each side of the striatum for a total of 5 µl virus per mouse. The AChE -/- mice for striatal injection were 17-29 days old.

Collection of blood. Blood samples were collected from the Saphenous vein in the hind leg into heparinized capillary tubes. Plasma was separated from red blood cells by centrifugation.

Tissue extraction. 3 adult mice were euthanized 3 days after being injected with rAAV/AChE. Mice were perfused transcardially with phosphate buffered saline to wash out the blood. Perfused tissues were homogenized in 10 volumes of ice-cold 50 mM potassium phosphate pH 7.4, 0.5% Tween 20 in a Polytron (Brinkmann Instruments) for 10 seconds. Cell debris was removed by centrifugation at 12,000 rpm in a microfuge at 4°C. Plasma and tissue extracts were assayed for AChE activity.

Ellman assay for AChE activity. 4 µl plasma was preincubated with 50 µM bambuterol in 2 ml of 0.1 M potassium phosphate pH 7.0, 0.5 mM DTNB for 20 min to inhibit butyrylcholinesterase (BChE). Bambuterol hydrochloride was a gift from Dr. Leif Svensson, Astra Draco, Lund, Sweden. Assay of AChE activity was begun by adding acetylthiocholine to a final concentration of 1 mM. Units of activity are µmoles acetylthiocholine hydrolyzed per min. Units of activity were calculated using the extinction coefficient 13,600 M^{-1} cm^{-1}.

Radiometric assay for AChE activity. The Johnson and Russell (1975) method was used. 5 µl of plasma diluted to 80.5 µl with phosphate buffer, or 80.5 µl of tissue extract was preincubated with 0.5 µM bambuterol for 30 min to inhibit BChE activity. This resulted in 97% inhibition of BChE activity. The reaction was started by adding C14-acetylcholine to a final concentration of 1 mM. Each reaction contained 0.05 microCuries (Catalog #1711103, ICN Radiochemicals, Costa Mesa, CA) in a total volume of 0.1 ml. The reaction was stopped after 50 minutes by adding 0.1 ml of stopping mixture that brought the pH to 2.5. The ^{14}C –acetate was extracted into 4 ml of scintillation cocktail and counted. The scintillation cocktail was prepared by mixing 8 ml of rpi scintillator (#111023 ppo-dimethyl-popop concentrated liquid scintillator, Research Products International, Mount Prospect, IL) with 33.3 ml of iso-amyl alcohol and 159 ml toluene.

A set of positive and negative controls was included in each assay. The positive controls were 1, 5, and 10 µl of wild-type plasma (n=4). The negative control was 5 µl of plasma from untreated AChE -/- mice (n=5).

Activity stained gel to visualize AChE. Nondenaturing 0.75 mm thick, 4-30% gradient polyacrylamide gels were prepared in a Hoefer apparatus. 3 µl plasma was treated with 1 mM iso-OMPA for 60 min before being loaded on the gel. Iso-OMPA is a specific BChE inhibitor. The upper buffer contained 600 ml of 0.021 M Tris base, 0.023 M glycine pH 9.0; the lower buffer contained 4.5 L of 0.06 M TrisCl pH 8.1. Electrophoresis was at 4˚C constant voltage for 4000 volt hours. Gels were stained for AChE activity by the method of Karnovsky and Roots (1961) in the presence of 1.7 mM acetylthiocholine.

Antibody detection. To detect serum antibodies reactive with human AChE, an enzyme-linked immunosorbent assay (ELISA) was performed using Nunc-Immuno Module (Nalge Nunc International) immunoassay plates coated with purified human AChE. Each well of a 96-well plate was coated with 1 µg of purified human AChE diluted to 200 µl with buffer. Human AChE was produced by expression of AChE in CHO cells. The secreted AChE was purified from culture medium on procainamide-Sepharose affinity gel. Plates were blocked with phosphate buffered saline, 0.05% Tween-20 overnight at 4˚C. 2 µl and 4 µl of mouse plasma or tissue extract diluted to 200 µl were added to each well and incubated for 3 hours at room temperature. Plates were washed three times with phosphate buffered saline, 0.05% Tween-20 and then incubated with goat anti-mouse IgG conjugated to horse radish peroxidase (1:2000 dilution) overnight at 4˚C. Plates were washed three times with phosphate buffered saline, 0.05% Tween-20 and then developed to reveal bound horseradish peroxidase. 0.4 mg/ml o-phenylenediamine dihydrochloride (Sigma) was dissolved in 0.05 M phosphate-citrate pH 5.0. Immediately before use, 10 ml of the 0.4 mg/ml substrate solution was mixed with 4 µl of 30% H_2O_2. 200 µl of this mixture was added to each well. After 5 minutes, the reaction was stopped by adding 50 µl of 3 M H_2SO_4. The absorbance at 492 nm was read on a microtiter plate reader.

Positive control antibodies were Mab304 (Chemicon International, Inc., Temecula, CA), a monoclonal generated against human red cell AChE (Fambrough et al, 1982) and Mab123 a gift from Dr. Steven Brimijoin, Mayo clinic, raised against human red cell AChE (Brimijoin et al., 1983). Positive control antibodies were diluted 1:100 – 1:2500. Negative controls included 200 µl of diluted plasma from uninjected AChE -/- mice, 200 µl from uninjected wild-type mice, 200 µl of phosphate buffered saline containing 0.05% Tween-20, and uncoated wells.

Results

Comparison of viral titer by two methods. Virus prepared in our laboratory, rAAV/AChE, and by the core facility at the University of North Carolina, rAAV/AChE (UNC) was titered by dot blot and by viral infectivity. The rAAV/AChE had a titer of 3 x 10^9 viral particles per ml in the dot blot assay and produced 510 µg AChE/ml in the infection assay. The value 510 µg AChE/ml was calculated from the experimental observation that 1 x 10^6 viral particles expressed 0.17 µg AChE in 3 ml culture medium in 23 hours. The rAAV/AChE(UNC) had a titer of 1 x 10^{12} viral particles per ml in the dot blot assay and produced 20 µg AChE/ml in the infection assay. The value of 20 µg AChE/ml was calculated from the observation that 1 x 10^6 viral particles expressed 0.0.00002 µg AChE in 3 ml culture medium in 23 hours. The rAAV/AChE expressed 8,500 times more AChE protein per viral particle than the rAAV/AChE (UNC). This result shows that the dot blot viral titer was not a reliable predictor of AChE expression. We used the dot blot method to identify virus-containing fractions when samples contained cesium chloride. We used infection of HEK293 cells and expression of AChE activity to quantify the desalted virus.

4.1. Adult AChE -/- mice treated with virus intramuscularly

Virally expressed human AChE in plasma of adult AChE -/-. 12 adult AChE -/- mice (2-3 months old) were injected i.m. with 100 µl of rAAV/AChE. The viral titer was 510 µg AChE per ml, as measured in the infectivity and expression assay. Two animals died of convulsions 2 and 15 days after injection. Convulsions and seizures are a common occurrence in AChE knockout mice and are the major cause of death in these animals.

Blood was collected on days 3, 6, 9, 14, and 30 post-injection from 7 animals and on day 150 from 2 animals. The plasma was tested for AChE activity in the Ellman assay. Figure 4.2 shows that AChE -/- plasma had no AChE activity before injection of virus but acquired 0.27±0.16 units/ml of AChE activity on day 3 after rAAV/AChE delivery. This level of AChE activity is 47% of the activity in wild-type mouse plasma. Wild-type mice have 0.57±0.06 units/ml AChE activity in plasma. AChE activity dropped significantly by day 6 to 0.039 units/ml and persisted unchanged for 30 days. Two mice tested on day 150 were found to express this

same low level of AChE, suggesting that the virus continued expressing AChE for at least 150 days.
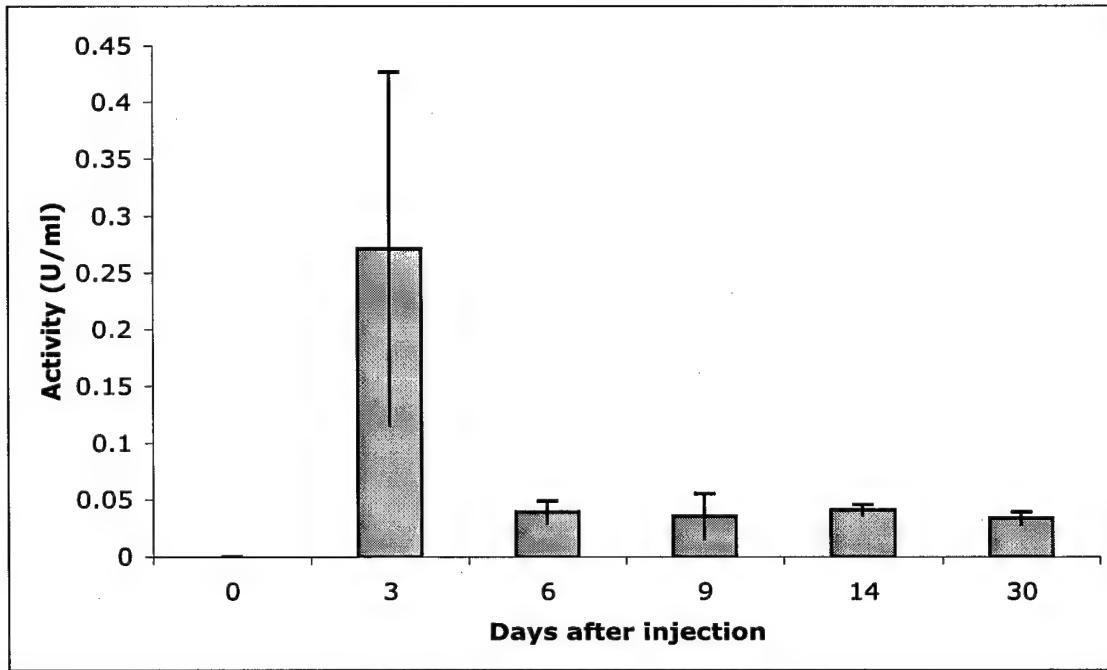
Figure 4.2. AChE activity in plasma of AChE -/- mice after rAAV/AChE delivery i.m. Plasma from 7 adult AChE -/- mice was tested for AChE activity in the Ellman assay. Day 0 values show zero AChE activity. The residual rate of hydrolysis of acetylthiocholine by BChE has been subtracted.

The presence of AChE activity in plasma of AChE -/- mice treated with rAAV/AChE was confirmed by Karnovsky and Roots activity staining of a nondenaturing polyacrylamide gel. The gel (Figure 4.3) separates AChE from BChE and therefore makes clear that the acetylthiocholine hydrolysis activity comes from the virally expressed AChE and not from BChE. The AChE -/- mouse has no AChE activity, so all AChE activity must have come from the gene therapy vector.

The finding of tetramers of AChE in the virus-treated knockout mice shows that the virally expressed human AChE assembled into tetramers. No exogenous administration of a polyproline rich peptide was required to get assembly into tetramers.
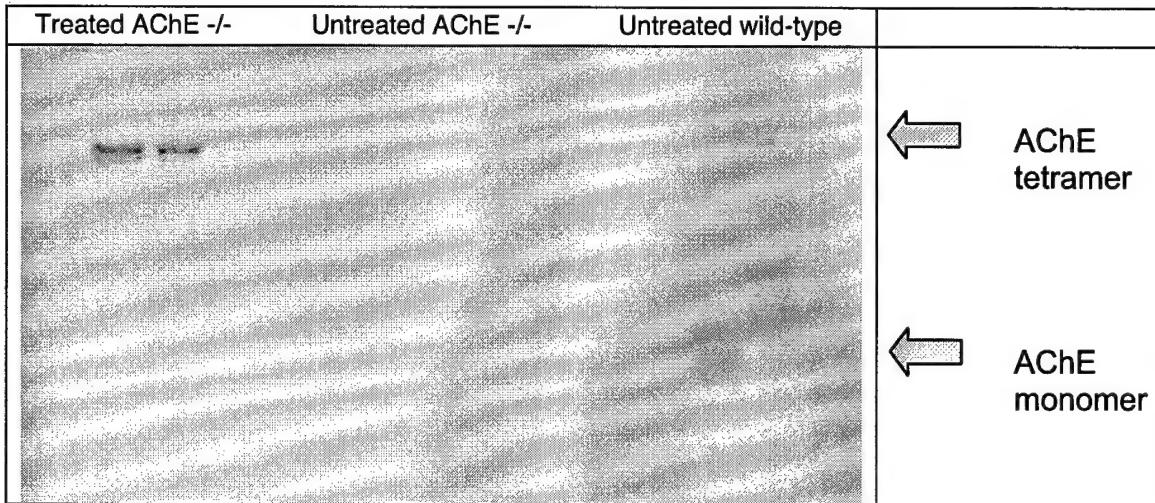
Figure 4.3. Nondenaturing gel to show AChE activity in virus-treated AChE -/- mice. Plasma from 2 AChE -/- mice treated with rAAV/AChE, 3 untreated AChE -/- mice, and 2 untreated wild-type mice was subjected to gel electrophoreses to separate AChE from BChE. The BChE activity was inhibited with iso-OMPA. AChE tetramers were visible in plasma of virus-treated AChE -/- mice and in untreated wild-type mice. No AChE activity was present in untreated AChE -/- mice. Wild-type mice had monomers and tetramers of AChE.

Virally expressed human AChE in tissues. Three of the 12 adult AChE -/- mice treated with rAAV/AChE and 3 uninjected AChE -/- mice were euthanized on day 3 post-injection. Tissue extracts from perfused mice were tested for AChE activity with the radiometric assay. Figure 4.4 shows that AChE activity was higher in heart, intestine, kidney, liver, spleen and stomach of mice that had been treated with virus, compared to untreated controls. However, the error bars are large due to the small number of animals tested, and the differences are statistically significant only for kidney, spleen, and stomach.
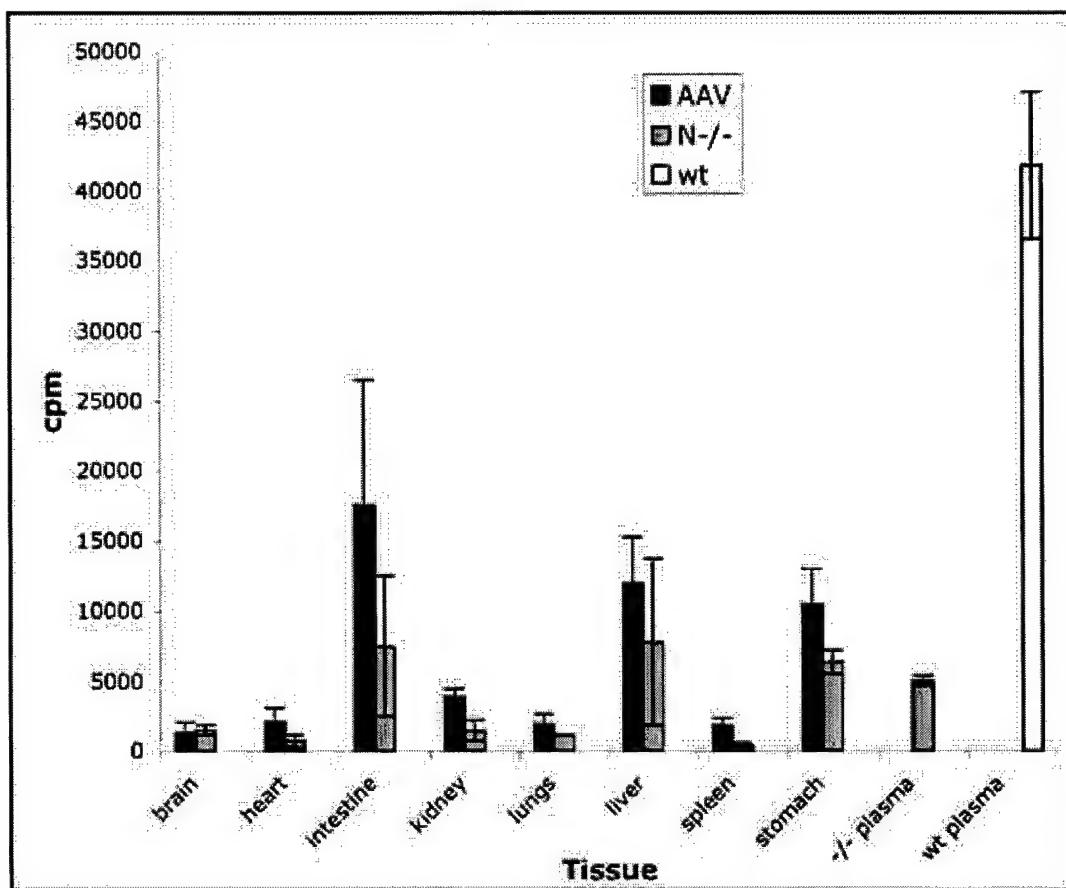
Figure 4.4. AChE activity in tissues of AChE -/- mice, 3 days after i.m. delivery of rAAV-AChE into adult mice. Black boxes are for AChE -/- mice treated with virus (n=3). Gray boxes are for untreated AChE -/- mice (n=3). Each 100 µl reaction contained 80.5 µl of tissue extract; since the tissues had been extracted in 10 volumes of buffer, 80.5 µl represents 8 µg tissue. The negative control is 5 µl of plasma from AChE -/- mice (n=5). The positive control is 1 µl of plasma from wild-type mice (n=4).

AChE -/- mice have no AChE activity in any tissue (Xie et al., 2000; Li et al., 2000). The C14-acetylcholine hydrolyzed by untreated AChE -/- tissues represents activity of residual BChE that was not inhibited by 0.5 µM bambuterol.

Production of antibodies against human AChE. Expression of AChE activity in plasma was found to be highest on day 3 post-injection and to decrease thereafter. The decrease in the level of human AChE activity led us to test the possibility that the AChE -/- mouse had produced antibodies against human AChE. Mice were bled on days 0, 3, 6, 10, 14, and 30 post-injection and the plasma was tested for the

presence of anti-human AChE antibodies. The ELISA assay results in Figure 4.5
show that antibody against human AChE was not present on day 0, but was present
on all other days tested.   The antibody level increased with time, suggesting that
AChE continued to be expressed and continued to stimulate the immune system for
at least 30 days after injection of adenoassociated virus. The presence of antibodies
to human AChE explains the low level of AChE activity in virus-treated mice.
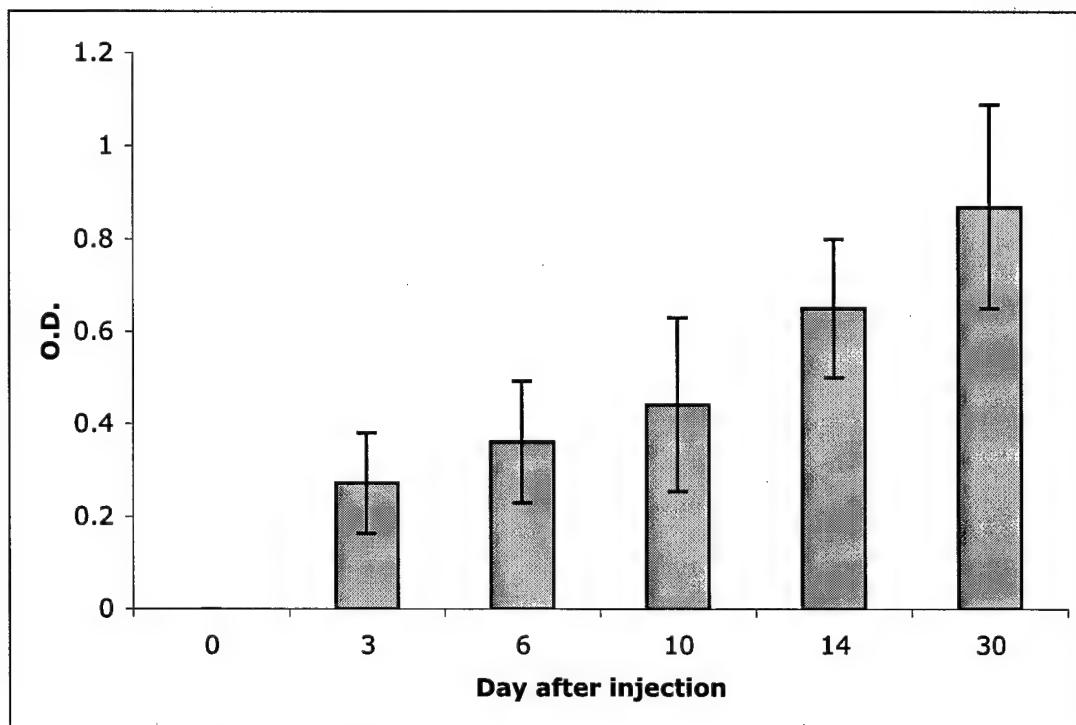
**Figure 4.5. Antibody against human AChE after i.m delivery of virus into adult
AChE -/- mice**. Plasma from 7 adult AChE -/- mice injected with rAAV/AChE was
tested for the presence of anti-human AChE antibodies by ELISA.

Two adult AChE +/- mice were injected with virus i.m. to see whether having
endogenous mouse AChE would prevent an immune response to human AChE.
Mice were bled on day 5 post-injection and tested for anti-human AChE antibody
and for AChE activity. The adult AChE +/- mice did form antibodies against human
AChE. No increase in AChE activity was found in the Ellman assay.

No effect on phenotype. The adenoassociated virus injected into adult AChE -/-
mice had no effect on phenotype. The mice continued to show whole body tremor,
abnormal body posture, splayed hind legs, twitching hind legs when the mouse was
held by the investigator, and inability to eat solid food. No changes in the rate of
gain in body weight, and no changes in body temperature were found. They still
vocalized during cage changing. Their climbing and rearing activity continued to be

lower than in normal littermates. They did not acquire grip strength, but fell off an inverted screen within seconds. They still died of seizures. Out of the 12 adult AChE -/- mice that received the virus, 4 have died of seizures. Three were euthanized for measurement of AChE expression in tissues and 5 are still alive at 120 to 180 days post-injection.

4.2. Newborn mice treated with virus subcutaneously

In vivo delivery of virus into newborn mice. In an attempt to avoid the immune reaction seen in adult mice, we decided to inject very young animals with the virus. All newborn mice in 3 litters were injected s.c. with rAAV/AChE (UNC). Of the 16 newborn mice, 6 had the AChE -/- genotype, 4 were AChE +/-, and 6 were AChE +/+. Two of the injected AChE -/- mice were neglected or killed by the parent mouse within one day. This is a normal response to handling of neonates. Two AChE -/- mice died on days 20 and 25 from convulsions. 12 mice are still alive 60 days post-injection.

Antibody to AChE. Mice injected with rAAV/AChE (UNC) when they were newly born were bled on day 30-40 post-injection and tested for antibodies to human AChE. A low level of antibody was detected in all plasma samples. This test result was ambiguous and needs to be repeated.

AChE activity. No AChE activity was detected in the blood on day 30 post-injection for the 4 AChE -/- mice that had received virus as newborns. However, the 6 wild-type and 4 AChE +/- mice had higher than normal AChE activity in their plasma.

Phenotype. Newborns treated with virus were observed for changes in weight. Duysen et al. (2002) had previously shown that AChE -/- mice were smaller than their littermates and that their small body size correlated with a slower rate of growth. We wanted to know whether treatment with rAAV/AChE would increase the weight of animals. Figure 4.6 shows that weight gain was unaffected by the virus. Treated AChE -/- and untreated AChE -/- had the same pattern of weight gain. Similarly, AChE +/+ and +/- mice had the same pattern of weight gain regardless of their treatment status (data not shown).

Duysen et al (2002) had shown that AChE -/- mice were slow to learn to regulate their body temperature. At postnatal day 15 wild-type mice no longer needed the warmth of a nest because they adjusted their body temperature to maintain a constant 37° C. However, AChE -/- mice had to be kept on heating pads from postnatal day 15 to 21 because of their low body temperature. It was of interest to determine whether the adenoassociated virus affected body temperature. Figures 4.7 shows no difference in body temperature between untreated and virus treated AChE -/- mice.
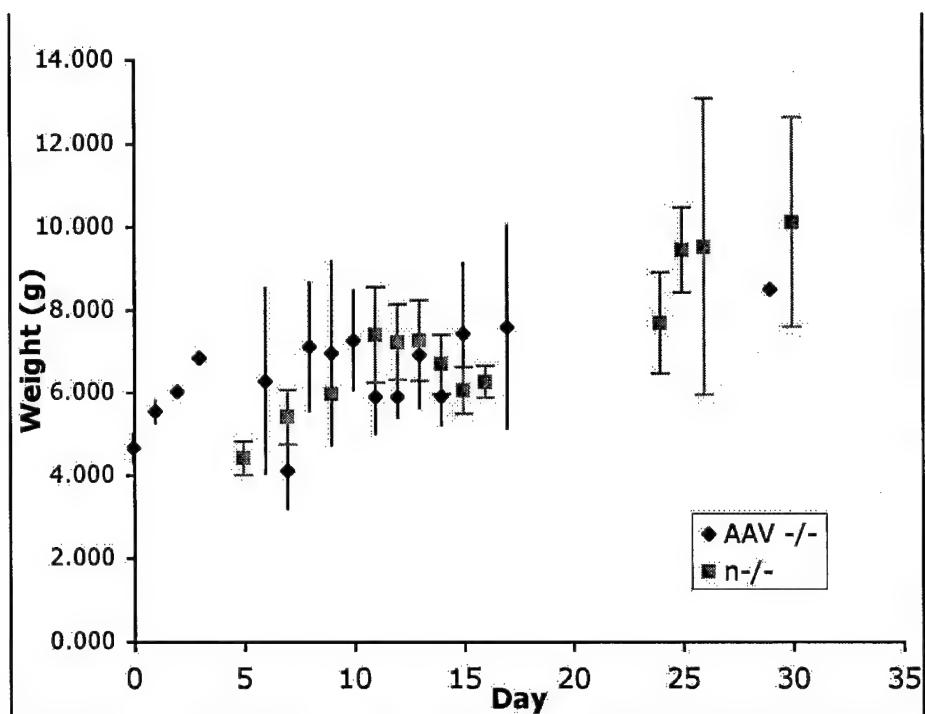
Figure 4.6. Weight increase in AChE -/- mice treated with virus on the day of birth. Newborn mice (4 AChE -/-) received 10 µl rAAV/AChE (UNC) s.c. on day 0. Weights for the 4 treated and 15 untreated AChE -/- mice are shown. There is no difference in the pattern of weight gain for the two groups.
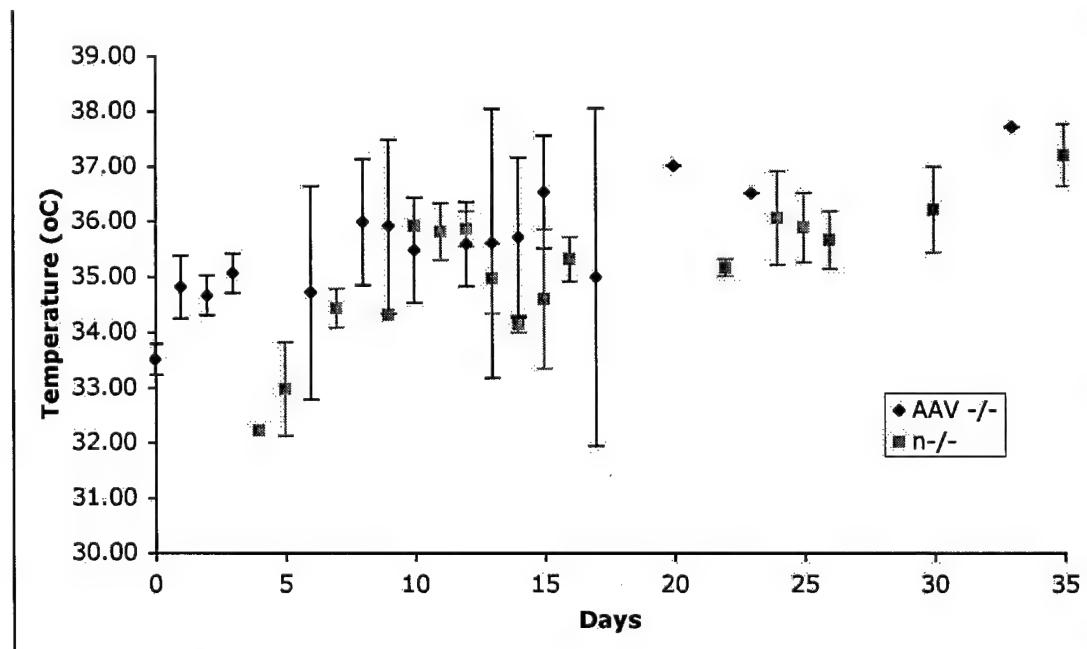
Figures 4.7. Thermoregulation in mice treated with virus on the day of birth. The same mice weighed in Figures 4.6 were measured for surface body temperature.

Newborn mice treated with virus developed in the same way as untreated mice (Duysen et al., 2002). The presence of virus did not change the phenotype. Weight drop on postnatal day 14 still occurred in AChE -/- mice. AChE -/- mice had tremor, abnormal body posture, splayed feet, tail dragging on the floor, and absence of grip strength.

4.3 Young AChE -/- mice treated with virus intrastriatally

Injection site. The brain was selected to receive rAAV/AChE for two reasons: to avoid antibody production, and to increase the possibility that treatment with virus would improve the phenotype of AChE -/- mice. The striatum has the highest number of cholinergic neurons in the brain, suggesting that this region would benefit most from expression of AChE. The striatum is involved in movement coordination, body posture, and tremor. Absence of AChE in AChE -/- mice causes problems with movement coordination, body posture and tremor. It was hoped that expression of AChE would have a positive effect on these behaviors.

Mice. 6 AChE -/- mice (ages 17, 17, 19, 19, 20, 29 days) and 1 wild-type mouse (age 27 days) were anesthetized with 20-30 µl/g Avertin i.p. Some animals required isoflurane inhalation because the depth of anesthesia as determined by the tail pinch test was inadequate with Avertin alone. The striatum was injected bilaterally with 2.5 µl of rAAV/AChE (titer 540 µg AChE/ml). The striatum of an additional 4 AChE -/- mice (all 20 days old) was injected with phosphate buffered saline. Mice completely recovered from anesthesia within one hour. During the recovery period they were placed on a heating pad. They were placed in cages and fed their usual diet of liquid Ensure. Mice were weighed and their temperature measured daily after surgery to make sure there was no infection.

Phenotype change. The inverted screen test was used to measure muscle coordination. Mice were placed on the screen when the screen was in a horizontal position. Then the screen was rotated 90° and the time the mice remained on the screen was measured. The test was videotaped to facilitate measurement of time. Each mouse was tested three times per session on days 3, 14, 19 and 28 after virus injection. The longest time was chosen.

On day 3 post-injection one mouse out of six stayed on the screen for 24 seconds. The others fell off in about 4 seconds. On day 14 post-injection 3 out of 5 mice stayed on the screen longer than 20 seconds (23, 37, 44 sec). The maximum time for the PBS injected mice was 7 sec. The 6th mouse was not tested because it died of convulsions on day 12 post-injection.

On day 19 post-injection 3 mice out of 5 stayed on the screen longer than 20 seconds (30, 33, 60 sec). The maximum time for the PBS injected mice was 10 sec. On day 28 post-injection all 5 mice stayed on the screen at least 20 sec (20, 23, 28, 33, 45 sec). The maximum for PBS injected mice was 15 sec.

The wild-type mouse stayed on the screen indefinitely. Intrastriatal injection of virus had no deleterious effect on its muscle coordination.

No other phenotype changes were found.

No antibody production. Plasma was collected from animals on days 19 and 20 after intrastriatal injection. None of the plasma samples had antibodies to human AChE.

No AChE activity in plasma. The same plasma samples that were tested for antibodies were also tested for AChE activity. None of the samples had AChE activity.

AChE activity in brain. One AChE -/- mouse that had been injected intrastriatally was perfused with PBS, and 4% paraformaldehyde and its brain sectioned with a cryostat. Sections were stained for AChE activity. AChE activity was found near the needle track in the striatum.

Discussion

This is the first gene therapy vector and gene therapy protocol to report expression of human AChE. Adenoassociated virus gave long-term expression of human AChE, up to 5 months. The activity of AChE in treated AChE -/- mice reached 50% of the endogenous level in wild-type mouse plasma. This level of expression is expected to provide protection against nerve agent toxicity, though toxicity studies have not yet begun. Since adenoassociated virus is an FDA approved vector for gene therapy in humans, it can be anticipated that use of this vector will be safe in humans.

Antibodies against human AChE were produced in virus-treated AChE -/- mice. Antibodies cleared a large percentage, but not all, of the human AChE from the blood of AChE -/- mice. No humans have been found to date that are deficient in AChE. Therefore humans are not expected to form antibodies against the human AChE expressed by adenoassociated virus.

We plan to make an adenoassociated virus that expresses mouse AChE. Expression of mouse AChE in mice is expected to prevent clearance of AChE by antibodies, and therefore to maintain a high level of expression of AChE for several months.

Key Research Accomplishments
• Stable transgenic mouse lines expressing a mutant form of human butyrylcholinesterase, G117H, have been made. One of these transgenic lines has been tested for resistance to the organophosphorus anti-glaucoma drug, echothiophate. It was found that the G117H mice are resistant to toxicity. A dose of echothiophate that kills wild-type mice, gives only very mild signs of toxicity in the transgenic animals.

• A gene therapy vector expressing human acetylcholinesterase has been constructed and tested in mice. Adenoassociated virus was selected as a vector because it gives expression in nondividing cells, it has no known deleterious effects in humans, and it continues to express the desired protein for long periods of time. Mice that have no acetylcholinesterase were tested first. Human AChE was found in their blood on day three after intramuscular delivery of the virus. The AChE activity was about 50% of that in uninjected wild-type mice. AChE activity levels decreased with time because of clearance by antibodies.

Reportable Outcomes
Published manuscript
Boeck AT, Schopfer LM, Lockridge O (2002) DNA sequence of butyrylcholinesterase from rat; expression of the protein and characterization of the properties of rat butyrylcholinesterase. Biochem Pharmacol 63: 2101-2110

Duysen EG, Fry DL, Lockridge O (2002) Early weaning and culling eradicated Helicobacter hepaticus from an acetylcholinesterase knockout 129S6/SvEvTac mouse colony. Comp Med 52: 461-466

Li B, Duysen EG, Volpicelli LA, Levey AI, Lockridge O (2003) Regulation of muscarinic acetylcholine receptor function in acetylcholinesterase knockout mice. Pharmacology, Biochemistry, and Behavior 74: 977-986

Volpicelli-Daley LA, Duysen EG, Lockridge O, Levey AI (2003) Altered hippocampal muscarinic receptors in acetylcholinesterase-deficient mice. Ann Neurol 53:788-96

Bernard V, Brana C, Liste I, Lockridge O, Bloch B (2003) Dramatic depletion of cell surface m2 muscarinic receptor due to limited delivery from intracytoplasmic stores in neurons of acetylcholinesterase-deficient mice. Mol Cell Neurosci 23:121-33

Nachon F, Masson P, Nicolet Y, Lockridge O, Fontecilla-Camps JC (2003) Comparison of the structures of butyrylcholinesterase and acetylcholinesterase. Chapter 4 in "Butyrylcholinesterase Its Function and Inhibitors" (Editor Ezio Giacobini). Martin Dunitz, London, p39-54

Lockridge O, Duysen EG, Li B (2003) Butyrylcholinesterase function in the acetylcholinesterase knockout mouse. Chapter 2 in "Butyrylcholinesterase Its Function and Inhibitors" (Editor Ezio Giacobini) Martin Dunitz, London, p21-28

Abstracts
Bytyqi A, Paraoanu L, Lockridge O, Duysen E, Layer P (2002) Early distortion of network formation in the inner retina of an AChE knockout mouse. Seventh International Meeting on Cholinesterases, November 8-12, 2002, Chile.

Bytyqi AH, Duysen EG, Lockridge O, Layer P (2002) Complete postnatal degeneration of the photoreceptor layer in an AChE knockout mouse. Seventh International Meeting on Cholinesterases, November 8-12, 2002, Chile.

Nachon F, Lockridge O, Nicolet Y, Fontecilla-Camps JC, Masson P (2002) X-ray structure of native and soman-aged human butyrylcholinesterase. NATO TG004 Meeting in Oslo, Norway, November 2002.

Nachon F, Nicolet Y, Masson P, Lockridge O, Fontecilla-Camps JC (2002) How do the crystal structures of human butyrylcholinesterase compare to Torpedo Californica acetylcholinesterase structures? Seventh International Meeting on Cholinesterases, November 8-12, 2002, Chile.

Hrabovska A, Lockridge O (2002) Acetylcholinesterase wild-type and knock-out mice show different locomotor activity after scopolamine injection. Seventh International Meeting on Cholinesterases, November 8-12, 2002, Chile.

Duysen EG, Kolar CH, Lockridge O. H. hepaticus infection in acetylcholinesterase knockout mice results in severe intestinal distension. Seventh International Meeting on Cholinesterases, November 8-12, 2002, Chile.

Li B, Duysen EG, Lockridge O. Acetylcholinesterase knockout mice are resistant to oxotremorine-induced hypothermia and pilocarpine-induced seizures. Seventh International Meeting on Cholinesterases, November 8-12, 2002, Chile.

Nicolet Y, Lockridge O, Masson P, Fontecilla-Camps JC, Nachon F. Crystallographic basis for substrate/product exchange in cholinesterases. Seventh International Meeting on Cholinesterases, November 8-12, 2002, Chile.

New reagents and animals created for this project

• A monoclonal antibody to human butyrylcholinesterase that recognizes denatured as well as folded enzyme
• Transgenic mice resistant to organophosphorus toxicants
• Adenoassociated virus that expresses human acetylcholinesterase
• A human butyrylcholinesterase gene made up entirely of codons preferred by bacteria

Conclusions. Summary of results to include the implications of the research.
Our goal is to provide new therapeutics, in the form of genes and proteins, for protection against organophosphorus nerve agents.

- o The transgenic G117H mouse is resistant to OP toxicity.
  - ▪ This shows that the right gene introduced into random positions in the chromosome provides protection.
  - ▪ The protection is life-long because the gene is a stable component of the genetic make-up of the animal.
  - ▪ Relatively low levels of G117H BChE provide protection.
  - ▪ These results imply that humans could be protected from nerve agent toxicity by gene therapy with G117H butyrylcholinesterase.
- o Gene therapy with adenoassociated virus results in expression of human AChE
  - ▪ Expression of human AChE is prolonged, continuing for at least 6

months.

- The maximum level of expression of human AChE in mouse plasma is about 50% of the level of endogenous mouse AChE.
- Antibodies against human AChE decreased the level of active human AChE in mouse blood.
- These results imply that a gene therapy vector could be used in humans to deliver acetylcholinesterase to provide protection against nerve agent toxicity.

References

Abu-Amer Y, Dowdy SF, Ross FP, Clohisy JC, Teitelbaum SL. TAT fusion proteins containing tyrosine 42-deleted IκBα arrest osteoclastogenesis. J Biol Chem 276: 30499-30503 (2001)

Allon N, Raveh L, Gilat E, Cohen E, Grunwald J, Ashani Y. Prophylaxis against soman inhalation toxicity in guinea pigs by pretreatment alone with human serum butyrylcholinesterase. Toxicol Sci 43: 121-128 (1998)

Altamirano CV, Lockridge O. Conserved aromatic residues of the C-terminus of human butyrylcholinesterase mediate the association of tetramers. Biochemistry 38: 13414-13422 (1999)

Amiss TJ, Samulski RJ. Methods for adeno-associated virus-mediated gene transfer into muscle. Methods Molec Biol 175: 455-469 (2001)

Angus LM, Chan RYY, Jasmin BJ. Role of intronic E- and N-box motifs in the transcriptional induction of the acetylcholinesterase gene during myogenic differentiation. J Biol Chem 276: 17603-17609 (2001)

Ashani Y, Shapira S, Levy D, Wolfe AD, Doctor BP, Raveh L. Butyrylcholinesterase and acetylcholinesterase prophylaxis against soman poisoning in mice. Biochem Pharmacol 41: 37-41 (1991)

Awatramani R, Soriano P, Mai JJ, Dymecki S. An Flp indicator mouse expressing alkaline phosphatase from the ROSA26 locus. Nature Genetics 29: 257-259 (2001)

Beeri R, Gnatt A, Lapidot-Lifson Y, Ginzberg D, Shani M, Soreq H, Zakut H. Testicular amplification and impaired transmission of human butyrylcholinesterase cDNA in transgenic mice. Hum Reprod 9: 284-292 (1994)

Blatter Garin MC, Abbott C, Messmer S, Mackness M, Durrington P, Pometta D, James RW. Quantification of humans serum paraoxonase by enzyme-linked immunoassay: population differences in protein concentrations. Biochem J 304: 549-554 (1994)

Bon S, Massoulié J. Quaternary associations of acetylcholinesterase. Oligomeric associations of T subunits with and without the amino-terminal domain of the collagen tail. J Biol Chem 272: 3007-3015 (1997)

Bon S, Coussen F, Massoulié J. Quaternary associations of acetylcholinesterase. II. The polyproline attachment domain of the collagen tail. J Biol Chem 272: 3016-3021 (1997)

Brandeis R, Raveh L, Grunwald J, Cohen E, Ashani Y. Prevention of soman-induced cognitive deficits by pretreatment with human butyrylcholinesterase in rats. Pharmacol Biochem Behav 46: 889-896 (1993)

Brimijoin S, Mintz KP, Alley MC. Production and characterization of separate monoclonal antibodies to human acetylcholinesterase and butyrylcholinesterase. Mol Pharmacol 24: 513-520 (1983)

Broomfield CA, Maxwell DM, Solana RP, Castro CA, Finger AV, Lenz DE. Protection by butyrylcholinesterase against organophosphorus poisoning in nonhuman primates. J Pharmacol Exp Ther 259: 633-638 (1991)

Cao G, Pei W, Ge H, Liang Q, Luo Y, Sharp FR, Lu A, Ran R, Graham SH, Chen J. In vivo delivery of a Bcl-xL fusion protein containing the TAT protein transduction domain protects against ischemic brain injury and neuronal apoptosis. J Neurosci 22: 5423-5431 (2002)

Cashman SM, Morris DJ, Kumar-Singh R. Evidence of protein transduction but not intercellular transport by proteins fused to HIV Tat in retinal cell culture and in vivo. Mol Ther 8: 130-142 (2003)

Castro CA, Gresham VC, Finger AV, Maxwell DM, Solana RP, Lenz DE, Broomfield CA. Behavioral decrements persist in Rhesus monkeys trained on a serial probe recognition task despite protection against soman lethality by butyrylcholinesterase. Neurotoxicol Teratol 16: 145-148 (1994)

Chan RY, Boudreau-Lariviere C, Angus LM, Mankal FA, Jasmin BJ. An intronic enhancer containing an N-box motif is required for synapse- and tissue-specific expression of the acetylcholinesterase gene in skeletal muscle fibers. Proc Natl Acad Sci USA 96: 4627-4632 (1999)

Choi T, Huang M, Gorman C, Jaenisch R. A generic intron increases gene expression in transgenic mice. Mol Cell Biol 11: 3070-3074 (1991)

Console S, Marty C, Garcia-Echeverria C, Schwendener R, Ballmer-Hofer K. antennapedia and HIV transactivator of transcription (TAT) "Protein Transduction Domains" promote endocytosis of high molecular weight cargo upon binding to cell surface glycosaminoglycans. J Biol Chem 278: 35109-35114 (2003)

Delbrück A, Henkel E. A rare genetically determined variant of pseudocholinesterase in two German families with high plasma enzyme activity. Eur J Biochem 99: 65-69 (1979)

Dietz GPH, Kilic E, Bähr M. Inhibition of neuronal apoptosis in vitro and in vivo using TAT-mediated protein transduction. Molec Cell Neurosci 21: 29-37 (2002)

Doctor BP, Raveh L, Wolfe AD, Maxwell DM, Ashani Y. Enzymes as pretreatment drugs for organophosphate toxicity. Neurosci Biobehavioral Review 15: 123-128 (1991)

Duysen EG, Li B, Xie W, Schopfer LM, Anderson RS, Broomfield CA, Lockridge O. Evidence for nonacetylcholinesterase targets of organophosphorus nerve agent: supersensitivity of acetylcholinesterase knockout mouse to VX lethality. J Pharmacol Exp Ther 299: 528-535 (2001)

Duysen EG, Stribley JA, Fry DL, Hinrichs S, Lockridge O. Rescue of the acetylcholinesterase knockout mouse by feeding a liquid diet; phenotype of the adult acetylcholinesterase deficient mouse. Brain Res Dev Brain Res 137: 43-54 (2002)

Elliger SS, Elliger CA, Lang C, Watson GL. Enhanced secretion and uptake of β-glucuronidase improves adeno-associated viral-mediated gene therapy of mucopolysaccharidosis type VII mice. Mol Ther 5: 617-626 (2002)

Ellman GL, Courtney KD, Andres V Jr, Featherstone RM. A new and rapid colorimetric determination of acetylcholinesterase activity. Biochem Pharmacol 7: 88-95 (1961)

Embury J, Klein D, Pileggi A, Ribeiro M, Jayaraman S, Molano RD, Fraker C, Kenyon N, Ricordi C, Inverardi L, Pastori RL. Proteins linked to a protein transduction domain efficiently transduce pancreatic islets. Diabetes 50: 1706-1713 (2001)

Falnes PO, Wesche J, Olsnes S. Ability of the Tat basic domain and VP22 to mediate cell binding, but not membrane translocation of the diphtheria toxin A-fragment. Biochemistry 40: 4349-4358 (2001)

Fambrough DM, Engel AG, Rosenberry TL. Acetylcholinesterase of human erythrocytes and neuromuscular junctions: homologies revealed by monoclonal antibodies. Proc Natl Acad Sci USA 79: 1078-1082 (1982)

Farley FW, Soriano P, Steffen LS, Dymecki SM. Widespread recombinase expression using FLPeR (Flipper) mice. Genesis 28: 106-110 (2000)

Genovese RF, Doctor BP Behavioral and pharmacological assessment of butyrylcholinesterase in rats. Pharmacol Biochem Behavior 51: 647-654 (1995)

Guedes RNC, Zhu KY, Kambhampati S, Dover BA. An altered acetylcholinesterase conferring negative cross-insensitivity to different insecticidal inhibitors in organophosphate-resistant lesser grain borer, Rhyzopertha dominica. Pestic Biochem Physiol 58: 55-62 (1997)

Haberman RA, Kroner-Lux G, Samulski RJ. Production of recombinant adeno-associated viral vectors. Current Protocols in Human Genetics 12.9.1-12.9.17 (1999)

Hada T, Yamawaki M, Moriwaki Y, Tamura S, Yamamoto T, Amuro Y, Nabeshima K, Higashino K. Hypercholinesterasemia with isoenzymic alteration in a family. Clin Chem 31: 1997-2000 (1985)

Hoffman RS, Morasco R, and Goldfrank LR. Administration of purified human plasma cholinesterase protects against cocaine toxicity in mice. JToxClinTox 34:259-266 (1996)

Jo D, Nashabi A, Doxsee C, Lin Q, Unutmaz D, Chen J, Ruley HE. Epigenetic regulation of gene structure and function with a cell-permeable Cre recombinase. Nature Biotechnology 19: 929-933 (2001)

Johnson CD, Russell RL. A rapid, simple radiometric assay for cholinesterase, suitable for multiple determinations. Anal Biochem 64: 229-238 (1975)

Joshi SK, Hashimoto K, Koni PA. Induced DNA recombination by Cre recombinase protein transduction. Genesis 33: 48-54 (2002)

Karnovsky MJ, Roots L. A direct-coloring thiocholine method for cholinesterases. J Histochem Cytochem 12: 219-221 (1964)

Kilic E, Dietz GPH, Hermann DM, Bähr M. Intravenous TAT-Bcl-XL is protective after middle cerebral artery occlusion in mice. Ann Neurol 52: 617-622 (2002)

Kisseberth WC, Brettingen NT, Lohse JK, Sandgren EP. Ubiquitous expression of marker transgenes in mice and rats. Dev Biology 214: 128-138 (1999)

Krejci E, Thomine S, Boschetti N, Legay C, Sketelj J, Massoulié J. The mammalian gene of acetylcholinesterase-associated collagen. J Biol Chem 272: 22840-22847 (1997)

Kronman C, Chitlaru T, Elhanany E, Velan B, Shafferman A. Hierarchy of post-translational modifications involved in the circulatory longevity of glycoproteins. Demonstration of concerted contributions of glycan sialylation and subunit assembly to the pharmacokinetic behavior of bovine acetylcholinesterase. J Biol Chem 275: 29488-29502 (2000)

Kwon HY, Eum WS, Jang HW, Kang JH, Ryu J, Lee BR, Jin LH, Park J, Choi SY. Transduction of Cu,Zn-superoxide dismutase mediated by an HIV-1 Tat protein basic domain into mammalian cells. FEBS Lett 485: 163-167 (2000)

Leifert JA, Harkins S, Whitton JL. Full-length proteins attached to the HIV tat protein transduction domain are neither transduced between cells, nor exhibit enhanced immunogenecity. Gene Ther 9: 1422-1428 (2002)

Leifert JA, Whitton JL. Translocatory proteins and protein transduction domains: a critical analysis of their biological effects and the underlying mechanisms. Mol Ther 8: 13-20 (2003)

Li B, Stribley JA, Ticu A, Xie W, Schopfer LM, Hammond P, Brimijoin S, Hinrichs SH, Lockridge O. Abundant tissue butyrylcholinesterase and its possible function in the acetylcholinesterase knockout mouse, J. Neurochem. 75: 1320-1331 (2000)

Lockridge O, Bartels CF, Vaughan TA, Wong CK, Norton SE, Johnson LL. Complete amino acid sequence of human serum cholinesterase. J Biol Chem 262: 549-557 (1987)

Lockridge O, Blong RM, Masson P, Froment MT, Millard CB, Broomfield CA. A single amino acid substitution, Gly117His, confers phosphotriesterase (organophosphorus acid anhydride hydrolase) activity on human butyrylcholinesterase. Biochemistry 36: 786-795 (1997)

Lundberg M, Wikström S, Johansson M. Cell surface adherence and endocytosis of protein transduction domains. Mol Ther 8: 143-150 (2003)

Luo ZD, Camp S, Mutero A, Taylor P. Splicing of 5' introns dictates alternative splice selection of acetylcholinesterase pre-mRNA and specific expression during myogenesis. J Biol Chem 273: 28486-28495 (1998)

Matsushita M, Tomizawa K, Moriwaki A, Li S, Terada H, Matsui H. A high-efficiency protein transduction system demonstrating the role of PKA in long-lasting long-term potentiation. J Neurosci 21: 6000-6007 (2001)

Matzke SM, Oubre JL, Caranto GR, Gentry MK, Galbicka G. Behavioral and immunological effects of exogenous butyrylcholinesterase in Rhesus monkeys. Pharmacol Biochem Behav 62: 523-530 (1999)

Maxwell DM, Castro CA, De La Hoz DM, Gentry MK, Gold MB, Solana RP, Wolfe AD, Doctor BP. Protection of rhesus monkeys against soman and prevention of performance decrement by pretreatment with acetylcholinesterase. Toxicol Appl Pharmacol 115: 44-49 (1992)

Maxwell DM, Brecht KM, Doctor BP, Wolfe AD. Comparison of antidote protection against soman by pyridostigmine, HI-6 and acetylcholinesterase. J Pharmacol Exp Ther 264: 1085-1089 (1993)

Millard CB, Lockridge O, Broomfield CA. Design and expression of organophosphorus acid anhydride hydrolase activity in human butyrylcholinesterase. Biochemistry 34: 15925-15933 (1995)

Millard CB, Lockridge O, Broomfield CA. Organophosphorus acid anhydride hydrolase activity in human butyrylcholinesterase: synergy results in a somanase. Biochemistry 37: 237-247 (1998)

Morris MC, Depollier J, Mery J, Heitz F, Divita G. A peptide carrier for the delivery of biolog ically active proteins into mammalian cells. Nature Biotechnology 19: 1173-1176 (2001)

Nachon F, Nicolet Y, Viguie N, Masson P, Fontecilla-Camps JC, Lockridge O. Engineering of a monomeric and low-glycosylated form of human butyrylcholinesterase: expression, purification, characterization and crystallization. Eur J Biochem 269: 630-637 (2002)

Nagahara H, Vocero-Akbani AM, Snyder EL, Ho A, Latham DG, Lissy NA, Becker-Hapak M, Ezhevsky SA, Dowdy SF. Transduction of full-length TAT fusion proteins into mammalian cells: TAT-p27 induces cell migration. Nature Medicine 4: 1449-1452 (1998)

Neitlich HW. Increased plasma cholinesterase activity and succinylcholine resistance: a genetic variant. J Clin Invest 45: 380-387 (1966)

Newcomb RD, Campbell PM, Ollis DL, Cheah E, Russell RJ, Oakeshott JG. A single amino acid substitution converts a carboxylesterase to an organophosphorus hydrolase and confers insecticide resistance on a blowfly. ProcNatlAcad Sci USA 94:7464-7468 (1997)

Nicolet Y, Lockridge O, Masson P, Fontecilla-Camps JC, Nachon F. Crystal structure of human butyryl cholinesterase and of its complexes with substrate and products. J Biol Chem. 2003 Jul 17 [Epub ahead of print]

Oppenoorth FJ. Two different paraoxon-resistant acetylcholinesterase mutants in the house fly. Pestic Biochem Physiol 18: 26-27 (1982)

Palmiter RD, Sandgren EP, Avarbock MR, Allen DD, Brinster RL. Heterologous introns can enhance expression of transgenes in mice. Proc Natl Acad Sci USA 88:478-482 (1991)

Park J, Ryu J, Kim K, Lee HJ, Bahn JH, Han K, Choi EY, Lee KS, Kwon HY, Choi SY. Mutational analysis of a human immunodeficiency virus type 1 Tat protein transduction domain which is required for delivery of an exogenous protein into mammalian cells. J Gen Virol 83: 1173-1181 (2002)

Perrier AL, Massoulié J, Krejci E. PRiMA: the membrane anchor of acetylcholinesterase in the brain. Neuron 33: 275-285 (2002)

Rachinsky TL, Camp S, Li Y, Ekström TJ, Newton M, Taylor P. Molecular cloning of mouse acetylcholinesterase: tissue distribution of alternatively spliced mRNA species. Neuron 5: 317-327 (1990)

Ralston JS, Rush RS, Doctor BP, Wolfe AD. Acetylcholinesterase from fetal bovine serum. Purification and characterization of soluble G4 enzyme.JBiolChem260:4312-4318(1985)

Raveh L, Ashani Y, Levy D, De La Hoz D, Wolfe AD, Doctor BP. Acetylcholinesterase prophylaxis against organophosphate poisoning. Quantitative correlation between protection and blood-enzyme level in mice, Biochem Pharmacol 38: 529-534 (1989)

Raveh L, Grunwald J, Macus D, Papier Y, Cohen E, Ashani Y Human butyrylcholinesterase as a general prophylactic antidote for nerve agent toxicity. In vitro and in vivo quantitative characterization. Biochem Pharmacol 45: 2465-2474 (1993)

Raveh L, Grauer E, Grunwald J, Cohen E, Ashani Y The stoichiometry of protection against soman and VX toxicity in monkeys pretreated with human butyrylcholinesterase. Toxicol Appl Pharmacol 145: 43-53 (1997)

Richard JP, Melikov K, Vives E, Ramos C, Berbeure B, Gait MJ, Chernomordik LV, Lebleu B. Cell-penetrating peptides: a reevaluation of the mechanism of cellular uptake. J Biol Chem 278: 585-590 (2003)

Rojas M, Donahue JP, Tan Z, Lin Y. Genetic engineering of proteins with cell membrane permeability. Nature Biotechnology 16: 370-375 (1998)

Rosenberry TL, Scoggin DM. Structure of human erythrocyte acetylcholinesterase. Characterization of intersubunit disulfide bonding and detergent interaction. J Biol Chem 259: 5643-5652 (1984)

Sambrook J, Fritsch EF, Maniatis T. Molecular Cloning, a Laboratory Manual. Second Edition. Cold Spring Harbor Laboratory Press, 1989, p16.66

Schmitteckert EM, Prokop CM, Hedrich HJ. DNA detection in hair of transgenic mice – a simple technique minimizing the distress on the animals. Lab Animals 33:385-389 (1999)

Schwarze SR, Ho A, Vocero-Akbani A, Dowdy SF. In vivo protein transduction: delivery of a biologically active protein into the mouse. Science 285: 1569-1572 (1999)

Simon S, Krejci E, Massoulié J. A four-to-one association between peptide motifs: four C-terminal domains from cholinesterase assemble with one proline-rich attachment domain (PRAD) in the secretory pathway. EMBO J 17: 6178-6187 (1998)

Soriano P. Generalized lacZ expression with the ROSA26 Cre reporter strain. Nature Genetics 21: 70-71 (1999)

Vocero-Akbani AM, Heyden NV, Lissy NA, Ratner L, Dowdy SF. Killing HIV-infected cells by transduction with an HIV protease-activated caspase-3 protein. Nature Medicine 5: 29-33 (1999)

Vocero-Akbani A, Lissy NA, Dowdy SA. Transduction of full-length Tat fusion proteins directly into mammalian cells: analysis of T cell receptor activation-induced cell death. Methods Enzymol 322: 508-521 (2000)

Vontas JG, Cosmidis N, Loukas M, Tsakas S, Hejazi MJ, Ayoutanti A, Hemingway J. Altered acetylcholinesterase confers organophosphate resistance in the olive fruit fly *Bactrocera oleae*. Pestic Biochem Physiol 71: 124-132 (2001)

Wolfe AD, Rush RS, Doctor BP, Koplovitz I, Jones D. Acetylcholinesterase prophylaxis against organophosphate toxicity. Fund Appl Toxicol 9: 266-270 (1987)

Wolfe AD, Blick DW, Murphy MR, Miller SA, Gentry MK, Hartgraves SL, Doctor BP Use of cholinesterases as pretreatment drugs for the protection of Rhesus monkeys against soman toxicity. Toxicol Appl Pharmacol 117: 189-193 (1992)

Xia H, Mao Q, Davidson BL. The HIV Tat protein transduction domain improves the biodistribution of β-glucuronidase expressed from recombinant viral vectors. Nature Biotechnology 19: 640-644 (2001)

Xiao X, Li J, Samulski RJ. Production of high-titer recombinant adeno-associated virus vectors in the absence of helper adenovirus. J Virol 72: 2224-2232 (1998)

Xie W, Stribley JA, Chatonnet A, Wilder PJ, Rizzino A, McComb RD, Taylor P, Hinrichs SH, Lockridge O. Postnatal developmental delay and supersensitivity to organophosphate in gene-targeted mice lacking acetylcholinesterase, J. Pharmacol. Exp. Ther. 293: 896-902 (2000)

Yang Y, Ballatori N, Smith HC. Apolipoprotein B mRNA editing and the reduction in synthesis and secretion of the atherogenic risk factor, apolipoprotein B100 can be effectively targeted through TAT-mediated protein transduction. Mol Pharmacol 61: 269-276 (2002)

Yoon HY, Lee SH, Cho SW, Lee JE, Yoon CS, Park J, Kim TU, Choi SY. TAT-mediated delivery of human glutamate dehydrogenase into PC12 cells. Neurochem Int 41: 37-42 (2002)

Yao FF, Savarese JJ. Pseudocholinesterase hyperactivity with succinylcholine resistance: an unusual cause of difficult intubation. J Clin Anesthesia 9: 328-330 (1997)

Yoshida A, Motulsky AG. A pseudocholinesterase variant (E Cynthiana) associated with elevated plasma enzyme activity. Am J Hum Genetics 21: 486-498 (1969)

Zambrowicz BP, Imamoto A, Fiering S, Herzenberg LA, Kerr WG, Soriano P. Disruption of overlapping transcripts in the ROSA βgeo 26 gene trap strain leads to widespread expression of β-galactosidase in mouse embryos and hematopoietic cells. Proc Natl Acad Sci USA 94: 3789-3794 (1997)

Zhu KY, Clark JM. Validation of a point mutation of acetylcholinesterase in Colorado potato beetle by polymerase chain reaction coupled to enzyme inhibition assay. Pestic Biochem Physiol 57: 28-35 (1997)

Zhu Y, Gao JR, Starkey SR. Organophosphate resistance mediated by alterations of acetylcholinesterase in a resistant clone of the greenbug, Schizaphis graminum (Homoptera: Aphididae). Pestic Biochem Physiol 68: 138-147 (2000)

Appendices   Published manuscript

Boeck AT, Schopfer LM, Lockridge O (2002) DNA sequence of butyrylcholinesterase from rat; expression of the protein and characterization of the properties of rat butyrylcholinesterase. Biochem Pharmacol 63: 2101-2110

Duysen EG, Fry DL, Lockridge O (2002) Early weaning and culling eradicated Helicobacter hepaticus from an acetylcholinesterase knockout 129S6/SvEvTac mouse colony. Comp Med 52: 461-466

Li B, Duysen EG, Volpicelli LA, Levey AI, Lockridge O (2003) Regulation of muscarinic acetylcholine receptor function in acetylcholinesterase knockout mice. Pharmacology, Biochemistry, and Behavior 74: 977-986

Volpicelli-Daley LA, Duysen EG, Lockridge O, Levey AI (2003) Altered hippocampal muscarinic receptors in acetylcholinesterase-deficient mice. Ann Neurol 53:788-96

Bernard V, Brana C, Liste I, Lockridge O, Bloch B (2003) Dramatic depletion of cell surface m2 muscarinic receptor due to limited delivery from intracytoplasmic stores in neurons of acetylcholinesterase-deficient mice. Mol Cell Neurosci 23:121-33

Nachon F, Masson P, Nicolet Y, Lockridge O, Fontecilla-Camps JC (2003) Comparison of the structures of butyrylcholinesterase and acetylcholinesterase. Chapter 4 in "Butyrylcholinesterase Its Function and Inhibitors" (Editor Ezio Giacobini). Martin Dunitz, London, p39-54

Lockridge O, Duysen EG, Li B (2003) Butyrylcholinesterase function in the acetylcholinesterase knockout mouse. Chapter 2 in "Butyrylcholinesterase Its Function and Inhibitors" (Editor Ezio Giacobini) Martin Dunitz, London, p21-28

DNA sequence of butyrylcholinesterase from the rat: expression of the protein and characterization of the properties of rat butyrylcholinesterase[☆]

Andreea Ticu Boeck, Lawrence M. Schopfer[*], Oksana Lockridge

Eppley Institute, 986805, University of Nebraska Medical Center, Omaha, NE 68198-6805, USA

Abstract

The rat is the model animal for toxicity studies. Butyrylcholinesterase (BChE), being sensitive to inhibition by some organophosphorus and carbamate pesticides, is a biomarker of toxic exposure. The goal of this work was to characterize the purified rat BChE enzyme. The cDNA sequence showed eight amino acid differences between the active site gorge of rat and human BChE, six clustered around the acyl binding pocket and two below the active site serine. A prominent difference in rat was the substitution of arginine for leucine at position 286 in the acyl pocket. Wild-type rat BChE, the mutant R286L, wild-type human BChE, and the mutant L286R were expressed in CHO cells and purified. Arg286 was found responsible for the resistance of rat BChE to inhibition by Triton X-100. Replacement of Arg286 with leucine caused the affinity for Triton X-100 to increase 20-fold, making it as sensitive as human BChE to inhibition by Triton X-100. Wild-type rat BChE had an 8- to 9-fold higher K_m for the positively charged substrates butyrylthiocholine, acetylthiocholine, propionylthiocholine, benzoylcholine, and cocaine compared with wild-type human BChE. Wild-type rat BChE catalyzed turnover 2- to 7-fold more rapidly than human BChE, showing the highest turnover with propionylthiocholine (201,000 min^{-1}). Human BChE does not reactivate spontaneously after inhibition by echothiophate, but rat BChE reactivates with a half-life of 4.3 hr. Human serum contains 5 mg/L of BChE and 0.01 mg/L of AChE. Male rat serum contains 0.2 mg/L of BChE and approximately 0.2 mg/L of AChE. © 2002 Elsevier Science Inc. All rights reserved.

Keywords: Steady-state kinetics; Triton X-100; Cocaine; Phosphorylation reactivation

1. Introduction

The rat is the most commonly used animal for toxicity testing. The results from toxicity tests in rats are then extrapolated to predict toxicity in humans. The enzyme components of the blood have a major influence on the potency of toxic agents. The major detoxifying enzyme in rat blood is carboxylesterase (EC 3.1.1.1, carboxylic-ester hydrolase), but human blood contains no carboxylesterase.

In humans, serum BChE (EC 3.1.1.8, acylcholine acyl-hydrolase) plays a role in the detoxication of cocaine, organophosphorus pesticides, carbamate pesticides, and chemical warfare agents [1,2].

Human BChE has been studied extensively [3,4]; however, relatively little is known about rat BChE. From what is known, it is clear that the reactivity of rat BChE differs from that of human BChE. For example: (a) human BChE shows a preference for the hydrolysis of BTC over PTC, while rat BChE shows the opposite preference [5,6]; (b) with 1 mM BTC as substrate, the reaction of human BChE is inhibited 39% by 0.025% Triton X-100, while rat BChE appears to be unaffected [7]; (c) reactivation of diethylphosphate-inhibited rat BChE proceeds 100-fold faster than diethylphosphate-inhibited human BChE [8]; and (d) rat serum has very little BChE activity compared with that in human serum [7], but whether the low activity was due to less BChE protein or to a BChE with intrinsically lower activity was unknown.

These observations prompted us to investigate the kinetic properties of rat BChE in detail. Since BChE is present at low levels in rat blood, we chose to use recombinant BChE for our studies. Therefore, we determined the nucleotide sequence for the rat BCHE cDNA (and consequently the amino acid sequence of the protein), and expressed it in cell culture. We found that the structure of the active site of rat BChE is substantially different from the active site of human BChE. Most of the differences are localized to the acyl-binding pocket. The most prominent of these differences was an arginine at position-286 in rat BChE, where a leucine is found in the human. We tested the importance of this difference on the kinetic properties of rat BChE by making mutants of both rat (R286L) and human (L286R) BChE. We found that the presence of an arginine at position-286 conferred resistance to Triton X-100 inhibition onto rat BChE. However, Arg286 alone does not account for the substrate selectivity of rat BChE, nor is it responsible for the increased rate of reactivation found with diethylphosphate-inhibited rat BChE.

2. Methods and materials

2.1. DNA amplification and sequencing

PCR amplification was performed on rat heart Marathon-Ready cDNA (Sprague–Dawley rat) and on rat genomic DNA (Sprague–Dawley rat) from Clontech, using a panel of oligonucleotide primers directed against human BChE sequences. After obtaining partial rat cDNA sequences, new primers specific for rat BChE were made for further DNA amplification. *Taq* polymerase (Promega), *HotStar-Taq* polymerase (Qiagen), or Platinum *Pfx* polymerase (Gibco BRL) were used for PCR. All of the rat BCHE cDNA sequences were amplified and sequenced at least twice, to identify potential errors caused by polymerases.

2.2. Mutagenesis and expression of rat and human BChE

Site-directed mutagenesis to make human L286R and rat R286L was performed with the PCR and *Pfu* DNA polymerase (Stratagene). Expression from CHO-KI cells was performed essentially as previously described [9].

2.3. Purification of BChE

Recombinant proteins of wild-type rat BChE, wild-type human BChE, and mutants R286L (rat) and L286R (human) were purified from serum-free culture medium using the affinity chromatography method of Lockridge [4], followed by ion exchange chromatography on DE52 essentially as described [9]. The concentration of the recombinant BChE proteins was determined by titration with chlorpyrifos-oxon [diethyl *O*-(3,5,6-trichloro-2-pyridinyl) phosphate, from ChemService Inc.] as proposed by Amitai et al. [10].

2.4. Steady-state kinetics

Substrate turnover was followed spectrophotometrically in a temperature-controlled, single-beam Gilford spectrophotometer, which was interfaced via a MacLab data recorder (ADInstruments) to a Macintosh computer. Initial rates for all reactions were measured in 0.1 M potassium phosphate buffer, pH 7.0, at 25°. All rates were corrected for spontaneous degradation of substrates and reagents. Unless otherwise indicated, all chemicals were obtained from the Sigma Chemical Co.

The hydrolysis of thioester substrates, ATC, PTC, or BTC, was measured by the method of Ellman et al. [11] as previously described [9]. Hydrolysis of the other substrates was followed by established methods: BzCh [9]; ONPB [12]; (+)-cocaine (National Institute on Drug Abuse Research Resources Drug Supply System) [13]; and (−)-cocaine [14].

Inhibition of BChE turnover by Triton X-100, Tween 20 (Fisher), and Brij 96 V (Fluka) was determined in the presence of BTC.

2.5. Analysis of steady-state turnover data

Steady-state data (velocity versus substrate concentration) for ATC, PTC, BTC, and BzCh were fit to an equation for excess substrate activation/inhibition [15], Eq. (1):

$$
k_{app} = \frac{k_{cat} + \dfrac{bk_{cat}[S]}{K_{ss}}}{1 + \left(\dfrac{K_m}{[S]}\right)1 + \left(\dfrac{[S]}{K_{ss}}\right)} \tag{1}
$$

In this equation, k_{app} is the apparent rate, in terms of moles of product per mole of BChE per minute; [S] is the concentration of substrate; k_{cat} is the turnover number (min^{-1}) when [S] $\ll K_{ss}$; K_m is the Michaelis constant; bk_{cat} is the turnover number (min^{-1}) when [S] $\gg K_{ss}$; and K_{ss} is the dissociation constant for excess substrate. The parameter b reflects the efficiency of product formation from the ternary complex (SES). When $b > 1$, there is substrate activation. When $b < 1$, there is substrate inhibition. When $b = 1$, the enzyme follows Michaelis–Menten kinetics. The k_{cat}, K_m, K_{ss}, and b values were obtained by non-linear, least-squares fitting of the apparent rate versus substrate concentration data to Eq. (1), using SigmaPlot v4.16 (Jandel Scientific). The value for bk_{cat} was obtained by multiplying k_{cat} by b.

Turnover data (velocity versus substrate concentration) for (+)-cocaine, (−)-cocaine, and ONPB were fit to the Michaelis–Menten equation [16], using a non-linear, least-squares algorithm with SigmaPlot v4.16, in order to extract K_m and k_{cat}.

2.6. Phosphorylation of BChE

Inhibition of BChE by ECHO (from Wyeth Ayerst) was performed in the absence of substrate as described by

Aldridge and Reiner [17]. BChE (0.3 to 3.0 nM) was incubated in 1,980 μL of 0.1 M potassium phosphate buffer, pH 7.0, containing 0.5 mM DTNB and variable amounts of ECHO (0.05 to 1.0 mM for L286R and 0.0125 to 0.1 μM for wild-type rat, wild-type human, and R286L), at 25°, in a series of quartz spectrophotometer cuvettes. At intervals, 20 μL of 100 mM ATC was added to a cuvette, and the BChE activity remaining at that time was determined by the rate of product formation (ΔA_{412}/min). ATC rather than BTC was used because ATC is a better substrate for rat BChE. The time interval for incubation of BChE with ECHO ranged from 10 sec to 10 min. The apparent rate of inhibition (k_{phos}) was determined by plotting $\log(\Delta A_{412}$/min) versus incubation time. This inhibition protocol relies on the substrate (ATC) to displace non-covalently bound ECHO from the BChE. The evidence that this was accomplished successfully is that extrapolation of the semilog plots to time zero yielded the uninhibited ΔA_{412}/min in every case (see Ref. [17]). A secondary plot of k_{app} versus the ECHO concentration was linear, yielding an apparent second order rate constant for phosphorylation.

2.7. Reactivation of diethylphosphorylated BChE

BChE (60–80 nM) was inhibited by reacting with 95 nM ECHO in 20 mM potassium phosphate buffer plus 1 mM EDTA, pH 7.0, at 25° for 30 min, after which time the activity was inhibited by greater than 95%. Then, 10-μL aliquots of the inhibited BChE were diluted into 1,920 μL of 0.1 M potassium phosphate buffer, pH 7.0, containing 0.1% bovine serum albumin, in a series of quartz spectrophotometer cuvettes. The cuvettes were sealed with Parafilm and incubated at 25°. At intervals, 20 μL of 100 mM ATC and 50 μL of 20 mM DTNB were added to a cuvette, and the activity of the reactivated BChE (ΔA_{412}/min) was determined. The bovine serum albumin stabilized the BChE against spontaneous loss of activity during the extended incubation required to follow reactivation. A parallel incubation of uninhibited BChE was also made to control for spontaneous loss of activity. Reactivation rate constants were extracted by fitting the activity versus incubation time data to a single exponential expression with SigmaPlot v4.16, using a non-linear, least-squares algorithm. We are employing the term reactivation to describe the process we are following in this section, because no effort was made to separate dephosphorylation from aging.

3. Results

3.1. BCHE sequence

Sequence information from both rat cDNA and rat genomic DNA was combined to produce the nucleotide sequence of the cDNA for the rat BCHE gene (GenBank Accession Number AF244349). The 1,791 nucleotides, which corresponded to the mature protein-coding sequence and the signal peptide, showed 81% identity with human BCHE at the nucleotide level [18] and 80% identity at the amino acid sequence level [19]. Fifty-seven percent of the nucleotides in this region were AT.

Translation of the nucleotide sequence yielded a mature protein-coding sequence of 574 amino acids, and a 23 amino acid signal peptide. The rat signal peptide is five amino acids shorter than the human signal peptide [18]. At 574 residues, rat BChE was exactly the same length as human BChE, which makes numbering for the two enzymes identical.

Human BChE carries nine asparagine-linked carbohydrates, which are located at positions 17(19), 57(59), 106(108), 241(243), 256(258), 341(343), 455(457), 481(483), and 486(488) [19]. By convention, the numbering of BChE from all species is referenced to the numbering of AChE (EC 3.1.1.7, acetylcholine hydrolase) from *Torpedo californica* [20]. The *T. californica* number is given in parentheses, following the number for the enzyme of interest. Rat BChE showed the Asn-X-Thr/Ser consensus sequence for an asparagine-linked, carbohydrate attachment site at seven of these locations. Positions 17 and 256 were missing. The rat sequence showed one additional site at position 87, for a total of eight potential carbohydrate attachment sites.

The six cysteines that form interchain disulfide bridges in human BChE, i.e. 65(67), 92(94), 252(254), 263(265), 400(402), and 519(521) [21], were all conserved in rat BChE. This strongly suggests that the same structurally important disulfide bridges are present in rat BChE. In addition, a cysteine at position 571(573), which is responsible for a disulfide bridge between monomers in human BChE [21], was conserved in rat BChE. This suggests that rat BChE retains the same dimer-of-dimers quaternary structure as human BChE [22]. An additional cysteine at position 210(212) was found in the rat sequence.

By analogy with the structure of *T. californica*, there are approximately 55 residues in the active site gorge of human BChE. The essential catalytic triad, consisting of S198(200), E325(327), and H438(440), was conserved in rat BChE. Out of the remaining 52 residues, eight differences were found between rat and human BChE. A schematic representation of those changes is shown in Fig. 1. Two of the changes were located below the catalytic triad, away from the substrate binding locus. One, F398(400)I, was a relatively conservative replacement. The other, Q223(225)E, was not. This latter change introduced a potential negative charge into the vicinity of the catalytic glutamate. The remaining six differences were clustered in the acyl binding pocket and along the gorge directly above the acyl binding pocket: V288(290)I, L286(288)R, P285(287)I, T284(286)S, V280(282)L, and A277(279)K. Three of these were conservative replacements, but L286R, P285I, and A277K were not.
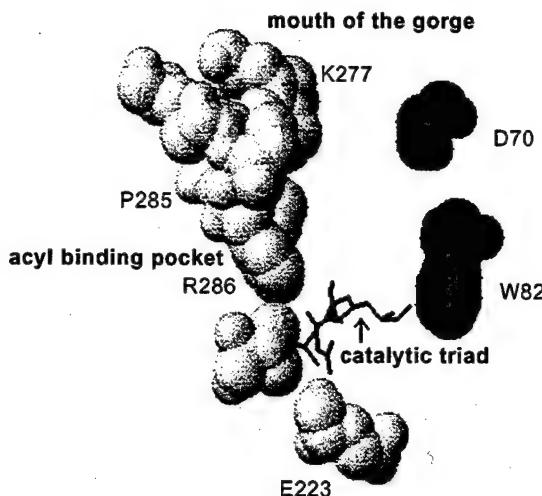
Fig. 1. Schematic representation of the amino acid differences between rat and human BChE in the active site and active site gorge. The catalytic triad is indicated by the stick structures. It is located at the bottom of a 10 Å deep gorge, the mouth of which is indicated by the residues at the top of the figure. The dark residues on the right side of the gorge are aspartate 70 (at the top) and tryptophan 82 (at the bottom). These residues are conserved in both rat and human BChE. Tryptophan 82 is generally considered to associate with the positively charged portion of cationic substrates. The acyl binding pocket, on the left side of the gorge, is generally considered to associate with the acyl end of the substrate. The light colored residues represent those amino acids that differ between rat and human BChE.

The 277 position is located at the mouth of the gorge. As such, the positive charge from the lysine in rat BChE might be expected to interact with the bulk solvent. If this is so, then this change in the rat structure might be relatively innocuous. Consistent with this interpretation is the fact that replacing A277 in human BChE with histidine had no significant effect on K_m or K_{ss} for the turnover of BTC [23].

Position 285 is in the midst of the acyl binding pocket. Replacing proline 285 with isoleucine undoubtedly will affect the structure of the acyl binding pocket, but the exact nature of this effect is unclear. In fact, with so many changes clustered in the vicinity of the acyl binding pocket, it would be difficult to accurately predict their overall effect on the structure of that region.

However, the L286R change is particularly intriguing. The special significance of this residue, in part, is extrapolated from studies on mouse and human AChE, where the size of the residue in the position equivalent to 286 defines the substrate specificity [24,25]. In addition, we have found that substituting a histidine into position-286 of human BChE increased the rate of reactivation for diethylphosphate-inhibited human BChE. Thus, we considered it possible that the presence of the arginine in position-286 could account for: (a) the substrate specificity of rat BChE; (b) the increased rate for reactivation from organophosphate inhibition by rat BChE; and (c) the lack of sensitivity of rat BChE toward inhibition by Triton X-100.

This encouraged us to investigate the role of the R286 in the activity of BChE. Consequently, we prepared the rat

mutant R286L and the complementary human mutant L286R. We compared the steady-state kinetics of these mutants to those of wild-type rat and wild-type human BChE. In addition, we examined the kinetics for reactivation from diethylphosphate inhibition, and the kinetics of Triton X-100 inhibition with each enzyme.

3.2. Steady-state turnover kinetics (ATC, PTC, BTC, BzCh, and ONPB)

Qualitatively, rat BChE behaved much the same as human BChE (Table 1). Both showed marked substrate activation with positively charged, acyl-choline substrates, ATC, BTC, and PTC, as reflected in b values ranging from 1.3 to 4.0. Both had normal Michaelis–Menten behavior with the neutral ONPB, as shown by b values equal to 1. Wild-type rat BChE showed a higher K_m for all substrates than did wild-type human. On the other hand, both k_{cat} and bk_{cat} generally were higher for wild-type rat BChE than they were for the wild-type human enzyme, suggesting that the catalytic machinery of the rat enzyme is more highly optimized. Our results are in reasonable agreement with reports from the literature (see Table 1).

When k_{cat}/K_m is used as a measure of catalytic efficiency, wild-type human BChE is more efficient with BTC, BzCh, ONPB, (+)-cocaine, and (−)-cocaine, whereas the wild-type rat enzyme is more efficient with ATC. Comparing efficiency within the acyl-choline series of substrates (ATC, PTC, and BTC), wild-type human BChE becomes increasingly efficient as the size of the acyl portion of the substrate increases (ATC < PTC < BTC). Wild-type rat BChE is least efficient with the larger BTC and equally efficient with the two smaller substrates. These findings suggest that the acyl-binding pocket in the active site of rat BChE is smaller than that of human BChE.

We had suggested that the arginine in position-286 of rat BChE might be responsible for the turnover differences between rat and human BChE. Accordingly, we examined the steady-state properties of the rat mutant, R286L, where the arginine in position-286 was replaced with the residue normally found in human BChE. The K_m values for R286L were reduced by about 2-fold, with all substrates (Table 1). The k_{cat} (bk_{cat}) values were also reduced (Table 1). The k_{cat}/K_m values indicated that the overall catalytic efficiency was improved only slightly by replacing Arg286 with leucine, and that the relative efficiency within the acyl-choline series of substrates was unchanged. Thus, the unique steady-state properties of rat BChE cannot be attributed simply to Arg286.

The converse mutation, L286R, in human BChE resulted in an enzyme with K_m values for positively charged substrates ATC, PTC, BTC, and BzCh, which were 20- to 50-fold higher for L286R than for wild-type human BChE (Table 1). The K_m value for the neutral ONPB was actually 2-fold lower for L286R. Although K_m is not a reliable measure of substrate affinity, these findings suggest that the

Table 1
Steady-state kinetic constants (determined in 0.1 M potassium phosphate at pH 7.0 and 25°)

Substrate	Species	Variant	K_m (μM)	K_{ss} (μM)	b	k_{cat} (min⁻¹)	bk_{cat} (min⁻¹)	k_{cat}/K_m (μM⁻¹ min⁻¹)
ATC	Human	WT	57 ± 6.4	2,890 ± 495	2.47 ± 0.1	20,200 ± 910	49,900 ± 3,000	354
ATC[a]	Human	WT	33	620	2.7	NR[b]	NR	NR
ATC	Human	L286R	2,340 ± 68	None[c]	1	11,800 ± 98	11,800 ± 98	5
ATC	Rat	WT	61 ± 6.7	2,580 ± 330	2.66 ± 0.11	66,200 ± 3,500	176,000 ± 11,800	1,090
ATC[d]	Rat	WT	80	NR	NR	NR	NR	NR
ATC	Rat	R286L	37 ± 6.8	1,630 ± 253	2.93 ± 0.23	47,000 ± 4,100	138,000 ± 16,200	1,270
PTC	Human	WT	25 ± 2.2	2,630 ± 130	4.09 ± 0.12	26,600 ± 860	109,000 ± 4,800	1,060
PTC[a]	Human	WT	24	410	2.2	NR	NR	NR
PTC	Human	L286R	510 ± 81	5,820 ± 3,600	1.59 ± 0.12	5,350 ± 610	8,510 ± 1,200	10
PTC	Rat	WT	189 ± 18	6,180 ± 1,200	1.99 ± 0.07	201,000 ± 9,300	400,000 ± 23,000	1,060
PTC	Rat	R286L	112 ± 6.8	4,800 ± 517	2.12 ± 0.05	144,000 ± 4,000	305,000 ± 11,000	1,290
BTC	Human	WT	14 ± 1.8	1,320 ± 78	3.60 ± 0.14	29,500 ± 1,100	106,000 ± 5,700	2,110
BTC[e]	Human	WT	23	1,400	2.5	33,900	84,900	1,470
BTC[f]	Human	WT	20	300	2.4	24,000	58,000	1,200
BTC	Human	L286R	738 ± 38	None	1	14,300 ± 410	14,300 ± 410	19
BTC	Rat	WT	134 ± 12	3,600 ± 2,500	1.32 ± 0.04	53,000 ± 26,500	70,000 ± 35,000	395
BTC[d]	Rat	WT	100	NR	NR	NR	NR	NR
BTC	Rat	R286L	94 ± 7.2	7,390 ± 2,900	1.63 ± 0.07	59,500 ± 1,900	97,000 ± 5,200	633
BzCh	Human	WT	5.6 ± 0.23	?[g]	<1	15,400 ± 140	?	2,750
BzCh[f]	Human	WT	8	?	<1	14,500	?	1,810
BzCh	Human	L286R	240 ± 54	None	1	23,300 ± 5,200	23,300 ± 5,200	97
BzCh	Rat	WT	43 ± 1.6	?	<1	23,300 ± 800	?	542
BzCh	Rat	R286L	21 ± 0.7	?	<1	14,600 ± 340	?	695
ONPB	Human	WT	106 ± 4.8	None	1	33,100 ± 420	33,100 ± 420	312
ONPB[h]	Human	WT	130	NR	NR	36,000	NR	277
ONPB	Human	L286R	42 ± 2	None	1	54,100 ± 830	54,100 ± 830	1,288
ONPB	Rat	WT	695 ± 36	None	1	76,900 ± 3,700	76,900 ± 3,700	111
ONPB	Rat	R286L	342 ± 14	None	1	66,500 ± 240		194
(+)-Coc[i,j]	Human	WT	13 ± 0.7	?	<1	8,900 ± 230	?	680
(+)-Coc[e,j]	Human	WT	10	None	1	7,500	7,500	750
(+)-Coc	Rat	WT	100 ± 15	None	1	7,800 ± 1,100	7,800 ± 1,100	78
(−)-Coc[i,j]	Human	WT	6.0 ± 1.4	None	1	1.8 ± 0.15	1.8 ± 0.15	0.30
(+)-Coc[e,j]	Human	WT	14	?	<1	3.9	?	0.27
(+)-Coc	Rat	WT	8.4 ± 3.0	None	1	0.43 ± 0.07	0.43 ± 0.07	0.05

Values are means ± SD, obtained using SigmaPlot.

[a] Data taken in 67 mM potassium phosphate, pH 7.0, at 25°, from [26].

[b] NR: not reported.

[c] "None" indicates that no indication of an excess substrate effect was detected at the highest concentration of substrate used.

[d] Data taken in 10 mM potassium phosphate, 150 mM sodium chloride, pH 7.4, at 25°, from [27].

[e] Data taken in 100 mM potassium phosphate, pH 7.0, at 25°, from [9].

[f] Data taken in 100 mM potassium phosphate, pH 7.4, at 25°, from [28].

[g] The "?" indicates that evidence for substrate inhibition was detected, but that insufficient data were collected to accurately define K_{ss} or b.

[h] Data taken in 100 mM potassium phosphate, pH 7.0, containing 5.5% methanol at from [12].

[i] (+)-Coc stands for (+)-cocaine, and (−)-Coc stands for (−)-cocaine.

[j] Substrate inhibition with cocaine becomes detectable at concentrations greater than 100 μM; refer to the present work with (+)-cocaine and to Xie et al. with (−)-cocaine [9]. We did not detect substrate inhibition with (−)-cocaine because we did not exceed 25 μM cocaine in our radioactive assay. Xie et al. did not report substrate inhibition with (+)-cocaine because they did not exceed 100 μM.

increased size of the arginine in position-286 did not obstruct substrate binding in L286R. Rather, the new positive charge in the active site of human BChE may selectively repel the positively charged substrates. Thus, the active site of human BChE tolerates the presence of a new positive charge poorly.

A similar charge-repulsion in rat BChE does not seem to occur. This is indicated by the fact that replacing Arg286 with leucine in rat BChE did not result in a large decrease in K_m for positively charged substrates. It follows that the positive charge on the arginine at position-286 in the rat enzyme is probably neutralized, most likely by the negatively charged Glu223.

Overall, the turnover results with the mutant BChE enzymes indicate that the structure of the active site of rat BChE is significantly different from the structure of the active site of human BChE. The observed differences in kinetic properties cannot be explained by a simple, single amino acid substitution. Furthermore, the active site of rat BChE is adapted to accommodate the presence of the

positively charged Arg286 in ways that cannot be easily mimicked by human BChE.

3.3. BChE levels in rat serum

It is well known that the measured activity of BChE in rat serum is low relative to that of human serum [5–7,29]. Having determined the specific activity of purified rat BChE to be 146 BzCh-units/mg, we were in a position to quantitate the amount of BChE protein in rat serum. Rat serum (adult male Sprague–Dawley, from RJO Biologicals Inc.), when measured with 50 μM BzCh in 0.1 M potassium phosphate, pH 7.0, at 25°, contained 0.027 units/mL of BChE activity. This is equivalent to 0.185 mg of BChE/L of rat serum. In contrast, there are 5 mg of BChE/L of human serum.

3.4. Inhibition of BChE by Triton X-100

Li et al. [7] showed that the monomeric form of Triton X-100 could inhibit activity of human BChE, but that rat serum BChE was resistant to Triton X-100 inhibition. It was proposed that the arginine in position-286 of rat BChE might be responsible for the rat's resistance. In those experiments, Triton X-100 appeared to behave as a competitive inhibitor of human BChE turnover. The investigation into Triton X-100 inhibition of wild-type BChE has been extended with a traditional steady-state inhibition study, using multiple concentrations of both substrate (BTC) and Triton X-100. BChE mutants at the 286-position of both rat and human BChE have been included in the study to test the proposal that resistance to Triton X-100 inhibition in rat BChE is due to the presence of arginine in position-286.

Both wild-type rat and human BChE showed classical competitive inhibition with Triton X-100. Plots of 1/[substrate] versus 1/velocity at different concentrations of Triton X-100 were linear and converged on the y-axis. Re-plots of the slopes as a function of Triton X-100 concentration were linear, yielding competitive inhibition constants of 13.1 ± 2.9 and 194 ± 19 μM for Triton X-100 binding to human and rat BChE, respectively. Thus, either Triton X-100 or BTC can bind to the enzyme, but not both. It was not clear whether this mutually exclusive binding results from direct competition between Triton X-100 and BTC for the same binding site, or whether it occurs allosterically with Triton X-100 and BTC binding to separate loci.

Replacing the arginine at position-286 in rat BChE with leucine (R286L) caused the inhibition to become mixed, with both the slopes and the y-axis intercepts of the double-reciprocal plot showing a dependence on Triton X-100 concentration. Analysis indicated classical, non-competitive, mixed-type inhibition with the lines on the double-reciprocal plot converging on the x-axis. The inhibition constant obtained from the slopes was 9.3 ± 0.79 μM, and that from the intercepts was 9.6 ± 1.1 μM. Thus, Triton X-100 bound to R286L 20-fold more tightly than it did to

wild-type rat BChE. This strongly suggests that the arginine in position-286 is responsible for the weak binding of Triton X-100 to rat BChE.

Replacing the leucine at position-286 in human BChE with arginine (L286R) resulted in an enzyme that retained competitive Triton X-100 inhibition, but with an inhibition constant, which was increased 3-fold, to 40.1 ± 3.6 μM. The decrease in affinity for Triton X-100 upon introduction of arginine into position-286 of human BChE is consistent with the results from rat BChE. However, the difference in affinity for human BChE was much smaller than for rat BChE. This result supports our suggestion, taken from the steady-state turnover findings, that the structures of the active sites of human and rat BChE are significantly different.

It is noteworthy that 250 μM is the critical micellar concentration for Triton X-100 [30]. The fact that all of the Triton X-100 inhibition constants were below the critical micellar concentration supports the proposal by Li et al. [7] that the monomeric form of Triton X-100 is responsible for the inhibition of BChE.

3.5. Triton X-100 and tissue extracts

It is common for investigators to extract tissues with 0.5% Triton X-100 when assaying for BChE activity. Tissue extracts containing 0.5% Triton X-100 are typically diluted directly into the assay mixture in order to measure BChE activity. For tissues with low activity, such as those from the rat, 50 μL of extract may be diluted into 1 mL of reaction medium. This results in a 40-fold dilution, or 0.025% Triton X-100 remaining in the assay [7]. We have determined the effect of Triton X-100 on the activity of wild-type rat and human BChE with 1 mM BTC (Fig. 2). Rat BChE was inhibited 24% at Triton X-100 concentrations greater than 250 μM (0.016%). Human BChE was inhibited 40% under the same conditions. Thus, in the
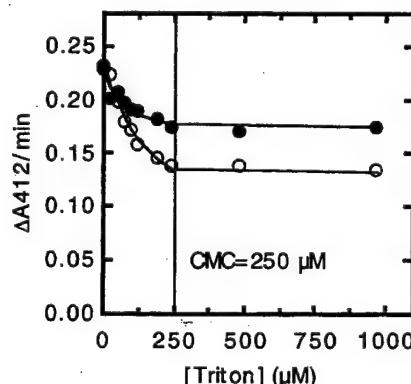
Fig. 2. Inhibition of wild-type BChE from rats and humans by Triton X-100. BChE was reacted with 1 mM BTC (0.1 M potassium phosphate buffer, pH 7.0, at 25°) in the presence of various concentrations of Triton X-100 (0–1 mM). The effect of Triton X-100 on BChE activity (ΔA_{412}/min) is shown: closed circles for rat BChE, open circles for human BChE. CMC denotes the critical micellar concentration for Triton X-100. The points are the average of triplicate assays.

presence of 0.025% Triton X-100, even rat BChE would be inhibited markedly by Triton X-100.

Li et al. [7] reported that BChE in rat serum was resistant to Triton X-100 inhibition, under conditions comparable to those described here. The data (see Table 4 from Ref. [7]) actually show a 23% inhibition of rat BChE activity in serum, in the presence of 0.025% Triton X-100. However, the low levels of activity with which Li et al. were working made this difference unreliable. In the present experiments, sufficiently high levels of the recombinant rat BChE were used that the observed 24% inhibition is reliable.

3.6. Other detergents

In addition to studying Triton X-100, the inhibition of BChE by Tween 20 was examined. It was found that with 1 mM BTC and 0.125% Tween 20 (1 mM) neither wild-type rat nor wild-type human BChE was inhibited. This is equivalent to the findings of Li et al. [7]. Inhibition by Brij 96 V was also examined. It was found that with 1 mM BTC and 0.07% Brij (1 mM) neither wild-type rat nor wild-type human BChE was inhibited.

3.7. Phosphorylation of BChE by ECHO

In the present work (in 0.1 M potassium phosphate buffer, pH 7.0, at 25°), the apparent rate constant for phosphorylation (k_{phos}) of wild-type human BChE, up to a value of 1.6 min^{-1}, was linearly dependent upon the ECHO concentration. Concentrations of ECHO ranged from 0.1 to 0.6 µM. The apparent second order rate constant was $2.5 \pm 0.2 \times 10^6$ M^{-1} min^{-1}. Masson et al. [31] have reported that phosphorylation of human BChE by ECHO is not linearly dependent upon ECHO in this concentration range. Rather, it showed saturating behavior, reaching a limiting rate at 0.48 min^{-1} (in 0.1 M potassium phosphate buffer, pH 7.0, plus 0.5% ethanol, at 25°). The reaction of wild-type human BChE with ECHO was repeated in the presence of 1% ethanol. The k_{phos} values were still linearly dependent upon the ECHO concentration, up to 1.5 min^{-1}, though the apparent second order rate constant was reduced to $1.23 \pm 0.04 \times 10^6$ M^{-1} min^{-1}. The reason for the discrepancy between these results and those of Masson et al. [31] is unclear.

A similar, linear relationship between the concentration of ECHO and the rate of phosphorylation was found for wild-type rat BChE, and mutants R286L (rat) and L286R (human). The apparent second order rate constant for the phosphorylation of wild-type rat BChE by ECHO ($1.86 \pm 0.04 \times 10^7$ M^{-1} min^{-1}) was 10-fold faster than that for wild-type human BChE. Replacement of Arg286 with leucine (R286L) did not have much effect on that value ($1.73 \pm 0.07 \times 10^7$ M^{-1} min^{-1}), despite the fact that ECHO is positively charged. This finding supports our interpretations of the steady-state turnover data from rat BChE, which concluded that: (a) the arginine does not create a major steric hindrance in the active site; and (b) the charge on the arginine is neutralized. The increased rate for phosphorylation of rat BChE is consistent with the increased rates observed for substrate turnover by rat BChE.

In contrast, introducing an arginine into the active site of human BChE at position-286 (L286R) reduced the apparent second order rate constant for phosphorylation by ECHO by 3 orders of magnitude (to $3.5 \pm 0.4 \times 10^4$ M^{-1} min^{-1}). Since ECHO is positively charged, this result is consistent with significant charge repulsion for positively charged compounds in the active site of human L286R.

3.8. Reactivation of diethylphosphorylated BChE

Davison [8] has shown that the reactivation rate for diethylphosphate-inhibited wild-type rat BChE (2.0×10^{-3} min^{-1} at pH 7.8 and 37°) is 100-fold faster than that for wild-type human BChE (1.6×10^{-5} min^{-1}). In the present study, reactivation of wild-type rat BChE after inhibition by ECHO (a diethylphosphate containing organophosphate) occurred at $2.7 \pm 0.08 \times 10^{-3}$ min^{-1} (half-life of 4.3 hr), which is in good agreement with the Davison report. Seventy-three percent of the starting activity was recovered after reactivation was complete, suggesting that aging was not a major contributor to the reactivation rate.

Replacing the arginine at position-286 in rat BChE with leucine (R286L) slowed the reactivation rate by only 30% (to $1.9 \pm 0.40 \times 10^{-3}$ min^{-1}), while yielding a 60% recovery of the starting activity. Thus, Arg286 is not the factor responsible for the fast reactivation of rat BChE. Consistent with this conclusion, the human L286R mutant showed no measurable reactivation after 6.5 hr, indicating that the arginine at this position did not promote reactivation in human BChE.

3.9. Hydrolysis of cocaine

The non-pharmacologically active (+)-cocaine has been reported to react well with wild-type human BChE, with a K_m of 6–10 µM and a k_{cat} of 7,500–8,900 min^{-1} [9,13]. Similar values for wild-type human BChE (Table 1) were found in this study. With wild-type rat BChE, the K_m for (+)-cocaine was 10-fold weaker ($K_m = 100$ µM), although the k_{cat} value was essentially the same as that for human BChE (Table 1). The higher K_m value for rat BChE reacting with (+)-cocaine is consistent with the increase in K_m found for rat BChE reacting with other substrates. When k_{cat}/K_m was used as a measure of relative catalytic efficiency, rat BChE was 10-fold less efficient than human BChE at hydrolyzing (+)-cocaine.

Xie et al. [9] have reported that wild-type human BChE hydrolyzes the pharmacologically active (−)-cocaine 2,000-fold more slowly than (+)-cocaine, although the (−)-cocaine bound with the same affinity as (+)-cocaine (Table 1). Similar results were obtained in the current work (Table 1). In addition, it was found that with wild-type rat

BChE the K_m for (−)-cocaine was much the same ($K_m = 8.4 \pm 3.0$ μM) as that for wild-type human BChE (6.0 ± 1.4 μM), and that the turnover rate with rat BChE (0.43 ± 0.07 min^{-1}) was nearly 4-fold slower than with human BChE (1.8 ± 0.15 min^{-1}). The net effect is that rat BChE is about 5-fold less efficient than human BChE at hydrolyzing (−)-cocaine.

Since the K_m values for both (+)- and (−)-cocaine were the same for human BChE, it was unexpected to find a 10-fold difference in the K_m for (+)-cocaine (100 μM) and (−)-cocaine (8.4 μM) for rat BChE. To test the reliability of the numbers, the affinity of (−)-cocaine for rat BChE was determined by using this slow substrate as an inhibitor for the hydrolysis of the faster substrate, ATC. Plots of 1/velocity versus 1/[ATC] at different (−)-cocaine concentrations were linear. Both the slopes and the y-axis intercepts were dependent upon the (−)-cocaine concentration, indicating mixed-type inhibition. The inhibition constant calculated from the slopes was 14.5 ± 1.2 μM, while the inhibition constant calculated from the intercepts was 24.8 ± 8.1 μM. These values are in reasonable agreement with the K_m of 8.4 μM for the reaction of (−)-cocaine with rat BChE.

3.10. AChE in rat serum

In addition to BChE, rat serum contains AChE. The presence of AChE is demonstrated in Fig. 3, where non-denaturing polyacrylamide gels have been stained for activity. The band labeled AChE was identified as AChE by its disappearance when the gel was treated with the AChE-selective inhibitor BW [1,5-bis(4-allyldimethylam-moniumphenyl)-pentan-3-one]. Fetal bovine serum, known to contain only AChE, served as a control. The

BChE bands were identified by treating the gel with the BChE-selective inhibitor iso-OMPA [tetraisopropylpyro-phosphoramide]. Rat serum, but not human serum or fetal bovine serum, contains carboxylesterase. The carboxylesterase migrates behind albumin.

4. Discussion

4.1. Rat BChE enzyme

We found that wild-type rat BChE generally binds substrates more weakly than wild-type human BChE, and that this effect is more prominent with larger substrates. This selectivity for smaller substrates probably reflects a decrease in the size of the acyl-binding pocket of rat BChE, which is the locus for most of the active site amino acid differences between rat and human BChE. This preference for smaller substrates, which is shared by mouse BChE [6], led Augustinsson to consider the rat enzyme to be a propionylcholinesterase rather than a butyrylcholi-nesterase [5]. We also found that Arg286, in the acyl-binding pocket of rat BChE, was intimately involved in the resistance of rat BChE to inhibition by Triton X-100, but that it had little-or-no role in determining substrate specificity or in promoting reactivation of the diethylphosphate-inhibited enzyme.

4.2. BChE and AChE in rat serum

Our measured value for male rat serum (0.185 BzCh-units/mg) was 25-fold lower than that of BChE in human serum. However, BChE is not the only cholinesterase in rat
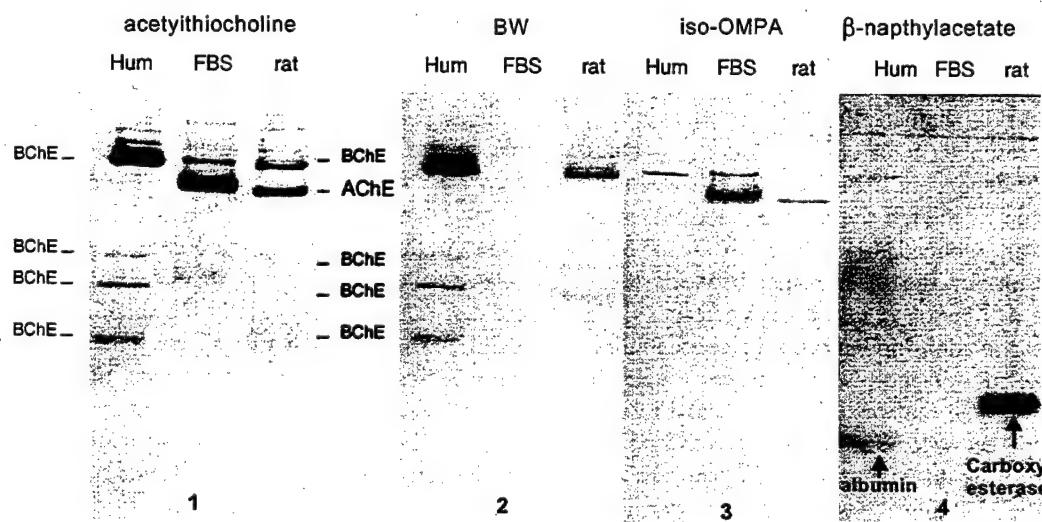
Fig. 3. Visualization of AChE, BChE, and carboxylesterase in rat serum. Lanes of non-denaturing gradient gels, 4 to 30% polyacrylamide, contained 3 μL of human serum, fetal bovine serum (FBS), or rat serum. Gel 1 was stained to reveal both AChE and BChE activity by the method of Karnovsky and Roots [32] using 1.7 mM ATC as substrate. Gel 2 was incubated in 30 μM BW for 30 min to inhibit AChE before ATC was added. Gel 3 was incubated in 0.1 mM iso-OMPA for 30 min to inhibit BChE before ATC was added. Gel 4 was stained for carboxylesterase with β-naphthylacetate and Fast Blue RR. The rat AChE band migrates at the same position as the AChE tetramer in fetal bovine serum. Rat serum has four BChE bands, similar to the four bands in human serum. The most intense BChE band is a tetramer. Carboxylesterase is present in rat serum but not in human serum or fetal bovine serum.

serum. In fact, the AChE activity in rat serum is 2.5-fold higher than the BChE activity with 1 mM ATC [7,29]. Considering the k_{cat} levels of rat AChE and BChE, it can be estimated that rat serum contains approximately the same amounts of AChE and BChE protein. This is an important point that is commonly overlooked when cholinesterase measurements on rat serum are made.

4.3. Triton X-100 inhibition

Triton X-100 is another important factor to consider when working with BChE. Li et al. [7] found that Triton X-100 could inhibit BChE from a variety of species. However, by reporting that rat BChE was resistant to Triton X-100, they implied that rat tissues extracted with Triton X-100 could be assayed without the concern of inhibiting BChE activity. We have found that although rat BChE is less sensitive than human BChE to inhibition by Triton X-100, it is still inhibited (see Fig. 2). Under conditions commonly used for the assay of rat BChE in tissue extracts, there is enough residual Triton X-100 to inhibit BChE activity by 24%. Li et al. report on BChE activities measured from various tissues, extracted with either Tween 20 or Triton X-100 (see Table 5 from Ref. [7]). They consistently report greater activity in the presence of Triton X-100. We suggest that this higher activity reflects more efficient solubilization of BChE by Triton X-100, and that the correct activities in the Triton X-100 samples are actually 24% higher than reported.

In conclusion, we can say that rat BChE and human BChE are remarkably similar. They are 80% identical in their amino acid sequences, and hydrolyze the same set of substrates, including cocaine, with similar kinetic constants. They are both inhibited by Triton X-100, in a competitive manner, and they are both readily inhibited by ECHO. Rat BChE is distinct from human BChE in that it favors the hydrolysis of PTC over BTC; it reactivates from diethylphosphate inhibition 100-fold more rapidly; and it is 15-fold less sensitive to Triton X-100 inhibition.

References

[1] Kalow W, Grant DM. Pharmacogenetics. In: Scriver CR, Beaudet AL, Sly WS, Valle D, Childs B, Kinzler K, Vogelstein B, editors. The metabolic and molecular bases of inherited disease. 8th ed. New York: McGraw-Hill, 2001. pp. 225–55.

[2] Lockridge O, Masson P. Pesticides and susceptible populations: people with butyrylcholinesterase genetic variants may be at risk. Neurotoxicology 2000;21:113–26.

[3] Main AR. Mode of action of anticholinesterases. Pharmacol Ther 1979;6:579–628.

[4] Lockridge O. Genetic variants of human serum cholinesterase influence metabolism of the muscle relaxant succinylcholine. Pharmacol Ther 1990;47:35–60.

[5] Augustinsson K-B. Electrophoresis studies on blood plasma esterases. I. Mammalian plasmata. Acta Chem Scand 1959;13:571–92.

[6] Ecobichon DJ, Comeau AM. Pseudocholinesterases of mammalian plasma: physiochemical properties and organophosphate inhibition in eleven species. Toxicol Appl Pharmacol 1973;24:92–100.

[7] Li B, Stribley JA, Ticu A, Xie W, Schopfer LM, Hammond P, Brimijoin S, Hinrichs SH, Lockridge O. Abundant tissue butyrylcholinesterase and its possible function in the acetylcholinesterase knockout mouse. J Neurochem 2000;75:1320–31.

[8] Davison AN. Return of cholinesterase activity in the rat after inhibition by organophosphate compounds. Biochem J 1955;60:339–46.

[9] Xie W, Varkey-Altamirano C, Bartels CF, Speirs RJ, Cashman JR, Lockridge O. An improved cocaine hydrolase: the A328Y mutant of human butyrylcholinesterase is 4-fold more efficient. Mol Pharmacol 1999;55:83–91.

[10] Amitai G, Moorad D, Adani R, Doctor BP. Inhibition of acetylcholinesterase and butyrylcholinesterase by chlorpyrifos-oxon. Biochem Pharmacol 1998;56:293–9.

[11] Ellman GL, Courtney KD, Andres Jr. V, Featherstone RM. A new and rapid colorimetric determination of acetylcholinesterase activity. Biochem Pharmacol 1961;7:88–95.

[12] Masson P, Legrand P, Bartels CF, Froment M-T, Schopfer LM, Lockridge O. Role of aspartate 70 and tryptophan 82 in binding of succinyldithiocholine to human butyrylcholinesterase. Biochemistry 1997;36:2266–77.

[13] Gatley SJ. Activities of the enantiomers of cocaine and some related compounds as substrates and inhibitors of plasma butyrylcholinesterase. Biochem Pharmacol 1991;41:1249–54.

[14] Sun H, El Yazal J, Lockridge O, Schopfer LM, Brimijoin S, Pang Y-P. Predicted Michaelis–Menten complexes of cocaine-butyrylcholinesterase. Engineering effective butyrylcholinesterase mutants for cocaine detoxication. J Biol Chem 2001;276:9330–6.

[15] Radic Z, Pickering NA, Vellom DC, Camp S, Taylor P. Three distinct domains in the cholinesterase molecule confer selectivity for acetyl- and butyrylcholinesterase inhibitors. Biochemistry 1993;32:12074–84.

[16] Michaelis L, Menten ML. Die kinetik der invertinwirkung. Biochem Z 1913;49:333–69.

[17] Aldridge WN, Reiner E. Acetylcholinesterase. Two types of inhibition by an organophosphorus compound: one the formation of phosphorylated enzyme and the other analogous to inhibition by substrate. Biochem J 1969;115:147–62.

[18] McTiernan C, Adkins S, Chatonnet A, Vaughan TA, Bartels CF, Kott M, Rosenberry TL, La Du BN, Lockridge O. Brain cDNA clone for human cholinesterase. Proc Natl Acad Sci USA 1987;84:6682–6.

[19] Lockridge O, Bartels CF, Vaughan TA, Wong CK, Norton SE, Johnson LL. Complete amino acid sequence of human serum cholinesterase. J Biol Chem 1987;262:549–57.

[20] Massoulie J, Sussman JL, Doctor BP, Soreq H, Velan B, Cygler M, Rotundo R, Shafferman A, Silman I, Taylor P. Recommendations for nomenclature in cholinesterase. In: Shafferman A, Velan B, editors. Multidisciplinary approaches to cholinesterase functions. New York: Plenum Press, 1992. pp. 285–8.

[21] Lockridge O, Adkins S, LaDu BN. Location of disulfide bonds within the sequence of human serum cholinesterase. J Biol Chem 1987;262:12945–52.

[22] Lockridge O, Eckerson HW, LaDu BN. Interchain disulfide bonds and subunit organization in human serum cholinesterase. J Biol Chem 1979;254:8324–30.

[23] Masson P, Froment M-T, Bartels CF, Lockridge O. Asp70 in the peripheral anionic site of human butyrylcholinesterase. Eur J Biochem 1996;235:36–48.

[24] Hosea NA, Berman HA, Taylor P. Specificity and orientation of trigonal carboxyl esters and tetrahedral alkylphosphonyl esters in cholinesterase. Biochemistry 1995;34:11528–36.

[25] Ordentlich A, Barak D, Kronman C, Flashner Y, Leitner M, Segall Y, Ariel N, Cohen S, Velan B, Shafferman A. Dissection of the human acetylcholinesterase active center determinants of substrate specificity. Identification of residues constituting the anionic site, the hydrophobic site, and the acyl pocket. J Biol Chem 1993;268:17083–95.

[26] Masson P, Adkins S, Gouet P, Lockridge O. Recombinant human butyrylcholinesterase G390V, the fluoride-2 variant, expressed in Chinese hamster ovary cells, is a low affinity variant. J Biol Chem 1993;268:14329–41.

[27] Sine J-P, Toutant J-P, Weigel P, Colas B. Amphiphilic forms of butyrylcholinesterase in mucosal cells of rat intestine. Biochemistry 1992;31:10893–900.

[28] Lockridge O, Blong RM, Masson P, Froment M-T, Millard CB, Broomfield CA. A single amino acid substitution, Gly117His, confers phosphotriesterase (organophosphorus acid anhydride hydrolase) activity on human butyrylcholinesterase. Biochemistry 1997;36:786–95.

[29] Arpagaus M, Chatonnet A, Masson P, Newton M, Vaughan TA, Bartels CF, Nogueira CP, LaDu BN, Lockridge O. Use of the polymerase chain reaction for homology probing of butyrylcholinesterase from several vertebrates. J Biol Chem 1991;266:6966–74.

[30] Helenius A, Simons K. Solubilization of membranes by detergents. Biochim Biophys Acta 1975;415:29–79.

[31] Masson P, Froment M-T, Bartels CF, Lockridge O. Importance of aspartate-70 in organophosphate inhibition, oxime re-activation and aging of human butyrylcholinesterase. Biochem J 1997;325:53–61.

[32] Karnovsky MJ, Roots L. A "direct-coloring" thiocholine method for cholinesterases. J Histochem Cytochem 1964;12:219–21.

Early Weaning and Culling Eradicated *Helicobacter hepaticus* from an Acetylcholinesterase Knockout 129S6/SvEvTac Mouse Colony

Ellen Gail Duysen,* Debra Lucie Fry, and Oksana Lockridge, PhD

The finding of *Helicobacter hepaticus* infection in our acetylcholinesterase (AChE) knockout mouse colony led to a search for a treatment. One-hundred percent of AChE +/+, 100% of AChE +/-, and 35% of AChE -/- mice tested positive. The lower infection rate in AChE -/- mice, who are routinely weaned on day 15, suggested that early weaning might be an effective eradication strategy. The AChE +/+ and +/- mice were weaned on days 13, 14, 15, or 16. Litters were placed in sterile, heated, isolator cages. Animals were fed liquid Ensure Fiber and 11% fat pelleted diet. Feces were tested for the presence of *H. hepaticus* by use of DNA amplification. Litters weaned on days 14, 15, or 16 had a high rate (68, 63, and 100%, respectively), whereas litters weaned on day 13 had a lower (8%) rate of infection. Uninfected animals have remained free of *H. hepaticus* through day 120. Pups weaned on day 13 lost body weight, beginning on day 14, but recovered by day 16. It is concluded that the non-coprophagic behavior of AChE -/- mice accounts for a low infection rate and that the combination of early weaning, routine testing, and culling provide an effective method for eradication of *H. hepaticus*.

Helicobacter hepaticus contamination of commercial and private mouse colonies has presented a treatment dilemma for researchers. Characterized as a novel bacterium in 1994 (1, 2), the gram-negative *H. hepaticus* bacterium has since been associated with chronic active hepatitis and liver tumors in various strains of mice (A/JCr, DBA/2NCr, C3H/HeNCr, B6C3F₁) (2-5). Colitis, typhlitis, and inflammatory bowel disease in immunodeficient mice have been linked to infection with *H. hepaticus* (6-10). Transmission of *H. hepaticus* has been reported to be by the oral-fecal route (11), an effective means of infection in coprophagic animals such as mice. Exposure of sentinel mice to *H. hepaticus*-contaminated bedding results in high rates of infection. (12, 13). A study by Truett and co-workers (14) indicated that pups raised by *Helicobacter*-positive dams all tested positive for the bacteria by day 19.

Initial identification of the *H. hepaticus* bacterium in this laboratory's acetylcholinesterase (AChE) knockout mouse colony was made during serologic and fecal screening of sentinel animals. Samples were analyzed at The Missouri University Research Animal Diagnostic Laboratory (RADIL, Columbia, Mo.). In-house testing of bacterial DNA from fecal pellets led to the discovery of widespread *H. hepaticus* infection. A surprise finding was that, although 100% of AChE wild type (AChE +/+) and heterozygote (AChE +/-) mice tested positive for *H. hepaticus*, only 35% of the group-housed AChE nullizygote (AChE -/-) mice were infected. An investigation into a feasible method for reestablishment of a *H. hepaticus*-negative breeding colony was undertaken. Reports of successful drug therapy involved oral gavage of affected animals three times daily, using a triple drug regimen

(15). The labor and cost involved in treating our large colony, as well as reports of inconsistent results, eliminated drug therapy as a practical treatment method. Neonatal transfer of pups from *H. hepaticus*-positive dams to negative dams was documented to be an effective method of eradication (14). Fostering the AChE knockout litters on an *H. hepaticus*-negative dam was worrisome because the AChE -/- pups are substantially smaller and weaker than their littermates and would have been targets for cannibalism or abandonment. This would have resulted in loss of valuable AChE -/- pups. Cross-fostering the pups would have required additional time to establish uninfected dams in the colony and would have necessitated implementing a protocol for synchronization of the dams' reproductive cycle prior to breeding. Re-deriving the colony by embryo transfer would have been cost and time prohibitive.

The AChE knockout mouse was developed in our laboratory by use of gene targeting and homologous recombination (16). All tissues of the AChE -/- animals are devoid of acetylcholinesterase enzyme activity and protein (16, 17). The AChE -/- animals, produced by heterozygote breeding, are characterized by weak muscles, manifested in lack of bite and suckling strength, no fore or hind limb grip strength, splayed limbs, and reduced locomotor activity. In addition, the AChE -/- animals do not manifest aggressive behaviors, do not breed, have continuous mild tremors, and have reduced body weight and body temperature, compared with their AChE +/+ and +/- littermates (18). Consequences of the bite strength deficit are that AChE -/- animals are unable to efficiently eat pelleted diet and are not coprophagic. Raised by *H. hepaticus*-positive dams, AChE -/- mice are weaned on day 15, placed on a heating pad through day 21, and fed a diet of liquid Ensure Fiber. The AChE -/- mice remain on the Ensure Fiber diet for the duration of their life, which averages 100 days. In a previous study conducted in this labora-

461

tory, feeding of a liquid diet of Ensure Fiber ad libitum to AChE +/+ and +/- mice did not reduce survival time or cause any detrimental health effects (18). Early weaning and lack of coprophagia are believed to be the factors responsible for the reduced incidence of infection in AChE -/- animals. Thus, the objective of the study reported here was to devise and describe use of an early-weaning regimen to prevent infection of the AChE +/+ and +/- mice with *H. hepaticus*.

Materials and Methods

Animals and husbandry. All animal procedures were performed in accordance with the Public Health Service Policy on Humane Care and Use of Laboratory Animals (PHS 1996). Protocols were approved by the University of Nebraska Medical Center Institutional Animal Care and Use Committee. Facilities were maintained at a temperature of 20-22°C, humidity of 35 to 40%, with lighting on a 12/12-h light/dark cycle. The AChE -/- mice were housed in a 17 × 8.5 × 8-in. hamster cage lined with paper towels in place of bedding. Cages were lined with paper towels to eliminate contamination of the liquid diet by loose bedding. Early-weaned pups and animals determined to be *H. hepaticus* free were housed in sterile static isolator top standard mouse cages. All procedures were conducted under a laminar flow hood, using Clidox spray as a decontaminant.

The animals studied were derived from an original breeding of Taconic 129S6/SvEvTac mice with a chimera from R1 embryonic stem cells, in which five kilobases of the ACHE gene from intron one through exon five had been deleted (16). Nullizygote mice, generated from AChE +/- breeding, have no AChE activity in any of their tissues (16, 17). By visual observation, AChE +/+ and AChE +/- mice are indistinguishable.

Males and nonpregnant females were fed a pelleted 5% (wt./wt.) fat maintenance diet (catalog No. 7912, Harlan Teklad LM-485 Harlan Teklad, Madison, Wis.). Gestating females were fed a pelleted 11% (wt./wt.) fat diet (catalog No. 7904, Harlan Teklad S-2335, Harlan Teklad). Early weaned pups (from day 13 to 21) and AChE -/- mice (from day 15 throughout their lifetime) were fed a liquid diet of Ensure Fiber, vanilla flavor (catalog No. 50650, Abbott Laboratories, Ross Products division, Columbus, Ohio). In addition, early-weaned pups were offered 11% (wt./wt.) fat diet pellets, placed on the floor of the cage for easy access.

Colony health status. Serologic testing of the colony was conducted quarterly at the RADIL. The Crl:CD-1(ICR)BR sentinels from Charles River Laboratories, Inc. (Wilmington, Mass.) were exposed to dirty bedding three times a week for three months. One sentinel was analyzed for every 21 cages of test animals. Serum samples from sentinel animals were tested for the presence of antibodies to: mouse hepatitis virus, Sendai virus, pneumonia virus of mice, reovirus 3, Theiler's murine encephalomyelitis virus, ectromelia virus, mouse adenovirus type I and mouse adenovirus type II, polyoma virus, *Mycoplasma pulmonis*, parvovirus, mouse rotavirus, lymphocytic choriomeningitis virus, *E. cuniculi*, cilia-associated respiratory bacillus, *Clostridium piliforme*, and Hantaan virus. Fecal samples were analyzed by use of a polymerase chain reaction (PCR) assay for the presence of *Helicobacter* species (*H. bilis, H. hepaticus, H. rodentium, and H. typhlonicus*) at the RADIL as well as at Charles River Diagnostic Laboratories (Wilmington, Mass.).

Detection methods for *H. hepaticus*. A DNA purification and amplification method was used to determine the presence

of *H. hepaticus* bacteria in fecal pellets. Using sterile forceps, feces were collected from the cage floor and placed in a sterile 2.0-ml microcentrifuge tube. The samples were tested within two hours of collection and were stored at 4°C in the interim. The bacterial DNA from the feces was purified, using the QIAamp DNA Stool Mini Kit (catalog No. 51504, QIAGEN Inc., Valencia, Calif.). This kit contains a matrix and a buffer that are designed to remove enzyme inhibitory substances and DNA degradation products from the fecal sample. The purified DNA was amplified by use of a PCR assay with primer sequences that recognized an *H. hepaticus*-specific region of the 16S rRNA gene (15). The oligonucleotides, 5' GCA TTT GAA ACT GTT ACT CTG 3', and 5' CTG TTT TCA AGC TCC CC 3' produced a 416-bp product. The PCR materials and conditions used were those outlined by Foltz and co-workers (15), with the exception that *Taq* polymerase in storage buffer B (catalog No. M116B-1, Promega, Madison, Wis.) was used. Samples were visualized by electrophoresis on a 1% agarose gel containing ethidium bromide and viewing by UV illumination.

***Helicobacter hepaticus* testing of group-housed AChE -/- mice.** The AChE -/- mice were group-housed, four to eight animals per cage, in hamster cages lined with paper towels. Mice were housed together beginning on postpartum day (PPD) 15, and remained together throughout their lifetime. The AChE -/- mice (n = 23) housed in four cages were individually tested for *H. hepaticus* infection. Mice ranged in age from 29 to 392 days. For fecal collection, mice were placed in separate cages lined with paper towels. Fecal samples were collected, and the DNA was purified and detected as described previously.

Weaning from contaminated breeding colony. During gestation and after parturition, *H. hepaticus*-positive heterozygote dams were housed in a cage containing nesting material, with 11% (wt./wt.) fat diet and water available ad libitum. Cage bedding was changed three times weekly. On PPD 13, 14, 15, or 16, AChE +/+ and AChE +/- pups from 56 litters (264 animals) were removed from the birth cage and placed in a sterile standard mouse cage lined with paper towels and fitted with an isolator top. The 37 AChE -/- mice of the 56 litters were not included in this part of the study. These developmentally delayed pups do not have their eyes open and are not fully mobile until PPD 15; therefore, weaning prior to this time would result in death of the pup. Day 13 was chosen as the earliest day of weaning of AChE +/+ and +/- pups because, by PPD 12, the pup's eyes are open, the animals are mobile, and they are able to regulate their body temperature.

A 12 × 8.3 × 3.2-cm sterile plastic box with a hole in the side was lined with paper towels and inverted in the cage to provide shelter and additional warmth. Shallow plastic petri dishes were placed on the floor of the cage to hold the Ensure Fiber liquid diet. Several 11% (wt./wt.) diet pellets were placed on the floor. Additional pellets and a water bottle were placed in the hopper on the cage lid. Approximately a third of the cage, the portion containing the lined box, was placed on a 11 × 13-in. heating pad, providing a surface temperature of 42°C. Cage bedding was changed, food dishes were washed, and the Ensure diet was replenished daily.

Determination of body weight and surface body temperature. Body weight and surface body temperature of pups in nine litters (45 pups) were measured daily from day 10 through day 21. Half the animals in each litter were weaned on

Table 1. Detection of *Helicobacter hepaticus* in group-housed acetylcholinesterase (AChE) -/- mice (n = 23)

Cage no.	Age at testing (days)	No. of *H. hepaticus*-positive mice	No. of *H. hepaticus*-negative mice
1	222-392	1	5
2	92-249	1	4
3	31-70	4	3
4	29-33	2	3

Mice were group housed from postpartum day (PPD) 15 onward.

day 13, while the remainder were left with the dam through day 21. Body weight was measured daily, using a top-loading balance. The axial body temperature was measured daily by use of a digital thermometer (Thermalert model TH-5 and a surface Microprobe MT-D, Type T thermocouple, Physitemp Instruments Inc., Clifton, N.J.). Data from male and female pups were analyzed separately to avoid having sex as a confounding variable in the results.

Statistical analysis. Body weight, surface temperature data, and litter size were analyzed, using the Microsoft Excel data analysis program. Statistical differences were determined by use of a two-tailed independent t test, with significance set at $P = 0.05$.

Results

Initial *H. hepaticus* detection. In one routine quarterly screening of our AChE knockout colony by RADIL, all sentinel mice (n = 6) were determined to be free of antibodies to MHV and all other pathogens. These same mice were all found to be infected with *H. hepaticus* on the basis of results of fecal analysis. Subsequent random testing of feces from the colony indicated that the infection was widespread, with 100% of the AChE +/+ (11/11) and AChE +/- (13/13) mice testing positive. Infection status was determined in house by PCR analysis of purified DNA from fecal samples.

Group-housed AChE -/- infection rate. Twenty three AChE -/- mice group-housed in four cages were individually tested for *H. hepaticus* infection (Table 1). The four cages had a total of 15 mice testing negative for *H. hepaticus* and eight testing positive, for a 35% infection rate.

Lack of coprophagia in AChE -/- mice. Observations that the AChE -/- mice are not coprophagic were made over a two-year period. The AChE -/- mice were never observed consuming feces, a behavior common to the AChE +/+ and +/- mice. The solid fecal pellets were not held or consumed by the AChE -/- mice, as they lack grip and bite strength (18). Although the AChE -/- mice do not have a deficit in their olfactory sense (18), they did not manifest interest in the feces of other animals when introduced to a new cage.

Early weaning. A total of 56 litters of mice, 264 AChE +/+ and +/- pups, were weaned on PPD 13 (n = 25 litters), 14 (n = 19 litters), 15 (n = 8 litters) or 16 (n = 4 litters) (Table 2). Average litter size for each group was: PPD 13, 6.1 pups/litter; PPD 14, 5.5 pups/litter; PPD 15, 5.8 pups/litter; and PPD 16, 6.1 pups/litter. There was no significant difference among litter sizes. Because of delayed eye opening and reduced locomotor activity, AChE -/- mice cannot be weaned until day 15; therefore, these mice were not included in this experiment. Each litter was tested for *H. hepaticus* infection on PPD 21 to 30. Because of time and cost considerations, pups were not housed or tested individually. Litters were group-housed, and it was assumed

Table 2. Effect of early weaning on infection rate

PPD of weaning	No. of litters *H. hepaticus* pos.	No. of litters *H. hepaticus* neg.	% of mice *H. hepaticus* pos.	% of mice converting to pos. status
13	2	23	8.0	0
14	13	6	68.4	0
15	5	3	62.5	0
16	4	0	100.0	NA

Mice in 56 litters (n = 264; AChE +/+ and +/- pups) were weaned on postpartum day (PPD) 13, 14, 15 or 16, and were tested for *H. hepaticus* on days 21 to 30 and again every 3 weeks through 120 days. Mice that were test negative in the first test period, remained negative in subsequent test periods.
Pos. = test positive; NA = all animals weaned on day 16 tested positive for *H. hepaticus*; therefore, the % conversion parameter is not applicable.
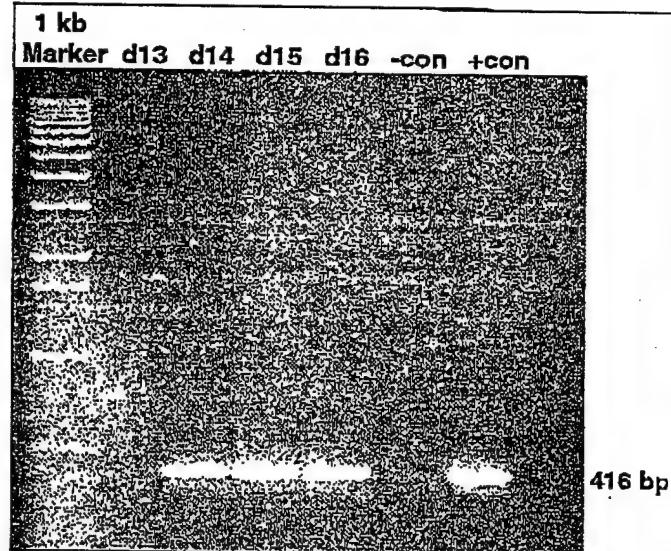
Figure 1. Detection of *Helicobacter hepaticus* by use of polymerase chain reaction (PCR) analysis. The DNA from the feces of acetylcholinesterase (AChE) +/+ and +/- mice pups was amplified by PCR analysis and was visualized on a 1% agarose gel containing ethidium bromide with a 1-kb marker. The 416-bp band indicates presence of *H. hepaticus* in mice weaned on postpartum day (PPD)14, 15, and 16. The absence of the band on day 13 indicates that the animal was not infected. The PCR product from a known infected animal was included as a positive control (+ con). The negative control (- con) is a PCR reaction containing no fecal DNA.

that if one animal became infected, the remainder would become infected (12, 18). Only two of 25 litters (8%) weaned on day 13 tested positive for *H. hepaticus*; however, 13 of 19 (68%) and three of five (60%) litters whose members were weaned on days 14 and 15, respectively, tested positive. All four (100%) of the litters whose members were weaned on PPD 16 tested *H. hepaticus* positive. An example of the PCR results from AChE +/+ and +/- mice weaned on PPD 13, 14, 15 or 16 is shown in Fig. 1. The 416-bp band is indicative of infection with *H. hepaticus*. Absence of the band on day 13 indicates that the pups in this litter were not infected. The litters whose members were deemed to be *H. hepaticus* negative were retested every three weeks after the initial testing. None of the previously test-negative litters converted to a positive status through 120 days of testing. The RADIL and Charles River Diagnostic Laboratories substantiated the findings by analyzing random samples previously tested in house.

Body weight and surface temperature of early-weaned pups. Body temperature (Fig. 2) and body weight (Fig. 3) were

463
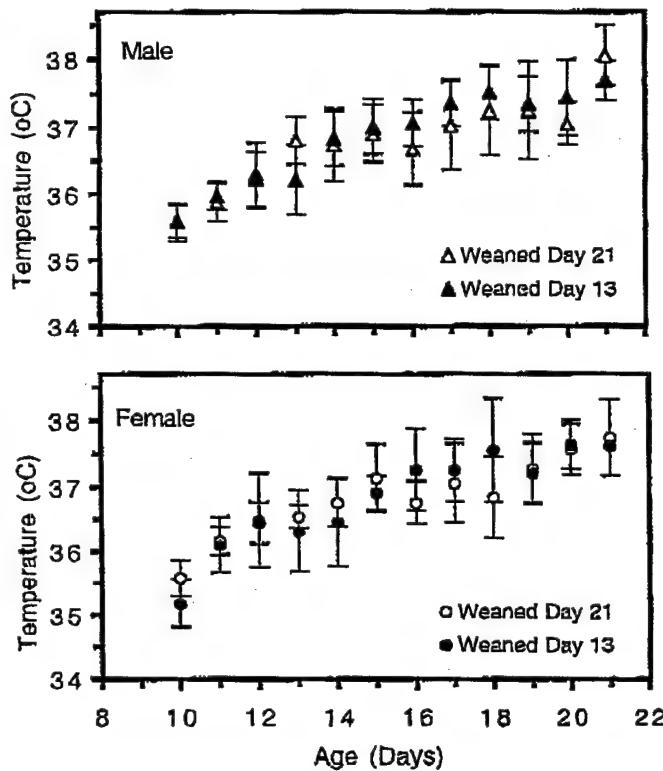
Figure 2. Surface body temperature of AChE +/+ and +/- pups weaned on day 13 (male, n = 13; female, n = 12) or day 21 (male, n = 11; female, n = 9). There was no significant difference at any time point (two-tailed independent *t* test with significance level of *P* < 0.05). Error bars represent ± SD.

Figure 3. Body weight of AChE +/+ and +/- pups weaned on day 13 (male, n = 13; female, n = 12) or day 21 (male, n = 11; female, n = 9). Pups weaned on day 13 had significantly lower body weight on day 14 (*P* = 0.001) and on day 15 (*P* = 0.007) than did the male littermates weaned on day 21 (two-tailed independent *t* test with significance level of *P* < 0.05). See Fig. 2 for key.

measured daily for nine litters. One half of each litter was weaned on day 13, and the other half was left with the dam through day 21, the routine day of weaning. There was no significant difference between surface body temperature of the early- weaned male (n = 13) and female (n = 12) pups and the day-21 weaned male (n = 11) and female (n = 9) pups (two-tailed independent samples *t*-test significance level, *P* = 0.05). Body weight of the male pups weaned on day 13 was significantly lower on days 14 (*P* = 0.001) and 15 (*P* = 0.007), compared with the weight of male pups that were left with the dam through day 21. From days 16 to 21, body weight did not differ significantly between the two male groups. There was no significant difference in body weight in pups of the female group at any time. Although it was not significant, there was a trend toward lower weight in pups of the early-weaned group from days 14 to 20, compared with that in the female pups weaned on day 21.

Mortality/morbidity of early-weaned pups. There were 264 individual pups in the 56 early-weaned litters. One animal died on day 18 during the weaning process (0.4% mortality). This animal did not manifest any untoward signs of disease prior to death. Other indicators of morbidity were not observed in any of the early-weaned pups.

Sexual development. On PPD 50 to 58, eight heterozygote, early-weaned, *H. hepaticus*-negative females were bred to sexually mature, heterozygote, early-weaned, *H. hepaticus*-negative males. All of the females (8/8) gave birth from 21 to 26 days after exposure to the males. Average litter size was 5.3 pups.

464

Discussion

Concerns regarding the long-term health of our *H. hepaticus*-infected AChE knockout colony prompted this laboratory to investigate a method of eradication of the organism. The possibility that infection could prove to be a confounding factor in the data generated from these animals was considered. Although clinical signs of disease ascribed to this infection were not apparent, and signs of disease were not observed by gross and microscopic examinations, long-term effects could not be ruled out. Infected animals could not be shipped to other facilities because of their *H. hepaticus*-positive status, resulting in delay in collaborative research efforts.

Early-weaning rationale. To facilitate feeding and to provide a constant warm environment, AChE -/- mice are weaned on day 15. This early-weaning protocol has made it possible to raise a high percentage of these fragile pups to adulthood (18). Remarkably, only 35% of the early-weaned, group-housed, non-coprophagic AChE -/- mice tested positive for *H. hepaticus*. The oldest AChE -/- animal in the colony (392 days) as well as four other animals in the same cage were negative for *H. hepaticus* even though they had been housed with an *H. hepaticus*-positive animal for seven months. This finding is in contrast to results of studies indicating rapid infection with *H. hepaticus*, either after exposure to contaminated bedding (12, 13) or by exposure to the bacteria in the birth cage (14). The AChE -/- mice testing positive may have originally contracted the bacteria from the dam's coat

while suckling. Our results substantiate the reported link between coprophagia and infection with *H. hepaticus*. It follows that, by using the same early-weaning protocol, the AChE +/+ and +/- mice could be weaned prior to becoming coprophagic, thereby eliminating spread of the bacteria. The stronger and more developmentally mature AChE +/+ and +/- mice were able to be weaned prior to day 15. Truett and co-workers (14) reported that, when 13-day-old *Helicobacter*-free mice were housed with *Helicobacter*-contaminated dams, they became *Helicobacter* positive by day 16. Ebino and co-workers (19) reported that suckling ICR mice manifested coprophagic behavior at 17 to 18 days of age. Considering these data we focused on a range of weaning times from days 13 to 16. Our data indicated marked difference in the infection rate between pups weaned on PPD 13 versus those weaned one day later. This may represent a transition period between non-coprophagic and coprophagic behavior in 129S6/SvEvTac mice. This 13- to 14-day postpartum period may also represent a time when the pups become more susceptible to intestinal invasion by the *Helicobacter* organism. There may be strain differences when it comes to the appropriate day to wean. Physically larger mouse strains may develop faster and become coprophagic by day 13, requiring that they be weaned before day 13. Smaller, fragile or slower developing strains may not yet have their eyes open, or be mobile enough to feed from a petri dish. The appropriate day to wean would have to be established for each colony.

Stress associated with early weaning. Concern about the stress that early weaning might cause prompted additional parameters, such as weight loss, decrease in body temperature, increase in morbidity or mortality, and delayed time to sexual development, to be examined. Although we saw significant weight loss in the early weaned male pups beginning on day 14, there was rapid and sustained recovery by day 16. Body temperature between the two groups was not significantly different. Morbidity was not observed in any of the early-weaned pups. There have been 225 pups weaned on day 13 and only one pup has died. Early-weaned females were successfully bred at eight weeks of age, producing 5.3 pups/litter. Females weaned on day 21 have routinely been bred in this time frame. The average litter size of 5.3 pups from the early-weaned dams (n = 8) is similar to the average litter (5.7 pups/litter) for a non-early-weaned first-litter dam (n = 27).

The lower body weight from days 14 through 16 after weaning suggested a minimal degree of stress involved in the early-weaning process. Reduction in the level of stress was accomplished by addition of a covered secure area in the cage for the pups to hide, by providing additional warmth, and by feeding a liquid diet. Different strains of mice may be more or less prone to stress than is the 129S6/SvEvTac strain used in this study.

Labor and cost factors. The early-weaning protocol is labor intensive. Cage bedding and liquid diet must be changed daily. If the early-weaned pups are housed in a room with infected animals, they must be handled prior to handling infected animals. Using sterile technique and isolator housing is important because fecal contamination can be easily transmitted from gloves, infected cages, or bedding that may be scattered from infected cages (12). The animals must be screened after weaning on day 13 and routinely screened to ensure that the test-negative animals have not converted to test-positive status. Animals testing positive for *H. hepaticus* must be culled from

the colony. Screening of feces from an entire cage verses individual animals saved time and expense. Using the commercially available QIAGEN fecal DNA purification kit proved to be convenient and rapid. The expense of screening numerous samples by use of this method could become prohibitive. An inexpensive alternative was proposed by Truett and co-workers (14), using a reagent termed HotSHOT for the purification procedure.

In conclusion, our experience with the successful early weaning of non-coprophagic AChE -/- mice led us to develop a safe, rapid, inexpensive procedure for eradication of *H. hepaticus*. By weaning pups on day 13, using sterile technique, reducing stress by feeding a liquid diet, providing a supplementary heat source and a sheltered area in the cage, and conducting routine fecal screening, we were able to re-establish a breeding colony free of infection with *H. hepaticus*.

Acknowledgments

References

1. Fox, J. G., F. E. Dewirst, J. G. Tully, B. J. Paster, L. Yan, N. S. Taylor, M. J. Collins, Jr., P. L. Gorelick, and J. M. Ward. 1994. *Helicobacter hepaticus* sp. nov., a microaerophilic bacterium isolated from livers and intestinal mucosal scrapings from mice. J. Clin. Microbiol. 32:1238-1245.

2. Ward, J. M., J. G. Fox, M. R. Anver, D. C. Haines, C. V. George, M. J. Collins, Jr, P. L. Gorelick, K. Nagashima, M. A. Gonda, R. V. Gilden, J. G. Tully, R. J. Russell, R. E. Benveniste, B. J. Paster, F. E. Dewhirst, J. C. Donovan, L. M. Anderson, and J. M. Rice. 1994. Chronic active hepatitis and associated liver tumors in mice caused by a persistent bacterial infection with a novel *Helicobacter* species. J. Natl Cancer Inst. 86:1222-1227.

3. Ward, J. M., M. R. Anver, D. C. Haines, and R. E. Benveniste. 1994. Chronic active hepatitis in mice caused by *Helicobacter hepaticus*. Am. J. Pathol. 145:959-968.

4. Fox, J. G., X. Li, L. Yan, R. J. Cahill, R. Hurley, R. Lewis, and J. C. Murphy. 1996. Chronic proliferative hepatitis in A/JCr mice associated with persistent *Helicobacter hepaticus* infection: a model of Helicobacter-induced carcinogenesis. Infect. Immun. 64:1548-1558.

5. Fox, J. G., J. A MacGregor, Z. Shen, X. Li, R. Lewis, and C. A. Dangler. 1998. Comparison of methods of identifying *Helicobacter hepaticus* in B6C3F₁ mice used in a carcinogenesis bioassay. J. Clin. Microbiol. 36:1382-1387.

6. Fox, J. G., L. Yan, B. Shames, J. Campbell, J. C. Murphy and X. Li. 1996. Persistent hepatitis and enterocolitis in germ-free mice infected with *Helicobacter hepaticus*. Infect. Immun. 64:3673-3681.

7. Cahill, R. J., C. J. Foltz, J. G. Fox, C. A. Dangler, F. Powrie, and D. B. Schauer. 1997. Inflammatory bowel disease: an immunity-mediated condition triggered by bacterial infection with *Helicobacter hepaticus*. Infect. Immun. 65:3126-3131.

8. Whary, M. T., T. J. Morgan, C. A. Dangler, K. J. Gaudes, N. S. Taylor, and J. G. Fox. 1998. Chronic active hepatitis induced by *Helicobacter hepaticus* in the A/JCr mouse is associated with a Th1 cell-mediated immune response. Infect. Immun. 66:3142-3148.

9. Foltz, C. J., J. G. Fox, R. Cahill, J. C. Murphy, L. Yan, B. Shames, and D. B. Schauer. 1998. Spontaneous inflammatory bowel disease in multiple mutant mouse lines: association with colonization by *Helicobacter hepaticus*. Helicobacter 3:69-78.

10. Kullberg, M. C., J. M. Ward, P. L. Gorelick, P. Caspar, S. Hieny, A. Cheever, D. Jankovic, and A. Sher. 1998. *Helicobacter hepaticus* triggers colitis in specific-pathogen-free interleukin-10 (IL-10)-deficient mice through an IL-12- and gamma interferon-dependent mechanism. Infect. Immun. 66:5157-5166.

11. Rice, J. M. 1995. *Helicobacter hepaticus*, a recently recognized bacterial pathogen, associated with chronic hepatitis and hepatocellular neoplasia in laboratory mice. Emerg. Infect. Dis. 1:1-2.

12. Whary, M. T., J. H. Cline, A. E. King, C. A. Corcoran, S. Xu, and J. G. Fox. 2000. Containment of *Helicobacter hepaticus* by use of husbandry practices. Comp. Med. 50:78-81.

13. Livingston, R. S., L. K. Riley, C. L. Besch-Williford, R. R. Hook, Jr., and C. L. Franklin. 1998. Transmission of *Helicobacter hepaticus* infection to sentinel mice by contaminated bedding. Lab. Anim. Sci. 48:291-293.

14. Truett, G. E., J. A. Walker, and D. G. Baker. 2000. Eradication of infection with *Helicobacter spp.* by use of neonatal transfer. Comp. Med. 50:444-451.

15. Foltz, C. J., J. G. Fox, L. Yan, and B. Shames. 1995. Evaluation of antibiotic therapies for eradication of *Helicobacter hepaticus*. Antimicrob. Agents Chemother. 39:1292-1294.

16. Xie, W., J. A. Stribley, A. Chatonnet, P. J. Wilder, A. Rizzino, R. D. McComb, P. Taylor, S. H. Hinrichs, and O. Lockridge. 2000. Postnatal developmental delay and supersensitivity to organophosphate in gene-targeted mice lacking acetylcholinesterase. J. Pharmacol. Exp. Ther. 293:896-902.

17. Li, B., J. A. Stribley, A. Ticu, W. Xie, L. M. Schopfer, P. Hammond, S. Brimijoin, S. H. Hinrichs, and O. Lockridge. 2000. Abundant tissue butyrylcholinesterase and its possible function in the acetylcholinesterase knockout mouse. J. Neurochem. 75:1320-1331.

18. Duysen, E., J. A. Stribley, D. L. Fry, S. H. Hinrichs, and O. Lockridge. 2002. Rescue of the acetylcholinesterase knockout mouse by feeding a liquid diet; phenotype of the adult acetylcholinesterase deficient mouse. Dev. Brain Res. 137:43-54.

19. Ebino K. Y., T. Suwa, Y. Kuwabara, T. R. Saito, and K. W. Takahashi. 1987. Lifelong coprophagy in male mice. Jikken Dobutsu. 36:273-276.

Regulation of muscarinic acetylcholine receptor function in acetylcholinesterase knockout mice ☆

Bin Li[a,b], Ellen G. Duysen[a], Laura A. Volpicelli-Daley[c], Allan I. Levey[c], Oksana Lockridge [a,b,*]

[a]Eppley Institute, University of Nebraska Medical Center, Omaha, NE 68198, USA
[b]Department of Biochemistry and Molecular Biology, University of Nebraska Medical Center, Omaha, NE 68198, USA
[c]Department of Neurology and Center for Neurodegenerative Disease, Emory University School of Medicine, Atlanta, GA 30322, USA

Abstract

Acetylcholinesterase (AChE) hydrolyzes acetylcholine to terminate cholinergic neurotransmission. Overstimulation of cholinergic receptors by excess acetylcholine is known to be lethal. However, AChE knockout mice live to adulthood, although they have weak muscles, do not eat solid food, and die early from seizures. We wanted to know what compensatory factors allowed these mice to survive. We had previously shown that their butyrylcholinesterase activity was normal and had not increased. In this report, we tested the hypothesis that AChE − / − mice adapted to the absence of AChE by downregulating cholinergic receptors. Receptor downregulation is expected to reduce sensitivity to agonists and to increase sensitivity to antagonists. Physiological response to the muscarinic agonists, oxotremorine (OXO) and pilocarpine, showed that AChE − / − mice were resistant to OXO-induced hypothermia, tremor, salivation, and analgesia, and to pilocarpine-induced seizures. AChE+/ − mice had an intermediate response. The muscarinic receptor binding sites measured with [³H]quinuclinyl benzilate, as well as the protein levels of M1, M2, and M4 receptors measured with specific antibodies on Western blots, were reduced to be approximately 50% in AChE − / − brain. However, mRNA levels for muscarinic receptors were unchanged. These results indicate that one adaptation to the absence of AChE is downregulation of muscarinic receptors, thus reducing response to cholinergic stimulation.
© 2003 Elsevier Science Inc. All rights reserved.

Keywords: Acetylcholinesterase; Knockout mice; Muscarinic receptor; Oxotremorine; Pilocarpine; Seizures

1. Introduction

Acetylcholinesterase (AChE; EC 3.1.1.7) has a crucial role in cholinergic neurotransmission, hydrolyzing the neurotransmitter acetylcholine to terminate nerve impulse transmission. Acute AChE inhibition by nerve agents or organophosphorus pesticides may be lethal. No case of total AChE deficiency in the human population has ever been reported, leading to the speculation that inactive AChE mutations may be embryonically lethal. Therefore, it was a surprise to find out that AChE knockout mice without AChE activity survived to adulthood (Duysen et al., 2002; Li et al., 2000; Xie et al., 2000).

The absence of AChE activity most likely results in abnormally high levels of acetylcholine in the cholinergic synapses. AChE − / − mice have motor tremor and pinpoint pupils, signs indicative of the presence of excess acetylcholine. Although acute overstimulation of acetylcholine receptors by excess acetylcholine is known to be lethal (Mileson et al., 1998), surprisingly, AChE − / − mice live to adulthood when maintained on a liquid diet (Duysen et al., 2002) and many have survived for nearly 2 years. Death occurs from seizures. The cholinergic marker, choline acetyl transferase, showed normal anatomical distribution in AChE − / − brain, indicating that the absence of AChE does not affect the development of cholinergic

pathways in the central nervous system (Mesulam et al., 2002).

The mice live despite the complete absence of AChE, suggesting that they have adapted to the absence of AChE, or that a backup enzyme substitutes for the missing AChE activity. Butyrylcholinesterase (BChE; EC 3.1.1.8) did not undergo compensatory increases in the AChE $-/-$ mouse (Li et al., 2000). However, inhibition of BChE was lethal to AChE $-/-$ mice (Xie et al., 2000). It is possible that the normal level of BChE plays a role in keeping AChE $-/-$ mice alive by hydrolyzing acetylcholine (Li et al., 2000; Mesulam et al., 2002). The present study examined whether AChE knockout mice have adapted to the absence of AChE by downregulating muscarinic receptors. Several other adaptation mechanisms are possible, but have not yet been tested. For example, nicotinic receptors may be downregulated, and there may be changes in rates of acetylcholine synthesis and release.

The action of acetylcholine is mediated by nicotinic and muscarinic acetylcholine receptors (mAChRs). The mAChR family belongs to the G protein-coupled receptor gene superfamily and consists of five subtypes (M1–M5), which regulate numerous fundamental physiological processes, including motor control, temperature regulation, pain perception, learning, and memory (Messer et al., 1990; van der Zee and Luiten, 1999). In the peripheral nervous system, mAChR mediates smooth muscle contraction, glandular secretion, and cardiac function (Caulfield and Birdsall, 1998; Eglen, 2001). Acetylcholine is known to regulate the level of both nicotinic and muscarinic receptors in many systems. Chronic agonist stimulation of mAChR results in desensitization and downregulation of mAChR (Honda et al., 1995). Downregulation of muscarinic receptors is generally accompanied by decreased sensitivity to muscarinic agonists and increased sensitivity to muscarinic antagonists. Conversely, upregulation of mAChR is found after chronic administration of muscarinic antagonists (Ben-Barak and Dudai, 1980). Therefore, we tested whether mice without AChE have adapted to the absence of AChE by downregulation of cholinergic receptors. We found that AChE knockout mice have a significant reduction in the number and responsiveness of muscarinic receptors, indicating that the chronic absence of AChE produces marked changes in the cholinergic system. Downregulation of muscarinic receptors is one of the mechanisms that explains the survival of AChE $-/-$ mice.

2. Materials and methods

2.1. Drugs

Oxotremorine (OXO) sesquifumarate salt, pilocarpine hydrochloride, and atropine sulfate salt were from Sigma (St. Louis, MO). OXO and atropine were dissolved in sterile water. Pilocarpine was dissolved in phosphate-buffered saline.

2.2. Pharmacological and behavioral studies

Animal studies were carried out in accordance with the Guide for the Care and Use of Laboratory Animals as adopted by the National Institutes of Health. The AChE $-/-$ mouse colony is maintained by breeding heterozygotes (Duysen et al., 2002; Xie et al., 2000). Two- to 4-month-old mice of both sexes were used. No significant differences in responses were found between male and female animals.

Mice from each genotype were injected subcutaneously with 1 or 0.2 mg/kg OXO, a nonselective muscarinic receptor agonist. Body temperature, salivation, and tremor were assessed immediately before and after injection. Body temperature was measured with a surface thermometer (Physitemp Instruments, Clifton, NJ). Salivation was scored as: $1 = no\ salivation$; $2 = moisture\ on\ face\ only$; and $3 = moisture\ on\ the\ face\ and\ chest$. Tremor was scored on a scale of $1 = no\ tremor$; $2 = intermittent\ head\ and\ body\ tremor$; and $3 = nearly\ continuous\ whole\ body\ tremor$. The data were expressed as a percent of the maximum possible score.

The antinociceptive effect of OXO was investigated using tail-flick and hot-plate tests. The tail-flick test was carried out by immersing approximately 1 cm of the tip of the mouse tail in a 55 °C water bath. The response latency for the animal to withdraw its tail was measured immediately before (baseline) and 30 min after drug injection. A 10-s maximum cut-off was imposed to prevent tissue damage. The hot-plate test was performed by using an electronically controlled hot plate set to 55 °C. The animal was placed on the hot plate and the time required for the animal to jump or lick its paws was measured before and 30 min after OXO injection. The cut-off time was 30 s.

Seizures were induced by injecting freshly dissolved pilocarpine at a dose of 200 mg/kg ip. Pilocarpine solutions, prepared the day before and stored at 4 °C, gave a decreased response. The mice were observed for 45 min for seizures after drug injection. Salivation and lacrimation were scored on the same scale as described above. Gastrointestinal mobility was observed as the amount of defecation.

To determine the LD_{50} of atropine in AChE+/+, +/$-$, and $-/-$ mice, the "up-and-down" procedure for acute toxicity testing was employed (Bruce, 1987). This method requires the use of fewer animals relative to other methods of estimating the LD_{50}. Adult female mice (56–91 days) were injected intraperitonally with atropine. AChE+/+ ($n=24$), +/$-$ ($n=27$), and $-/-$ ($n=15$) animals were monitored continuously throughout the treatment period. Moribund animals were euthanized immediately.

The LD_{50} values were estimated by a probit regression analysis of the data, using the PROBIT procedure of the SAS system.

2.3. Ligand binding assay

Mouse whole brains from wild type and nullizygous mice were flash frozen in liquid nitrogen, and stored at −70 °C until use. Plasma membrane was prepared by the method of Gray and Whittaker (1962). Two wild type brains or two nullizygous brains were pooled and homogenized by hand with 20 strokes of a Dounce tissue homogenizer in 10 vol of ice-cold 50 mM Tris−Cl (pH 8.0) containing 0.32 M sucrose and protease inhibitor cocktail (Roche, Germany). The homogenate was centrifuged for 10 min at $1000 \times g$. The pellet (crude nuclear fraction) was discarded and the supernatant was centrifuged at $17,000 \times g$ for 55 min. The membrane pellet was suspended in 2 ml of 50 mM Tris buffer (pH 7.4). Protein concentrations were determined by the BCA protein assay (Pierce Chemical, Rockford, IL).

The ligand binding properties of mAChR from wild type and AChE − / − brain extracts were determined by titration with [^{3}H]quinuclinyl benzilate ([^{3}H]QNB; 39 Ci/mmol; Perkin-Elmer, Boston, MA) (Peterson and Schimerlik, 1984). [^{3}H]QNB is a nonselective muscarinic antagonist, which labels all five muscarinic receptor subtypes. Briefly, membrane factions (100 μg of protein) were mixed with 2 ml of 50 mM potassium phosphate buffer (pH 7.4), containing various concentrations of [^{3}H]QNB, ranging from 10 to 400 pM. The mixture was incubated for 1.5 h at room temperature. Nonspecific binding was determined in the presence of 10 μM atropine. The reaction was terminated by addition of 3 ml of ice-cold 50 mM potassium phosphate buffer, then immediately filtered under vacuum through Whatman GF/B glass fiber filter, and washed three times with 3 ml of ice-cold 50 mM potassium phosphate buffer. The filters were placed in 7-ml plastic minivials and dried. Four milliliters of EcoLume scintillation cocktail (ICN) was added and radioactivity was measured using a Beckman liquid scintillation counter. Titration data were fit to the equation for a single dissociation process using nonlinear regression analysis (SigmaPlot, version 4.16). [Comp]= $\{[M][QNB]\}/\{K_d+[QNB]\}$, where [M] = total concentration of muscarinic receptor per milligram of protein; [QNB] = total concentration of QNB; K_d = dissociation constant; [Comp] = measured concentration of QNB receptor complex per milligram of protein.

Total QNB binding sites in brain plasma membranes were determined using a saturating concentration of [^{3}H]QNB (3 nM). Brain plasma membranes were prepared from three 23-day-old AChE+/+ and three 23-day-old AChE − / − mice.

2.4. Northern analysis

Total RNA was extracted from tissues of 20- to 40-day-old mice using Trizol reagent (GibcoBRL, Rockville, MD) according to the manufacturer's instructions. To prepare probes, DNA fragments corresponding to parts of the coding regions from M1, M3, and M4 muscarinic receptors were amplified by polymerase chain reaction (PCR) from 129SvJ mouse genomic DNA. The primers were: M1 receptor sense (5′-GCTACATCCAGTTCCTCTCCCAA C) and M1 receptor antisense (5′-TGCCTTCTTCTCCTTGA-CCAGTG); M3 receptor sense (5′-CAGAAGCGGA-AGCAGAAAACTTTG) and M3 receptor antisense (5′-TTTGAAGGACAGAGGTAGAGCGGC); M4 receptor sense (5′-AGCCATTGCT GCCTTCTACCTG) and M4 receptor antisense (5′-TCACTGCCTGTCTGCTTTGT-CAC). The Genbank accession numbers for the M1, M3, and M4 sequence are NM007698, AF264050, and NM007699, respectively. The PCR products were sequenced to check for correctness and then used directly as templates to synthesize ^{32}P-labeled single-stranded probes. The M2 receptor probe was a 519-bp $BstxI$ fragment from mM2-PCDPS vector (kindly provided by Dr. Jurgen Wess). Northern hybridization was performed using ExpressHyb hybridization solution (Clontech, Palo Alto, CA) according to the manufacturer's instructions. Blots were hybridized at 68 °C, and washed at 25 and 50 °C.

2.5. Western analysis

Total forebrains from two 33-day-old AChE+/+ and two 33-day-old AChE − / − mice were flash frozen in liquid nitrogen. Homogenization buffer (50 mM Tris−HCl, pH 7.5; 50 mM NaCl; 10 mM EGTA; 5 mM EDTA) and protease inhibitor cocktail (Roche) were added and the samples were sonicated. Samples were solubilized in 0.125 M Tris−Cl, pH 6.8, buffer containing 4% sodium dodecyl sulfate (SDS), 20% glycerol, and 10% mercaptoethanol. Fifty micrograms of each sample was loaded onto 8% polyacrylamide SDS gels and then transferred to PVDF membrane. The blots were incubated in primary antibody diluted in blocking buffer (M1, 1 μg/ml; M2, 1:500; M4, 1 μg/ml), followed by horseradish peroxidase-conjugated goat antirabbit secondary antibody, and detected by Renaissance Western Blot Chemiluminescence Reagent (Perkin-Elmer). The blots were reprobed for total extracellular signal-regulated kinase 2 (ERK2; 1:500) (Cell Signaling, Beverly, MA).

The M1, M2, and M4 are polyclonal antibodies prepared in the laboratory of Levey et al. (1991). A fusion protein of glutathione-S-transferase and the i3 loop of each human receptor were expressed in bacteria to make the antigen. The purified antigen was injected into rabbits. Negative controls to show the specificity of the M1, M2, and M4 receptor antibodies were brain extracts from muscarinic receptor knockout mice (Gerber et al., 2001; Gomeza et al., 1999a,b).

Commercially available antibodies did not give the same results as the antibodies from Levey et al. The mAChR M1 (C-20) goat polyclonal antibody raised against a carboxy terminal peptide of human M1 (catalog no. sc-7470; Santa Cruz Biotechnology, Santa Cruz, CA) gave a single strong band of 100 kDa. The rabbit polyclonal antibody against a

10-amino-acid peptide from the carboxyl terminus of human M2 receptor (catalog no. WR-3721; Research and Diagnostic Antibodies, Benicia, CA) hybridized with proteins that were larger than 65 kDa. The mouse monoclonal antibody against purified porcine cardiac M2 receptor (catalog no. MA3-044, clone 31-1D1; ABR, Golden, CO) recognized no proteins in the mouse brain. The goat polyclonal antibody against a peptide from the carboxyl terminus of human muscarinic M3 receptor (catalog no. sc-7474; Santa Cruz Biotechnology) gave many bands including a band of the expected size of 75 kDa. The mouse monoclonal antibody against the i3 loop of human M4 receptor, fused to GST (catalog no. MAB1576; Chemicon International, Temecula, CA), gave a single strong band of 70 kDa. None of the commercial antibodies showed a difference in band intensity between AChE+/+ and −/− muscarinic receptors.

3. Results

Behavioral studies were undertaken to test the status of muscarinic receptors in AChE knockout mice. It was expected that receptor downregulation will reduce sensitivity to agonists (pilocarpine and OXO), but will increase sensitivity to antagonists (atropine).

3.1. AChE−/− mice are resistant to pilocarpine-induced seizures

The administration of pilocarpine, the mAChR agonist, produces seizures in mice via activation of the M1 receptors (Hamilton et al., 1997). Pilocarpine was used to investigate the functional status of M1 receptors in AChE −/− mice. In response to pilocarpine, 200 mg/kg ip, all the wild type mice experienced multiple seizures and only 20% survived the treatment. AChE+/− mice, with 50% of normal AChE activity, showed intermediate sensitivity to pilocarpine-induced seizures, with 50% having seizures and 60% surviving. In contrast, none of the AChE −/− mice experienced seizures. All the AChE −/− mice survived (Table 1). The reduced sensitivity to pilocarpine-induced seizures in AChE −/− and +/− mice indicates that functional levels of M1 muscarinic receptors are reduced in both the complete and partial AChE deficiency states.

Table 1
AChE −/− mice are resistant to pilocarpine-induced seizures (200 mg/kg ip)

AChE genotype	Number of mice	Seizures [%]	Survival [%]
+/+	10	100	20
+/−	10	50	60
−/−	6	0	100

Mice of the indicated genotypes were injected with a fresh pilocarpine solution at a dose of 200 mg/kg ip. The animals were observed for seizures for 45 min after injection.
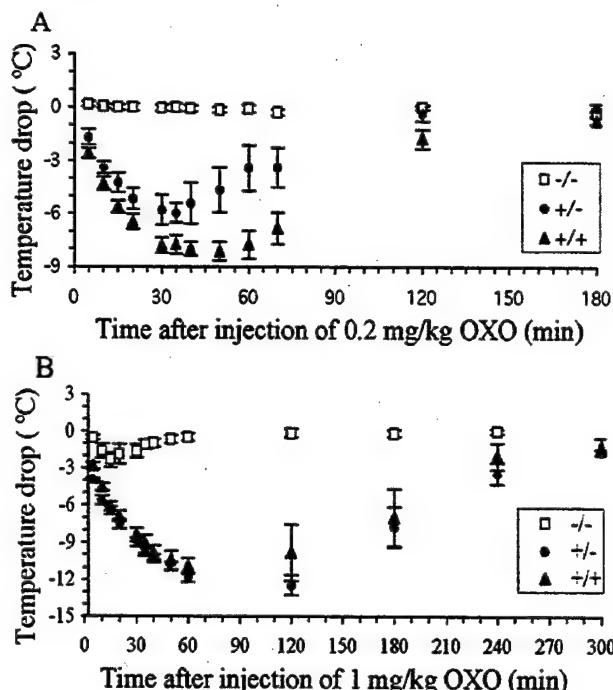
Fig. 1. Hypothermic response to OXO administration in mice. Mice of the indicated genotypes ($n = 6$ for each treated group) were injected subcutaneously with a dose 0.2 mg/kg (Panel A) or 1 mg/kg (Panel B) of the nonselective muscarinic agonist, OXO. The data are presented as mean ± S.E. AChE −/− response to OXO-induced hypothermia was significantly reduced compared to AChE+/+ and +/− mice ($P < .00001$, t test).

3.2. AChE−/− mice are resistant to OXO-induced hypothermia, tremor, salivation, and analgesia

One of the effects of the administration of the nonselective mAChR agonist, OXO, in normal mice is induction of hypothermia (Gomeza et al., 1999a). Following administration of 0.2 mg/kg OXO, AChE+/+ mice showed an 8 °C decrease in body temperature 30–60 min after agonist injection. The body temperature of AChE+/+ mice recovered to baseline 37.1 °C approximately 2–3 h after agonist injection (Fig. 1A). In contrast, there was no effect of this dose of OXO on body temperature in the AChE −/− mice. The decrease in temperature was less pronounced in AChE+/− mice (6 °C) and began to recover to baseline sooner than in AChE+/+ mice. Following a higher dose of OXO (1 mg/kg), AChE −/− mice showed only a slight 2 °C decrease in temperature that returned to baseline 36.5 °C by 45 min, whereas AChE+/+ and +/− mice showed an equivalent 12 °C drop in temperature that recovered 5 h after agonist injection (Fig. 1B). These results indicate that AChE −/− and +/− mice had decreased hypothermic response, an effect mediated by central M2 receptors (Gomeza et al., 1999a).

OXO also induces motor tremor (Gomeza et al., 1999a). As expected, OXO induced massive whole body tremor in AChE+/+ mice. The tremorogenic effects of OXO were

significantly reduced in AChE $-/-$ mice, even when the dose was increased to 1 mg/kg (Fig. 2A and B). The fact that OXO did induce some tremor in AChE $-/-$ mice indicates the presence of some functional M2 receptors. Heterozygous mice showed an intermediate response (Fig. 2A), but only at low doses of OXO. Recovery from OXO-induced tremor was rapid in AChE $-/-$, intermediate in AChE+/$-$, and slowest in AChE+/+ mice (Fig. 2A). Because the OXO-induced tremor response is primarily mediated by central M2 receptors (Gomeza et al., 1999a), it can be concluded that AChE deficiency at the 100% level and, surprisingly, also at the 50% level reduces the number of functional M2 receptors.

Administration of 0.2 mg/kg OXO resulted in salivary secretion in wild type and heterozygous mice, but not in AChE $-/-$ mice (Fig. 3A). The response was intermediate in AChE+/$-$ mice. When the dose was increased to 1 mg/kg, the AChE $-/-$ mice had a mild salivation response, indicating that they did have some functional receptors (Fig. 3B). At the higher dose, the response of AChE+/+ and +/$-$ mice was indistinguishable. These results indicate that AChE $-/-$ and +/$-$ mice have decreased levels of functional M3 receptors because sal-
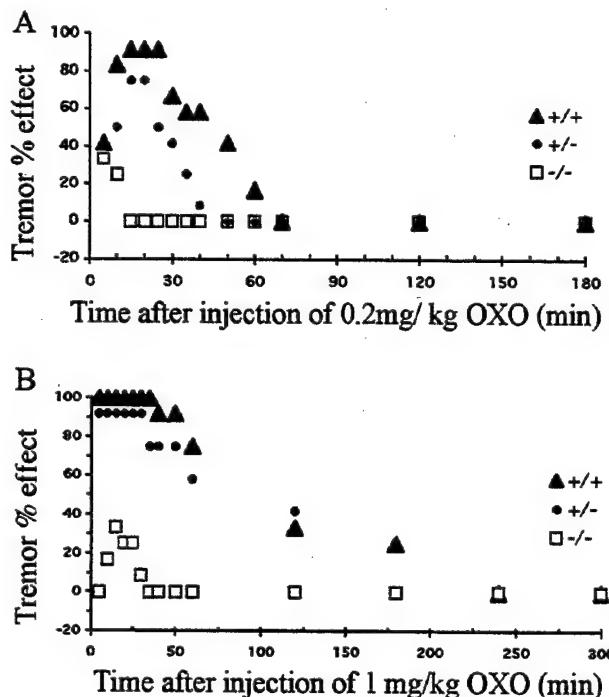
Fig. 2. Tremorogenic response to OXO administration in mice. Mice of the indicated genotypes ($n=6$ for each treated group) were injected subcutaneously with 0.2 mg/kg (Panel A) or 1 mg/kg (Panel B) of OXO. Data are presented as percent effect, where the score for each group was averaged and expressed as a percent of the maximum possible score. Standard error ranged from 0% to 16%. AChE $-/-$ response to OXO-induced tremor was significantly reduced compared to AChE+/+ and +/$-$ mice ($P<.0001$, AChE+/+ vs. AChE $-/-$; $P<.005$, AChE+/$-$ vs. AChE $-/-$, by t test).
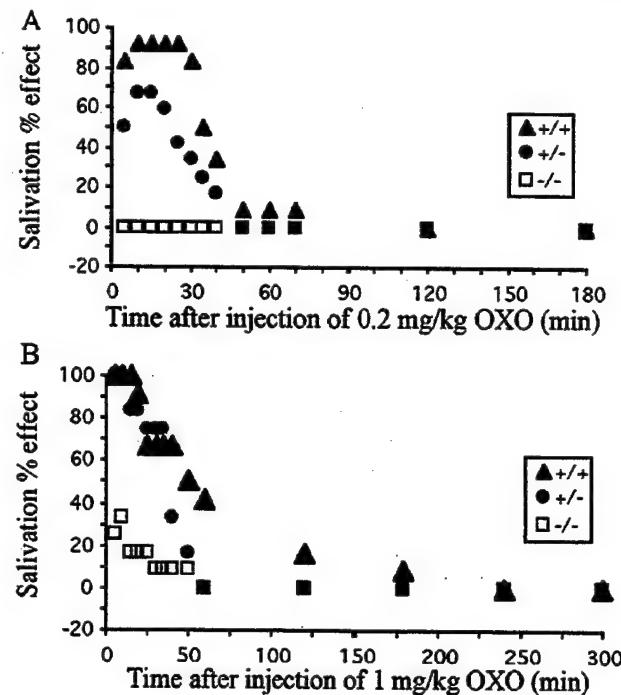
Fig. 3. Salivation response to OXO administration in mice. Mice of the indicated genotypes ($n=6$ for each treated group) were injected subcutaneously with a dose 0.2 mg/kg (Panel A) or 1 mg/kg (Panel B) of OXO. Data are presented as percent effect, where the score for each group was averaged and expressed as a percent of the maximum possible score. Standard error ranged from 0% to 20%. AChE $-/-$ response to OXO-induced salivation was significantly reduced compared to AChE+/+ and +/$-$ mice ($P<.00001$, AChE+/+ vs. AChE $-/-$; $P<.005$, AChE+/$-$ vs. AChE $-/-$, by t test).

ivation is primarily mediated by M3 receptors (Matsui et al., 2000).

Muscarinic agonists can cause analgesic effects by activating the muscarinic receptors in the pain pathway (Eisenach, 1999). The analgesic effect of OXO was investigated by using the tail-flick and hot-plate tests. The tail-flick test assesses pain sensitivity primarily at the spinal level and the hot-plate test measures pain responses mediated by supraspinal mechanisms (Konig et al., 1996). Normal baseline response to thermal stimuli with the hot-plate test (5–6 s) and tail-flick test (1–2 s) did not differ significantly in AChE+/+, +/$-$, and $-/-$ mice (Fig. 4A and B). In contrast, OXO administration (0.2 mg/kg) induced strong analgesic effects in AChE+/+ as well as AChE+/$-$ mice in both tests. OXO-dependent analgesic responses in AChE $-/-$ mice were significantly reduced compared to AChE+/+ and +/$-$ mice. AChE+/$-$ mice were almost as sensitive as wild type mice to OXO-induced analgesia in the tail-flick test. However, AChE+/$-$ mice showed intermediate analgesic response to OXO in the hot-plate test. Reduced analgesic response to OXO in AChE $-/-$ and +/$-$ mice indicates that the functional M2 and M4 muscarinic receptors are reduced in AChE-deficient mice. Muscarinic analgesia is exclusively mediated by a combination of M2 and
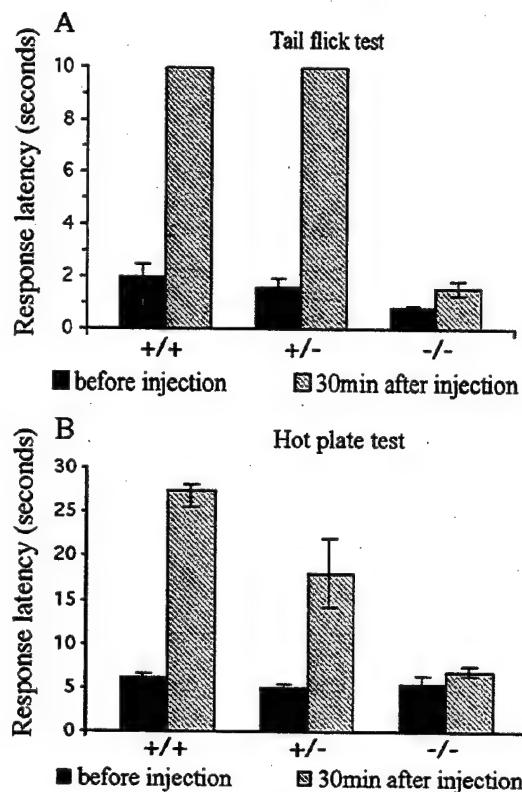
Fig. 4. Analgesic response to OXO administration in mice. Mice of the indicated genotypes ($n = 6$ per group) were injected with OXO subcutaneously (0.2 mg/kg) and analgesic responses were measured by the tail-flick and hot-plate tests. Data are presented as mean ± S.E. In (A), AChE −/− response to OXO was significantly reduced compared to AChE+/+ and +/− mice in tail-flick test ($P < .00001$, t test). In (B), AChE −/− response to OXO was significantly reduced compared to AChE+/+ and +/− mice in hot-plate test ($P < .00001$, AChE+/+ vs. −/−; $P < .01$ AChE+/− vs. AChE −/−, by t test).

M4 receptors at both spinal and supraspinal sites (Duttaroy et al., 2002).

The intermediate response of AChE+/− mice to OXO-induced effects suggests that efficient M2, M3, and M4 receptor-induced effects require a relatively high fractional receptor occupancy.

3.3. AChE−/− mice have low LD_{50} for atropine

Atropine, a specific muscarinic receptor antagonist, was used to further confirm that AChE −/− mice have reduced functional muscarinic receptors. The toxicity of atropine was determined by measuring the LD_{50} of atropine. Animals, regardless of genotype, experienced severe whole body tremor, initial hyperlocomotion, and clonic convulsions prior to death. The median lethal dose of atropine was 251 mg/kg (95% CI = 233; 272) in AChE+/+ mice, 216 mg/kg (95% CI = 209; 226) in AChE+/− mice, and 97 mg/kg (95% CI = 72; 107) in AChE −/− mice. The lower LD_{50} values of atropine for AChE −/− and +/− mice further confirmed that functional muscarinic receptors are reduced in AChE-deficient mice.

3.4. Muscarinic receptor binding sites are reduced in AChE−/− mice

Reduced responsiveness to the behavioral effects of central mAChR stimulation could result from decreased levels of mAChR. Radioligand binding assays were performed to determine the total number of mAChR in mouse brain plasma membranes using [^{3}H]QNB, a muscarinic antagonist that binds to all muscarinic subtypes with high affinity and specificity. The total number of muscarinic receptor binding sites in brain plasma membrane of AChE −/− mice was approximately 50% of that in wild type mice (Fig. 5). Heterozygotes showed an intermediate value, corresponding to a 25% loss in total [^{3}H]QNB binding. Titration of receptors with [^{3}H]QNB indicated that the binding characteristics of muscarinic receptors in wild type and AChE −/− mice were not significantly different, within the limits of the standard deviation. The dissociation constant was 176 ± 33 pM for AChE+/+ and 98 ± 22 pM for AChE −/− (Fig. 6). These data suggest that it is the number of muscarinic receptors, not their reactivity, which is reduced in AChE −/− mice. Thus, loss of muscarinic receptors is a major factor responsible for loss of physiological responses to agonist stimulation in AChE −/− mice.

3.5. Muscarinic receptor mRNA levels are unchanged in AChE−/− mice

Reduced levels of mAChR binding sites in AChE −/− mice could result from enhanced receptor degradation or decreased receptor expression. To determine whether alteration in mRNA expression of muscarinic receptors was responsible for reduced muscarinic receptor level in AChE −/− mice, mRNA levels of the M1–M4 subtypes
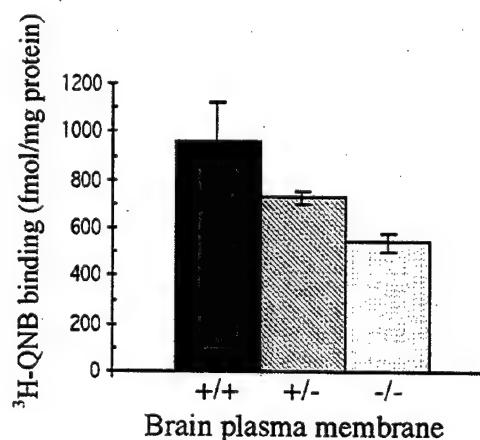
Fig. 5. Radioligand binding analysis of muscarinic receptor densities in AChE+/+, +/−, and −/− mice ($n = 3$ for each group). Brain membranes were prepared from the indicated genotypes. Muscarinic receptor densities were determined by radioligand binding using a saturating concentration (3 nM) of the muscarinic antagonist, [^{3}H]QNB. Data are given as mean ± S.E.
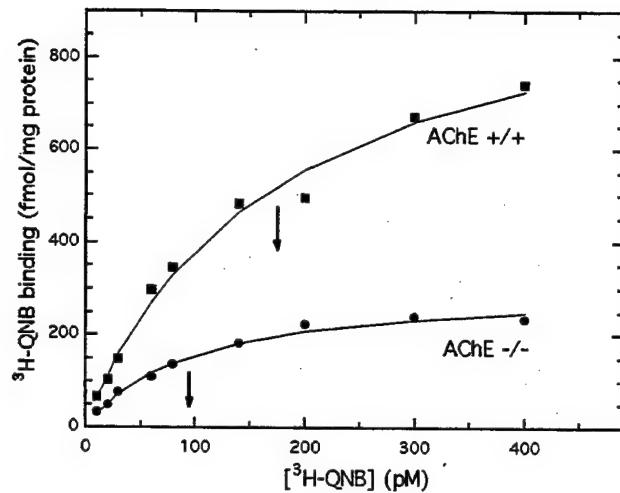
Fig. 6. Titration of [³H]QNB binding to muscarinic receptors in brain plasma membranes. Brain plasma membranes were prepared from two 32-day-old AChE+/+ and two 32-day-old AChE −/− mice. Titration was performed as described in Materials and Methods. Square (■) represents AChE+/+, and circle (●) represents AChE −/−. The arrows indicate the position of dissociation constants. The lines are fitted to the data using the following parameters: AChE+/+, $K_d = 176$ pM, $B_{max} = 1050$ fmol/mg protein; AChE −/−, $K_d = 98$ pM, $B_{max} = 306$ fmol/mg protein. Each point was the average of three measurements. The titration experiment was performed twice with essentially the same results.

were determined by Northern blotting. As shown in Fig. 7, mRNA levels of M1–M4 receptors were unchanged in the brain, intestines, and heart of AChE −/− mice. It is concluded that downregulation of functional muscarinic receptors in AChE −/− mice is not associated with a decrease of muscarinic receptor mRNA levels.
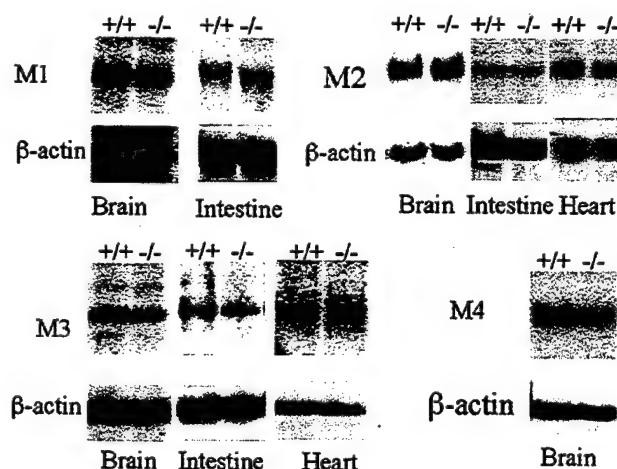
Fig. 7. Northern blot analysis of muscarinic receptor gene expression in AChE+/+ and −/− mice. Total RNA was extracted from the indicated tissues and hybridized with ³²P-labeled specific probes for muscarinic receptors M1–M4. Membranes were rehybridized with a β-actin probe as a loading control. Northern blotting was quantitated by ImageQuant software (Molecular Dynamics).

3.6. M1, M2, and M4 mAChR proteins are markedly reduced in AChE−/− mice

Binding assays demonstrated that total mAChR levels were reduced in the brains of AChE −/− mice. Because [³H]QNB does not distinguish among individual mAChR subtypes, the reduction in binding sites might preferentially involve one or more of the subtypes. The protein levels of M1, M2, and M4 muscarinic receptors, which are the primary mAChR expressed in the brain, were determined by Western blotting with specific antibodies (Levey et al., 1991). Brains from two AChE+/+ and two AChE −/− mice were used for these studies; individual results are shown in Fig. 8. The protein levels for M1, M2, and M4 muscarinic receptors in AChE −/− mice were each reduced approximately by 50% (M1, 38%; M2, 57%; and M4, 52%) compared to wild type mice. These findings suggest that
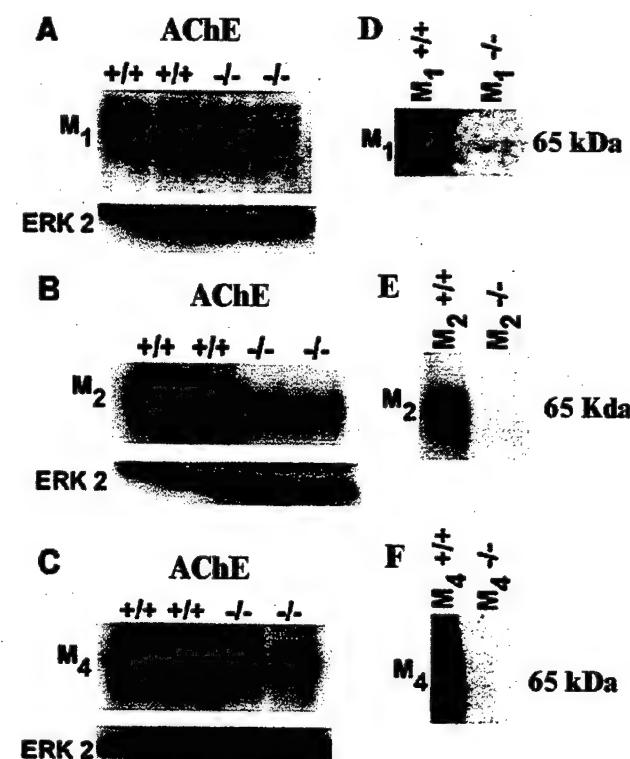
Fig. 8. Western blot analysis of muscarinic receptor proteins in AChE+/+ and −/− brains. Total forebrain homogenates from AChE+/+ and −/− mice were immunoblotted with M1 (Panel A), M2 (Panel B), and M4 (Panel C) antibodies. Each lane represents homogenates from individual AChE+/+ and −/− mice. Membranes were rehybridized with an ERK2 antibody as a loading control. The intensity of bands was quantitated by Kodak 1-D Image Analysis software and normalized using the intensities of total ERK2. Panels (D), (E), and (F) demonstrate the specificity of M1, M2, and M4 antibodies. Total brain homogenates from M1+/+ and −/− mice (Gerber et al., 2001), M2+/+ and −/− (Gomeza et al., 1999a), or M4+/+ and −/− (Gomeza et al., 1999b) knockout mice were immunoblotted with M1, M2, and M4 antibodies. The blots show M1, M2, and M4 immunoreactivity in the respective +/+ mice, but no immunoreactivity in the respective muscarinic receptor knockout mice.

the muscarinic receptor binding sites and proteins are down-regulated in AChE − / − mice.

4. Discussion

The presence of tremor, pinpoint pupils, and seizures in AChE − / − mice implies a dysfunction of central and peripheral pathways. Such conditions are consistent with impaired function of the cholinergic receptors. The absence of AChE from cholinergic synapses would be expected to result in elevated levels of the cholinergic transmitter, acetylcholine. It is known that chronic agonist stimulation of muscarinic receptors induces downregulation of the receptors and results in loss of the cell response to further agonist stimulation in cultured cells (Fukamauchi et al., 1993; Lenz et al., 1994; Waugh et al., 1999). Myasthenia gravis patients treated chronically with the cholinesterase inhibitor, pyridostigmine, develop tolerance to the toxic effects of the drug (Johns and McQuillen, 1966). Similarly, rats and mice treated chronically with cholinesterase inhibitors develop tolerance. The tolerance is explained by downregulation of cholinergic receptors (Bushnell et al., 1994; Costa et al., 1982; Gupta et al., 1986; Russell et al., 1981; Schiller, 1979). AChE − / − mice can be regarded as an extreme example of tolerance to anticholinesterase agents. As such, they are expected to downregulate not only muscarinic but also nicotinic receptors.

4.1. Downregulation of multiple muscarinic receptor subtypes

Downregulation of receptors is generally associated with decreased sensitivity to agonists and hypersensitivity to antagonists. We have found that AChE − / − mice are remarkably insensitive to the muscarinic receptor agonists, OXO and pilocarpine. In addition, AChE − / − mice are supersensitive to the muscarinic receptor antagonist, atropine. Together, these results strongly suggest that muscarinic receptors have undergone a compensatory downregulation in AChE − / − mice.

Comparison of our functional studies on the AChE − / − mouse to similar studies with muscarinic receptor knockout mice makes this conclusion more compelling. For example, it is known that the M1 receptor is required for the initiation of seizures in the pilocarpine model of epilepsy. M1 receptor knockout mice do not exhibit seizures following the administration of a dose of pilocarpine, which causes multiple tonic–clonic seizures in wild type mice (Hamilton et al., 1997). Similarly, AChE − / − mice were completely insensitive to pilocarpine-induced seizures. These results indicate that the level of M1 receptors is reduced in AChE − / − mice.

The M2 receptor plays a key role in the regulation of heart rate, temperature, and pain response (Gomeza et al., 1999a,b). M2 receptor knockout mice show strikingly

reduced OXO-induced tremor, hypothermia, and analgesia, similar to the reduced response in AChE knockout mice. These results indicate that the level of functional M2 receptors is reduced in AChE − / − mice.

The M3 receptor is the major muscarinic receptor involved in glandular secretion. M3 receptor knockout mice, unlike M1 and M2 knockout mice, are resistant to agonist-induced salivation (Matsui et al., 2000). As shown here, AChE − / − mice had a dramatic decrease in OXO-induced salivation. We also observed a marked decrease in pilocarpine-induced glandular secretion in AChE − / − mice (data not shown), suggesting that the level of M3 receptors is reduced in AChE − / − mice. Overall, these data indicate a pronounced reduction in functional responses of multiple mAChR subtypes in AChE − / − mice.

4.2. Quantitation of the total number of muscarinic receptors

Receptor binding studies using [^{3}H]QNB indicated that the total number of muscarinic receptors in the AChE − / − mouse brain was reduced by 50%. On the other hand, the reactivity of the muscarinic receptors remained essentially unchanged—with the affinity for QNB binding being less than two-fold lower for wild type mice. This suggested that AChE − / − mice have adapted to excess acetylcholine by reducing the total number of muscarinic receptors rather than altering binding affinity. The overall decrease in the number of muscarinic receptors is a major factor responsible for loss of response to the muscarinic agonists, OXO and pilocarpine, in AChE − / − mice.

4.3. mRNA levels

The regulation of muscarinic gene expression by muscarinic receptor agonists differs according to cell type and muscarinic receptor subtype. Our results showed that the function of muscarinic receptors was downregulated without reducing the total receptor mRNA levels in AChE − / − mice. Our results are supported by the work of others in rats and cells. Studies in the rat brain in vivo demonstrated that acute and chronic treatments with AChE inhibitors induced a decrease of M4 receptors in the striatum without altering the mRNA level (Liste et al., 2002). Long-term muscarinic agonist treatment induced downregulation of M2, M3, and M4 receptors, but was not associated with a decrease of muscarinic receptor mRNA levels in cultured cell lines and primary cells (Haddad et al., 1995; Janossy et al., 2001; Lenz et al., 1994).

We did not detect any significant change in muscarinic receptor mRNA levels using whole brain homogenate. However, we cannot rule out the possibility that muscarinic receptor mRNA levels may have changed in selected areas. Yagle and Costa (1996) found that OP exposure can differentially regulate mRNA levels for muscarinic receptor subtypes in different brain areas. Rats treated with 2 mg/kg/

day disulfoton for 14 days had a 28% decrease in $[^3H]QNB$ binding and 81% decrease in AChE activity in the cortex. There was a 23% decrease in M1 receptor mRNA levels in the hippocampus after the disulfoton treatment, while no change was observed in the cortex, corpus striatum, medulla, or cerebellum. The M2 subtype mRNA was decreased in both hippocampus (24%) and medulla (19%), but not in the cortex, striatum, or cerebellum. The M3 receptor mRNA levels were decreased in the cortex (10%), but no change was observed in the hippocampus, medulla, cerebellum, or lymphocytes.

4.4. Protein levels

Downregulation of G protein-coupled receptors, defined as a decrease in the total number of receptors in a cell, is observed following activation of G-coupled receptors (Bohm et al., 1997). Downregulation serves to decrease the responsiveness of a cell to a certain stimulus. We found that the protein levels for M1, M2, and M4 receptors in whole forebrain homogenates were reduced in AChE $-/-$ mice. This indicates that the downregulation of functional mAChR in AChE $-/-$ mice, as observed in behavioral assays, was accompanied by a net loss in the total number of mAChR.

Multiple processes are involved in the regulation of mAChR in response to agonist stimulation. The abundance and availability of G protein-coupled receptors at the cell surface are regulated by the neuronal environment and is the result of complex intraneuronal trafficking (Bernard et al., 1998, 1999; Edwardson and Szekeres, 1999; Koenig and Edwardson, 1996; Liste et al., 2002; Logsdon, 1999; Roseberry et al., 2001). Sequestration of receptors within the cell is an established mechanism for downregulation of functional muscarinic receptors. Studies by Bernard et al. found a marked depletion of cell surface M2 receptor, associated with an accumulation of M2 receptors in the endoplasmic reticulum and Golgi complex of AChE $-/-$ mouse brain (Bernard et al., in press). Therefore, it is possible that enhanced mAChR downregulation results from muscarinic receptor sequestration in AChE $-/-$ mice. Bernard et al. also demonstrated that blockade of cholinergic stimulation in AChE $-/-$ mouse neurons provokes translocation of M2 receptors from the cytoplasm to the cell surface. These data strongly suggested that the absence of M2 receptors at the cell surface was due to chronic hyperstimulation by endogenous acetylcholine.

Phosphorylation is also involved in muscarinic receptor regulation. When muscarinic receptors are phosphorylated by G protein-coupled receptor kinases and other kinases (Tobin and Nahorski, 1993; Tsuga et al., 1998; Waugh et al., 1999), they become uncoupled from the G protein signaling system. It will be interesting to determine in future studies whether phosphorylation of muscarinic receptors is also involved in downregulation of muscarinic receptors in AChE $-/-$ mice.

4.5. Functional implications

The finding that heterozygous mice, with 50% of the normal AChE activity, had intermediate sensitivity to low-dose OXO-induced hypothermia, tremor, and salivation, as well as intermediate sensitivity to pilocarpine-induced seizures and an intermediate LD_{50} value for atropine, suggested that the functional muscarinic receptors were reduced in AChE$+/-$ mice. Duysen et al. (2001) have shown that AChE$+/-$ mice are more sensitive to organophosphorus toxicants than wild type mice. However, by visual inspection, AChE$+/-$ mice are indistinguishable from AChE$+/+$ mice. They do not have any obvious impairment. They have a normal lifespan and have normal reproductive abilities. This report shows that AChE$+/-$ mice respond differently to muscarinic agonists. We expect that, in the future, people who have one deficient AChE allele will be identified. These people will be healthy, but will have an unexpected response to muscarinic agonists, muscarinic antagonists, and organophosphorus pesticides.

Acknowledgements

References

Ben-Barak J, Dudai Y. Scopolamine induces an increase in muscarinic receptor level in rat hippocampus. Brain Res 1980;193:309–13.

Bernard V, Laribi O, Levey AI, Bloch B. Subcellular redistribution of m2 muscarinic acetylcholine receptors in striatal interneurons in vivo after acute cholinergic stimulation. J Neurosci 1998;18:10207–18.

Bernard V, Levey AI, Bloch B. Regulation of the subcellular distribution of m4 muscarinic acetylcholine receptors in striatal neurons in vivo by the cholinergic environment: evidence for regulation of cell surface receptors by endogenous and exogenous stimulation. J Neurosci 1999;19: 10237–49.

Bernard V, Brana C, Liste I, Lockridge O, Bloch B. Dramatic depletion of cell surface muscarinic acetylcholine receptor M2R due to limited delivery from intracytoplasmic stores in neurons of acetylcholinesterase (AChE) deficient mice. Cholinergic Mechanism Symposium, in press.

Bohm SK, Grady EF, Bunnett NW. Regulatory mechanisms that modulate signalling by G-protein-coupled receptors. Biochem J 1997;322:1–18.

Bruce RD. A confirmatory study of the up-and-down method for acute oral toxicity testing. Fundam Appl Toxicol 1987;8:97–100.

Bushnell PJ, Kelly KL, Ward TR. Repeated inhibition of cholinesterase by chlorpyrifos in rats: behavioral, neurochemical and pharmacological indices of tolerance. J Pharmacol Exp Ther 1994;270:15–25.

Caulfield MP, Birdsall NJ. International Union of Pharmacology. XVII. Classification of muscarinic acetylcholine receptors. Pharmacol Rev 1998;50:279–90.

Costa LG, Schwab BW, Murphy SD. Tolerance to anticholinesterase compounds in mammals. Toxicology 1982;25:79–97.

Duttaroy A, Gomeza J, Gan JW, Siddiqui N, Basile AS, Harman WD, et al.

Evaluation of muscarinic agonist-induced analgesia in muscarinic acetylcholine receptor knockout mice. Mol Pharmacol 2002;62:1084–93.

Duysen EG, Li B, Xie W, Schopfer LM, Anderson RS, Broomfield CA, et al. Evidence for nonacetylcholinesterase targets of organophosphorus nerve agent: supersensitivity of acetylcholinesterase knockout mouse to VX lethality. J Pharmacol Exp Ther 2001;299:528–35.

Duysen EG, Stribley JA, Fry DL, Hinrichs SH, Lockridge O. Rescue of the acetylcholinesterase knockout mouse by feeding a liquid diet; phenotype of the adult acetylcholinesterase deficient mouse. Brain Res Dev Brain Res 2002;137:43–54.

Edwardson JM, Szekeres PG. Endocytosis and recycling of muscarinic receptors. Life Sci 1999;64:487–94.

Eglen RM. Muscarinic receptors and gastrointestinal tract smooth muscle function. Life Sci 2001;68:2573–8.

Eisenach JC. Muscarinic-mediated analgesia. Life Sci 1999;64:549–54.

Fukamauchi F, Saunders PA, Hough C, Chuang DM. Agonist-induced down-regulation and antagonist-induced up-regulation of m2- and m3-muscarinic acetylcholine receptor mRNA and protein in cultured cerebellar granule cells. Mol Pharmacol 1993;44:940–9.

Gerber DJ, Sotnikova TD, Gainetdinov RR, Huang SY, Caron MG, Tonegawa S. Hyperactivity, elevated dopaminergic transmission, and response to amphetamine in M1 muscarinic acetylcholine receptor-deficient mice. Proc Natl Acad Sci USA 2001;98:15312–7.

Gomeza J, Shannon H, Kostenis E, Felder C, Zhang L, Brodkin J, et al. Pronounced pharmacologic deficits in M2 muscarinic acetylcholine receptor knockout mice. Proc Natl Acad Sci USA 1999a;96:1692–7.

Gomeza J, Zhang L, Kostenis E, Felder C, Bymaster F, Brodkin J, et al. Enhancement of D1 dopamine receptor-mediated locomotor stimulation in M(4) muscarinic acetylcholine receptor knockout mice. Proc Natl Acad Sci USA 1999b;96:10483–8.

Gray EG, Whittaker VP. The isolation of nerve endings from brain: an electron microscopic study of cell fragments derived by homogenization and centrifugation. J Anat 1962;96:79–88.

Gupta RC, Patterson GT, Dettbarn WD. Mechanisms of toxicity and tolerance to diisopropylphosphorofluoridate at the neuromuscular junction of the rat. Toxicol Appl Pharmacol 1986;84:541–50.

Haddad EB, Rousell J, Mak JC, Barnes PJ. Long-term carbachol treatment-induced down-regulation of muscarinic M2-receptors but not m2 receptor mRNA in a human lung cell line. Br J Pharmacol 1995;116:2027–32.

Hamilton SE, Loose MD, Qi M, Levey AI, Hille B, McKnight GS, et al. Disruption of the m1 receptor gene ablates muscarinic receptor-dependent M current regulation and seizure activity in mice. Proc Natl Acad Sci USA 1997;94:13311–6.

Honda K, Takano Y, Kamiya H. Changes in ^{3}H-quinuclidinyl benzilate binding and protein synthesis in the striatum following chronic administrations of muscarinic agonist. Jpn J Pharmacol 1995;67:83–6.

Janossy A, Saez JM, Li JY. Carbachol induces homologous steroidogenic refractoriness of bovine fasciculata-reticularis cells. Mol Cell Endocrinol 2001;172:147–55.

Johns RJ, McQuillen MP. Syndromes simulating myasthenia gravis: asthenia with anticholinesterase tolerance. Ann NY Acad Sci 1966;135:385–97.

Koenig JA, Edwardson JM. Intracellular trafficking of the muscarinic acetylcholine receptor: importance of subtype and cell type. Mol Pharmacol 1996;49:351–9.

Konig M, Zimmer AM, Steiner H, Holmes PV, Crawley JN, Brownstein MJ, et al. Pain responses, anxiety and aggression in mice deficient in pre-proenkephalin. Nature 1996;383:535–8.

Lenz W, Petrusch C, Jakobs KH, van Koppen CJ. Agonist-induced down-regulation of the m4 muscarinic acetylcholine receptor occurs without changes in receptor mRNA steady-state levels. Naunyn-Schmiedeberg's Arch Pharmacol 1994;350:507–13.

Levey AI, Kitt CA, Simonds WF, Price DL, Brann MR. Identification and localization of muscarinic acetylcholine receptor proteins in brain with subtype-specific antibodies. J Neurosci 1991;11:3218–26.

Li B, Stribley JA, Ticu A, Xie W, Schopfer LM, Hammond P, et al. Abundant tissue butyrylcholinesterase and its possible function in the acetylcholinesterase knockout mouse. J Neurochem 2000;75:1320–31.

Liste I, Bernard V, Bloch B. Acute and chronic acetylcholinesterase inhibition regulates in vivo the localization and abundance of muscarinic receptors m2 and m4 at the cell surface and in the cytoplasm of striatal neurons. Mol Cell Neurosci 2002;20:244–56.

Logsdon CD. The influence of the cellular context on receptor function: a necessary consideration for physiologic interpretations of receptor expression studies. Life Sci 1999;64:369–74.

Matsui M, Motomura D, Karasawa H, Fujikawa T, Jiang J, Komiya Y, et al. Multiple functional defects in peripheral autonomic organs in mice lacking muscarinic acetylcholine receptor gene for the M3 subtype. Proc Natl Acad Sci USA 2000;97:9579–84.

Messer Jr WS, Bohnett M, Stibbe J. Evidence for a preferential involvement of M1 muscarinic receptors in representational memory. Neurosci Lett 1990;116:184–9.

Mesulam MM, Guillozet A, Shaw P, Levey A, Duysen EG, Lockridge O. Acetylcholinesterase knockouts establish central cholinergic pathways and can use butyrylcholinesterase to hydrolyze acetylcholine. Neuroscience 2002;110:627–39.

Mileson BE, Chambers JE, Chen WL, Dettbarn W, Ehrich M, Eldefrawi AT, et al. Common mechanism of toxicity: a case study of organophosphorus pesticides. Toxicol Sci 1998;41:8–20.

Peterson GL, Schimerlik MI. Large scale preparation and characterization of membrane-bound and detergent-solubilized muscarinic acetylcholine receptor from pig atria. Prep Biochem 1984;14:33–74.

Roseberry AG, Bunemann M, Elavunkal J, Hosey MM. Agonist-dependent delivery of M(2) muscarinic acetylcholine receptors to the cell surface after pertussis toxin treatment. Mol Pharmacol 2001;59:1256–68.

Russell RW, Carson VG, Booth RA, Jenden DJ. Mechanisms of tolerance to the anticholinesterase, DFP: acetylcholine levels and dynamics in the rat brain. Neuropharmacology 1981;20:1197–201.

Schiller GD. Reduced binding of (^{3}H)-quinuclidinyl benzilate associated with chronically low acetylcholinesterase activity. Life Sci 1979;24:1159–63.

Tobin AB, Nahorski SR. Rapid agonist-mediated phosphorylation of m3-muscarinic receptors revealed by immunoprecipitation. J Biol Chem 1993;268:9817–23.

Tsuga H, Kameyama K, Haga T, Honma T, Lameh J, Sadee W. Internalization and down-regulation of human muscarinic acetylcholine receptor m2 subtypes. Role of third intracellular m2 loop and G protein-coupled receptor kinase 2. J Biol Chem 1998;273:5323–30.

van der Zee EA, Luiten PG. Muscarinic acetylcholine receptors in the hippocampus, neocortex and amygdala: a review of immunocytochemical localization in relation to learning and memory. Prog Neurobiol 1999;58:409–71.

Waugh MG, Challiss RA, Berstein G, Nahorski SR, Tobin AB. Agonist-induced desensitization and phosphorylation of m1-muscarinic receptors. Biochem J 1999;338:175–83.

Xie W, Stribley JA, Chatonnet A, Wilder PJ, Rizzino A, McComb RD, et al. Postnatal developmental delay and supersensitivity to organophosphate in gene-targeted mice lacking acetylcholinesterase. J Pharmacol Exp Ther 2000;293:896–902.

Yagle K, Costa LG. Effects of organophosphate exposure on muscarinic acetylcholine receptor subtype mRNA levels in the adult rat. Neurotoxicology 1996;17:523–30.

Altered Hippocampal Muscarinic Receptors in Acetylcholinesterase-Deficient Mice

Laura A. Volpicelli-Daley, PhD,[1] Ellen G. Duysen, BS,[2] Oksana Lockridge, PhD,[2] and Allan I. Levey, MD, PhD[1]

A primary therapeutic strategy for Alzheimer's disease includes acetylcholinesterase (AChE) inhibitors with the goal of enhancing cholinergic transmission. Stimulation of muscarinic acetylcholine receptors (mAChRs) by elevated levels of ACh plays a role in the effects of AChE inhibitors on cognition and behavior. However, AChE inhibitors only demonstrate modest symptomatic improvements. Chronic treatment with these drugs may cause mAChR downregulation and consequently limit the treatment efficacy. AChE knockout (−/−) mice were utilized in this study as a model for investigating the effects of selective, complete, and chronic diminished AChE activity on mAChR expression and function. In AChE −/− mice, the M_1, M_2, and M_4 mAChRs showed strikingly 50 to 80% decreased expression in brain regions associated with memory. In addition, mAChRs showed decreased presynaptic, cell surface, and dendritic distributions and increased localization to intracellular puncta. Furthermore, mAChR agonist–induced activation of extracellular signal–regulated kinase, a signaling pathway associated with synaptic plasticity and amyloidogenesis, is diminished in the hippocampus and cortex of AChE −/− mice. Therefore, chronic diminished ACh metabolism produces profound effects on mAChR expression and function. The alterations of mAChRs in AChE −/− mice suggest that mAChR downregulation may contribute to the limited efficacy of AChE inhibitors in Alzheimer's disease treatment.

One of the primary characteristics of Alzheimer's disease (AD) involves degeneration of cholinergic projections to the cortex and hippocampus.[1] Accordingly, current therapeutic strategies for AD use acetylcholinesterase (AChE) inhibitors with the goal of enhancing cholinergic transmission. However, AChE inhibitor treatment only modestly improves cognition,[2,3] suggesting the existence of adaptive mechanisms that downregulate the neuronal response to elevated ACh levels. A potential adaptive target includes metabotropic muscarinic acetylcholine receptors (mAChRs). mAChRs regulate attention, memory, behavior, and amyloidogenesis[4,5] and therefore are key targets for AD treatment. The M_1, M_2, and M_4 subtypes of mAChRs are expressed throughout the central nervous system including in vulnerable brain regions in AD.[6-8]

AD requires chronic treatment with cholinesterase inhibitors, and thus an important issue is the fate of mAChRs upon prolonged stimulation. Cellular mechanisms that reduce mAChR responsiveness to stimulation include agonist-induced internalization from the cell surface and lysosomal degradation/downregulation.[9] Recently developed AChE knockout (AChE −/−) mice provide a novel approach for determining the effects of selective, complete, and long-term inhibition of ACh metabolism on mAChR expression and trafficking.[10,11] AChE −/− mice survive to adulthood,[11] show normal development of cholinergic pathways,[12] and symptoms of hypercholinergic activity such as motor tremor[10] and mAChR antagonist–induced hyperlocomotion (L. Volpicelli-Daley, A. Hrabovskey, E. Duysen, S. Ferguson, R. Blakely, O. Lockridge, A. Levey, unpublished observations). This study shows that AChE −/− mice exhibit drastic alterations in mAChR expression, subcellular localization, and function in the hippocampus and cortex. These findings provide important implications for the chronic use of cholinergic-based therapeutics in AD treatment.

Materials and Methods

Acetylcholinesterase −/− Mice
The mice were generated in the 129Sv strain and characterized as described.[10,11] Six male AChE +/+ mice ranging from 43 to 80 days old, six male AChE −/− mice ranging

From the [1]Center for Neurodegenerative Disease and Department of Neurology, Emory University School of Medicine, Atlanta, GA; and [2]Eppley Institute, Department of Biochemistry and Molecular Biology, University of Nebraska Medical Center, Omaha, NE.

Address correspondence to Dr Levey, Emory University School of Medicine, Whitehead Biomedical Research Building, 615 Michael Street, 5th Floor, Atlanta, GA 30322. E-mail: alevey@emory.edu

from 43 to 83 days old, and one male AChE −/− 118-day-old mouse were included in the study.

Immunoblotting and Quantitation

The hippocampus and the forebrain cortex dorsal to the rhinal fissure were dissected from three individual AChE +/+ mice and three individual AChE −/− mice. The samples were prepared by sonication in buffer containing 10mM Tris Cl (pH 7.4), 1mM EDTA (pH 8.0), and protease inhibitor cocktail (Roche Diagnostics Corporation, Indianapolis, IN) and solubilization in Laemmli sample buffer. The samples were subjected to sodium dodecyl sulfate polyacrylamide gel electrophoresis and transferred to Immobilon-P transfer membrane (Millipore, Bedford, MA). Blots were blocked in Odyssey blocking buffer (Li-Cor Biosciences, Lincoln, NE) and incubated in the following primary antibodies diluted in blocking buffer overnight at 4°C with gentle agitation: M_1 rabbit polyclonal (1μg/ml), M_2 rat monoclonal (1:500), and M_4 rabbit polyclonal (1μg/ml)[7]. To control for loading, we coincubated blots with Na^+/K^+ ATPase mouse monoclonal antibody (1:40,000; Upstate Biotechnologies, Waltham, MA) or total extracellular signal–regulated kinase (ERK1/2) rabbit polyclonal antibody (1:500; Cell Signaling Technologies, Beverly, MA). Blots were rinsed in Tris-buffered saline and incubated in AlexaFluor 680 donkey anti–mouse or rat (1:10,000; Molecular Probes, Eugene, OR) and IRDye 800 goat anti–rabbit (1:10,000; Rockland, Gilbertsville, PA) secondary antibodies in blocking buffer at room temperature for 1 hour with gentle agitation. After rinsing, blots were dried, scanned, and quantitated using Odyssey Infrared Imaging System (Li-Cor Biosciences). The samples were blotted a minimum of three times. Data were analyzed using an independent t test using SPSS software.

Immunofluorescence

Mice were anesthetized with pentobarbital and perfused with 0.9% NaCl followed by 4% paraformaldehyde in 0.1M phosphate buffer. The brain was cryoprotected and 50μm sections were cut using a freezing microtome. All incubations were performed at 4°C with gentle agitation and all solutions were diluted in Tris-buffered saline. After rinsing, the sections were treated with 3% hydrogen peroxide for 10 minutes, rinsed, and blocked with 5% normal horse serum, 0.05% Triton X-100, and 10μg/ml avidin. The sections were incubated with the following antibodies diluted in primary antibody buffer containing 1% normal horse serum and 50μg/ml biotin: M_1 (1μg/ml), M_2 (1:100), M_4 (1μg/ml), phospho-ERK1/2 (1:500; Cell Signaling Technologies) or the vesicular acetylcholine transporter (1μg/ml).[13] For double-labeling, both primary antibodies were included in the incubation buffer. Sections were rinsed and incubated in biotin-conjugated donkey anti–rat or anti–rabbit secondary antibodies (1:100; Jackson Immunoresearch Laboratories, West Grove, PA) diluted in buffer containing 1% normal horse serum. The sections were then rinsed and incubated in avidin-biotin-horseradish peroxidase complex (Vector Laboratories, Burlingame, CA) for 3 hours. The sections were rinsed and incubated in tyramide-fluorescein (1:100; Perkin-Elmer, Oak Brook, IL) diluted in amplification diluent (provided by manufacturer) at room temperature for 10 minutes.

The sections were rinsed and incubated in 10mM cupric sulfate in 50mM ammonium acetate buffer (pH 5) for 30 minutes to eliminate autofluorescence,[14] followed by rinsing. For double-labeling, the sections were incubated in donkey anti–rabbit rhodamine red-X (1:100, Jackson Immunoresearch), rinsed, and then incubated in biotin conjugated secondary antibodies. The sections were mounted onto slides using Vectashield mounting media for fluorescence (Vector Laboratories). Controls included omission of primary antibodies to test nonspecific secondary antibody binding. Sections were scanned using a Zeiss LSM 510 laser-scanning confocal microscope coupled to a Zeiss 100M axiovert (Heidelberg, Germany).

Drug Treatments

Mice received intraperitoneal injections of either saline, 0.5mg/kg oxotremorine, or 5mg/kg atropine dissolved in saline. For the oxotremorine experiments, the mice were perfused 30 minutes after injections. For the atropine experiments, mice received three injections with 30 minutes between each injection (total treatment time, 90 minutes).

Results

M_1, M_2 and M_4 Immunoreactivity in Acetylcholinesterase −/− Mice

Stimulation of mAChRs in the cortex and hippocampus plays an important role in learning and memory.[4] An adaptive response to chronic reduced ACh metabolism in AChE −/− mice could include alterations in mAChR levels. Therefore, the immunoreactivities of M_1, M_2, and M_4 were analyzed in AChE −/− mice compared with AChE +/+ control mice. M_1 is primarily expressed in pyramidal neurons of the hippocampus and cortex.[8] Immunoreactivity of M_1 was analyzed in cortical and hippocampal homogenates from three individual AChE +/+ and three AChE −/− mice. M_1 immunoreactivity was substantially reduced in AChE −/− mice relative to AChE +/+ control mice (Fig 1A) with 83% and 56% reductions in the cortex and hippocampus, respectively. M_2 is expressed in presynaptic terminals[15] and intrinsic interneurons of hippocampus.[16] M_2 showed 70% reduced immunoreactivity in the hippocampus of AChE −/− mice compared with AChE +/+ control mice (see Fig 1B). In the hippocampus, M_4 localizes to presynaptic terminals of the associational, commissural, and perforant pathways.[17–19] M_4 immunoreactivity also was reduced by 54% in the hippocampus of AChE −/− mice relative to AChE +/+ mice (see Fig 1C). Therefore, AChE −/− mice showed drastic reductions in the immunoreactivity of M_1, M_2, and M_4 mAChRs in brain regions associated with learning and memory and implicated in AD.

M_1 Subcellular Localization in Hippocampus of Acetylcholinesterase −/− Mice

M_1 localizes postsynaptically to dendrites in the pyramidal cell layer of the hippocampus where it activates
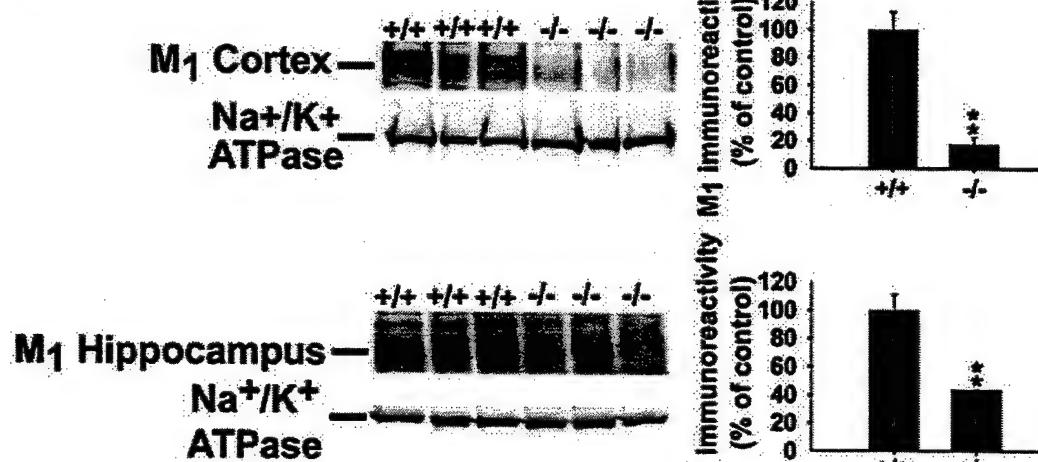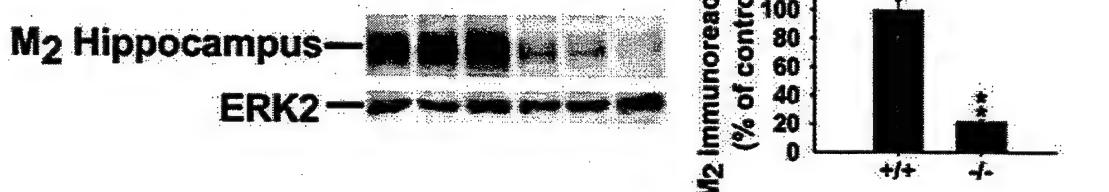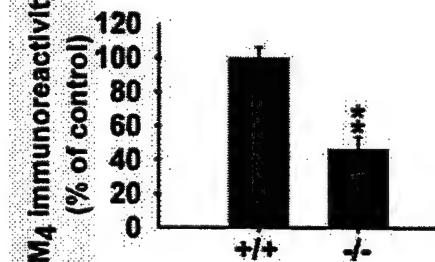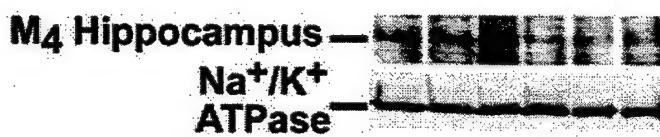
Fig 1. The M_1, M_2, and M_4 subtypes of muscarinic acetylcholine receptors (mAChRs) show decreased immunoreactivity in acetylcholinesterase (AChE) $-/-$ mice compared with AChE $+/+$ mice. Immunoreactivities of M_1, M_2, and M_4 were measured in homogenates from three individual AChE $-/-$ mice and three individual AChE $+/+$ mice. To control for loading, we also probed the immunoblots for Na^+/K^+ ATPase or total ERK2. For quantitation of the immunoblots, the receptor immunoreactivities were normalized to the loading controls. (A) M_1 showed a drastic decrease in immunoreactivity in cortical and hippocampal homogenates of AChE $-/-$ mice compared with control mice. Quantitation of immunoblots showed that M_1 immunoreactivity in the cortex (17% ± 5%) is decreased relative to AChE $+/+$ mice (100% ± 13%; **$p < 0.01$). M_1 immunoreactivity in the hippocampus of AChE $-/-$ mice (44% ± 0.3%) was also significantly reduced compared with AChE $+/+$ mice (100% ± 11%; **$p < 0.01$). (B) M_2 showed reduced immunoreactivity in the hippocampus of AChE $-/-$ mice compared with AChE $+/+$ mice. Quantitation of immunoblots showed that M_2 immunoreactivity in the hippocampus of AChE $-/-$ mice (31% ± 11%) was significantly reduced relative to M_2 immunoreactivity in AChE $+/+$ mice (100% ±3%; **$p < 0.01$). (C) M_4 also showed drastically reduced immunoreactivity in the hippocampus of AChE $-/-$ mice relative to AChE $+/+$ control mice. Quantitative analysis showed M_4 immunoreactivity in AChE $-/-$ mice (46% ± 8%) that was significantly reduced compared with AChE $+/+$ mice (100% ± 6%; **$p < 0.01$).

signaling cascades associated with synaptic plasticity and cell excitability.[8,20,21] Alterations in dendritic availability of M_1 could change the responsiveness of pyramidal cells to agonist activation. Therefore, the subcellular localization of M_1 was analyzed using confocal microscopy in the hippocampus of AChE $-/-$

mice. In the cornu ammonis 1 region of the hippocampus (CA1) pyramidal cell layer of the hippocampus of AChE +/+ mice, M_1 localized predominantly to apical and basal dendrites that extend into stratum radiatum and stratum oriens (Fig 2). In AChE −/− mice, M_1 showed a drastic reduction in dendritic distribution and enhanced perikaryal localization, particularly to intracellular puncta . M_1 in the cortex of AChE −/− mice also showed similarly reduced dendritic neuropil staining relative to AChE +/+ mice (data not shown).

Decreased M_1 localization to dendrites could result from enhanced internalization or reduced trafficking from biosynthetic compartments to the cell surface. To distinguish between these possibilities, we treated AChE +/+ mice and AChE −/− mice with the mAChR antagonist, atropine, for a total of 90 minutes to prevent M_1 activation and consequent internalization. In atropine-treated AChE −/− mice, M_1 showed a strikingly increased localization to the dendritic neuropil and reduced intracellular localization compared with saline-treated AChE −/− mice (see Fig 2). The distribution of M_1 in atropine-treated AChE +/+ mice was similar to saline-treated AChE +/+ mice (data not shown). These data indicate that M_1 can traffic from intracellular localizations to the plasma membrane and dendrites. Immunoblots of forebrain homogenates performed after 90 minutes of atropine treatment did not show a statistically significant increase in M_1 immunoreactivity in atropine-treated AChE −/− mice compared with saline-treated AChE −/− mice (data not shown). Therefore, M_1 recovery

to the dendrites resulted primarily from the return of pre-existing internalized receptors to the dendrites. Overall, in AChE −/− mice, M_1 showed an activity-dependent, reduced localization to dendrites.

Subcellular Localization of Postsynaptic and Presynaptic M_2 in the Hippocampus

In the hippocampus, M_2 localizes postsynaptically to GABAergic interneurons of the oriens/alveus (O/A) region. These neurons have dendrites that extend horizontally along the O/A border and send local axonal projections to the pyramidal layer of the hippocampus and distant projections to the medial septum.[16] As expected, in AChE +/+ mice, M_2 in the O/A region showed a continuous distribution along dendritic and axonal processes (Fig 3A). In AChE −/− mice, M_2 dendritic/axonal staining appeared diminished and punctate compared with the AChE +/+ mice. In addition, M_2 showed a drastic redistribution from the cell surface of O/A interneuron perikarya in AChE +/+ mice to intracellular puncta in AChE −/− mice.

M_2 also localizes presynaptically to GABAergic and cholinergic terminals in the pyramidal cell layer of the hippocampus[8,15] where it acts as an autoreceptor to regulate ACh release.[22] Thus, M_2 localization in presynaptic terminals in the hippocampus could be altered in response to changes in ACh levels in AChE −/− mice. In AChE +/+ mice, M_2 showed a punctate localization throughout the pyramidal cell layer of the hippocampus (see Fig 3B). Immunofluorescence for vesicular acetylcholine choline transporter demonstrated
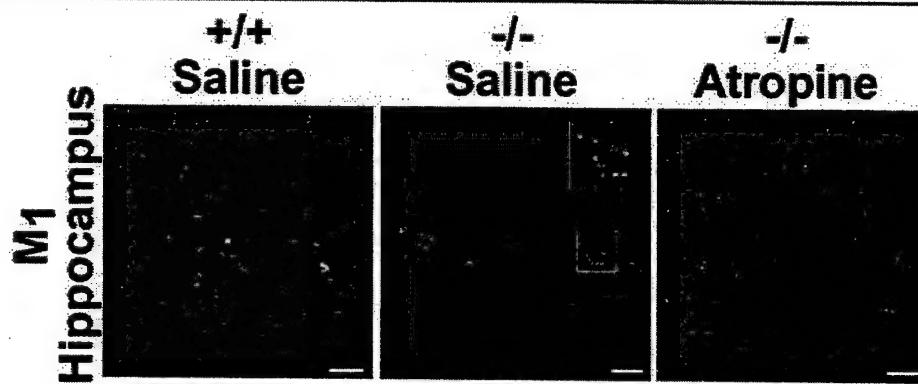
Fig 2. The M_1 muscarinic acetylcholine receptor (mAChR) shows an activity-dependent shift in dendritic distribution in the hippocampus of acetylcholinesterase (AChE) −/− mice. AChE +/+ mice and AChE −/− mice received three intraperitoneal injections every 30 minutes of either saline or atropine (total treatment time, 90 minutes). Hippocampal sections were processed for immunofluorescence and scanned using confocal microscopy as described in the Materials and Methods section. In the cornu ammonis 1 region of the hippocampus region of the hippocampus of saline-treated AChE +/+ mice (N = 2), M_1 localized primarily to the dendritic neuropil. In saline-treated AChE −/− mice (N = 2), M_1 distribution throughout the neuropil was reduced, and localization to cell bodies in the pyramidal cell layer was enhanced. A higher magnification inset demonstrates that M_1 localized to intracellular puncta within the pyramidal cell layer perikarya (untreated AChE +/+ mice [N = 3] and untreated AChE −/− mice [N = 3] showed similar M_1 hippocampal distributions to saline-treated mice; data not shown). In AChE −/− mice treated with atropine (N = 3), M_1 localization returned to the dendritic neuropil, the intracellular localization was reduced, and the distribution was similar to saline-treated AChE +/+ mice. Scale bars = 20μm.

the presence of cholinergic terminals throughout the pyramidal cell layer. In AChE −/− mice, M_2 localization to presynaptic terminals in the pyramidal cell layer was abolished. Staining for the vesicular acetylcholine choline transporter was not altered in AChE −/− mice compared with AChE +/+ mice, demonstrating that presynaptic cholinergic terminals were still present throughout the pyramidal cell layer of AChE −/− mice. Therefore, immunoreactivity of the presynaptic M_2 autoreceptor in the hippocampus is selectively decreased in AChE −/− mice. Overall, these data demonstrate drastic redistributions of postsynaptic and presynaptic M_2.

Hippocampus: Oriens

Hippocampus: Pyramidal
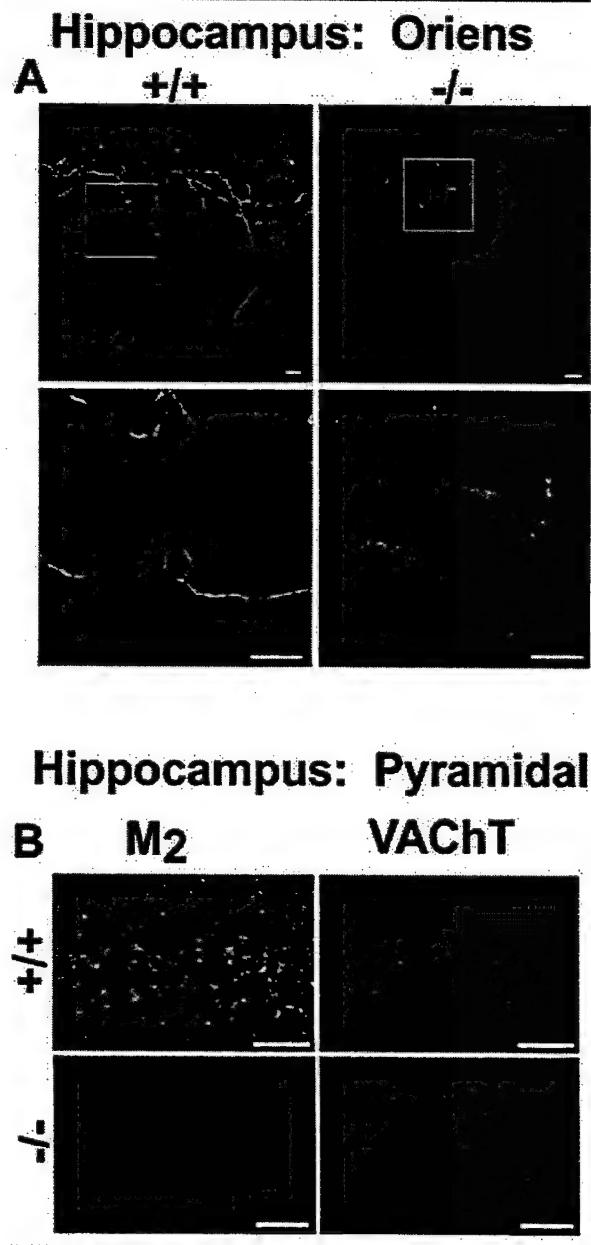
Muscarinic Acetylcholine Receptor–Mediated Activation of Signaling Cascades in Acetylcholinesterase −/− Mice

Decreased mAChR expression and cell surface localization could influence the cellular responsiveness to ACh. However, other factors such as receptor reserve could serve to maintain cholinergic signaling capabilities in AChE −/− mice. Therefore, mAChR signaling in hippocampus and cortex was tested, focusing on activation of ERKs. The ERK pathway is associated with synaptic plasticity, memory[23] and amyloidogenesis.[24,25] Cholinergic stimulation of the ERK signaling cascade is mediated by the M_1 mAChR that results in phosphorylation and activation of ERK in cell bodies and dendrites in CA1 pyramidal neurons of the hippocampus[21] and in primary cultures of cortical neurons.[26] To determine if the capacity of mAChRs to activate signaling cascades is reduced in AChE −/− mice, we evaluated the extent of mAChR-induced phosphorylation of ERK in the hippocampus and cortex using immunofluorescence. In the CA1 region of the hippocampus, saline-treated AChE +/+ mice showed basal phospho-ERK immunoreactivity in a few cell bodies scattered throughout the pyramidal cell layer (Fig 4A). AChE +/+ mice treated with oxotremorine showed a striking increase in phospho-ERK over baseline, particularly in dendrites of pyramidal neurons in the hippocampus. Saline-treated AChE −/− mice showed basal levels of phospho-ERK similar to saline-treated AChE +/+ mice. Unlike AChE +/+ mice, oxotremorine treatment did not increase ERK activation in the hippocampus of AChE −/− mice over baseline.

◄ *Fig 3. The M_2 muscarinic acetylcholine receptor (mAChR) shows altered postsynaptic and presynaptic localizations in the hippocampus and medial septum. (A) Immunofluorescent images of M_2 in the cornu ammonis 1 region of the hippocampus (CA1) demonstrated that in the oriens/alveus (O/A) region of the hippocampus, postsynaptic M_2 showed a continuous distribution along dendritic and axonal processes in acetylcholinesterase (AChE) +/+ mice (top row; N = 3) and a diminished and more beaded distribution in AChE −/− mice (N = 3). A higher magnification image (second row) showed that M_2 localized to the cell surface in O/A interneuron cell bodies of AChE +/+ mice. In AChE −/− mice, M_2 showed reduced cell surface distribution and enhanced localization to intracellular puncta. Scale bars = 20μm. (B) Presynaptic M_2 in the hippocampus (first column) showed a punctate distribution throughout the pyramidal cell layer of AChE +/+ mice (top row; N = 3). The vesicular acetylcholine transporter also showed punctate localization, corresponding to cholinergic terminals throughout the pyramidal cell layer. In AChE −/− mice (N = 3), presynaptic M_2 staining in the pyramidal cell layer was abolished. However, vesicular acetylcholine transporter immunofluorescence in AChE −/− mice was not altered demonstrating that cholinergic terminals remain distributed throughout the pyramidal cell layer. Scale bars = 20μm.*

The retrosplenial cortex receives cholinergic projections[27] and is involved in memory.[28] This area of the cortex also shows reduced metabolic activity in the early stages of AD.[29] The retrosplenial cortex of saline-treated AChE +/+ mice, showed slight phospho-ERK staining in the neuropil (see Fig 4B). Treatment of AChE +/+ mice with oxotremorine caused a striking increase in phospho-ERK immunoreactivity in cell bodies and dendrites. Saline-treated AChE −/− mice showed baseline phospho- ERK staining similar to saline-treated AChE +/+ mice. Treatment with oxotremorine did not cause an increase in phospho-ERK staining in AChE −/− mice. Overall, these findings indicate that decreased mAChR expression and dendritic availability are associated with reduced agonist-induced activation of signaling cascades in the hippocampus and cortex of AChE −/− mice.

Discussion

The use of cholinesterase inhibitors to enhance cholinergic transmission is one of the primary goals of the treatment of AD. However, AChE inhibitors only modestly improve AD symptoms, which may result from the regulation of receptors that mediate cholinergic transmission.[2,3] mAChRs are key targets for AD treatment because of their role in learning and memory,[4] behavioral symptoms in AD,[30] and amyloidogenesis.[5] This study demonstrates that chronic reduced metabolism of ACh decreases levels of M_1, M_2, and M_4 in the hippocampus and cortex. In addition, M_1 and M_2 show reduced localization to dendrites, the cell surface, and presynaptic terminals. Furthermore, alterations in mAChR expression and subcellular localization are associated with diminished ability of mAChRs to activate signaling cascades in the hippocampus and cortex.

Therefore, these data provide the first demonstration that selective, complete abolishment of AChE activity alters mAChR expression, cell surface availability, and function in brain regions associated with learning and memory. These results provide important implications regarding the chronic use of AChE inhibitors and other mAChR agonists in the treatment of AD.

M_1, M_2 and M_4 in AChE −/− Mice Show Altered Expression and Subcellular Distributions
The hippocampus and cortex of AChE −/− mice show reduced mAChR levels which could result from

Fig 4. Muscarinic acetylcholine receptor (mAChR)–induced activation of extracellular signal–regulated kinase 1/2 is diminished in the hippocampus and cortex of acetylcholinesterase (AChE) −/− mice. AChE +/+ mice and AChE −/− mice were treated with either saline or oxotremorine and perfused 30 minutes later. Sections were processed for immunofluorescent staining of active, phospho-ERK as described in the Materials and Methods section. Saline-treated AChE +/+ mice (N = 2) showed a small amount of basal phospho-ERK immunoreactivity in cell bodies and neuropil in the pyramidal cell layer of the cornu ammonis 1 region of the hippocampus (A) and retrosplenial cortex (B). Oxotremorine treatment caused a drastic increase in phospho-ERK staining in the hippocampus (A) and cortex (B) of AChE +/+ mice (N = 2), particularly in the dendrites. Saline-treated AChE −/− mice (N = 2) showed basal phospho-ERK immunoreactivity similar to saline-treated AChE +/+ mice. Oxotremorine did not cause an increase in phospho-ERK immunoreactivity in the hippocampus (A) or cortex (B) of AChE −/− mice (N = 2). Scale bar = 10μm.

decreased synthesis at the transcriptional level or enhanced targeting to lysosomes. Binding assays using ^{3}H-quinuclidinyl benzilate demonstrate 50% reductions in total mAChR binding in AChE $-/-$ mice compared with AChE $+/+$ mice, although levels of M_1, M_2, and M_4 mRNA are not altered.[31] These data indicate that mAChR synthesis is not reduced in AChE $-/-$ mice but that degradation is enhanced. In addition, the subcellular distribution of mAChRs is strikingly altered in AChE $-/-$ mice. M_1 shows reduced localization to dendrites and enhanced intracellular localization in the hippocampus and cortex. Postsynaptic M_2 shows decreased localization to the cell surface and increased localization to intracellular puncta in neuronal perikarya of the hippocampus. In addition, presynaptic M_2 shows decreased localization to terminals in the pyramidal cell layer of the hippocampus. Treatment of AChE $-/-$ mice with atropine causes M_1 to return to a dendritic distribution similar to saline-treated AChE $+/+$ mice. Therefore, the decreased localization of M_1 to dendrites in the hippocampus of AChE $-/-$ mice results from ACh-induced mAChR internalization and not impaired trafficking from biosynthetic compartments. The recovery of M_1 to the dendritic neuropil after 90-minute atropine treatment in AChE $-/-$ mice results from the return of internalized M_1 to the dendrites. Overall, these data indicate that although AChE $-/-$ mice show striking alterations in mAChR expression and subcellular localization in the hippocampus and cortex these changes are rapidly reversible.

Functional Implications
Decreased mAChR expression at the cell surface and dendrites is associated with diminished ability of mAChRs to activate signaling cascades in AChE $-/-$ mice. The hippocampus and cortex of AChE $+/+$ mice show robust agonist-induced increases in phospho-ERK which plays an important role in learning and memory.[23] In contrast, AChE $-/-$ mice show no agonist-induced increases in phospho-ERK. M_1 activates ERK in the hippocampus and cortex,[21,26] suggesting prolonged reduced ACh metabolism diminishes the functional capacity of M_1. On a behavioral level, pilocarpine-induced seizures, which are mediated by M_1,[32] are abolished in AChE $-/-$ mice,[31] also consistent with diminished M_1 function in AChE $-/-$ mice. Other functions attributed to M_1 include potentiation of N-methyl-D-aspartate current in the hippocampus[20] and ACh-induced excitation of cortical cells, possibly through inhibition of a K^+ current defined as I_M.[33] Recently, M_1 has been shown to play an important role in hippocampal and cortical memory function and in long-term potentiation induced by θ burst stimulation.[34] Therefore, it is likely that chronic reduced ACh metabolism diminishes the capacity of M_1 to modulate synaptic plasticity, neuronal excitability, and learning and memory in hippocampus and cortex.

M_2 and M_4 also show decreased expression in the hippocampus. In the hippocampus, M_4 localizes to presynaptic terminals of the perforant, associational, and commissural pathways where it may act as a heteroreceptor regulating the release of excitatory neurotransmitters.[17–19] M_2 is the primary autoreceptor in the hippocampus where it controls ACh release by feedback inhibition.[22] Although the functions of M_2 and M_4 were not addressed in this study, AChE $-/-$ mice show impairments in behaviors attributed to these receptor subtypes such as diminished agonist-induced hypothermia, tremor, and analgesia[31] and enhanced sensitivity to mAChR antagonist–induced increases in locomotor activity (L. Volpicelli-Daley, A. Hrabovskey, E. Duysen, S. Ferguson, R. Blakely, O. Lockridge, A. Levey, unpublished observations). Therefore, reduced function of these receptors in AChE $-/-$ mice suggests that the ability of M_2 and M_4 to regulate neurotransmitter release in the hippocampus of AChE $-/-$ mice also may be diminished.

Implications for the Treatment of Alzheimer's Disease
Reduced mAChR function in AChE $-/-$ mice suggests important consequences for the treatment of cognitive disorders such as AD. For example, mAChR downregulation in response to chronic diminished ACh metabolism may impair the ability of mAChRs to enhance cognition or improve behavior. Decreased mAChR expression and cell surface availability in AChE $-/-$ mice may explain the modest efficacy of AChE inhibitors in the treatment of AD. This is particularly relevant for M_1, because loss of function of this subtype could be detrimental for cholinergic effects on synaptic plasticity, memory and learning, and amyloidogenesis. Loss of M_2 and M_4 may also be important in behavioral effects of cholinergic therapies. However, unlike AChE $-/-$ mice, AChE inhibitors show differences in selectivity for AChE, pharmacokinetics, and maximal inhibition of cholinesterase activity.[2,3,35,36] Therefore, the effects on mAChR expression, subcellular distribution, and function may vary depending on the AChE inhibitor used. Chronic treatment with organophosphorus cholinesterase inhibitors reduces mAChR binding sites and inhibits mAChR function.[37,38] In addition, chronic treatment with the cholinesterase inhibitor, metrifonate, causes altered subcellular distribution of M_2 and M_4 in striatal neurons.[39] Therefore, these data suggest that, similar to our findings in AChE $-/-$ mice, chronic administration of AChE inhibitors most likely produces diminished mAChR expression and altered subcellular distributions in brain regions associated with learning and memory. However, mAChR alterations produced by chronic diminished ACh me-

tabolism may differ in age-related diseases, including AD, which is characterized by perturbed cholinergic transmission[40] and altered mAChR protein levels.[6] We have not examined age dependence on mAChR alterations in the AChE−/− mice. Future studies are required to determine if chronic diminished ACh metabolism causes similar alterations in mAChRs in AD brains.

This study demonstrates that although chronic diminished ACh metabolism can drastically alter mAChR subcellular distribution, the mAChRs can return to baseline distributions when ACh-induced activation and internalization is inhibited. It is possible that altering the temporal pattern of the AChE inhibitor treatment regimen to allow mAChRs return to basal distributions could enhance treatment efficacy. Another option is the development of mAChR subtype–specific agonists that do not cause receptor internalization, as has been demonstrated for μ-opioid receptor ligands,[41] which may prevent mAChR downregulation and enhance the efficacy of cholinomimetics in AD treatment.

In conclusion, we provide evidence that chronic reduced ACh metabolism results in striking reductions in mAChR expression, cell surface availability, and function in brain regions crucial for learning and memory. In addition to AD, cholinomimetics have been implicated in the treatment of other central nervous system disorders characterized by perturbed cholinergic functions such as Huntington's chorea, schizophrenia, and tardive dyskinesia.[42–45] Therefore, these data provide important implications regarding the chronic use of cholinesterase inhibitors and other cholinomimetics not only for the treatment of AD but also for a variety of central nervous system disorders.

References

1. Burns A, Whitehouse P, Arendt T, Forsti H. Alzheimer's disease in senile dementia: loss of neurones in the basal forebrain: Whitehouse P, Price D, Struble R, Clarke A, Coyle J, Delong M. Science 1982;215:1237–1239. Int J Geriatr Psychiatry 1997;12:7–10.
2. Farlow MR, Evans RM. Pharmacologic treatment of cognition in Alzheimer's dementia. Neurology 1998;51:S36–S44; discussion, S65–S67.
3. Francis PT, Palmer AM, Snape M, Wilcock GK. The cholinergic hypothesis of Alzheimer's disease: a review of progress. J Neurol Neurosurg Psychiatry 1999;66:137–147.
4. Jerusalinsky D, Kornisiuk E, Izquierdo I. Cholinergic neurotransmission and synaptic plasticity concerning memory processing. Neurochem Res 1997;22:507–515
5. Hellstrom-Lindahl E. Modulation of beta-amyloid precursor protein processing and tau phosphorylation by acetylcholine receptors. Eur J Pharmacol 2000;393:255–263.
6. Flynn DD, Ferrari-DiLeo G, Mash DC, Levey AI. Differential regulation of molecular subtypes of muscarinic receptors in Alzheimer's disease. J Neurochem 1995;64:1888–1891
7. Levey AI, Kitt CA, Simonds WF, et al. Identification and localization of muscarinic acetylcholine receptor proteins in brain with subtype-specific antibodies. J Neurosci 1991;11:3218–3226.
8. Levey AI, Edmunds SM, Koliatsos V, et al. Expression of m1–m4 muscarinic acetylcholine receptor proteins in rat hippocampus and regulation by cholinergic innervation. J Neurosci1995;15:4077–4092.
9. Koenig JA, Edwardson JM. Endocytosis and recycling of G protein-coupled receptors. Trends Pharmacol Sci 1997;18:276–287.
10. Xie W, Stribley JA, Chatonnet A, et al. Postnatal developmental delay and supersensitivity to organophosphate in gene-targeted mice lacking acetylcholinesterase. J Pharmacol Exp Ther 2000;293:896–902.
11. Duysen EG, Stribley JA, Fry DL, et al. Rescue of the acetylcholinesterase knockout mouse by feeding a liquid diet; phenotype of the adult acetylcholinesterase deficient mouse. Brain Res Dev Brain Res 2002;137:43–54.
12. Mesulam MM, Guillozet A, Shaw P, et al. Acetylcholinesterase knockouts establish central cholinergic pathways and can use butyrylcholinesterase to hydrolyze acetylcholine. Neuroscience 2002;110:627–639.
13. Gilmor ML, Nash NR, Roghani A, et al. Expression of the putative vesicular acetylcholine transporter in rat brain and localization in cholinergic synaptic vesicles. J Neurosci 1996;16:2179–2190.
14. Schnell SA, Staines WA, Wessendorf MW. Reduction of lipofuscin-like autofluorescence in fluorescently labeled tissue. J Histochem Cytochem 1999;47:719–730.
15. Rouse ST, Edmunds SM, Yi H, et al. Localization of M(2) muscarinic acetylcholine receptor protein in cholinergic and non-cholinergic terminals in rat hippocampus. Neurosci Lett 2000;284:182–186.
16. Hajos N, Papp EC, Acsady L, et al. Distinct interneuron types express m2 muscarinic receptor immunoreactivity on their dendrites or axon terminals in the hippocampus. Neuroscience 1998;82:355–376.
17. Rouse ST, Levey AI. Expression of m1–m4 muscarinic acetylcholine receptor immunoreactivity in septohippocampal neurons and other identified hippocampal afferents. J Comp Neurol 1996;375:406–416.
18. Rouse ST, Gilmor ML, Levey AI. Differential presynaptic and postsynaptic expression of m1–m4 muscarinic acetylcholine receptors at the perforant pathway/granule cell synapse. Neuroscience 1998;86:221–232.
19. Rouse ST, Marino MJ, Potter LT, et al. Muscarinic receptor subtypes involved in hippocampal circuits. Life Sci 1999;64:501–509.
20. Marino MJ, Rouse ST, Levey AI, et al. Activation of the genetically defined m1 muscarinic receptor potentiates N-methyl-D-aspartate (NMDA) receptor currents in hippocampal pyramidal cells. Proc Natl Acad Sci USA 1998;95:11465–11470.
21. Berkeley JL, Gomeza J, Wess J, et al. M1 muscarinic acetylcholine receptors activate extracellular signal-regulated kinase in CA1 pyramidal neurons in mouse hippocampal slices. Mol Cell Neurosci 2001;18:512–524.
22. Zhang W, Basile AS, Gomeza J, et al. Characterization of central inhibitory muscarinic autoreceptors by the use of muscarinic acetylcholine receptor knock-out mice. J Neurosci 2002;22:1709–1717.

23. Adams JP, Sweatt JD. Molecular psychology: roles for the ERK MAP kinase cascade in memory. Annu Rev Pharmacol Toxicol 2002;42:135–163.

24. Mills J, Laurent Charest D, Lam F, et al. Regulation of amyloid precursor protein catabolism involves the mitogen-activated protein kinase signal transduction pathway. J Neurosci 1997; 17:9415–9422.

25. Haring R, Fisher A, Marciano D, et al. Mitogen-activated protein kinase-dependent and protein kinase C-dependent pathways link the m1 muscarinic receptor to beta-amyloid precursor protein secretion. J Neurochem 1998;71:2094–2103.

26. Hamilton SE, Nathanson NM. The M1 receptor is required for muscarinic activation of mitogen-activated protein (MAP) kinase in murine cerebral cortical neurons. J Biol Chem 2001; 276:15850–15853.

27. Selden NR, Gitelman DR, Salamon-Murayama N, et al. Trajectories of cholinergic pathways within the cerebral hemispheres of the human brain. Brain 1998;121:2249–2257.

28. Maddock RJ. The retrosplenial cortex and emotion: new insights from functional neuroimaging of the human brain. Trends Neurosci 1999;22:310–316.

29. Minoshima S, Giordani B, Berent S, et al. Metabolic reduction in the posterior cingulate cortex in very early Alzheimer's disease. Ann Neurol 1997;42:85–94.

30. Bodick NC, Offen WW, Levey AI, et al. Effects of xanomeline, a selective muscarinic receptor agonist, on cognitive function and behavioral symptoms in Alzheimer disease. Arch Neurol 1997;54:465–473.

31. Li B, Duysen EG, Volpicelli LA, et al. Regulation of muscarinic acetylcholine receptor function in acetylcholinesterase knockout mice. Pharmacol Biochem Behav 2003;74:977–986.

32. Hamilton SE, Loose MD, Qi M, et al. Disruption of the m1 receptor gene ablates muscarinic receptor-dependent M current regulation and seizure activity in mice. Proc Natl Acad Sci USA 1997;94:13311–13316.

33. McCormick DA, Prince DA. Two types of muscarinic response to acetylcholine in mammalian cortical neurons. Proc Natl Acad Sci USA 1985;82:6344–6348.

34. Anagnostaras SG, Murphy GG, Hamilton SE, et al. Selective cognitive dysfunction in acetylcholine M(1) muscarinic receptor mutant mice. Nat Neurosci 2003;6:51–58.

35. Bullock R. New drugs for Alzheimer's disease and other dementias. Br J Psychiatry 2002;180:135–139.

36. Poirier J. Evidence that the clinical effects of cholinesterase inhibitors are related to potency and targeting of action. Int J Clin Pract Suppl 2002:6–19.

37. Olianas MC, Onali P, Schwartz JP, et al. The muscarinic receptor adenylate cyclase complex of rat striatum: desensitization following chronic inhibition of acetylcholinesterase activity. J Neurochem 1984;42:1439–1443.

38. Gazit H, Silman I, Dudai Y. Administration of an organophosphate causes a decrease in muscarinic receptor levels in rat brain. Brain Res 1979;174:351–356.

39. Liste I, Bernard V, Bloch B. Acute and chronic acetylcholinesterase inhibition regulates in vivo the localization and abundance of muscarinic receptors m2 and m4 at the cell surface and in the cytoplasm of striatal neurons. Mol Cell Neurosci 2002;20:244–256.

40. Giacobini E. Cholinesterase inhibitors: from the Calabar bean to Alzheimer therapy. In: Giacobini E, eds. Cholinesterases and cholinesterase inhibitors. London: Martin Dunitz, 2000: 181–226.

41. Keith DE, Anton B, Murray SR, et al. mu-Opioid receptor internalization: opiate drugs have differential effects on a conserved endocytic mechanism in vitro and in the mammalian brain. Mol Pharmacol 1998;53:377–384.

42. Davis KL, Berger PA. Pharmacological investigations of the cholinergic imbalance hypotheses of movement disorders and psychosis. Biol Psychiatry 1978;13:23–49.

43. Tammenmaa IA, McGrath JJ, Sailas E, Soares-Weiser K. Cholinergic medication for neuroleptic-induced tardive dyskinesia. Cochrane Database Syst Rev 2002;3:CD000207.

44. Shannon HE, Rasmussen K, Bymaster FP, et al. Xanomeline, an M(1)/M(4) preferring muscarinic cholinergic receptor agonist, produces antipsychotic-like activity in rats and mice. Schizophr Res 2000;42:249–259.

45. Assal F, Cummings JL. Neuropsychiatric symptoms in the dementias. Curr Opin Neurol 2002;15:445–450.

Dramatic depletion of cell surface m2 muscarinic receptor due to limited delivery from intracytoplasmic stores in neurons of acetylcholinesterase-deficient mice

Véronique Bernard,[a],* Corinne Brana,[b] Isabel Liste,[a] Oksana Lockridge,[c] and Bertrand Bloch[a]

[a] Centre National de la Recherche Scientifique, Unité Mixte de Recherche 5541, Laboratoire d'Histologie-Embryologie, Université Victor Ségalen-Bordeaux 2, 146 rue Léo-Saignat, 33076 Bordeaux cedex, France
[b] Laboratoire d'Epileptologie Expérimentale et Clinique, Université Victor Ségalen-Bordeaux 2, 146 rue Léo-Saignat, 33076 Bordeaux cedex, France
[c] Eppley Institute, University of Nebraska, Omaha, USA

Abstract

We have studied the consequences of the constitutive acetylcholinesterase (AChE) deficiency in knockout mice for the AChE gene on the subcellular localization of the m2 receptor (m2R) and the regulation of its intraneuronal compartmentalization by the cholinergic environment, using immunohistochemistry at light and electron microscopic levels. (1) In AChE +/+ mice in vivo, m2R is mainly located at the neuronal membrane in striatum, hippocampus, and cortex. In AChE −/− mice, m2R is almost absent at the membrane but is accumulated in the endoplasmic reticulum and Golgi complex. (2) In vivo and in vitro (organotypic culture) dynamic studies demonstrate that the balance between membrane and intracytoplasmic m2R can be regulated by the cholinergic influence: In AChE −/− mice, m2R is translocated from the cytoplasm to the cell surface after (1) blockade of muscarinic receptors by atropine, (2) supplementation of AChE −/− neurons with AChE in vitro, and (3) disruption of the cortical and hippocampal cholinergic afferents in vitro. Our results suggest that the neurochemical environment may contribute to the control of the abundance and availability of cell surface receptors, and consequently to the control of neuronal sensitivity to neurotransmitters or drugs, by regulating their delivery from the endoplasmic reticulum and Golgi complex.
© 2003 Elsevier Science (USA). All rights reserved.

Introduction

The effects of most neurotransmitters and related drugs in the brain are mediated by G protein-coupled receptors (GPCRs[1]), which are synthetized in the cytoplasm of the neurons and targeted to the plasma membrane to interact with neurotransmitters. In vitro and in vivo studies have widely demonstrated that the abundance and availability of these receptors at the cell surface is regulated by the neuronal environment and is the result of complex intraneuronal trafficking (Faure et al., 1995; Mantyh et al., 1995a, 1995b; Sternini et al., 1996; Koenig and Edwardson, 1997; Marvizon et al., 1997; Bernard et al., 1998, 1999; Dournaud et al., 1998; Dumartin et al., 1998; Bloch et al., 1999; Dumartin et al., 2000; Csaba et al., 2001; Liste et al., 2002). Modifications of the quantity of receptors available at the plasma membrane have been suggested to contribute to functional responses to stimulation, including desensitization and resensitization (Hertel et al., 1985; Pippig et al., 1995; McDonald et al., 1998; Mundell and Kelly, 1998). There is much evidence that under acute stimulation, the quantity of receptors located at the plasma membrane is regulated by endocytosis. Indeed, acute stimulation of GPCRs induces different subcellular events including cell surface receptor depletion through internalization of these

---

* Corresponding author. Fax: +33-5-56-98-61-82.

E-mail address: Veronique.Bernard@umr5541.u-bordeaux2.fr (V. Bernard).

[1] Abbreviations: GPCR, G protein-coupled receptor; AChE, acetylcholinesterase; m2R, m2 receptor; ACh, acetylcholine; LM, light microscopy; Cath D, cathepsin D; TF, fluorescein-conjugated transferrin; EM, electron microscopy; VAChT, vesicular acetylcholine transporter; NDS, normal donkey serum.

receptors in endosomes, degradation, or recycling to the plasma membrane (Faure et al., 1995; Mantyh et al., 1995a, 1995b; Koenig and Edwardson, 1996, 1997; Sternini et al., 1996; Marvizon et al., 1997; Bernard et al., 1998, 1999; Dumartin et al., 1998; Csaba et al., 2001; Tsao et al., 2001; Liste et al., 2002).

Some evidence suggests that in the brain, the availability and abundance of GPCRs at the plasma membrane and the intracytoplasmic localization is regulated by several cellular mechanisms that operate over a long time scale and that contribute to downregulation of these receptors (Heck and Bylund, 1998; Jockers et al., 1999; Ko et al., 1999; Tsao et al., 2001). Under chronic hyperstimulation D1 and m2 receptors have been shown to display dramatic redistribution in striatal neurons. This includes a depletion of cell surface receptors associated with exaggerated storage in the endoplasmic reticulum and in the Golgi complex of neurons (Dumartin et al., 2000; Liste et al., 2002). These data suggest that the delivery of GPCRs from the endoplasmic reticulum and Golgi apparatus to the plasma membrane is involved in vivo in the regulation of the abundance of cell surface neurotransmitter receptors. However, the environmental conditions regulating this redistribution of receptors are still unclear. Yet, by modulating the quantity of the receptors available for stimulation, such redistribution may play key roles in the neuronal response to long-lasting modifications of the neurochemical environment in physiological, experimental, or pathological conditions.

To bring insight on the influence of chronic changes in the neurochemical environment on receptor trafficking and subcellular compartmentalization, we have used acetylcholinesterase (AChE) knockout mice that present chronic AChE deficiency (Xie et al., 2000) to study the consequences of chronic hypercholinergy on the intraneuronal localization of m2 receptor (m2R) in neurons of different brain areas. The m2R is involved as a presynaptic autoreceptor in the autoregulation of acetylcholine (ACh) release in striatum and as an heteroreceptor in the heteroregulation of the release of gamino butytic acid (GABA) or somatostatin (James and Cubeddu, 1984; Weiler et al., 1984; Murakami et al., 1989; Bernard et al., 1992; Billard et al., 1995; Rouse et al., 1997; Hajos et al., 1998). Modifications of the membrane availability of m2R as a consequence of perturbations of the cholinergic environment may play a key role in the regulation of the functions of cholinoceptive neurons, including the neuronal activity and/or the neurotransmitter release. By using immunohistochemistry at light and microscopic levels, we have determined in neurons of the central nervous system (1) the effect of the absence of expression of AChE on the subcellular distribution of m2R, and (2) the neurochemical factors governing the intraneuronal distribution of m2R and its targeting to the plasma membrane. We have shown that in normal mice, m2R is expressed mainly at the plasma membrane of cell bodies in striatum, hippocampus, and cortex. In AChE −/− mice, neurons display nearly no m2R at the plasma membrane of cell bodies and

proximal dendrites, but do accumulate this receptor in the endoplasmic reticulum and Golgi apparatus. We have demonstrated that blockade of the effects of cholinergic stimulation of AChE −/− neurons in vivo and in vitro (in organotypic cultures) reversed the alterations of the subcellular distribution of neuronal m2R.

Results

Cellular and subcellular distribution of m2R immunoreactivity in striatum, cortex, and hippocampus

AChE +/+ mice

The analysis at the light microscopy (LM) level demonstrated immunoreactivity for m2R in few neurons of striatum, cortex, and hippocampus. In striatum, these neurons were characterized as aspiny cholinergic and somatostatinergic interneurons as previously described in rats (Bernard et al., 1998) (data not shown). In cortex, some m2R-immunopositive scattered neurons were identified in layer 2. In hippocampus, m2R-immunoreactive perikarya were seen mostly in stratum oriens. In all three areas, in vivo and in vitro, the cell bodies displayed an intense labeling restricted to the neuronal membrane and proximal dendritic shafts (Fig. 1A, D, and G). Ultrastructural studies in the striatum in vivo confirmed that immunoparticles were mostly associated with the plasma membrane (47% of the total number of particles) (Figs. 2A and 3A). Immunoparticles were also detected in the cytoplasm in association with endoplasmic reticulum (7%), Golgi apparatus (15%), small vesicles (2%), and nuclear membrane (1%). Twenty-eight percent of immunoparticles could not be associated with one of the previous subcellular elements (Fig. 3A). In vivo, lysosomes where identified as cathepsin D (Cath D)-immunoreactive structures. The double-labeling experiments at the florescence microscopic level (m2R + Cath D) demonstrated that 1.4% of the surface of m2R immunolabeling colocalized with Cath D-immunopositive structures (Figs. 4 and 5). In vitro, endosomes were identified as structures having endocyted fluorescein-conjugated transferrin (Tf) (see Experimental Methods). The double-labeling experiments at the fluorescence microscopic level (m2R + Tf) demonstrated that 6% of the surface of m2R immunolabeling colocalized with fluorescein-labeled endosomes (Figs. 6 and 7).

AChE −/− mice

In vivo, the observations at the LM level showed dramatic modifications of the distribution of the immunofluorescence for m2R in striatum, cortex, and hippocampus. The m2R labeling was intense in the cytoplasm, especially in the perinuclear area, but was absent at the plasma membrane of cell bodies and proximal dendrites (Figs. 1B, E, H, and 4B). All m2R-immunoreactive neurons in all three areas displayed the same subcellular distribution of the labeling. The quantitative analysis at the electron microscopy (EM) level
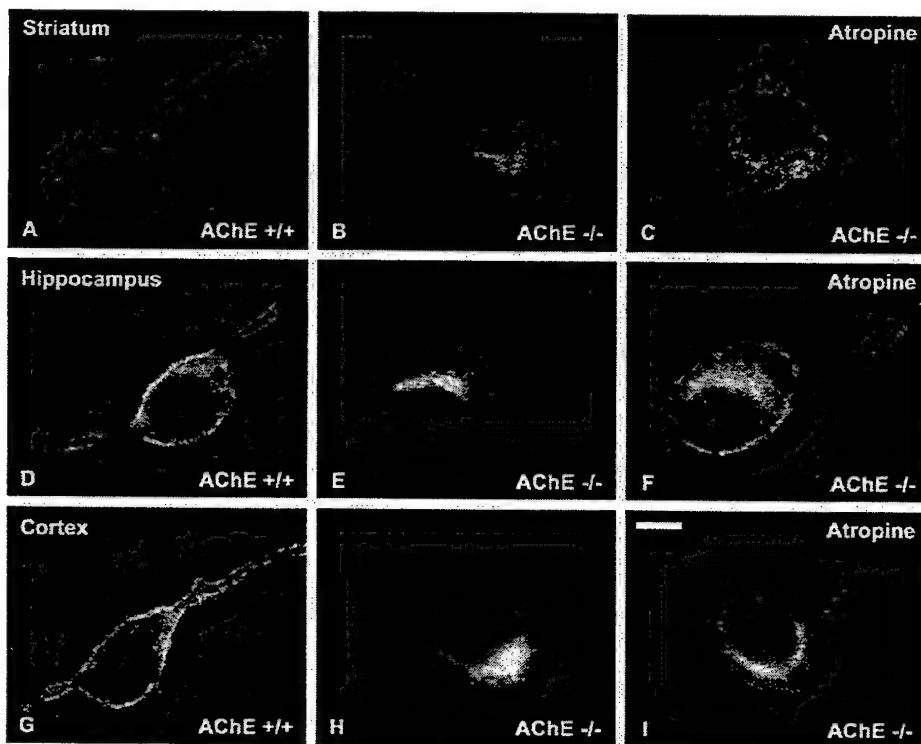
Fig. 1. Detection of m2R in neurons of striatum (A, B, and C), hippocampus (D, E, and F), and cortex (G, H, and I) in wild-type (AChE +/+) and knockout (AChE −/−) mice for the ACHE gene and effect of blockade of the muscarinic receptors on the subcellular distribution of m2R in neurons of AChE −/− mice in vivo. (A, D, and G) In AChE +/+ mice, m2R fluorescent immunoreactivity is detected at the plasma membrane. (B, E, and H) In contrast, in AChE −/− mice, no staining is seen at the plasma membrane, whereas a strong immunolabeling is detected in the cytoplasm. (C, F, and I) In AChE −/− mice, atropine, a muscarinic receptor antagonist, restores the presence of m2R immunoreactivity at the plasma membrane in striatum (C), cortex (F), and hippocampus (I). m2R immunoreactivity is also detected in the cytoplasm. m2R, m2 receptor; AChE, acetylcholinesterase. Bar: 10 μm.

in the striatum demonstrated that 96% of immunoparticles were located in the cytoplasm and only 4% of them were detected at the plasma membrane (Figs. 2B and C and 3A). In the cytoplasm, the majority of immunoparticles were detected in association with the endoplasmic reticulum and the Golgi apparatus, representing 21% and 33% of the total number of immunoparticles (Figs. 2B and C and 3A). Indeed, we have shown a large and significant decrease of the density of immunoparticles located at the plasma membrane (−93%) and a significant increase in the number of immunoparticles associated with the endoplasmic reticulum (+136%) and Golgi apparatus (+69%) (Fig. 3B). No difference in the total number of immunoparticles per neuronal surface was seen. In vivo, the statistical analysis (Mann-Whitney U test) showed that the percentage of the surface of m2R labeling colocalized with Cath D-immunopositive structures strongly increases in AChE −/− striatal neurons (+686%; $P < 0.001$) (Figs. 4 and 5). In vitro, the statistical analysis (Kruskal-Wallis test) showed that the percentage of the surface of m2R labeling colocalized with Tf labeling is not different in AChE −/− and in AChE +/+ mice (Fig. 7). In contrast, in oxotremorine-treated mice, the surface of m2R immunoreactivity colocalized with Tf labeling strongly increases compared to AChE +/+ (+266%; $P <$

0.001) and AChE −/− mice (+266%; $P < 0.001$) (Figs. 6 and 7).

In AChE −/− mice striatum, the same intracytoplasmic distribution of m2R was observed in vivo and in vitro (Figs. 1B, 4B, and 6C). In contrast, in vitro, in cortex and in hippocampus, m2R immunoreactivity was very similar to the labeling obtained in AChE +/+ mice, i.e., restricted to the plasma membrane (Fig. 8B).

Dynamic study of the influence of cholinergic transmission on the subcellular redistribution of m2R in AChE −/− mice

Effect of supplementation of AChE on the subcellular distribution of m2R in striatal neurons of AChE −/− mice in vitro

In AChE −/− striatum cultured alone in vitro for at least 2 weeks, m2R displayed a subcellular distribution similar to the localization observed in vivo: no labeling at the membrane, but intense staining in the cytoplasm (Figs. 6C, 9B, and 10B). AChE +/+ and AChE −/− mice were cocultured to determine the role of AChE on the subcellular distribution of the m2R in AChE −/− striatum. AChE +/+ and AChE −/− striatal explants were cultured side by side.
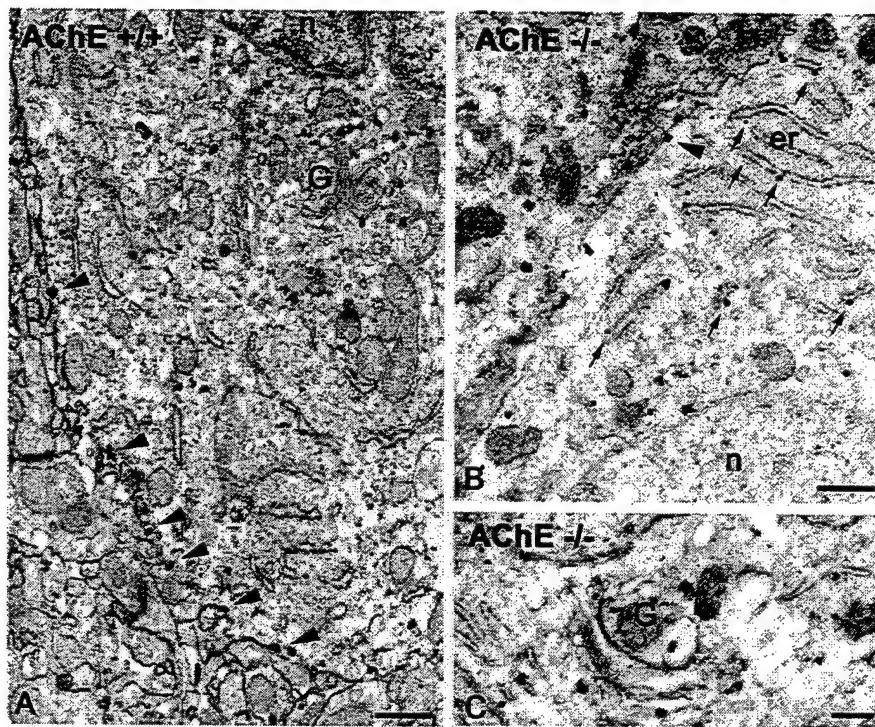
Fig. 2. Subcellular distribution of m2R immunoreactivity in striatal neurons of AChE +/+ (A) and AChE −/− (B and C) mice, using the preembedding immunogold method with silver intensification. (A) In an AChE +/+ mouse, immunoparticles are associated mostly with the internal side of the plasma membrane (arrowheads). Some immunoparticles are associated with the endoplasmic reticulum (er, small arrows) and the Golgi apparatus (G). (B and C) In an AChE −/− mouse, very few immunoparticles are detected in association with the plasma membrane. In contrast, numerous particles are seen in the cytoplasm associated with the endoplasmic reticulum (small arrows) and the Golgi apparatus. m2R, m2 receptor; AChE, acetylcholinesterase; n, nucleus. Bars: A and B, 500 nm; C, 50 nm.

The AChE −/− explant was innervated by AChE +/+ neurons as demonstrated by the presence of AChE-immunoreactive fibers (Fig. 9D′ and D″). In this condition, AChE −/− neurons displayed m2R at the plasma membrane (Fig. 9D and 9D″). The intracytoplasmic receptor disappeared and the localization became similar to that observed in AChE +/+ mice.

Influence of the cholinergic afferents on the subcellular distribution of m2R in hippocampal neurons in AChE −/− mice in vitro

When neurons from AChE −/− mice (cortex and hippocampus) are cultured alone, and are thus no longer subjected to their cholinergic afferents, they express m2R at the membrane (Fig. 4E). When cholinergic neurons from septum of AChE −/− mice, the native afferents, are cocultured with hippocampus from AChE −/−, m2R keeps the distribution observed in vivo in target hippocampal neurons, i.e., cytoplasmic accumulation and cell surface depletion (Fig. 4F). When cholinergic neurons from septum of AChE +/+ mice are cocultured with hippocampus from AChE +/+ or AChE −/−, m2R is located at the plasma membrane. When cholinergic neurons from septum from AChE −/− mice are cocultured with hippocampus from AChE +/+, m2R is

located at the plasma membrane, but an intracytoplasmic labeling is also seen (data not shown).

Effect of the blockade of muscarinic receptors on the subcellular distribution of m2R in striatal, hippocampal, and cortical neurons in AChE −/− mice

In AChE −/− mice, atropine restored immunoreactivity for m2R at the plasma membrane in vivo (striatum, hippocampus, and cortex; 10 mg/kg i.p. for 22 days) and in vitro (striatum, 100 μM for 2 h) (Fig. 1C, F, and I). In the striatum in vivo, but not in vitro, m2R was also detected in the cytoplasm, especially in association with the endoplasmic reticulum. In vivo and in vitro, chronic treatment with mecamylamine, a nicotinic receptor antagonist, has no effect on the subcellular localization of m2R in AChE −/− mice.

Discussion

We report that chronic AChE deficiency in mice lacking the ACHE gene induces a dramatic redistribution of m2R in neurons of the central nervous system including striatum, cortex, and hippocampus in vivo and in vitro (Fig. 5). We

Subcellular distribution of m2R in perikarya of striatal neurons
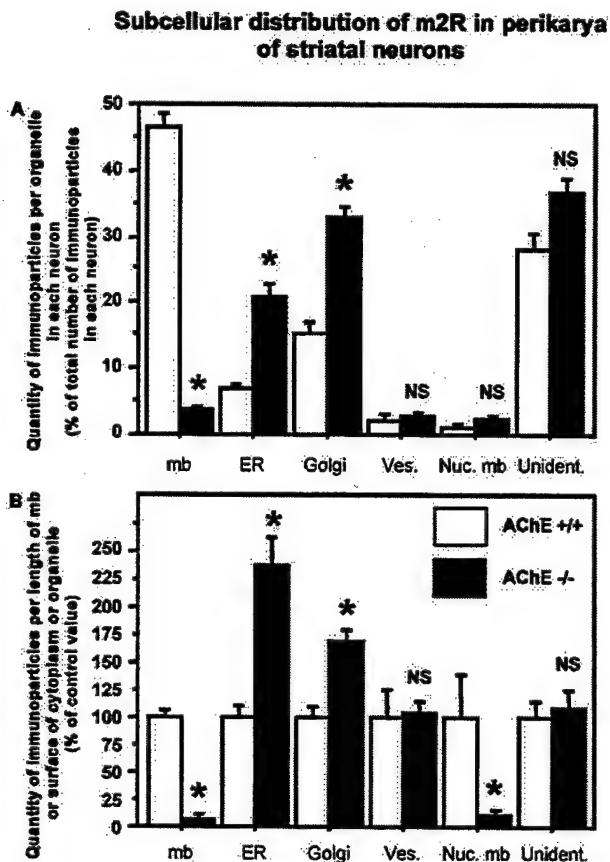
Fig. 3. Quantitative analysis of the subcellular distribution of m2R in the striatum of AChE +/+ and AChE −/− mice, using the preembedding immunogold method with silver intensification. (A) Proportion of immunoparticles for m2R associated with different subcellular neuronal compartments of each neuron. For each neuron, the number of immunoparticles associated with each subcellular compartment was counted and the proportion in relation to the total number was calculated. In AChE +/+ mice, the largest part of immunoparticles for m2R was associated with the plasma membrane. In the cytoplasm, the largest part of immunoparticles associated with an identified compartment was detected in association with endoplasmic reticulum (ER) and Golgi apparatus. A small proportion of immunoparticles was associated with small vesicles and the nuclear membrane. Some immunoparticles are seen associated with none of an identified compartment (unident.). In AChE −/− mice, most of the immunoparticles was detected in the cytoplasm associated with the endoplasmic reticulum (ER), Golgi apparatus, and the identified compartment. The statistical analysis (nonparametric Mann-Whitney U test) shows that the proportion of labeling strongly decreases at the plasma membrane (−92%; $P < 0.01$) and strongly increases in the endoplasmic reticulum (+203%; $P < 0.01$) and in the Golgi apparatus (+118%; $P < 0.001$). (B) Comparison of the density of immunolabeling for m2R in each subcellular compartment between AChE +/+ and AChE −/− mice. For each neuron, the number of immunoparticles associated with each compartment was counted in relation to the membrane length (μm) for the plasma membrane, to the surface of cytoplasm for the endoplasmic reticulum (μm^2). For the Golgi apparatus, the values are expressed as the number of immunoparticles per Golgi apparatus. Data are the result of counting in 5 AChE +/+ mice and 5 AChE −/− mice about 10 neurons per animal. To be able to compare more easily the variations of immunolabeling in the different compartments, the results are expressed in relation to an arbitrary unit (100) of the control values. The statistical analysis (nonparametric Mann-Whitney U test) shows that the labeling strongly decreases at the plasma membrane

have demonstrated in neurons of AChE −/− mice an almost complete depletion of cell surface receptors associated with an accumulation of m2R in endoplasmic reticulum and Golgi complex. Such an intraneuronal redistribution was reversed by blockade of cholinergic transmission in acute and subacute conditions leading to a recovery of normal abundance of m2R at the plasma membrane. The inhibition of protein synthesis inhibited this recovery of m2R at the plasma membrane induced by the blockade of muscarinic receptors.

Effect of AChE deficiency on the cellular and subcellular distribution of m2R immunoreactivity in striatum, cortex, and hippocampus

We have demonstrated that AChE deficiency provokes an almost complete depletion of m2R normally located at the plasma membrane of cell bodies and dendrites and an accumulation of the same receptor at the sites of synthesis and maturation in striatum, cortex, and hippocampus. This intraneuronal redistribution of m2R and especially the decrease of the density of m2R at the plasma membrane in AChE −/− mice would be an adaptive downregulation in response to AChE deficiency-induced hypercholinergy. Indeed, several arguments are in favor of chronic hypercholinergy in AChE −/− mice including behavioral signs of hypercholinergy (tremor and seizures in stressing conditions). We assume also that the absence of AChE leads to the absence of degradation of ACh and thus increases ACh levels as demonstrated by the fact the AChE inhibition induced by metrifonate has been demonstrated to increase ACh concentrations in differents brain areas including striatum and cortex (Giovannini et al., 1997; Scali et al., 1997).

Our results expand previous results showing that the membrane receptor availability is regulated by the neurochemical environment. We have recently shown that the direct or indirect acute stimulation of muscarinic receptors induced partial depletion of m2R and m4R at the membrane of striatal neurons (Bernard et al., 1998, 1999; Liste et al., 2002). We have especially shown that under the AChE inhibition induced by metrifonate in conditions known to provoke increased ACh concentrations in differents brain areas including striatum and cortex (Giovannini et al., 1997; Scali et al., 1997), m2R is stored in the cytoplasm of striatal neurons (Liste et al., 2002). We have also shown that chronic hyperdopaminergy in knockout mice for the dopamine transporter and chronic hypercholinergy induced in rats by chronic treatment with metrifonate, an AChE inhibitor, provokes both a robust and reversible decrease of the membrane abundance of D1, m2R, and m4R, with an exaggerated abundance in endoplasmic reticulum and Golgi

(−93%; $P < 0.001$) and strongly increases in the endoplasmic reticulum (+136%; $P < 0.001$) and in the Golgi apparatus (+69%; $P < 0.001$). m2R, m2 receptor; AChE, acetylcholinesterase.
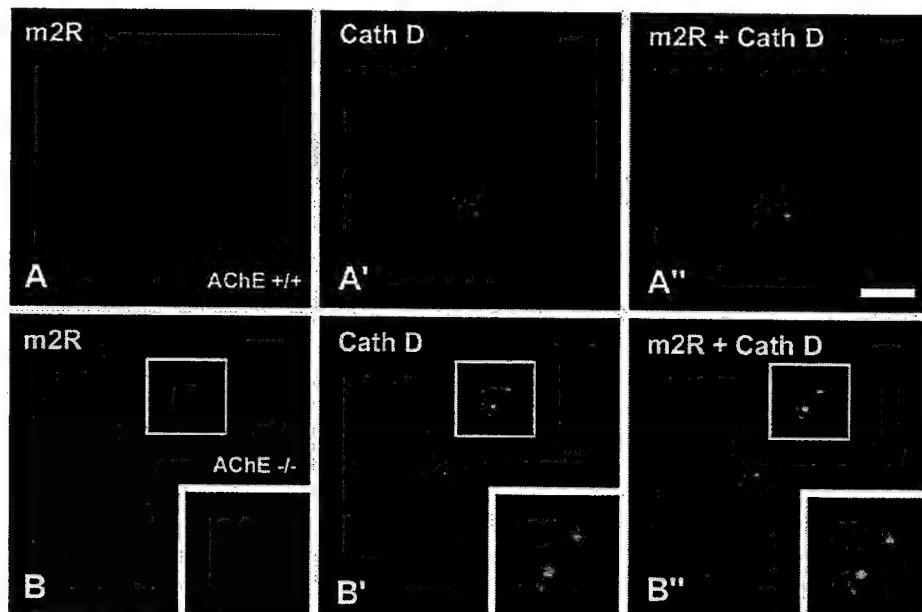
Fig. 4. Immunodetection of m2R and Cath D in striatal neurons in wild-type (AChE +/+) and knockout (AChE −/−) mice for the ACHE gene in vivo by using fluorescence microscopy. The same neurons were observed by using selective optical filters for red Alexa 568 (m2R; A and B) or green fluorescein isothiocyanate (Cath D; A' and B'). The colocalization of m2R and Cath D labelings was visualized as a yellow signal (m2R + Cath D; A″ and B″). (A″) In AChE +/+, m2R signal does not colocalize with Cath D immunolabeling. (B″) In contrast, in AChE −/− mice, m2R immunoreactivity colocalizes with Cath D labeling. m2R, m2 receptor; Cath D, cathepsin D; AChE, acetylcholinesterase. Bar: 10 μm.
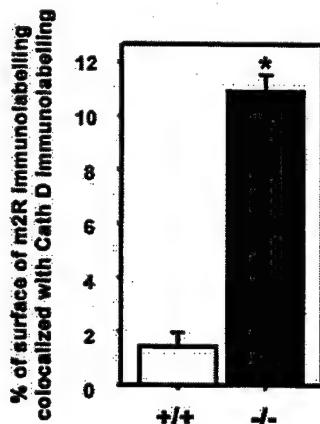

Fig. 5. Quantitative analysis of the colocalization of m2R and Cath D immunolabelings in striatum of AChE +/+ and AChE −/− mice in vivo. The localization of m2R in Cath D-immunoreactive lysosomes was analyzed at the fluorescent microscopic level in sections double-labeled for m2R and Cath D in AChE +/+ and AChE −/− mice. Both fluorescent signals (m2R and Cath D) were acquired by using suitable optical filters for Alexa 568 or fluorescein isothiocyanate, respectively, with a camera coupled to the microscope. Their colocalization was analyzed by using Metamorph software on a personal computer (Universal Imaging, Paris, France). The measures were performed on three animals per group. A mean of 10 neurons per animal were analyzed. For each neuron, the surface occupied by each labeling and the surface of colocalization of both labelings was calculated. The results were expressed as the percentage of the surface of m2R immunolabeling colocalized with the Cath D labeling. The statistical analysis (nonparametric Mann-Whitney U test) shows that the percentage of the surface of m2R labeling colocalized with Cath D labeling strongly increases in AChE −/− mice (+666%; $P < 0.05$). m2R, m2 receptor; Cath D, cathepsin D; AChE, acetylcholinesterase. Bar: 10 μM.

apparatus (Dumartin et al., 2000; Liste et al., 2002). However, our data are the first demonstration of a complete depletion of a GPCR at the neuronal membrane after hyperstimulation. The more robust and long-lasting stimulation may explain this absence of receptor at the plasma membrane since in vitro experiments on CHO cells expressing the m2R have shown that the density of m2R at the plasma membrane decreased when the concentration of the agonist increased (Tsuga et al., 1998).

We have shown that the total number of immunoparticles for m2R in neurons is similar in AChE +/+ and AChE −/− mice. This suggests that the decrease of the m2R abundance at the membrane in AChE −/− mice is not accompanied by a loss of the total number of receptors and that there is a redistribution of m2R in different intraneuronal compartments. The mechanisms involved in the disappearance of the m2R from the membrane are still unclear. However, the most relevant hypothesis is that there is an alteration of the delivery of the m2R from intracytoplasmic stores. Indeed, we have shown that the m2R is accumulated in the cytoplasm of neurons in the neuronal compartments involved in synthesis (endoplasmic reticulum) and maturation (Golgi apparatus). The molecular mechanisms that allow the delivery of newly synthetized receptors from the endoplasmic reticulum-Golgi secretory system to the plasma membrane are still poorly understood. However, it has been recently shown that an endoplasmic reticulum membrane-associated protein, DRIP78, may regulate the transport of a GPCR by binding to a specific endoplasmic
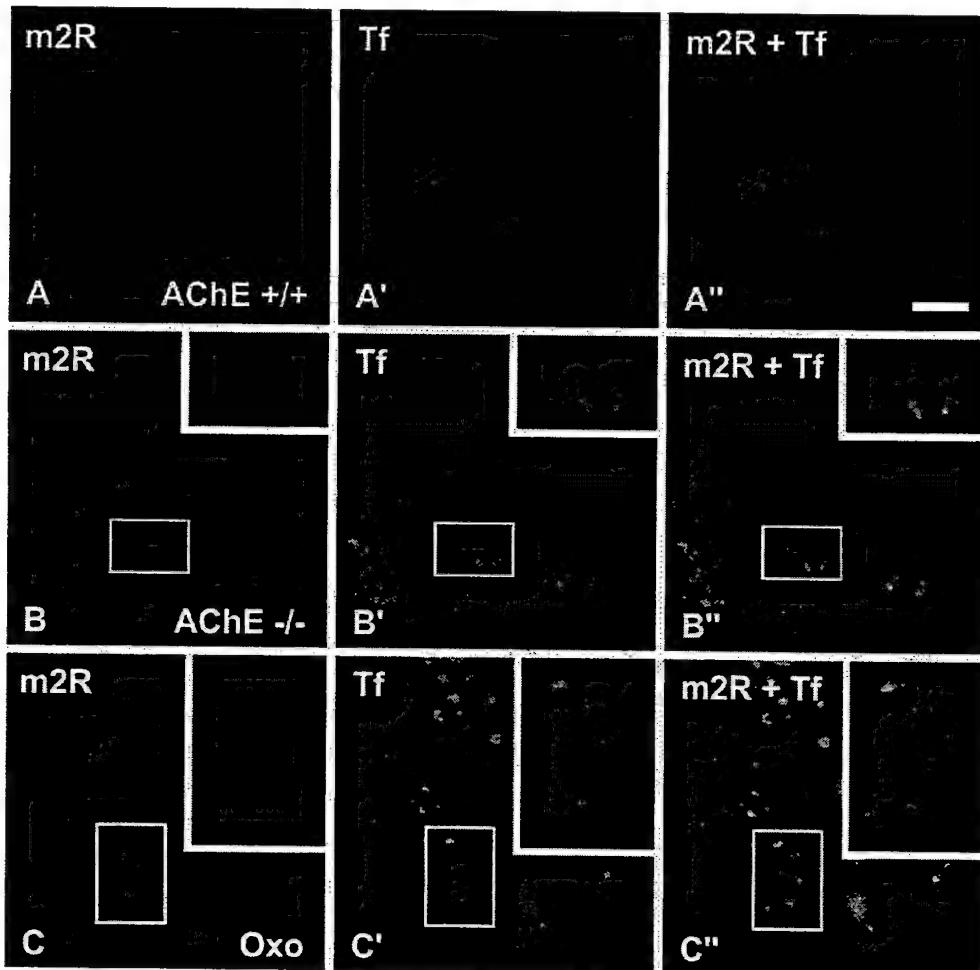
Fig. 6. Detection of m2R immunolabeling and fluorescein-conjugated transferrin (Tf) in striatal neurons in AChE +/+, AChE −/−, and oxotremorine-treated mice in vitro by using fluorescence microscopy. The same neurons were observed by using selective optical filters for red Alexa 568 (m2R; A, B, and C) or green fluorescein (Tf; A′, B′, and C′). The colocalization of m2R and Tf labelings was visualized as a yellow signal (m2R + Tf; A″, B″, and C″). (A″ and B″) In AChE +/+ and AChE −/− mice, m2R signal does not colocalize with Tf labeling. (B″) In contrast, in oxotremorine-treated mice, m2R immunoreactivity colocalizes with Tf labeling. m2R, m2 receptor; AChE, acetylcholinesterase. Bar: 10 μm.

reticulum export signal (Bermak et al., 2001). A dysfunction of the trafficking from the synthesis compartments to the membrane involving DRIP78 may occur in AChE −/− mice. As shown by Bermak et al. (2001), overexpression or sequestration of DRIP78 leads to the retention of m2R in the endoplasmic reticulum. In AChE −/− mice, in vivo, the absence of m2R at the plasma membrane may thus result from the dysfunction of available proteins involved in the targeting of the m2R to the plasma membrane. Nevertheless, this would be a reversible process since m2R can be targeted to the membrane even in AChE −/− mice when the normal cholinergic environment is restored. The absence of m2R at the plasma membrane in AChE −/− mice is unlikely to be due to the blockade of m2R synthesis. Indeed, since the cause leading to the redistribution of m2R is considered to be the permanent modification of the ACh levels due to the absence of AChE, the production of m2R would have been blocked early during ontogenesis and

definitively. It would have led to the disappearance of this subtype of receptor in the cell, whereas we have shown that the total number of immunoparticles for m2R did not differ between AChE +/+ and AChE −/− mice.

We have demonstrated that the proportion of m2R associated to lysosomes was highly increased in AChE −/− mice, which suggests an activation of the degradation of this receptor. In AChE +/+ mice, m2R may be mostly targeted to the plasma membrane and then endocyted and degraded, or recycled to the membrane. In contrast, in AChE −/− mice, the pool of newly synthesized m2R may be directly led to the lysosomal compartment to be degraded.

It is most unlikely that the absence of m2R at the plasma membrane is due to increased endocytosis in contrast to what we have shown after acute stimulation of muscarinic receptors in vivo (Bernard et al., 1998, 1999; Liste et al., 2002) or in vitro in the present study. Indeed, we have demonstrated in AChE −/− mice that striatal neurons in
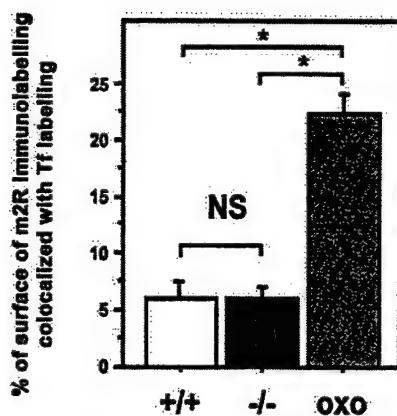
Fig. 7. Quantitative analysis of the colocalization of m2R and Tf labelings in striatum of AChE +/+ and AChE −/− mice in vitro. The localization of m2R in Tf-positive structures was analyzed at the fluorescent microscopic level in sections double labeled for m2R and Tf in AChE +/+, AChE −/−, and oxotremorine-treated mice. Both fluorescent signals (m2R and Tf) were acquired by using suitable optical filters for Alexa 568 or fluorescein isothiocyanate, respectively, with a camera coupled to the microscope. Their colocalization was analyzed by using Metamorph software on a personal computer (Universal Imaging, Paris, France). The measures were performed on three animals per group. A mean of 10 neurons per animal were analyzed. For each neuron, the surface occupied by each labeling and the surface of colocalization of both labelings were calculated. The results were expressed as the percentage of the surface of m2R immunolabeling colocalized with the Tf labeling. The statistical analysis (nonparametric Mann-Whitney U test) shows that the percentage of the surface of m2R labeling colocalized with Tf labeling is not different in AChE −/− and in AChE +/+ mice. In contrast, in oxotremorine-treated mice, the surface of m2R immunoreactivity colocalized with Tf labeling strongly increases compared to AChE +/+ (+266%; $P < 0.001$) and AChE −/− mice (+266%; $P < 0.001$). m2R, m2 receptor; Tf, fluorescein-conjugated transferrin; AChE, acetylcholinesterase; OXO, oxotremorine.

vitro did not display an activation of the coincorporation of m2R with transferrin, i.e., did not show m2R endocytosis. This was confirmed in vivo at the EM level by the absence of any morphological evidence of increased endocytosis, i.e., the presence of m2R-immunoreactive endosomes while such events are clearly observed in other models (Bernard et al., 1998; Liste et al., 2002). This is in agreement with in vitro experiments for m2R but also for the β2-adrenergic receptor, suggesting that the decrease of the membrane density of a GPCR after chronic activation does not involve endocytosis (Tsuga et al., 1998; Jockers et al., 1999). Taken together, this suggests that the absence of m2R at the membrane in AChE −/− mice does not involve a regulation by endocytosis and recycling.

Regulation of the balance between intracytoplasmic and membrane m2R stores

It is likely that the abundance of m2R at the plasma membrane is the result of a balance between intracytoplasmic and membrane stores and that variations in ACh levels regulate this balance. Our evidence suggests that the cholinergic environment is a key factor regulating the mem-

brane availability of m2R. We were able to induce the delivery of the m2R to the plasma membrane in AChE −/− mice by modulating the cholinergic transmission by different ways. When hippocampal and cortical slices from AChE −/− mice were cultured alone, without their cholinergic afferents, m2R was present at the membrane and did not accumulate in the cytoplasm. When hippocampus from AChE −/− mice was cocultured with septum from AChE −/− mice, its native cholinergic afferent, m2R kept the distribution seen in hippocampus in vivo, i.e., cytoplasmic storage and membrane depletion. In AChE −/− striatum, in which cholinergic afferents were intrinsic, m2R stayed blocked in the cytoplasm. Moreover, the supplementation of AChE −/− neurons with AChE by the coculture of AChE −/− with AChE +/+ striatum, leading probably to the decrease of ACh levels in the microenvironment of AChE −/− cells, provoked a translocation of m2R from the cytoplasm to the membrane. These data strongly suggest that the blockade of m2R in endoplasmic reticulum and Golgi apparatus and the absence of m2R at the membrane were due to chronic overstimulation by endogenous ACh. Our data suggest also that the absence of m2R at the plasma membrane is a muscarinic receptor-mediated effect, since the blockade of muscarinic receptors by atropine in AChE −/− mice in vivo and in vitro induced the expression of m2R at the plasma membrane. The nicotinic transmission does not seem to be playing a role in the storage of m2R in the cytoplasm, since the blockade of nicotinic receptors has no effect on the subcellular localization of m2R observed in AChE −/− mice.

Functional implications

Since it is likely that the quantity of receptors located at the plasma membrane is conditioning the neuronal activity, the neuronal function regulated through m2R must be deeply modified in the AChE −/− mice. Interestingly, preliminary results have shown that these animals are resistant to oxotremorine-induced hypothermia and salivation (Li et al., in press). These pharmacological effects were demonstrated to be triggered by m2R, since the same absence of response to oxotremorine has been shown in knockout mice for the m2R (Gomeza et al., 1999). Our data thus give a strong anatomical basis for a functional link between the decrease of the number of receptors located at the plasma membrane and the modification of the function modulated by the same receptors. The m2R is not available for the ligand and thus is not able to transduce the cholinergic effects. This would be in agreement with work in CHO cells showing that the downregulation of m3R induced by chronic stimulation provokes desensitization of the cell response (Detjen et al., 1995). Further experiments coupling electrophysiology and muscarinic receptor trafficking analysis may help to understand the functional consequences of the m2R intraneuronal redistribution. Since the m2R is involved in the autoregulation of ACh release, one may

suggest that AChE deficiency contributes, through the regulation of the membrane m2R availability at the surface of cholinergic neurons, to the modulation of the ACh release in the striatum (Weiler et al., 1984; Billard et al., 1995). Dysfunctions of cholinergic transmission have been shown in several neurodegenerative disorders including Alzheimer's disease and Parkinson's disease. The efficiency of muscarinic antagonists in the treatment of motor disorders in Parkinson's disease suggest a chronic striatal cholinergic overactivity (Calne, 1993). Thus, changes in the availability of m2R at the plasma membrane may be involved in the changes in the neuronal activity and in the clinical symptoms of the disease. In view of the dramatic changes in m2R subcellular compartmentalization under chronic stimulation, our results may be relevant to understanding reduced efficiency with time of the AChE inhibitors used in the treatment of Alzheimer's disease.

Experimental methods

Animals

Knockout mice for the ACHE gene were generated as previously described (Xie et al., 2000). The experiments were performed on the following three groups of animals: wild-type (AChE +/+) mice, nullizygous (AChE −/−) mice, and AChE −/− mice treated for 22 days from the age of 6 days with atropine sulfate salt, or mecamylamine, an antagonist of muscarinic or nicotinic receptors, respectively (Sigma; St. Louis, MO; 5 mg/kg). The genotypes were determined by polymerase chain reaction. Mice were used at the age of 28 days (in vivo) or 2 to 7 days (in vitro). All experiments were performed in accordance with the policies of the French Agriculture and Forestry Ministry and the Centre National de la Recherche Scientifique and in accordance with the policy on the use of animals in neuroscience research issued by the Society for Neuroscience. The experiments were performed in vivo, i.e., in the whole animal, which reflects what happens in the living mouse, and in vitro in organotypic cultures.

Organotypic cultures

Organotypic slice cultures were prepared by the method originally described by Stoppini et al. (1991). Briefly, the mice pups were quickly decapitated and their brains removed from the skull. Frontal slices (400 μm) including cortex, striatum, septum, or hippocampus, obtained from AChE +/+ or AChE −/− pups, were cut by using a tissue chopper. Striatum, septum, and hippocampus were dissected from the slices of whole brain in a dissecting minimum essential medium (GibcoBRL, Rockville, USA) containing glucose (5 mg/ml). The subcellular distribution of m2R was studied in single cultures of striatum, cortex, and

hippocampus from AChE +/+ or AChE −/− mice. Some cultures were treated with different pharmacological agents (Table 1). Atropine sulfate salt (Sigma; 100 μM) or mecamylamine (Sigma; 100 μM) were used to study the effect of blockade of muscarinic or nicotinic receptors, respectively, on the subcellular distribution of m2R in AChE −/− striatum. To determine if endocytosis may be involved in the subcellular redistribution of m2R in AChE −/− striatum, Tf (fluorescein-conjugated transferrin), a molecule that is internalized in endosomes, was incubated for 1 h with striatal AChE −/− cultures and the colocalization of m2R and Tf was investigated. AChE +/+ striatal cultures, incubated together with Tf, with oxotremorine (25 μM), a muscarinic receptor agonist known to induce m2R endocytosis, were used as a control of endocytosis. Alternatively, to determine the role of AChE on the subcellular distribution of the m2R in AChE −/− striatum, cocultures of striatum from AChE +/+ and AChE −/− mice were developed. To study the influence of septal cholinergic neurons innervating hippocampus, septum and hippocampus were cocultured. For that, the explants were cultured side by side. The presence of the innervation of AChE −/− striatal explant by the neurons from the AChE striatal AChE +/+ explant was determined by the detection of a dense network of AChE-immunopositive fibers in the AChE −/− explant (Fig. 9B'). We assume that the AChE produced by neurons from the AChE +/+ explant innervating the AChE −/− explant hydrolyses and thus downregulates ACh levels in the AChE −/− striatum. Moreover, we have shown that this enzyme is active, since we were also able to detect it by histochemistry (data not shown). The presence of the innervation of hippocampus by cholinergic septal neurons was determined by the detection of fibers immunopositive for the vesicular acetylcholine transporter (VAChT) in the hippocampal explant (Fig. 8C). See Table 1 for the treatments, number, and age of animals. The slices were maintained in culture on Millicell membrane inserts in a humidified incubator (36.5°C; 5% CO_2) for at least 14 days before use. Culture medium consisted of 50% minimum essential medium (GibcoBRL), 33% Hanks' balanced salt solution (GibcoBRL), and 15% heat-inactivated horse serum (GibcoBRL) supplemented with glucose (5 mg/ml), 1 mM glutamine, 1% anti-mycoplasm agent, and 1% fungizone (GibcoBRL).

Tissue preparation for immunohistochemistry

For in vivo experiments, the mice were deeply anesthetized with sodium chloral hydrate and at least five animals per group were perfused transcardiacally with a mixture of 2% paraformaldehyde and 0.2% glutaraldehyde as previously described (Bernard et al., 1999). Sections from neostriatum were cut on a vibrating microtome at 70 μm and collected in phosphate-buffered saline. For in vitro experiments, the cultures were fixed in 4% (wt/vol) paraformaldehyde in 0.1 M phosphate buffer (pH 7.4) at 4°C for 4 h,
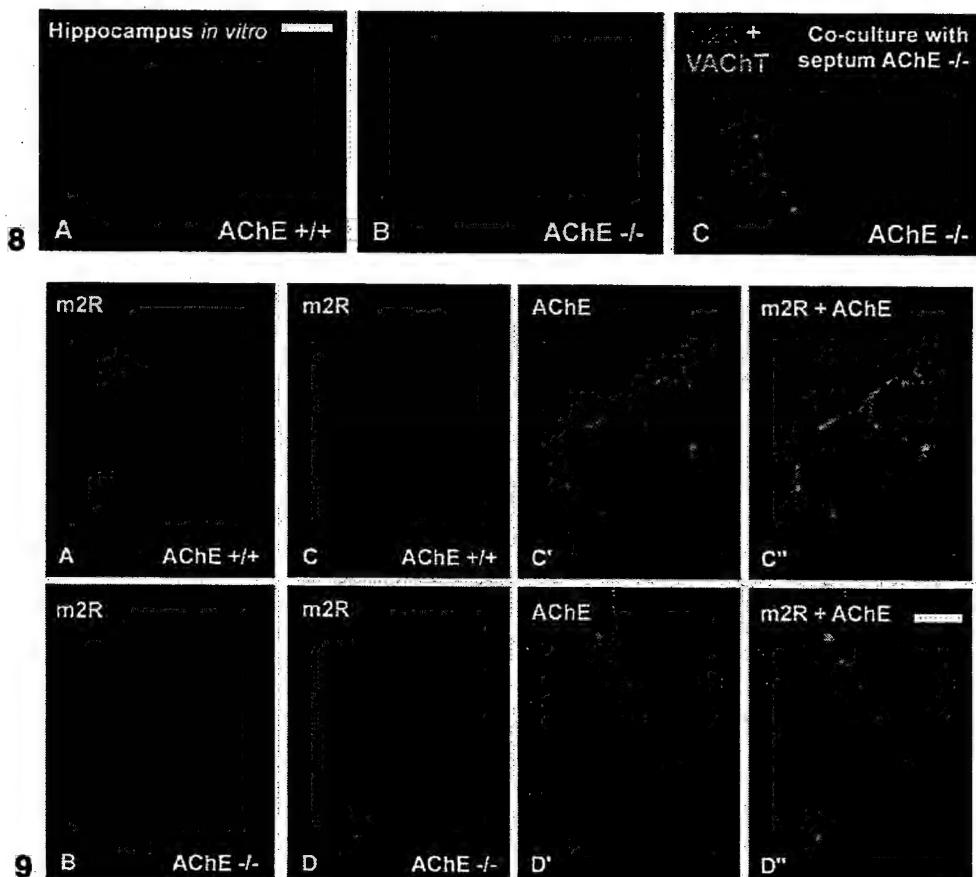
Fig. 8. Regulation of the subcellular distribution of the m2R in absence of AChE in the hippocampus in vitro. The m2R was detected in organotypic cultures of hippocampus from AChE +/+ and AChE −/− mice. (A and B) In AChE +/+ but also in AChE −/− mice, m2R is seen at the plasma membrane. (C) When AChE −/− hippocampus is cocultured with septum of AChE −/− mice (F), its native afferent, m2R (red), is detected stored in the cytoplasm of neurons of the hippocampus. The presence of septohippocampal cholinergic fibers was shown by the presence of VAChT-immunopositive fibers (green). m2R, m2 receptor; AChE, acetylcholinesterase; VAChT, vesicular acetylcholine transporter. Bar: 10 μm.

Fig. 9. Regulation of the subcellular distribution of the m2R in single striatal cultures of AChE +/+ and AChE −/− mice and in cocultures of AChE +/+ and AChE −/− mice striatal explants. (A and B) The m2R was detected in single organotypic cultures of striatum from AChE +/+ and AChE −/− mice. In AChE +/+ mice (A), m2R immunoreactivity is detected at the plasma membrane. In contrast, in AChE −/− mice (B), no staining is seen at the plasma membrane, whereas a strong immunolabeling is detected in the cytoplasm. (C–D″) AChE +/+ and AChE −/− mice were cocultured to determine the role of AChE on the subcellular distribution of the m2R in AChE −/− striatum. AChE +/+ and AChE −/− explants were cultured side by side. (C and D) The m2R was detected in striatum from AChE +/+ and AChE −/− mice. (C′ and D′) AChE immunoreactivity was used as a marker of AChE +/+ neurons and fibers. (C and C′) In an AChE +/+ mouse explant, the same neuron displaying m2R immunolabeling at the plasma membrane also shows AChE immunoreactivity. (D and D′) In the AChE −/− adjacent explant, which is innervated by AChE-containing fibers coming from the AChE tissue as shown by the presence of AChE immunoreactivity (B′), m2R is detected at the plasma membrane. m2R, m2 receptor; AChE, acetylcholinesterase.

removed from the membranes, and processed for immunocytochemistry as free-floating sections. The sections and cultures were cryoprotected, freeze-thawed, and stored in phosphate-buffered saline until use.

Immunohistochemistry

The m2R was detected by immunohistochemistry using a monoclonal antibody raised in rat against an intracellular epitope of the receptor (Chemicon, Temecula, USA; dilution: 1:500). The m2R was detected at the LM level on brain sections and on cultures by immunofluorescence, as previously described (Bernard et al., 1998). The m2R immuno-

reactivity was detected either alone or in combination with AChE, VAChT, or Cath D immunoreactivities, or Tf. The immunohistochemical detection of AChE (Chemicon) was used to identify AChE +/+ fibers in cocultures of AChE +/+ and AChE −/− striatum. The immunohistochemical detection of VAChT (Chemicon) was used to identify septal cholinergic fibers in hippocampal explants in cocultures of septum and hippocampus. The immunohistochemical detection of CathDs (Santa Cruz Biotechnology Inc., Santa Cruz, USA) was used as a marker of lysosomes on fixed brain sections. Tf was used to identify endosomes in cultures (see above). For the single detection of m2R, after fixation (in vitro) or perfusion-fixation (in vivo) as described above, sections were incubated in 4% normal donkey serum (NDS)
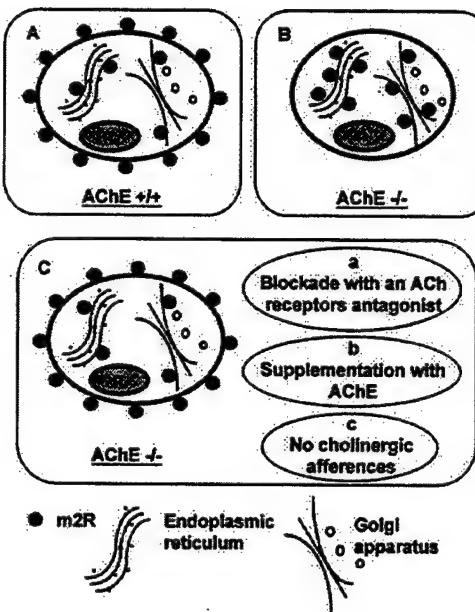
Fig. 10. Schematic representation of the regulation of the subcellular distribution of m2R in neurons of the central nervous system. (A and B) In AChE +/+ mice (A), m2R is mainly located at the plasma membrane, whereas in AChE −/− mice (B), m2R is accumulated mostly in the cytoplasm in association with the endoplasmic reticulum and Golgi apparatus. (C) In three conditions of blockade of the cholinergic transmission in AChE −/− mice, m2R is back on the plasma membrane, i.e., when the muscarinic receptors are blocked with an antagonist (a); when neurons from AChE −/− mice are supplemented with AChE coming from cocultures of neurons of AChE +/+ mice (b); and when neurons from AChE −/− mice are grown without cholinergic afferents (c). m2R, m2 receptor; AChE, acetylcholinesterase; ACh, acetylcholine.

for 30 min and then in m2R (1:500) antibody supplemented with 1% NDS for 15 h at room temperature. After washing, the sections were incubated with cyanine 3-conjugated goat anti-rat secondary antibody. For the double detection of m2R and AChE, VAChT, or Cath D antibodies, after fixation (in vitro) or perfusion-fixation (in vivo) as described above, sections were incubated in 4% NDS for 30 min and then in a mixture of m2R (1:500), and AChE (1:1000), VAChT (1:1000), or Cath D antibodies supplemented with 1% NDS for 15 h at room temperature. For the simultaneous detection of m2R and AChE, the sections were incubated in a mixture of goat anti-rat IgG coupled to Alexa 568 (Molecular Probes, Eugene, USA; 1:1000) and goat anti-rabbit coupled to fluorescein isothiocyanate (Jackson ImmunoResearch). For the simultaneous detection of m2R and VAChT or Cath D, the sections were incubated in donkey anti-goat IgG coupled to biotin (Amersham Biosciences, Amersham, UK; 1:200), saturated in 4% normal goat serum, and finally incubated in a mixture of goat anti-rat IgG coupled to Alexa 568 (Molecular Probes; 1:1000) and streptavidin coupled to DTAF (Jackson ImmunoResearch; 1:1000). For the simultaneous detection of m2R and Tf in vitro, transferrin was incubated in living cultures just before fixation as described above. Cultures were then incubated in 4% NDS for 30 min

and then in m2R (1:500) antibody supplemented with 1% NDS for 15 h at room temperature. After washing, the sections were incubated with Alexa 568-conjugated goat anti-rat secondary antibody (Molecular Probes; 1:1000). After washing, the sections were mounted in Vectashield mounting medium (Vector Laboratories, Burlingame, CA) and examined in a fluorescence microscope (Zeiss).

The m2R was detected at the EM level on sections from in vivo experiments using the preembedding immunogold method as previously described (Bernard et al., 1998). After treatment of sections with 1% osmium, dehydration, and embedding in resin, ultrathin sections were cut, stained with lead citrate, and examined in a Philips CM10 EM or Tecnai 20.

Quantitative analysis of the distribution of m2R in neuronal compartments

The subcellular distribution of m2R in perikarya of striatum of AChE +/+ and AChE −/− mice was analyzed from sections (in vivo) or cultures (in vitro).

The localization in different subcellular compartments was analyzed from immunogold-treated sections at the EM level. The analysis was performed on negatives of micrographs at a final magnification of 3900×, using Metamorph software on a personal computer (Universal Imaging, Paris, France). After scanning the negative (Magic Scan, version 3.1; Umax), the image was converted into a positive picture and magnified to allow the identification of the subcellular elements showing immunoparticles. The measures were performed on five animals per group. A mean of 10 perikarya per animal were analyzed. The immunoparticles were identified and counted in the cytoplasm of perikarya in association with six subcellular compartments. Five compartments are the plasma membrane, small vesicles, the Golgi apparatus, the endoplasmic reticulum, and the outer nuclear membrane. Some immunoparticles were classified as associated with a sixth unidentified compartment because they were associated either with no detectable organelles or with an organelle that could not be identified as one of the previous ones. The results were expressed in two ways. First, the data were expressed as the proportion of immunoparticles for m2R associated with the different subcellular compartments in each neuron. For that, for each neuron, the number of immunoparticles associated with each subcellular compartment was counted and the proportion in relation to the total number was calculated. Second, the results were also expressed to be able to compare the variations of the immunolabeling for m2R in each subcellular compartment between AChE +/+ and AChE −/− mice. For that, for each neuron, the number of immunoparticles associated with each compartment was counted in relation to membrane length (μm) for the plasma and nuclear membrane, to the surface of cytoplasm for the endoplasmic reticulum

Table 1
Animals and structures used for organotypic cultures[a]

Structure (No. of animals)	Age (postnatal days)	Treatment (dose, delay)
Single cultures		
Basal conditions		
Striatum AChE +/+ (10)	4–5	None
Striatum AChE −/− (10)	4–5	None
Cortex AChE +/+ (10)	4–5	None
Cortex AChE −/− (10)	4–5	None
Hippocampus AChE +/+ (5)	5–7	None
Hippocampus AChE −/− (5)	5–7	None
Blockade experiments		
Striatum AChE +/+ (5)	4–5	Atropine (100 μM, 2 h)
Striatum AChE −/− (5)	4–5	Atropine (100 μM, 2 h)
Striatum AChE +/+ (5)	4–5	Mecamylamine (100 μM, 2 h)
Striatum AChE −/− (5)	4–5	Mecamylamine (100 μM, 2 h)
Endocytosis experiments		
Striatum AChE +/+ (5)	4–5	NaCl (9 mg/L) + Tf (50 μg/ml) (1 h)
Striatum AChE +/+ (5)	4–5	Oxotremorine (25 μM) + Tf (50 μg/ml) (1 h)
Striatum AChE −/− (5)	4–5	NaCl (9 mg/L) + Tf (50 μg/ml) (1 h)
Cocultures		
Striatum AChE +/+ (5)	2	None
+ Striatum AChE −/− (5)	2	
Hippocampus AChE +/+ (5)	7	None
+ septum AChE +/+ (5)	2	
Hippocampus AChE +/+ (5)	7	None
+ septum AChE −/− (5)	2	
Hippocampus AChE −/− (5)	7	None
+ septum AChE +/+ (5)	2	
Hippocampus AChE −/− (5)	7	None
+ septum AChE −/− (5)	2	

[a] AChE, acetylcholinesterase; Tf, fluorescein-conjugated transferrin.

(μm^2). For the Golgi apparatus, the values are expressed as the number of immunoparticles per Golgi apparatus.

The localization in endosomes and lysosomes was analyzed at the fluorescent microscopic level in sections or cultures double labeled for m2R and transferrin or m2R and Cath D, respectively, in AChE +/+, AChE −/−, and oxotremorine-treated mice. Both fluorescent signals (m2R and transferrin or Cath D) were acquired by using suitable optical filters for Alexa 568 or fluorescein isothiocyanate, respectively, with a camera coupled to the microscope. Their colocalization was analyzed by using Metamorph software on a personal computer (Universal Imaging). The measures were performed on three animals per group. A mean of 10 neurons per animal were analyzed. For each neuron, the surface occupied by each labeling and the surface of colocalization of both labelings were calculated. The results were expressed as the percentage of the surface of m2R immunolabeling colocalized with the transferrin or Cath D labelings.

The values from immunogold experiments were analyzed by using the nonparametric Mann-Whitney U test. The comparisons of the values from fluorescence experiments were analyzed by using the Mann-Whitney U test (m2R/Cath D labeling, one-factor analysis) or the Kruskal-Wallis test followed by a post hoc Dunn test (m2R/transferrin, two-factor analysis).

References

Bermak, J.C., Li, M., Bullock, C., Zhou, Q.Y., 2001. Regulation of transport of the dopamine D1 receptor by a new membrane-associated ER protein. Nat. Cell. Biol. 3, 492–498.

Bernard, V., Laribi, O., Levey, A.I., Bloch, B., 1998. Subcellular redistribution of m2 muscarinic acetylcholine receptors in striatal interneurons in vivo after acute cholinergic stimulation. J. Neurosci. 18, 10207–10218.

Bernard, V., Levey, A.I., Bloch, B., 1999. Regulation of the subcellular distribution of m4 muscarinic acetylcholine receptors in striatal neurons in vivo by the cholinergic environment: evidence for regulation of cell surface receptors by endogenous and exogenous stimulation. J. Neurosci. 19, 10237–10249.

Bernard, V., Normand, E., Bloch, B., 1992. Phenotypical characterization of the rat striatal neurons expressing muscarinic receptor genes. J. Neurosci. 12, 3591–3600.

Billard, W., Binch, H.R., Crosby, G., McQuade, R.D., 1995. Identification of the primary muscarinic autoreceptor subtype in rat striatum as m2 through a correlation of in vivo microdialysis and in vitro receptor binding data. J. Pharmacol. Exp. Ther. 273, 273–279.

Bloch, B., Dumartin, B., Bernard, V., 1999. In vivo regulation of intraneuronal trafficking of G protein-coupled receptors for neurotransmitters. Trends Pharmacol. Sci. 20, 315–319.

Calne, D.B., 1993. Treatment of Parkinson's disease. N. Engl. J. Med. 329, 1021–1027.

Csaba, Z., Bernard, V., Helboe, L., Bluet-Pajot, M.T., Bloch, B., Epelbaum, J., Dournaud, P., 2001. In vivo internalization of the somatostatin sst2A receptor in rat brain: evidence for translocation of cell-surface receptors into the endosomal recycling pathway. Mol. Cell. Neurosci. 17, 646–661.

Detjen, K., Yang, J., Logsdon, C.D., 1995. Muscarinic acetylcholine receptor down-regulation limits the extent of inhibition of cell cycle progression in Chinese hamster ovary cells. Proc. Natl. Acad. Sci. USA 92, 10929–10933.

Dournaud, P., Boudin, H., Schonbrunn, A., Tannenbaum, G.S., Beaudet, A., 1998. Interrelationships between somatostatin sst2A receptors and somatostatin-containing axons in rat brain: evidence for regulation of cell surface receptors by endogenous somatostatin. J. Neurosci. 18, 1056–1071.

Dumartin, B., Caille, I., Gonon, F., Bloch, B., 1998. Internalization of D1 dopamine receptor in striatal neurons in vivo as evidence of activation by dopamine agonists. J. Neurosci. 18, 1650–1661.

Dumartin, B., Jaber, M., Gonon, F., Caron, M.G., Giros, B., Bloch, B., 2000. Dopamine tone regulates D1 receptor trafficking and delivery in striatal neurons in dopamine transporter-deficient mice [in process citation]. Proc. Natl. Acad. Sci. USA 97, 1879–1884.

Faure, M.P., Alonso, A., Nouel, D., Gaudriault, G., Dennis, M., Vincent, J.P., Beaudet, A., 1995. Somatodendritic internalization and perinuclear targeting of neurotensin in the mammalian brain. J. Neurosci. 15, 4140–4147.

Giovannini, M.G., Giovannelli, L., Bianchi, L., Kalfin, R., Pepeu, G., 1997. Glutamatergic modulation of cortical acetylcholine release in the rat: a combined in vivo microdialysis, retrograde tracing and immunohistochemical study. Eur. J. Neurosci. 9, 1678–1689.

Gomeza, J., Shannon, H., Kostenis, E., Felder, C., Zhang, L., Brodkin, J., Grinberg, A., Sheng, H., Wess, J., 1999. Pronounced pharmacologic deficits in M2 muscarinic acetylcholine receptor knockout mice. Proc. Natl. Acad. Sci. USA 96, 1692–1697.

Hajos, N., Papp, E.C., Acsady, L., Levey, A.I., Freund, T.F., 1998. Distinct interneuron types express m2 muscarinic receptor immunoreactivity on their dendrites or axon terminals in the hippocampus. Neuroscience 82, 355–376.

Heck, D.A., Bylund, D.B., 1998. Differential down-regulation of alpha-2 adrenergic receptor subtypes. Life Sci. 62, 1467–1472.

Hertel, C., Coulter, S.J., Perkins, J.P., 1985. A comparison of catecholamine-induced internalization of beta-adrenergic receptors and receptor-mediated endocytosis of epidermal growth factor in human astrocytoma cells. Inhibition by phenylarsine oxide. J. Biol. Chem. 260, 12547–12553.

James, M.K., Cubeddu, L.X., 1984. Frequency-dependent muscarinic receptor modulation of acetylcholine and dopamine release from rabbit striatum. J. Pharmacol. Exp. Ther. 229, 98–104.

Jockers, R., Angers, S., Da Silva, A., Benaroch, P., Strosberg, A.D., Bouvier, M., Marullo, S., 1999. Beta(2)-adrenergic receptor downregulation. Evidence for a pathway that does not require endocytosis. J. Biol. Chem. 274, 28900–28908.

Ko, J.L., Arvidsson, U., Williams, F.G., Law, P.Y., Elde, R., Loh, H.H., 1999. Visualization of time-dependent redistribution of delta-opioid receptors in neuronal cells during prolonged agonist exposure. Brain Res. Mol. Brain Res. 69, 171–185.

Koenig, J.A., Edwardson, J.M., 1996. Intracellular trafficking of the muscarinic acetylcholine receptor: importance of subtype and cell type. Mol. Pharmacol. 49, 351–359.

Koenig, J.A., Edwardson, J.M., 1997. Endocytosis and recycling of G protein-coupled receptors. Trends Pharmacol. Sci. 18, 276–287.

Li, B., Duysen, E.G., Volpicelli, L.A., Levey, A.I., Lockridge, O., 2003. Regulation of muscarinic acetylcholine receptor function in acetylcholinesterase knockout mice. Pharmacol. Biochem. Behav. (in press).

Liste, I., Bernard, V., Bloch, B., 2002. Acute and chronic acetylcholinesterase inhibition regulates in vivo the localization and abundance of muscarinic receptors m2 and m4 at the cell surface and in the cytoplasm of striatal neurons. Mol. Cell. Neurosci. 20, 244–256.

Mantyh, P.W., Allen, C.J., Ghilardi, J.R., Rogers, S.D., Mantyh, C.R., Liu, H.T., Basbaum, A.I., Vigna, S.R., Maggio, J.E., 1995a. Rapid endocytosis of a G protein-coupled receptor: substance P-evoked internalization of its receptor in the rat striatum in vivo. Proc. Natl. Acad. Sci. USA 92, 2622–2626.

Mantyh, P.W., DeMaster, E., Malhotra, A., Ghilardi, J.R., Rogers, S.D., Mantyh, C.R., Liu, H., Basbaum, A.I., Vigna, S.R., Maggio, J.E., 1995b. Receptor endocytosis and dendrite reshaping in spinal neurons after somatosensory stimulation. Science 268, 1629–1632.

Marvizon, J.C., Martinez, V., Grady, E.F., Bunnett, N.W., Mayer, E.A., 1997. Neurokinin 1 receptor internalization in spinal cord slices induced by dorsal root stimulation is mediated by NMDA receptors. J. Neurosci. 17, 8129–8136.

McDonald, T.P., Dinnis, D.M., Morrison, C.F., Harmar, A.J., 1998. Desensitization of the human vasoactive intestinal peptide receptor (hVIP2/PACAP R): evidence for agonist-induced receptor phosphorylation and internalization. Ann. NY Acad. Sci. 865, 64–72.

Mundell, S.J., Kelly, E., 1998. The effect of inhibitors of receptor internalization on the desensitization and resensitization of three Gs-coupled receptor responses. Br. J. Pharmacol. 125, 1594–1600.

Murakami, S., Kubota, Y., Kito, S., Shimada, S., Takagi, H., Wu, J.-Y., Inagaki, S., 1989. The coexistence of substance P- and glutamic acid decarboxylase-like immunoreactivity in entopeduncular neurons of the rat. Brain Res. 485, 403–406.

Pippig, S., Andexinger, S., Lohse, M.J., 1995. Sequestration and recycling of beta 2-adrenergic receptors permit receptor resensitization. Mol. Pharmacol. 47, 666–676.

Rouse, S.T., Thomas, T.M., Levey, A.I., 1997. Muscarinic acetylcholine receptor subtype, m2: diverse functional implications of differential synaptic localization. Life Sci. 60, 1031–1038.

Scali, C., Giovannini, M.G., Bartolini, L., Prosperi, C., Hinz, V., Schmidt, B., Pepeu, G., 1997. Effect of metrifonate on extracellular brain acetylcholine and object recognition in aged rats. Eur. J. Pharmacol. 325, 173–180.

Sternini, C., Spann, M., Anton, B., Keith Jr., D.E., Bunnett, N.W., von Zastrow, M., Evans, C., Brecha, N.C., 1996. Agonist-selective endocytosis of mu opioid receptor by neurons in vivo. Proc. Natl. Acad. Sci. USA 93, 9241–9246.

Stoppini, L., Buchs, P.A., Muller, D., 1991. A simple method for organotypic cultures of nervous tissue. J. Neurosci. Methods 37, 173–182.

Tsao, P., Cao, T., von Zastrow, M., 2001. Role of endocytosis in mediating downregulation of G-protein-coupled receptors. Trends Pharmacol. Sci. 22, 91–96.

Tsuga, H., Kameyama, K., Haga, T., Honma, T., Lameh, J., Sadee, W., 1998. Internalization and down-regulation of human muscarinic acetylcholine receptor m2 subtypes. Role of third intracellular m2 loop and G protein-coupled receptor kinase 2. J. Biol. Chem. 273, 5323–5330.

Weiler, M.H., Misgeld, U., Gheong, D.K., 1984. Presynaptic muscarinic modulation of nicotinic excitation in the rat neostriatum. Brain Res. 296, 111–120.

Xie, W., Stribley, J.A., Chatonnet, A., Wilder, P.J., Rizzino, A., McComb, R.D., Taylor, P., Hinrichs, S.H., Lockridge, O., 2000. Postnatal developmental delay and supersensitivity to organophosphate in gene-targeted mice lacking acetylcholinesterase. J. Pharmacol. Exp. Ther. 293, 896–902.

BUTYRYLCHOLINESTERASE
ITS FUNCTION AND INHIBITORS

Ezio Giacobini MD PhD
Department of Geriatrics
University of Geneva
School of Medicine
Geneva
Switzerland

Editor

Nachon et al

4

Comparison of the structures of butyrylcholinesterase and acetylcholinesterase

Florian Nachon, Patrick Masson, Yvain Nicolet, Oksana Lockridge and Juan C Fontecilla-Camps

Introduction

Early studies revealed that cholinesterases (ChEs) differ in their substrate specificity and sensitivity to inhibitors. Subsequently, ChEs were divided into two types on the basis of their catalytic properties: enzymes that preferentially hydrolysed small substrates such as acetylcholine were called acetylcholinesterase (AChE; EC 3.1.1.7) and enzymes able to accommodate bulkier substrates such as butyrylcholine were named butyrylcholinesterase (BuChE; EC 3.1.1.8). Cross-checking of data from sequence and structure databases showed that ChEs belong to a large family of proteins, sharing a common α/β-hydrolase fold. This family includes proteins with a broad range of functions such as lipases, peptidases, dehalogenases and even adhesion proteins. A dedicated database, available on the World Wide Web, has been created to consolidate most of the information concerning this family of proteins (ESTHER:http://meleze.ensam.inra.fr/cholinesterase/).

AChE and BuChE are so closely related that it is unthinkable to describe the structure of one enzyme without referring to the other. Actually, until the crystal structure of human BuChE (hBuChE) was solved, all structural studies on BuChE relied on homology models based on the crystal structure of *Torpedo californica* AChE (*Tc*AChE). Therefore, this chapter will cover knowledge on the structure of both enzymes and their differences. The literature on structural studies of ChEs being extremely extensive, the references in this chapter are only representative of the considerable work that has been done in the field.

At first, we will highlight key residues in the primary sequence of ChEs, focusing on the catalytic triad and the associated catalytic mechanism. We will also talk about the supramolecular organization of ChEs with a description of the tetramer, which represents the main molecular form of hBuChE, in particular in plasma. Then we will go on with the description and comparison of the crystal structures of both hBuChE and *Tc*AChE. We will describe in detail the active site gorge and its subsites: the cation-π site, the peripheral anionic site (PAS) and the acylation site. This issue is of particular interest regarding the future of ChE inhibitors in the treatment of Alzheimer's disease. Finally, we will discuss the relationship between the subsites, and develop hypotheses concerning the trafficking of substrates and products in the gorge, the electrostatic steering of cationic ligands and a possible alternative exit route for the products of the hydrolysis reaction.

Primary structure and catalytic mechanism

The peptide sequence of ChEs is very well conserved among species. For example, the size of the catalytic subunit of hBuChE is almost identical to that of TcAChE (respectively, 574 and 575 residues for the tailed molecular forms) and their sequences are 54% identical (Figure 4.1).[1] It is noteworthy that sequence conservation is generally very high among α/β hydrolases. For instance, the sequence of lipase 1 from the fungus Candida rugosa is about 30% identical to that of hBuChE. ChEs have three conserved disulphide bridges. An additional cysteine at the fourth position from the C-terminus, which is involved in dimerization of subunits, is fully conserved. One of the most important differences between AChE and BuChE is the number of potential N-glycosyla-

tion sites. AChEs are generally less glycosylated than BuChEs. For example, TcAChE has four N-glycosylation sites whereas hBuChE has 10 (two of them are contiguous). In native hBuChE nine of these sites are glycosylated. For these enzymes, the calculated molecular weight of the peptide chain is 65.6 and 65.1 kDa, whereas their molecular weights are 70–75 and 85 kDa, respectively, on denaturating polyacrylamide gel electrophoresis. Glycosylation affects the folding, stability, immunogenicity, and pharmacokinetic properties of ChEs but not their catalytic properties.

Among the most conserved residues is the catalytic triad of α/β hydrolases: Ser, His and Glu. The triad differs from that of serine proteases by having glutamate instead of aspartate indicating a convergent evolution of both enzyme families. The catalytic mechanism of hydrolases consists of two steps (Figure 4.2A):[2]

```
BCHE_HUMAN    1 --EDDIIIAT KNGKVRGMNL TVFGGTVTAF LGIPYAQPPL GRLRFKKPQS LTKWSDIWNA TKYANSCCQN IDQSFPGFHG SEMWNPNTDL  88
ACHE_TORCA    1 DDHSELLVNT KSGKVMGTRV PVLSSHISAF LGIPFAEPPV GNMRFRRPEP KKPWSGVWNA STYPNNCQQY VDEQFPGFSG SEMWNPNREM  90
                   .... * *** *    *    ..** ****.*.**.* .* .**.*.    ** .***  * * *.  *    .*. **** * *******  ..

BCHE_HUMAN   89 SEDCLYLNVW IPAPKPKNAT VLIWIYGGGF QTGTSSLHVY DGKFLARVER VIVVSMNYRV GALGFLALP GNPEAPGNMG LFDQQLALQWV 178
ACHE_TORCA   91 SEDCLYLNIW VPSPRPKSTT VMVWIYGGGF YSGSSTLDVY NGKYLAYTEE VVLVSLSYRV GAFGFLALH GSQEAPGNVG LLDQRMALQWV 180
                ******** .*  .*.*.** .* *  *.  .*******    .*.* .* **  **.**   * * ..**  *** ** ***** *  *****.* * **.*****

BCHE_HUMAN  179 QKNIAAFGGN PKSVTLFGES AGAASVSLHL LSPGSHSLFT RAILQSGSFN APWAVTSLYE ARNRTLNLA KLTGCSRENE TEIIKCLRNKD 268
ACHE_TORCA  181 HDNIQFFGGD PKTVTIFGES AGGASVGMHI LSPGSRDLFR RAILQSGSPN CPWASVSVAE GRRRAVELG RNLNCNLNSD EELIHCLREKK 270
                . ** .** .*** .*** "** *** .*. .***** .** ******** **    * .*** * .  *  * .*.   .  *  . .*.*.*** *

BCHE_HUMAN  269 PQEILLNEAF VVPYGTPLSV NFGPTVDGDF LTDMPDILLE LGQFKKTQIL VGVNKDEGTA FLVYGAPGF SKDNNSIITR KEFQEGLKIFF 358
ACHE_TORCA  271 PQELIDVEWN VLPFDSIFRF SFVPVIDGEF FPTSLESMLN SGNFKKTQIL LGVNKDEGSF FLLYGAPGF SKDSESKISR EDFMSGVKLSV 360
                ***.. *   *.*. .     * * .**.*    .*     .* .******* .*****  *. ** ****** ***  * *. .  .*  *.*.

BCHE_HUMAN  359 PGVSEFGKES ILFHYTDWVD DQRPENYREA LGDVVGDYNF ICPALEFTKK FSEWGNNAFF YYFEHRSSK LPWPEWMGVM HGYEIEFVFGL 448
ACHE_TORCA  361 PHANDLGLDA VTLQYTDWMD DNNGIKNRDG LDDIVGDHNV ICPLMHFVNK YTKFGNGTYL YFFNHRASN LVWPEWMGVI HGYEIEFVFGL 450
                *    . * ...   .****.* *.    *.   * * .*** *  **.    * . * *  .. **...  *.* **.*  * ******* .  **********.

BCHE_HUMAN  449 PLERRDNYTK AEEILSRSIV KRWANFAKYG NPNETQNNST SWPVFKSTEQ KYLTLNTEST RIMTKLRAQ QCRFWTSFFP KVLEMTGNIDE 538
ACHE_TORCA  451 PLVKELNYTA EEEALSRRIM HYWATFAKTG NPNEPHSQES KWPLFTTKEQ KFIDLNTEPM KVHQRLRVQ MCVFWNQFLP KLLNATETIDE 540
                ** .* ***  ** *** *.. *.**.*** * .** *** * *.*   ** ... ****  .. .* ** . * **.* * * *.  * .***

BCHE_HUMAN  539 AEWEWKAGFH RWNNYMMDWK NQFNDYTSKK ESCVGL 574
ACHE_TORCA  541 AERQWKPEFH RWSSYMMHWK NQFDHYS-RH ESCAEL 575
                ** .**  ** **  *** ** ***  *. .. *** *
```

Figure 4.1

Alignment of the amino-acid sequences of human butyrylcholinesterase (BCHE_HUMAN, figure) and Torpedo californica acetylcholinesterase (ACHE_TORCA, figure). The sequences were aligned using the software ClustalW. Asterisks, full stops and triangles denote identity, high similarity and catalytic triad residues, respectively. Boxes joined by lines denote cysteines involved in disulphide bridges. N-glycosylated asparagine residues are highlighted in grey. Although Asn485 belongs to a potential N-glycosylation site, it is glycosylated only when Asn486 is mutated.
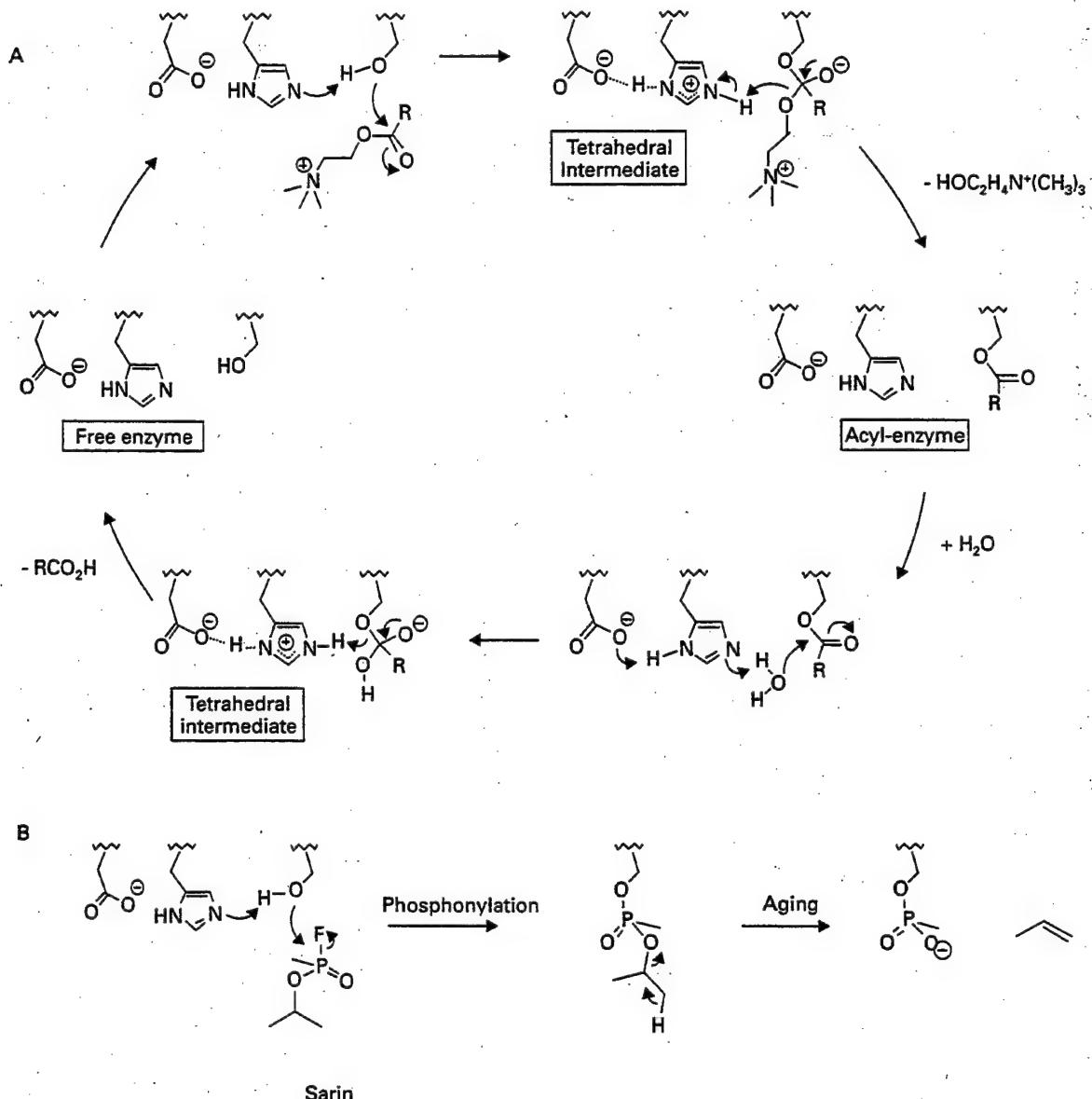
Figure 4.2
Catalytic (A) and aging (B) mechanisms.

(1) the carboxyl ester reacts with the catalytic serine, forming a tetrahedral intermediate state that collapses to an acyl-enzyme intermediate with release of the alcohol product; (2) a water molecule makes a nucleophilic attack on the acyl-enzyme, leading to the formation of a second tetrahedral intermediate that evolves to the free enzyme and the carboxylic acid product. This mechanism is very efficient, and the catalytic rate is close to the upper limit imposed by the molecular diffusion rate of the substrate. For example, AChE from the electric

eel (*Electrophorus electricus*), one of the most efficient enzymes known, is capable of hydrolysing 16,000 molecules of substrate per second. The driving force of this mechanism, shared by all serine hydrolases, is still controversial; it will be discussed below. It should be noted that hBuChE hydrolyses a wide range of substrates, including bulky neutral esters and even negatively charged esters (aspirin), at rates close to that for butyrylcholine.

With regard to their catalytic function, ChEs are the target of numerous reversible and irreversible or pseudo-irreversible inhibitors. Reversible inhibitors include a wide variety of aromatic ternary amines (e.g. tacrine, E2020) and quaternary ammonium derivatives. Pseudo-irreversible inhibitors can interact in a strong manner with the catalytic serine by mimicking the acylation tetrahedral intermediate. This is the case for boronates and m- (N,N,N-trimethyl-ammonium) trifluoroacetophenone (TMTFA) which have K_i values in the femto molar range. Other pseudo-irreversible inhibitors form stable alkyl intermediates that are very difficult to hydrolyse. These include carbamates (e.g. physostigmine, rivastigmine) and organophosphates (e.g. DDVP, the active product of metrifonate). For organophosphorus compounds, the use of nucleophiles stronger than water is needed to rapidly reactivate the phosphylated enzyme. Oxime derivatives are generally good reactivators. However, organophosphylates bearing an alkoxy group on the phosphorus atom undergo a side reaction (dealkylation of the alkoxy chain) a short time after phosphyla-tion of the enzyme (Figure 4.2B). This phenom-enon, called 'aging', can be very fast. For example, the half-life is shorter than 10 minutes for the soman-inhibited hBuChE, which carries a secondary alkoxy group. Because of this rapid aging, many alkylphosphonate monoester-ChE adducts are not reactivatable by oximes. Aging confers a very high toxicity to these compounds making them potent chemical warfare agents (such as the nerve gases soman and sarin).

Quaternary structure

The AChE displays molecular polymorphisms, which differ according to species and tissue distribution (for a review see Massoulié et al[3]). The different forms result from alternative splicing of a single gene. The AChE gene yields three main transcripts coding for three different molecular forms that differ by their C-terminal peptide. These forms are called H (Hydrophobic), T (Tailed) and S (Soluble). $AChE_S$ is a monomeric soluble form found in *Bungarus fasciatus* venom. A supplementary transcript (R; Read-through) has been identified in *Torpedo* and mammals; in human AChE (hAChE) it results from the absence of splicing after exon 4. In contrast to AChE, the BuChE gene yields a single transcript coding for the T form.

The H form of AChE is predominant in invertebrates. It is also expressed at the surface of mammalian blood cells (white cells and erythrocytes), but its physiological importance there is unclear. Each subunit of this dimeric form is anchored to the membrane by a glycophosphatidylinositol moiety. The free cysteine located close to the C-terminal forms a disulphide bridge between the two subunits. The abundance of this form in the electric organ of the *Torpedo* fish provided a large amount of material for early structural studies of cholinesterases. Ultimately, this form was used to solve the first structure of AChE by crystallography[4] in the early 1990s. The structure revealed a dimer, the two subunits interacting through a four-helix bundle. The helices involved in this bundle are different from those involved in the tetramerization domain.

This type of dimer was found in every AChE structure solved (mouse, human, *drosophila*). The subunits are arranged in an antiparallel manner with active site openings located on opposite sides of the dimer. All four helices of the bundle are aligned in an antiparallel fashion. The dimer is formed as soon as the concentration of subunits is sufficiently high. Surprisingly, the crystal structure of hBuChE does not display the same kind of dimer. Unlike *Tc*AChE, the two subunits of hBuChE are not antiparallel and the active site openings are located on the same side of the dimer (Figure 4.3). The helices are crossed ($\approx 45°$) rather than being aligned in an antiparallel fashion. Constraints resulting from the crystal packing could be at the origin of this exception.

The T form of AChE and BuChE is predominant in mammals. A multitude of supramolecular forms exist from the monomeric G1, the tetrameric G4 (95% of plasma BuChE) to the asymmetric complexes A_4, A_8 and A_{12} in which one to three tetramers are associated via a collagen-like tail. These tetramers are dimers of disulphide-linked dimers. The best illustration of the arrangement of the T form tetramer is provided by AChE from a non-mammal, the electric eel (*E. electricus*). Two different crystal forms were obtained, showing that the arrangement of the dimers in a tetramer is relatively flexible (Figure 4.4).[5] In frame A, the dimers are aligned antiparallel,
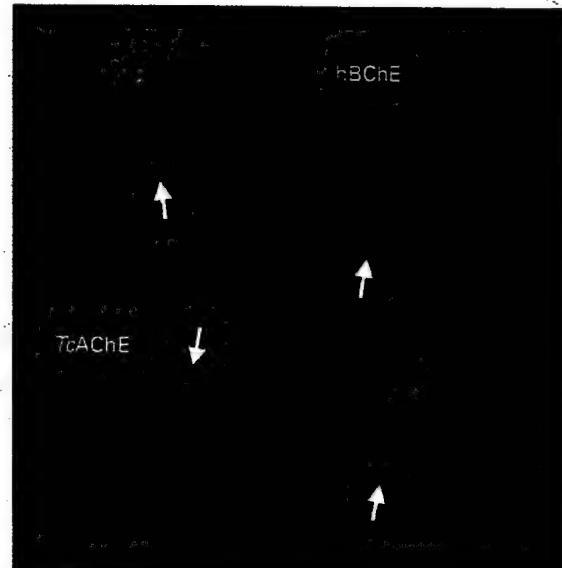
Figure 4.3
Ribbon representation of the dimers of human butyrylcholinesterase (hBChE, figure), top) and Torpedo californica acetylcholinesterase (TcAChE) (bottom). The right-hand subunits of hBChE (hBuChE) and TcAChE have the same orientation. An arrow indicates the entrance of the active site gorges. The β-strands are shown as arrows and the key helices (four-helix bundles for TcAChE) are shown as coils. The helices in cyan correspond to residues 362–375 of hBuChE and 365–375 of TcAChE. The helices in red correspond to residues 514–529 of hBuChE and 519–532 of TcAChE.

Figure 4.4
Ribbon representation of the crystal structures of tetrameric electric eel (Electrophorus electricus) acetylcholinesterase. (A) pseudo-square planar tetramer. (B) compact square nonplanar tetramer. The helices involved in the four-helix bundles are shown in red coils.

forming a pseudo-square planar tetramer with a large central space for the C-terminal peptide (T peptide). The T peptide is not visible in the crystal structure. In frame B, the tetramer is compact and nonplanar with all C-termini pointing to the same side.

The T peptide consists of the last 40 residues of the catalytic subunit. It is responsible for the formation of the tetramer. Secondary structure prediction of the T peptide showed that its C-terminus folds as an α-helix with an array of aromatic residues on the same face (called the WAT domain). Site-directed mutagenesis of these residues in hBuChE proved that they are necessary for the formation of the tetramers. Aromatic residues in this helix can interact with proline-rich peptides. Two peptides able to interact with the $AChE_T$ and $BuChE_T$ were identified: (a) PRAD (Proline Rich Attachment Domain) constitutes the N-terminal part of the collagen-tail of the asymmetric forms; it anchors $AChE_T$ at the neuromuscular junction. (b) PriMA anchors $AChE_T$ and $BuChE_T$ to cell membranes in muscle and brain. PRAD contains two nonessential cysteines that may form disulphide bridges with the ChE subunits. The group of Joel Sussman[6] recently solved the structure formed by interaction of the PRAD and four WAT domains. In this complex, the PRAD domain adopts a polyproline II type conformation. The WAT domains are parallel and form a super helix that surrounds the PRAD peptide. The stability of the structure is achieved through multiple stacking interactions between the conserved tryptophan residues of the WAT and the proline and phenylalanine residues of the PRAD. The T peptide also contains a free cysteine before the C-terminal end that is able to form a disulphide bridge with its equivalent of the other subunits.

No PRAD-like peptide has yet been identified in the tetrameric form of plasma hBuChE. However, adding L-polyproline to the culture media of Chinese hamster ovary (CHO) cells significantly increases the proportion of recombinant hBuChE tetramers. Therefore, a PRAD-like peptide is likely to promote the formation of tetrameric BuChE even if it only acts as a catalyst. If this peptide is still associated with the circulating BuChE tetramer, it could be identified. Among other curiosities of plasma BuChE, about 10% of the tetramer population consists of nonreducible dimers visible on denaturing polyacrylamide gel electrophoresis. The nature of the covalent bond that cross-links subunits has not yet been identified. Several heterologous molecular forms of BuChE have also been found in human plasma. The C_2 form is composed of a monomer of BuChE disulphide-linked to serum albumin. The C_5 isozyme is a G4-X form, present in 8–10% of the Caucasian population. It is a noncovalent complex of the G4 tetramer and an unknown protein of 60 kDa. The gene coding for this noncatalytic subunit is called locus E_2, and has been mapped to chromosome 2.

hBuChE displays many important genetic mutations, which have long been known. They are characterized by polyallelism of locus E_1, producing homozygous and heterozygous allelozymes or variants of the enzyme. Different aspects of BuChE mutants are dealt with in this book. By contrast, only one natural mutant of hAChE has been identified.

Structure

Structural studies on ChEs were boosted after the crystal structure of TcAChE was solved by Joel Sussman's group, in 1991.[4] Some really unexpected features were revealed. First, the 3D structure showed that the carboxylic residue of the catalytic triad was a glutamate instead of an aspartate, as in serine proteases. Because of the very efficient catalytic cycle of ChEs, it was commonly thought that the catalytic triad was located at the surface of the

protein. Actually, the active site is located at the bottom of a deep and narrow gorge lined by conserved aromatic residues. Due to the restrictive dimensions of the active site gorge, (20 Å depth, Ø ≈ 5 Å), the substrate hydrolysis takes place in a closed space virtually isolated from the bulk solvent. It was also thought for decades that the main component of the binding site for the quaternary head of acetylcholine was an anionic residue. Affinity labeling experiments, supported by the 3D structure, revealed that even though a negative charge is present close to the binding site (Glu199), the essential residues were aromatic: Trp84 and to a lesser extent Phe330.[7] These residues form what is called a cation-π binding site. Site-directed mutagenesis and 3D structures of complexes with inhibitors reinforced this interpretation. The cation-π interaction sites are now frequently found in other proteins, such as the acetylcholine receptors.

Later, the crystal structures of human, mouse and *Drosophila* AChE were solved; all of them are similar to the *Torpedo* enzyme. By relying on the high peptide sequence identity between *Tc*AChE and hBuChE (54%), a 3D model of hBuChE was soon built,[8] based on the 3D structure of *Tc*AChE. Most structural and mechanistic studies on hBuChE used this model as a starting template. Many attempts were made to crystallize human plasma BuChE without success. Failure was partly due to the heavy glycosylation of the enzyme (25% of its mass), which is not favorable for crystallization. Therefore, a recombinant BuChE lacking four out of the 10 potential glycosylation sites was designed. The C-terminal oligomerization domain was deleted to get a monomeric molecular form of the enzyme. This engineered hBuChE was expressed in CHO cells, purified to homogeneity and successfully crystallized.[9] The structure was solved to 2.0 Å by molecular replacement using the *Tc*AChE structure as the starting model.

As for AChE, the 3D structure of hBuChE is roughly represented by two hemispheres sandwiching the catalytic serine between two loops forming the sidewalls of the active site gorge (Figure 4.5). The active site gorge of hBuChE is much larger than its *Tc*AChE counterpart

Figure 4.5
Global structure of human butyrylcholinesterase. Left: side view of a ribbon diagram with α-helices shown as coils and β-strands as arrows. The ribbon is rainbow coloured from N-terminal in violet to C-terminal in red. Residue side chains of the omega-loop (violet) and acyl-loop (green) are shown as sticks. The butyrate and the catalytic serine are represented as balls and sticks. Right: Solvent accessibility surface with a view down to the active site gorge. The surfaces of the omega-loop, the acyl-loop and the catalytic serine are in violet, green and cyan, respectively.

($\approx$ 500 Å^3 vs 300 Å^3). Of the 14 aromatic residues, which line the active site gorge of TcAChE and determine its narrow aspect, six are substituted in hBuChE by smaller aliphatic or even polar residues. These residues account for most of the differences in catalytic properties observed between the two enzymes. Those differences have been extensively investigated by combining crystallography, specific labeling and site-directed mutagenesis. These studies led to the identification of four subsites in the active site gorge of ChEs: (1) the peripheral site at the rim of the gorge, which is the first encounter binding site for positively charged substrates and inhibitors, (2) the cation-π interaction site where the quaternary ammonium of choline binds, (3) the acylation site with its oxyanion hole, and (4) the acyl-binding pocket.

Cation-π site

Till the end of the 1980s, there was controversy over the nature of the binding site for the quaternary head of positively charged ligands in ChEs. An early hypothesis by Nachmansohn[10] stated that negatively charged carboxylic residues were the key elements of the binding site, providing Coulombian interactions with the quaternary ammonium group of ligands. However, chemical modifications showed the importance of tyrosine residues, and fluorescence studies showed that the binding site contained several tryptophan residues. Further labeling experiments, in the late 1980s and early 1990s, showed that aromatic residues, particularly Trp84, were directly involved in the interaction with positively charged groups of ligands. Finally, the crystal structure of TcAChE[4] provided a complete picture of the actual binding site for quaternary ammonium and protonated amines (Figure 4.6). The ammonium head of the acetylcholine molecule modeled into the binding site is in close contact with Phe330 and Trp84. Thus, interaction

between the enzyme binding site and the ligand is of the cation-π type. This type of interaction is now widely accepted. Shortly after the TcAChE crystal structure was published, mutagenesis studies confirmed the importance of these aromatic residues. Photoaffinity labeling of TcAChE and the crystal structures of inhibitor-AChE complexes provided an accurate view of the interaction between Phe330 and Trp84 and positively charged ligands.[7] In the structures of all complexes, the geometry of the binding site is unchanged, except for Phe330 whose orientation adjusts to better fit the shape of inhibitors. Some other residues, such as Tyr130, which interacts directly with Trp84, play an important role by stabilizing the functional conformation of the cation-π site.

In BuChE the key tryptophan (Trp82) is conserved but not the phenylalanine residue (Ala328) (see Figure 4.6). Absence of the phenylalanine affects the affinity for some inhibitors. For instance, huperzine has a high affinity for AChE because its protonated primary amine makes a strong interaction with Phe330 in TcAChE (Tyr337 in hAChE), whereas affinity for hBuChE is weaker because of an alanine residue (Ala328) in that position. Site-directed mutagenesis and affinity labeling confirmed the importance of Trp82 for the binding of ligands to hBuChE.[11,12]

The cation-π site is not specific to charged ligands as shown by the crystal structure of hBuChE. In that structure the cation-π site is occupied by a molecule of glycerol that was used as a cryoprotectant for freezing the crystal used for data collection (Figure 4.6). Similarly, a PEG-SH molecule was recently seen on the cation-π site of TcAChE.

Peripheral anionic site

Jean-Pierre Changeux[13] was the first to propose the existence of a regulatory site in TcAChE to explain noncompetitive inhibition
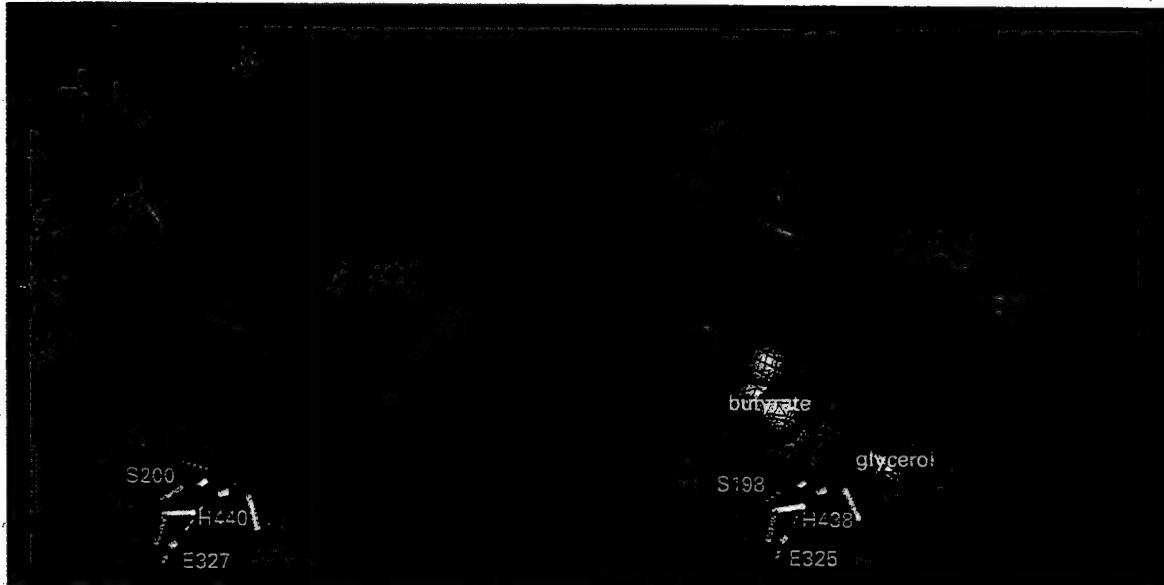
Figure 4.6
Active side gorge of Torpedo californica acetylcholinesterase (TcAChE) (left) and human butyrylcholinesterase (hBuChE) (right). The acyl-loop (green) and the omega-loop (violet) are represented as ribbons. The solvent accessibility surface is represented as a blue mesh. Key residues are represented as sticks: cation-π site in violet, acyl-binding pocket in green, key peripheral site residues for TcAChE in red, key peripheral site residues for hBuChE residues in orange, catalytic triad (carbon, blue; nitrogen, violet; oxygen, red). The butyrate and glycerol molecules bound in hBuChE's active site gorge are represented as space-filling models.

by certain ligands. This site was later characterized using propidium, a fluorescent inhibitor, whose binding does not affect the affinity of ligands specific to the cation-π site. According to the crystal structure of TcAChE and to affinity labeling experiments, Trp279, Tyr70 and Tyr121 are the key residues of the PAS. These residues are located at the rim of the gorge (Figure 4.6). Complexes of TcAChE with the bis-quaternary ligand decamethonium showed that one quaternary head binds to the cation-π on this site, whereas the other cationic head binds to the aromatic cluster formed by Trp279, Tyr70 and Tyr121.[7] Site-directed mutagenesis confirmed these results. For example, mutating these three aromatic residues into aliphatic ones dramatically reduced the affinity of fasciculin, a snake three-finger toxin specific for the PAS.[14] Crystal structures of complexes between AChEs and fasciculin clearly showed multiple interactions at the PAS.

Early studies using different approaches have suggested a conformational linkage between the PAS and the acylation site. Recently, De Ferrari et al showed that the binding of edrophonium or TMTFA at the acylation site quenches the fluorescence of thioflavin T bound to the PAS.[15] These molecules are sufficiently small and far apart that the quenching cannot be attributed to a steric interaction. Therefore, the binding of a ligand to one site affects the conformation of the other. It is clear that residues Tyr334, Asp72, Phe330 or even Glu199, contiguous to the catalytic serine, are part of a relay, transmitting

the information between the two sites, but the underlying molecular events are still unknown. At high substrate concentrations a molecule of substrate binds to the PAS to cause substrate inhibition. This inhibition could be a consequence of a similar conformational change.

In hBuChE, the three aromatic residues present in the AChE PAS are missing (Figure 4.6). Thus, it was thought that hBuChE had no PAS. Indeed, hBuChE has a weaker affinity than AChE for typical PAS ligands, such as propidium or fasciculin; and it is not subject to inhibition by excess substrate. By contrast, hBuChE is activated by excess substrate. Note that using inhibition and activation by excess substrate to describe the turnover kinetics of AChE and BuChE is only valid at physiological pH since these properties are pH-dependent. Substrate activation of hBuChE was found to be related to two residues located at the rim of the gorge: Asp70 and Tyr332 (Figure 4.6). These residues form the PAS of BuChE.

Based on early studies of natural variants of hBuChE, Asp70 was thought to be a key residue for the binding of cationic ligands to hBuChE. The natural Asp70Gly mutant, also called the 'atypical' variant, binds succinylcholine, a bis-quaternary myorelaxant,[11] weakly. This mutant does not show substrate activation and is slow at dealkylation of the phosphonyl residue after phosphylation by branched organophosphates (OPs) such as soman.[16] These factors support the existence of a conformational linkage between residues at the rim and at the bottom of the gorge. In addition, photo affinity labeling and site-directed mutagenesis showed that Tyr332, hydrogen bonded to Asp70, is important for substrate activation and for the binding of cationic ligands. Recent studies showed that Asp70 is the initial binding site of positively charged substrates before they slide down the gorge into a position favorable for the catalysis.[11] A similar role was assigned to the homologous residue Asp74 of hAChE.[17]

The acylation site

The acylation site or the active site is where the chemistry of the reaction takes place. It is located at the bottom of the gorge, about 20 Å from the protein surface. In hBuChE, it consists of the catalytic triad Ser198, His 438 and Glu325 (Figure 4.6). The catalytic role of Ser198 was first demonstrated in the 1950s by irreversible labeling with [^{32}P]diisopropyl-fluorophosphate. The roles of His438 and Glu325 were deduced from the sequence alignment with *Tc*AChE, and subsequently confirmed by mutagenesis. As a reminder, His440 of *Tc*AChE was identified as part of the catalytic triad by site-directed mutagenesis whereas Glu327 was assigned from the crystallographic structure.

Recent proton nuclear magnetic resonance studies on horse BuChE showed the presence of a short, strong hydrogen bond between these two residues when an inhibitor mimicking the acylation transition state is bound to the enzyme.[18] As in serine proteases, this short, strong hydrogen bond is thought to form when the catalytic histidine catches the Oγ proton of the catalytic serine. In this way, the histidine is more likely to accept the proton from the serine, thus improving the efficiency of the catalytic mechanism.

One of the main characteristics of serine hydrolases is H-bond stabilization of the transition state by the oxyanion hole. In hBuChE, the oxyanion hole is composed of three highly conserved N–H dipoles from the main chain of residues Gly116, Gly117 and Ala119 (Figure 4.7). There is one additional H-bond donor, compared to serine proteases like chy-
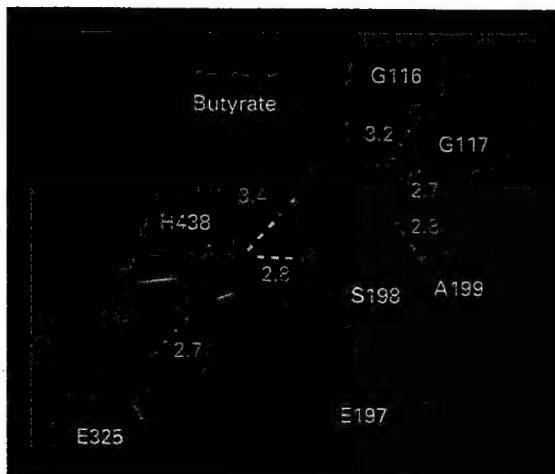
Figure 4.7
Acylation site of human butyrylcholinesterase. The residues of the catalytic triad (S198, H438, and E325) are represented as thick sticks, the bound butyrate as balls and sticks. The oxyanion hole residues (G116, G117, and A199) are represented as thin sticks. Yellow dotted lines represent hydrogen bonds with lengths indicated in Å. The depicted electron density of the butyryl moiety and the side chain of the catalytic serine Ser198 (violet mesh) is calculated at 2.0 Å resolution.

motrypsin, which may account for the superior efficiency of ChEs in the stabilization of the tetrahedral transition state. The catalytic role of the oxyanion hole was clearly pictured in the crystal structure of TcAChE complexed with TMTFA, but it is even more striking in the recent structure of hBuChE. In the latter case, the catalytic serine is bound to a butyryl moiety, i.e. the second product of the catalytic hydrolysis of a butyryl ester (Figure 4.7). This butyrate can be displaced in the crystals by high concentrations of the isosteric analog 3-bromopropionate.

The bound butyryl moiety displays a strong tetrahedral character. Thus the butyrate-BuChE tetrahedral complex is more stable than the free enzyme or the trigonal planar

butyryl-enzyme. However, there is an abnormally long distance between the butyrate carbonyl-carbon and the Oγ of Ser198 (2.16 Å), indicating labilization of this bond. This suggests that the tetrahedral structure of the butyrate is stabilized by interaction of the carbonyl-oxygen with the oxyanion hole. This provides a good illustration of the power of the oxyanion hole to promote the formation of transition states.

The origin of this butyryl moiety is still unknown. No butyryl ester was added either in the cell culture medium or during the steps leading to crystallization of the enzyme. It is likely that it originates from metabolism within the CHO cells in which the recombinant enzyme was expressed. Such enzyme-product adducts have already been described in other serine hydrolases such as γ-chymotrypsin but, to our knowledge, never in α/β-hydrolases. New refinements of several AChE crystal structures have shown that similar adducts are also present in their active site gorges. Therefore, it is likely that the resting state of ChEs in general corresponds to the acyl-enzyme form.

The mutation Gly117His allows OP-inhibited hBuChE to reactivate more rapidly than wild-type hBuChE. This effectively creates an OP hydrolase activity for hBuChE.[19] Optimally engineered mutants of hBuChE based on Gly117His may be used in the future for prophylaxis, treatment of nerve agent poisoning and skin decontamination.

The acylation site of ChEs contains a glutamic acid residue (Glu197 in hBuChE and Glu199 in TcAChE) adjacent to the catalytic serine (Figure 4.7); it stabilizes the transition states by electrostatic interaction with the protonated catalytic histidine and also promotes the dealkylation (aging) of alkoxy groups on the phosphylate after inhibition by OPs such as soman.[20,21] This residue and Trp82 form a

high electronic density that stabilizes the developing carbocation during the dealkylation reaction.

The acyl-binding pocket

Comparison of the hBuChE and the TcAChE structures shows a difference in the size of the acyl-binding pocket (Figure 4.6). The shape of the acyl-binding pocket is defined essentially by two residues, located at the bottom of the acyl-loop. These residues are aromatic in TcAChE (Phe288 and Phe290) but aliphatic in BuChE (Leu286 and Val288). Mutagenesis experiments confirmed that when the TcAChE acyl pocket residues are replaced by the smaller hBuChE residues, then this mutated enzyme is capable of hydrolysing bulkier substrates and is more sensitive to inhibitors, such as hBuChE.[8,22,23] Moreover, the global conformations of the acyl-loops of hBuChE (residues 277–288) and TcAChE are somewhat different (Figure 4.8). Flexibility of the acyl-loop has been suggested by molecular dynamics simulation for TcAChE.[24] A movement of the

loop has also been observed in the crystal structure of the 'aged' diisopropylfluorophosphate conjuguate of TcAChE. In both AChE and BuChE, the acyl-loop makes a thin shield against the external solvent and a limited movement could be sufficient to provide an exit route for the acidic product of substrate hydrolysis.

Relation between subsites and functional mechanism

Traffic of substrate

The PAS of AChE plays a role in allosteric regulation of catalysis. Kinetic measurements and site-directed mutagenesis by the groups of Shafferman,[25] Rosenberry[17] and Taylor[26] showed that the peripheral site is involved in inhibition by excess substrate. It was proposed that binding of acetylcholine to the PAS promotes a conformational change at the acylation and cation-π sites. In TcAChE, this event involves numerous residues of the gorge, par-

Figure 4.8
Superposition of the acyl-loops of Torpedo californica acetylcholinesterase (TcAChE) (blue) and human butyrylcholinesterase (hBuChE) (green). A front view on the left and a side view on the right are displayed. The acyl-loops are represented as ribbons. Key residues of hBuChE (V286, S287, and L288) and TcAChE (F288, R289, and F290) are represented as thick sticks and other acyl-loops residues as thin sticks. The bound butyrate is represented as balls and sticks.

ticularly Trp279, Asp72, Tyr334, Phe330, and Glu199, contiguous to the catalytic serine. Thus, binding of peripheral sites ligands, such as propidium or fasciculin, may induce a change of the position of Trp84 of the cation-π site.

Kinetic studies of substrate hydrolysis showed that when PAS inhibitors, such as fasciculin or propidium, are bound to the PAS, the acylation and deacylation rates decrease. However, this can be simply explained by a steric effect. This is in good agreement with molecular dynamics studies, showing that substrates should travel through a narrow channel to enter the gorge. This channel could be opened for a very short time to allow access to the active site. Recently, it has been shown that cationic substrates bind to the PAS as a first step of the catalytic mechanism.[17]

A possible physiological role of the PAS of *Tc*AChE could be to increase the local concentration of substrate at the entrance of the gorge, thereby improving the efficiency of substrate binding to the gorge. A similar scheme has been proposed for hBuChE to describe the path of substrate to the cation-π and acylation sites.[11] However, Tyr332 and Asp70 are the only residues conserved from *Tc*AChE to hBuChE. These two residues alone constitute the PAS of hBuChE, i.e. the primary binding site for positively charged substrate at the rim of the gorge. The substrate then slides down to Trp82 of the cation-π site. This model can be described in three steps, each step corresponding to one enzyme-substrate complex: the first complex is the substrate interacting with the PAS; the second one is the substrate vertically bound in the gorge with its head interacting with Trp82; finally, in the third complex, the substrate adopts a position favorable to the catalysis. For monocharged substrates like butyrylcholine, the PAS residues are only involved in the formation of the first encounter complex. On the other hand, the PAS residues are involved in the two first complexes with bis-quaternary ammonium compounds such as succinylcholine. This is the reason why the hydrolysis of succinylcholine is more affected by mutations in the PAS than is the hydrolysis of butyrylcholine.

Electrostatic steering

Computer calculations based on the crystal structures of *Tc*AChE and hBuChE indicate the existence of a strong electrostatic dipole aligned with the active site gorge of ChEs. This dipole, which results from an asymmetric distribution of charged residues in the enzyme, might steer positively charged ligands to the active site. Negatively charged carboxylic residues, located above the active site, are shielded by aromatic side chains that cover the gorge. This prevents the cationic substrates from direct interactions. In this way, substrates/ligands can smoothly slide on a 'carpet' of aromatic residues. However this mechanism is not completely accepted. Indeed, site-directed mutagenesis on seven carboxylic residues around the gorge of hAChE had no influence on the catalytic activity.[27] Brownian dynamics simulations show that the electrostatic steering generated by the dipole is weak[28] (up to 2-fold enhancement); most of the rate enhancement arises from short-range trapping of the substrate after it has entered the gorge.

Back door hypothesis

One of the most controversial issues about the mechanism of ChEs concerns the possibility that exit routes other than the gorge exist for the products of the hydrolysis reaction. The issue arises from a simple question. Since the catalytic residues are located at the bottom of a deep and narrow gorge, how can the enzyme manage to control the traffic of product and

substrate molecules to achieve a rate close to the limits imposed by the diffusion? This question has led some investigators to propose a back door, for release of products.

In BuChE, activation by excess substrate and the concomitant conformational change could be linked to the back door hypothesis. Under standard conditions, the PAS Asp70Gly mutant is not subject to excess substrate activation. This indicates that activation by excess substrate is directly related to the binding of a second substrate molecule to the PAS. It has been proposed that this binding promotes a conformational change of the Ω-loop (Cys65–Cys92) in which key residues Asp70 and Trp82 belong (Figure 4.6).[11,29] This loop attracted a lot of interest because of its homology to a highly flexible loop of the lipase1 from *Candida rugosa*. In this latter case, the Ω-loop can adopt two conformations leading to a fully open or completely closed active site. Several authors have hypothesized that a similar flexibility exists in the Ω-loop of ChEs. If true, such flexibility might allow opening and closing of a hole at the bottom of the gorge, through which products could exit. This could explain their catalytic efficiency in spite of the relatively buried active site. Flexibility of the Ω-loop is reasonable because it is weakly anchored to the core of the protein by three hydrogen bonds, two of them involving Tyr332 of the peripheral site. Molecular dynamics simulations on *Tc*AChE show that small movements of the loop, especially in the Trp84 (Trp82) area could provide an opening large enough to give access to water molecules, substrates or inhibitors. Attempts to reduce the mobility of the Ω-loop either by mutating key residues[30] or by introducing a cysteine bridge[31] gave disappointing results: the enzyme activity was only marginally affected. However, molecular dynamics revealed that even when the loop was tethered, substantial mobility remained in the immediate vicinity of the cation-π site. A limited movement could be sufficient to provide an access route to the active site.

The X-ray structure of a complex of *Tc*AChE and a carbamoylating agent (MF268) showed that although the rim of the gorge entrance was blocked with the long chain of the carbamylester, the bulky leaving group of MF268 was not found in the structure.[32] This strongly suggests that the product may leave the active site gorge via a back door. The recently solved crystal structure of the rabbit liver carboxylesterase – an enzyme closely related to ChEs – complexed with a cancer prodrug (CPT-11), provides further support to the existence of a secondary exit pore.[33] In this structure, the leaving group was bound at a site on the surface of the enzyme, which was separated from the catalytic gorge by only a thin wall of amino acid side chains. Despite all of these data in favour of a back door, direct evidence is still needed to definitively prove its existence.

Acknowledgments

References

1. Lockridge O, Bartels CF, Vaughan TA et al. Complete amino acid sequence of human serum cholinesterase. J Biol Chem 1987; 262:549–557.

2. Quinn D. Acetylcholinesterase: enzyme structure, reactions dynamics and virtual transition states. Chem Rev 1987; 87:955–979.

3. Massoulié J, Anselmet A, Bon S et al. The polymorphism of acetylcholinesterase: post-translational processing, quaternary associations and localization. Chem Biol Interact 1999; 120: 29–42.

4. Sussman JL, Harel M, Frolow F et al. Atomic structure of acetylcholinesterase from *Torpedo californica*: a prototypic acetylcholine-binding protein. Science 1991; 253:872–879.

5. Bourne Y, Grassi J, Bougis PE, Marchot P. Conformational flexibility of the acetylcholinesterase tetramer suggested by X-ray crystallography. J Biol Chem 1999; 274:30370–30376.

6. Harel M, Dvir H, Bon S et al. Crystal structure of the tetramerization domain of acetylcholinesterase at 2.3Å Resolution. XI International Symposium on Cholinergic Mechanisms-Function and Dysfunction, St Moritz (Switzerland), May 5–9, 2002.

7. Harel M, Schalk I, Ehret-Sabatier L et al. Quaternary ligand binding to aromatic residues in the active-site gorge of acetylcholinesterase. Proc Natl Acad Sci USA 1993; 90:9031–9035.

8. Harel M, Sussman JL, Krejci E et al. Conversion of acetylcholinesterase to butyrylcholinesterase: modeling and mutagenesis. Proc Natl Acad Sci USA 1992; 89:10827–10831.

9. Nachon F, Nicolet Y, Viguie N et al. Engineering of a monomeric and low-glycosylated form of human butyrylcholinesterase: expression, purification, characterization and crystallization. Eur J Biochem 2002; 269:630–637.

10. Bergman H., Wilson I, Nachmansohn D. The inhibitory effect of stilbamidine, curare and related compounds and their relationship to the active group of acetylcholinesterase. Biochem Biophys Acta 1950; 6:217–224.

11. Masson P, Legrand P, Bartels CF et al. Role of aspartate 70 and tryptophan 82 in binding of succinyldithiocholine to human butyrylcholinesterase. Biochemistry 1997; 36:2266–2277.

12. Nachon F, Ehret-Sabatier L, Loew D et al. Trp82 and Tyr332 are involved in two quaternary ammonium binding domains of human butyrylcholinesterase as revealed by photoaffinity labeling with [3H]DDF. Biochemistry 1998; 37: 10507–10513.

13. Changeux JP. Responses of acetylcholinesterase from Torpedo marmorata to salts and curarizing drugs. Mol Pharmacol 1966; 2:369–392.

14. Radic Z, Duran R, Vellom DC et al. Site of fasciculin interaction with acetylcholinesterase. J Biol Chem 1994; 269:11233–11239.

15. De Ferrari GV, Mallender WD, Inestrosa NC, Rosenberry TL. Thioflavin T is a fluorescent probe of the acetylcholinesterase peripheral site that reveals conformational interactions between the peripheral and acylation sites. J Biol Chem 2001; 276:23282–23287.

16. Masson P, Froment MT, Bartels CF, Lockridge O. Importance of aspartate-70 in organophosphate inhibition, oxime re-activation and aging of human butyrylcholinesterase. Biochem J 1997; 325:53–61.

17. Mallender WD, Szegletes T, Rosenberry TL. Acetylthiocholine binds to asp74 at the peripheral site of human acetylcholinesterase as the first step in the catalytic pathway. Biochemistry 2000; 39:7753–7763.

18. Viragh C, Harris TK, Reddy PM et al. NMR evidence for a short, strong hydrogen bond at the active site of a cholinesterase. Biochemistry 2000; 39:16200–16205.

19. Millard CB, Lockridge O, Broomfield CA. Organophosphorus acid anhydride hydrolase activity in human butyrylcholinesterase: synergy results in a somanase. Biochemistry 1998; 37:237–247.

20. Shafferman A, Ordentlich A, Barak D et al. Aging of phosphylated human acetylcholinesterase: catalytic processes mediated by aromatic and polar residues of the active centre. Biochem J 1996; 318:833–840.

21. Masson P, Fortier PL, Albaret C et al. Aging of di-isopropyl-phosphorylated human butyrylcholinesterase. Biochem J 1997; 327:601–607.

22. Radic Z, Pickering NA, Vellom DC et al. Three distinct domains in the cholinesterase molecule confer selectivity for acetyl- and butyrylcholinesterase inhibitors. Biochemistry 1993; 32:12074–12084.

23. Kaplan D, Ordentlich A, Barak D et al. Does 'butyrylization' of acetylcholinesterase through substitution of the six divergent aromatic amino acids in the active center gorge generate an enzyme mimic of butyrylcholinesterase? Biochemistry 2001; 40:7433–7445.

24. Enyedy IJ, Kovach IM, Bencsura A. Molecular dynamics study of active-site interactions with tetracoordinate transients in acetylcholinesterase and its mutants. Biochem J 2001; 353:645–653.

25. Shafferman A, Velan B, Ordentlich A et al. Substrate inhibition of acetylcholinesterase: residues affecting signal transduction from the surface to the catalytic center. Embo J 1992; 11:3561–3568.

26. Radic Z, Reiner E, Taylor P. Role of the peripheral anionic site on acetylcholinesterase: inhibition by substrates and coumarin derivatives. Mol Pharmacol 1991; 39:98–104.

27. Shafferman A, Ordentlich A, Barak D et al. Electrostatic attraction by surface charge does not contribute to the catalytic efficiency of acetylcholinesterase. EMBO J 1994; 13:3448–3455.

28. Botti SA, Felder CE, Lifson S et al. A modular treatment of molecular traffic through the active site of cholinesterase. Biophys J 1999; 77: 2430–2450.

29. Masson P, Xie W, Froment M, Lockridge O. Effects of mutations of active site residues and amino acids interacting with the Omega loop on substrate activation of butyrylcholinesterase. Biochim Biophys Acta 2001; 1544:166–176.

30. Velan B, Barak D, Ariel N et al. Structural modifications of the Omega loop in human acetylcholinesterase. FEBS Lett 1996; 395:22–28.

31. Faerman C, Ripoll D, Bon S et al. Site-directed mutants designed to test back-door hypotheses of acetylcholinesterase function. FEBS Lett 1996; 386:65–71.

32. Bartolucci C, Perola E, Cellai L et al. 'Back door' opening implied by the crystal structure of a carbamoylated acetylcholinesterase. Biochemistry 1999; 38:5714–5719.

33. Bencharit S, Morton CL, Howard-Williams EL et al. Structural insights into CPT-11 activation by mammalian carboxylesterases. Nat Struct Biol 2002; 9:337–342.

2

Butyrylcholinesterase function in the acetylcholinesterase knockout mouse

Oksana Lockridge, Ellen G Duysen and Bin Li

Introduction

All vertebrates have two distinct cholinesterases, acetylcholinesterase (AChE, EC 3.1.1.7) and butyrylcholinesterase (BuChE, EC 3.1.1.8). However, *Drosophila* flies and zebrafish have only AChE. The fact that mice can live to adulthood without AChE,[1,2] whereas insects and zebrafish cannot,[3,4] suggests that BuChE partly compensates for the loss of AChE. It is hypothesized that BuChE functions in nerve impulse transmission. This chapter summarizes the new view of BuChE function based on observations of the AChE knockout mouse.

Historical

When Mendel and Rudney first identified BuChE as an enzyme distinct from AChE, they named it pseudocholinesterase.[5] They were convinced that BuChE has no vital function. Dogs treated with cholinesterase inhibitor could lose 95% of their serum BuChE activity, yet show no toxic signs.[6] This view was reinforced by the finding that people with zero BuChE activity were healthy. About 2% of the Inuit population in Alaska, and 1 in 100,000 Caucasians have zero BuChE activity due to a genetic variant called 'silent' BuChE.[7] People with silent BuChE have no obvious health problems, though a detailed study has never been done.

AChE knockout mouse

The AChE knockout mouse was made by deleting 5 kb of the ACHE gene, making it impossible to produce any AChE protein.[1] All tissues in AChE–/– mice are completely deficient in AChE activity. Their BuChE activity is normal, and is not higher than in wild-type mice.[8,9] The genetic background of the knockout mice is strain 129Sv.

It was a surprise that AChE–/– mice were born alive, and that they could breathe and move. In our first report their average life span was 14 days.[1] Later we learned to keep them alive to adulthood by feeding them a liquid diet of Ensure (Abbott Laboratories, Abbott Park, IL).[2]

AChE–/– mice are not normal. They have a number of problems described below. Their phenotype suggests that, if BuChE is indeed responsible for the fact they are alive, BuChE is an inadequate substitute for AChE. The poor performance of BuChE can be attributed to location, low abundance in the brain, and slower rate of catalysis. BuChE is not in the right location for optimal function in nerve impulse transmission. BuChE is in glial cells, adjacent to rather than inside nerve synapses.[9] BuChE is highly abundant in most tissues, so that the total amount of BuChE in the mouse body is 10 times higher than the total AChE content.[10] However, the brain has low amounts of BuChE compared to AChE. The

affinity of BuChE for acetylcholine is the same as the affinity of AChE for acetylcholine,[11] though the catalytic activity of BuChE is about 4-fold lower.

Weak muscles

AChE-/- mice have very weak muscles. Pups are incapable of sucking enough milk to sustain life. When the diet of the dams was enriched by feeding them 11% fat food pellets and liquid Ensure, the dam's milk acquired more nutritional value with the result that AChE-/- pups survived. AChE-/- pups are weaned on day 14 and fed liquid Ensure in a dish.[2] They do not eat solid food. They never bite the handler or each other.

Their weak muscles cause them to have an unusual posture of splayed feet, an abnormal gait with the abdomen and tail dragging on the ground, and absence of grip strength. They are less active than their littermates. Young AChE-/- mice run, climb, and take a bipedal stance to look over the edge of a barrier. After 1 year of age AChE-/- mice are inactive; they walk to their food dish, but they do not climb or run. Adult AChE-/- mice have a hunched back. Weak muscles can be explained by the absence of AChE in the neuromuscular junction. People with end-plate AChE deficiency, due to mutations in the collagen tail protein (COLQ) gene, have the same weak muscles and scoliosis as AChE-/- mice.[12,13]

BuChE activity is found in the neuromuscular junction as shown by colocalization of BuChE activity and nicotinic receptors in AChE-/- muscle.[8] Electrophysiological experiments show that AChE-/- muscle is capable of contracting and of functioning. However, twitch tension, rise, and decay times in response to a single supramaximal stimuli are abnormal.[14] Diaphragm muscles from AChE-/- mice maintain tension when repetitively stimulated at 70 and 100 Hz, but show tetanic fade at 20, 50, 200, and 400 Hz. Two mechanisms explain the ability of AChE-/- muscle to maintain tension: downregulation of nicotinic acetylcholine receptors and reliance on BuChE activity. A role for BuChE in acetylcholine hydrolysis was shown by exposing AChE-/- diaphragm muscle to the selective BuChE inhibitor (BuChEI) tetra-(monoisopropyl)-pyrophosphortetramide (iso-OMPA). Inhibition of BuChE induced tetanic fade at 70 and 100 Hz. It was concluded that BuChE hydrolysed acetylcholine in the muscle of AChE-/- mice.

Minic et al[15] measured release of quanta of acetylcholine from AChE-/- muscle and came to a different conclusion regarding BuChE function. They found that inhibition of BuChE decreased evoked-quantal transmitter release. They concluded that BuChE has a role in the release of acetylcholine quanta from presynaptic membranes and that BuChE is not involved in regulating the duration of acetylcholine action at the post-synaptic membrane.

Sexual dysfunction

Male and female AChE-/- mice are housed together from postnatal day 14 to the end of their lives. No AChE-/- mouse has become pregnant in 4 years (n = 700). No mating behavior has been noticed; there is no sniffing and no mounting. An explanation for this sexual dysfunction is not yet available. Males have normal levels of testosterone and females have normal levels of estradiol. The seminiferous tubules contain sperm, and evidence of estrous has been found in females.[2]

Another behavioral abnormality is the absence of competition between males. Unrelated sexually mature wild-type males cannot be housed together because they fight to death. In contrast, AChE-/- males display no aggression to other males.

Eyes

AChE–/– mice have pinpoint pupils all their life, an observation consistent with the presence of excess acetylcholine. Other than the pinpoint pupils, the eyes of young mice look normal to visual inspection. However, by 1 year of age many AChE–/– mice have gross deformations in their eyes. In some mice the eyes bulge out, suggesting excessive pressure within the eye as in glaucoma. A vascular carpet covers the bulging eyes of some animals. Other mice have a different deformity; their eyes are resorbed. Mucus covers the sunken eyes, and a hairless ring of skin surrounds the eye.

The laboratory of Paul Layer has found degeneration of inner retina neural layers as early as postnatal day 60. By day 86, the photoreceptor layer is gone.[16] It is unknown whether young AChE–/– mice can see, but they are certainly blind when the photoreceptor layer is gone at day 86.

Postnatal developmental delay

AChE–/– pups can be distinguished from littermates from the day of birth. They tremble more, and hold their head and tail in unnatural, characteristic positions. With each day the differences become more pronounced. AChE–/– pups are smaller. The average weight of a 4-month-old AChE–/– female is 18 g, whereas a wild-type female weighs 27–32 g. Male AChE–/– mice also average 18 g though a few have grown to be 20–30 g, almost as large as wild-type males (30–35 g). Despite their small size, AChE–/– mice are not gaunt or emaciated. They have body fat and do not appear to be starving. Their body length to weight ratio is equivalent to that of wild-type animals.

AChE–/– mice are late in displaying the following developmental milestones. They open their eyes one day late (day 13 vs 12); they acquire the righting reflex 6 days late (day 18 vs 12); they acquire the ability to maintain their body temperature 7 days late (day 22 vs 15); their testes descend 4 weeks late (week 7–8 vs 4); estrous is up to 10 weeks late (week 15–16 vs 6–7).[2]

Gastrointestinal tract bloating

Wild-type and AChE+/– mice infected with *Helicobacter hepaticus* showed no symptoms. In contrast, infected AChE–/– mice had severe gastrointestinal (GI) bloating. Gas distended the walls of the stomach and the intestines. Gas filled the GI tract from the esophagus to the anus in some living animals. After our colony was freed of infection,[17] bloating was never seen again.

The bloating had caused distress to the animals as indicated by loss of body weight, loss of body temperature, and premature death. Currently no premature death is caused by GI ileus.

An explanation for the unusual response to infection is not yet available. The hypothesis was tested that intestinal motility might be reduced in AChE–/– mice.[18] To test motility, Evans blue dye was gavaged into 12 wild-type and six AChE–/– mice. Twenty minutes later the animals were euthanized and the distance traveled by the dye was measured relative to the length of the GI tract. Motility in AChE–/– mice was 16% higher than in wild-type mice. This experiment ruled out the possibility that reduced motility in AChE–/– mice fostered growth of inappropriate intestinal flora. Other possibilities being tested are that the immune function might be compromised, or that the environment in the GI tract might be abnormal due to improper functioning of pancreatic and gall bladder sphincters.

Seizures

Many AChE–/– mice have seizures when they are startled or undergo prolonged restraint. Pups less than 15 days of age do not have seizures. A critical period for seizure activity is postnatal days 20–50. AChE–/– mice older than 100 days have seizures less frequently. Many mice recover, but some die from the seizures. The major cause of early death in AChE–/– mice is seizures.

Normal brain structure

Mesulam et al[9] stained brain sections for choline acetyltransferase immunoreactivity. They reported that AChE–/– brains displayed an overall pattern of choline acetyltransferase immunoreactivity that did not qualitatively differ from wild-type. This indicated that cholinergic perikarya, axons, and terminals are viable even in the absence of AChE. It was concluded that AChE is not absolutely essential for the development or maintenance of cholinergic pathways. Staining for BuChE activity showed that the brain contains widespread BuChE activity which can be used to hydrolyse acetylcholine. In the wild-type mouse brain, BuChE activity is 10% of AChE activity. BuChE is found in capillaries, glial cells, and a few neurons, while AChE activity is found in axons and neurons. Mesulam et al[9] reported that BuChE activity extended to all regions known to have cholinergic neurotransmission. These studies were at the light microscopic level. More subtle quantitative studies are needed before it is known whether absence of AChE causes changes in connectivity, dendritic branching, cell number, and cell size.

Darvesh et al[19] stained human brain for BuChE activity. They concluded that BuChE may have specific functions including coregulation of cholinergic and noncholinergic neu-rotransmission in amygdala and in the hippocampal formation.

Downregulation of muscarinic and nicotinic receptors

BuChE is an inefficient substitute for AChE. The AChE–/– mouse has had to make drastic adaptations to survive in the absence of AChE. Muscarinic receptor levels are downregulated to 50% of normal.[20] The low level of muscarinic receptors suggests overstimulation by excess acetylcholine. This in turn suggests that BuChE does not adequately protect receptors from overstimulation. Nicotinic receptors are also downregulated as shown by the work of Adler et al[14] and Minic et al[15] in isolated muscle preparations.

Memory and learning

Memory and learning are difficult to measure in an animal that is blind, cannot swim well or for an extended period, and has poor locomotor activity. Thus, no measures of this type are available for AChE–/– mice. A clue to higher brain function is housekeeping behavior. Adult wild-type mice select one corner of their cage for urination. In contrast, AChE–/– mice urinate and defecate in their nest. This lack of housekeeping behavior suggests that higher brain function is undeveloped in AChE–/– mice.[2]

AChE is not present in excess concentrations in the mammalian brain

It is generally thought that AChE is present in excess concentrations in the mammalian brain and that AChE activity is not a limiting factor in brain acetylcholine metabolism.[21] Our results question this. Heterozygote AChE+/– mice with 50% of normal AChE activity have intermedi-

ate levels of muscarinic receptors in the brain.[20] This means that 50% AChE activity is too little to handle normal levels of acetylcholine. There is too much acetylcholine, and the receptors are overstimulated. In response to overstimulation, receptors are downregulated.

Inhibition of BuChE is lethal to AChE–/– mice

AChE–/– mice are supersensitive to the lethality of organophosphorus agents and carbamate inhibitors. Doses of the specific BuChEIs iso-OMPA and bambuterol, which are not toxic to wild-type mice, are lethal to AChE–/– mice. VX, the most potent nerve agent known, is lethal to AChE–/– mice at a lower dose (LD_{50} = 12 μg/kg) than the dose for lethality in wild-type mice (LD_{50} = 24 μg/kg).[10] The organophosphorus agents, DFP and chlorpyrifos oxon, which are relatively selective for BuChE over AChE, are lethal to AChE–/– mice at a lower dose compared to the lethal dose for wild-type mice. AChE–/– mice die when 50% of their brain BuChE is inhibited.[10]

Possible function of BuChE and implications for treatment of Alzheimer's disease

BuChE appears to have a function based on the following observations. (1) Mice live to adulthood despite the complete absence of AChE. It is thought that the presence of BuChE in mice partly compensates for AChE deficiency. (2) Inhibition of BuChE in the AChE–/– mouse is lethal. Low doses of DFP, iso-OMPA, and chlorpyrifos oxon are lethal to AChE–/– mice but not to AChE+/+ mice. (3) There is 10 times more BuChE than AChE in a wild-type mouse.

Would the body have so much BuChE if BuChE had no function? (4) BuChE is widely distributed in the brain of mice[9] and humans,[19] though its cellular localization is different from that of AChE. BuChE is present mainly in glial cells and capillaries, whereas AChE is in neurons and axons. (5) BuChE hydrolyses acetylcholine and therefore could have a role in terminating nerve impulse transmission.

The normal brain structure and intact cholinergic system found by Mesulam et al[9] suggested that BuChE compensated for the absence of AChE in AChE knockout brains. It was hypothesized that BuChE hydrolysed acetylcholine after the acetylcholine diffused out of synapses. Thus, BuChE could have a function in terminating nerve impulse transmission. This conclusion is supported by the work of Giacobini.[21] Giacobini specifically inhibited BuChE activity in the rat brain by perfusing a selective carbamate, MF-8622, into the cortex. Extracellular fluid was removed by microdialysis for quantitation of acetylcholine. A 15-fold increase in the concentration of acetylcholine was found in cortical cholinergic synapses (from 5 nM to 75 nM). There were no cholinergic adverse effects, thus supporting the finding that AChE was not significantly inhibited. Another specific BuChEI, phenethylcymserine, improved learning in elderly rats.[22] Mesulam et al's and Giacobini's results lead to the conclusion that inhibition of BuChE will increase the amount of acetylcholine in the brain, and thus BuChEIs are expected to be beneficial to Alzheimer's disease patients.

Acknowledgments

herein belong to the authors and should not be construed as the official views of the US Army or the Department of Defense.

References

1. Xie W, Stribley JA, Chatonnet A et al. Postnatal developmental delay and supersensitivity to organophosphate in gene-targeted mice lacking acetylcholinesterase. J Pharmacol Exp Ther 2000; 293:896–902.

2. Duysen EG, Stribley JA, Fry DL et al. Rescue of the acetylcholinesterase knockout mouse by feeding a liquid diet; phenotype of the adult acetylcholinesterase deficient mouse. Brain Res Dev Brain Res 2002; 137:43–54.

3. Greenspan RJ, Finn JA, Hall JC. Acetylcholinesterase mutants in Drosophila and their effects on the structure and function of the central nervous system. J Comp Neurol 1980; 189: 741–774.

4. Behra M, Cousin X, Bertrand C et al. Acetylcholinesterase is required for neuronal and muscular development in the zebrafish embryo. Nat Neurosci 2002; 5:111–118.

5. Mendel B, Rudney H. Studies on cholinesterase. I. Cholinesterase and pseudocholinesterase. Biochem J 1943; 37:59–63.

6. Hawkins RD, Gunter JM. Studies on cholinesterase. 5. The selective inhibition of pseudocholinesterase in vivo. Biochem J 1946; 40: 192–197.

7. Primo-Parmo SL, Bartels CF, Wiersema B et al. Characterization of 12 silent alleles of the human butyrylcholinesterase (BCHE) gene. Am J Hum Genet 1996; 58:52–64.

8. Li B, Stribley JA, Ticu A et al. Abundant tissue butyrylcholinesterase and its possible function in the acetylcholinesterase knockout mouse. J Neurochem 2000; 75:1320–1331.

9. Mesulam MM, Guillozet A, Shaw P et al. Acetylcholinesterase knockouts establish central cholinergic pathways and can use butyrylcholinesterase to hydrolyze acetylcholine. Neuroscience 2002; 110:627–639.

10. Duysen EG, Li B, Xie W et al. Evidence for nonacetylcholinesterase targets of organophosphorus nerve agent: supersensitivity of acetyl-

cholinesterase knockout mouse to VX lethality. J Pharmacol Exp Ther 2001; 299:528–535.

11. Radic Z, Pickering NA, Vellom DC et al. Three distinct domains in the cholinesterase molecule confer selectivity for acetyl- and butyrylcholinesterase inhibitors. Biochemistry 1993; 32:12074–12084.

12. Hutchinson DO, Walls TJ, Nakano S et al. Congenital endplate acetylcholinesterase deficiency. Brain 1993; 116:633–653.

13. Ohno K, Brengman J, Tsujino A, Engel AG. Human endplate acetylcholinesterase deficiency caused by mutations in the collagen-like tail subunit (COLQ) of the asymmetric enzyme. Proc Natl Acad Sci USA 1998; 95:9654–9659.

14. Adler M, Deshpande SS, Oyler G et al. Contractile and morphological properties of diaphragm muscle in acetylcholinesterase knockout mice. US Army Medical Defense Bioscience Review. Hunt Valley, MD June 2–5, 2002.

15. Minic J, Barbier J, Chatonnet A et al. Synaptic transmission at AChE–/– and COLQ–/– knockout mouse neuromuscular junctions. Seventh International Meeting On Cholinesterases; Pucon, Chile; November 8–12, 2002.

16. Bytyqi AH, Duysen EG, Lockridge O, Layer PG. Complete postnatal degeneration of the photoreceptor layer in an AChE knockout mouse. Seventh International Meeting On Cholinesterases; Pucon, Chile; November 8–12, 2002.

17. Duysen EG, Fry DL, Lockridge O. Early weaning and culling eradicated Helicobacter hepaticus from an acetylcholinesterase knockout 129S6/SvEvTac mouse colony. J Comp Med 2002; 52:461–466.

18. Duysen EG, Kolar CH, Lockridge O. H. hepaticus infection in acetylcholinesterase knockout mice results in severe intestinal distension. Seventh International Meeting On Cholinesterases; Pucon, Chile; November 8–12, 2002.

19. Darvesh S, Grantham DL, Hopkins DA. Distribution of butyrylcholinesterase in the human amygdala and hippocampal formation. J Comp Neurol 1998; 393:374–390.

20. Li B, Duysen EG, Lockridge O. Acetylcholinesterase knockout mice are resistant to oxotremorine-induced hypothermia and pilocarpine-induced seizures. Seventh International Meeting On Cholinesterases; Pucon, Chile; November 8–12, 2002.

21. Giacobini E. Selective inhibitors of butyry-cholinesterase. A valid alternative for therapy of Alzheimer's Disease? Drug Aging 2001; 18: 891–898.

22. Greig NH, Utsuki T, Yu Q et al. A new therapeutic target in Alzheimer's disease treatment: attention to butyrylcholinesterase. Curr Med Res Opin 2001; 17:159–165.

BUTYRYLCHOLINESTERASE
ITS FUNCTION AND INHIBITORS

Ezio Giacobini MD PhD
Department of Geriatrics
University of Geneva
School of Medicine
Geneva
Switzerland

Editor

Lochridge, Duysen, Li